Mechanisms of Sensory Signal Transduction Across the Envelope in the CpxRA System of *Escherichia coli*

by

Timothy Hyun Seok Cho

A thesis submitted in partial fulfillment of the requirements for the degree of

Doctor of Philosophy

Department of Biological Sciences
University of Alberta

Abstract

The bacterial envelope is a critical barrier that not only shields bacteria from harsh environments but also serves as a key organizing centre for processes such as metabolism, virulence, and even DNA replication. In Gram-negative bacteria, the envelope is composed of inner and outer membranes and a peptidoglycan cell wall and is especially resistant to environmental threats. The envelope is carefully constructed through a number of interconnected biogenesis pathways. Furthermore, bacteria monitor the envelope through several envelope stress responses. The Cpx response of the model organism *Escherichia coli* is a conserved system for maintaining the integrity of protein folding in the envelope. In this system, the sensor kinase CpxA detects stresses and activates its response regulator, CpxR, by phosphorylation. The Cpx response also utilizes accessory proteins such as the periplasmic chaperone CpxP and the outer membrane lipoprotein protein NlpE to fine-tune signaling. NlpE is an activator of the system, alerting the system to surface adhesion, lipoprotein biogenesis defects, and changes in periplasmic redox state. While much is known about what genes the Cpx response regulates and what signals induce CpxA, much less is known about how signals are sensed and transduced in this system.

In this thesis, we explore the molecular mechanisms of CpxA activation. In a collaborative study (Chapter 2), we investigate the structure of CpxA's sensor domain as a unique and novel dimer of Per-ARNT-Sim (PAS) domains. This novel dimer structure explains the phenotypes of several historical *cpxA** alleles and regulates CpxA's activity by preventing activation in the absence of inducing cues. Mutations in the dimer interface strongly activate CpxA and render it blind to stimuli. This novel PAS dimer orientation may be present in other sensor kinases, revealing a previously unknown diversity in the structure of these common sensory domains. In Chapters 3 and 4, we investigate how the outer membrane lipoprotein NlpE activates CpxA in

the presence of diverse inducing signals. We report the molecular details of the interaction between NlpE and CpxA when NlpE is mislocalized to the inner membrane and examine the structural features of NlpE and their contribution to activating CpxA. We also find a role for the Cpx-regulated proteolytic factors CpxP and DegP in stabilizing NlpE, a novel axis of regulating NlpE signaling. At the outer membrane, NlpE interacts with the major outer membrane protein OmpA via its N-terminal domain and signals to CpxA through its C-terminal domain. We also find that the ability of OmpA to bind the cell wall is important for activating the Cpx response, suggesting that NlpE signaling from the outer membrane is coordinated through the cell wall. Finally, we report that NlpE can become surface-exposed, which may explain its ability to sense adhesion to surfaces. Thus, NlpE's versatility in signaling comes from its ability to localize to both the inner and outer membranes, the proteins it interacts with in these locales (CpxA or OmpA), and the different functions of each of its domains. Taken together, the work presented in this thesis significantly expands our understanding of how Gram-negative bacteria sense and transduce signals across the envelope.

Preface

Minor parts of Chapter 1 (Introduction) were adapted from two reviews I co-wrote. “Bacterial envelope stress responses: Essential adaptors and attractive targets” in *Biochimica et Biophysica Acta (BBA) Molecular Cell Research* (2022) volume 1870, issue 2, 119387 was co-written by me, Kat Pick (fellow Raivio lab PhD student), and Dr. Tracy Raivio. Kat Pick and I were responsible for most of the literature search and writing, while Dr Raivio wrote the introduction, reviewed, and edited the manuscript. “Maintaining Integrity Under Stress: Envelope Stress Regulation of Pathogenesis in Gram-Negative Bacteria” in *Frontiers in Cellular and Infection Microbiology* (2019) volume 9, 313 was co-written by me and Claire Hews (University of East Anglia), and Drs. Gary Rowley, and Tracy Raivio. Claire Hews and I were responsible for the literature search and writing while Drs. Rowley and Raivio reviewed and edited the manuscript.

Chapter 2 of this thesis is published as “The sensor of the bacterial histidine kinase CpxA is a novel dimer of extracytoplasmic Per-ARNT-Sim domains” in the *Journal of Biological Chemistry* (2024) volume 300, issue 5, 107265 and is presented in this thesis with minimal modifications. This publication was the result of a longstanding collaboration between the labs of Dr. Tracy Raivio and Dr. J.N. Mark Glover (Department of Biochemistry, University of Alberta) and is a co-first authored publication with Glover lab PhD student Cameron Murray. Cameron Murray and I co-wrote the manuscript with both Drs. Tracy Raivio and Mark Glover providing feedback on and reviewing the manuscript. Cameron Murray and I were responsible for the majority of the experimental (me) and modelling (Cameron Murray) work presented in this chapter with the following essential contributions to the manuscript: Gina L. Thede was responsible for purifying the sensor domain of CpxA and crystallization; Ross A. Edwards assisted with the refinement of the crystallographic data; Jun Lu contributed to biochemical work on CpxA; Roxana Malpica generated the data shown in Figure 2-2; Rodrigo Margain-Quevedo provided some of the supplementary data used in the article (Figures 2-4, 2-9, 2-12, 2-15).

Chapter 4 of this thesis is modified from the publication “NlpE is an OmpA-associated outer membrane sensor of the Cpx envelope stress response” in the *Journal of Bacteriology* volume 205, issue 4 (Epub). The publication was a co-first authored publication with previous Raivio lab PhD student Dr Junshu Wang in recognition of her initial discovery of the NlpE-OmpA complex. I was responsible for writing the manuscript and Dr Tracy Raivio provided feedback on

and edited the manuscript. This chapter contains the work contained in the publication with additions and minus the work directly taken from Dr. Junshu Wang's thesis.

Work on this thesis was supported by the Canada Graduate Scholarship – Doctoral (2023-2024), Postgraduate Scholarship – Doctoral (2021-2023), and Canada Graduate Scholarship – Masters (2018-2019) from the Natural Sciences and Engineering Research Council of Canada.

Acknowledgments

This thesis only exists because of the contributions and support of a wide network of individuals and organizations. I would like to express my immense gratitude to my supervisor Dr. Tracy Raivio. From my first days in the lab as a second-year summer student to my 10th year of post-secondary schooling as a 6th year PhD student, Tracy's expertise, mentorship, and support has been constant and uplifting. Besides being an excellent scientist, Tracy is also one of the biggest-hearted individuals I know. I will always admire and carry with me her compassion, professionalism, and recognition that science is a fundamentally human endeavor, best conducted with kindness and empathy.

Second, I would like to thank my collaborators and PhD advisory committee members Dr. J.N. Mark Glover and Dr. Casey Fowler for providing invaluable feedback and direction for my thesis work. Thank you also to fellow graduate student Cameron Murray, without whom our study on CpxA's sensor domain would never have been published.

I would also like to thank the many organizations who supported my doctoral work through funding and scholarships. Particularly, thank you to the National Science and Engineering Research Council as well as the Department of Biological Sciences and Faculty of Graduate and Postdoctoral Studies, who supported me through many scholarships and TAships.

Finally, I would like to extend my gratitude to all my family and friends. Thank you especially to my Raivio lab family (Valeria Tsviklist, Kat Pick, Brent Weber, Shaina Selles, Justin Bishop, and Ashley Gilliland). You have stuck with me through all the ups and downs of grad school, and I'm thankful to have been on this journey with all of you! To Ve; thank you for always believing in and supporting me in all my endeavours. And finally, thank you to my parents who faced the hardships of immigrating to strange lands but always supported me and encouraged me to become a 훌륭한 person. I am always thankful for your support and love!

S.D.G.

Table of Contents

List of Tables

List of Figures

Chapter 1 – General Introduction

The Gram-negative envelope

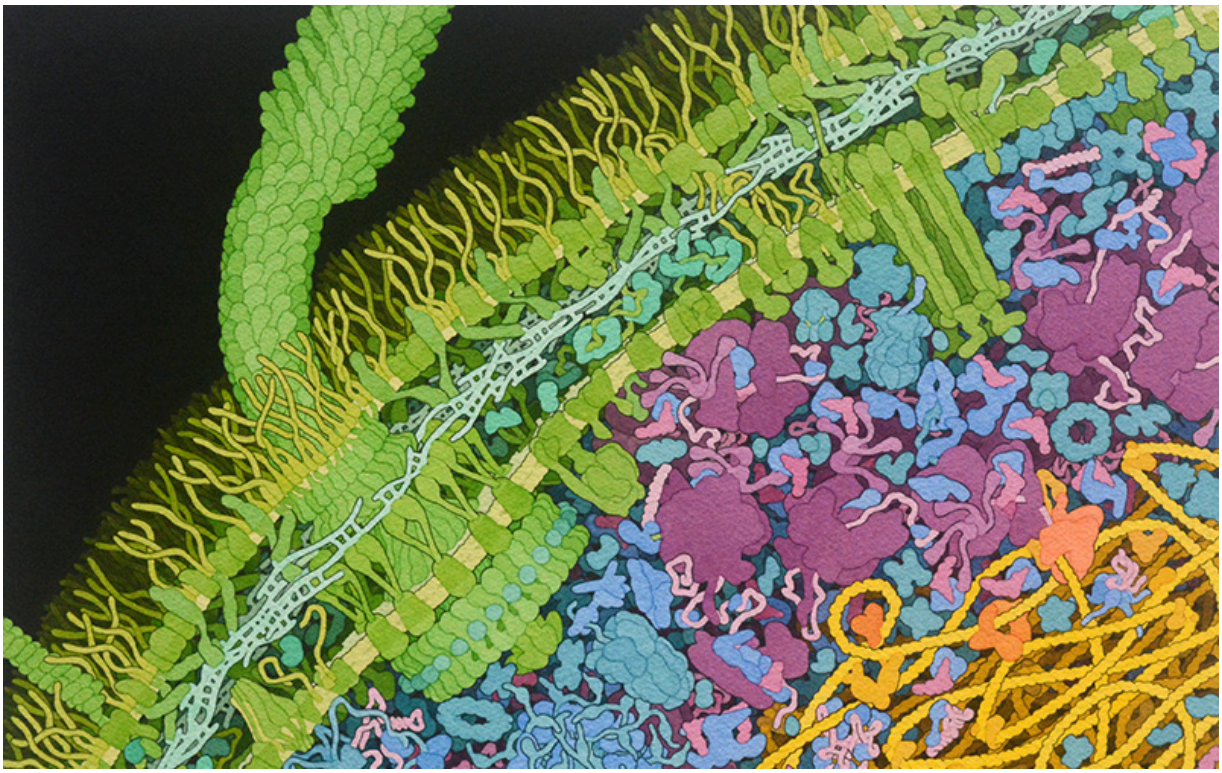

Figure 1-1. The Gram-negative envelope is a complex and beautiful structure.
Watercolor rendering of the *Escherichia coli* envelope (shown mostly in shades of green) by David S. Goodsell, RCSB Protein Data Bank. doi: 10.2210/rcsb_pdb/goodsell-gallery-028 (used with permission under CC BY 4.0). Several structures can be seen, including lipopolysaccharide, peptidoglycan complexed with OmpA/Lpp, and appendages such as pili and flagellum.

A dual-membrane envelope is the hallmark feature of Gram-negative bacteria. While the divergence between diderm (Gram-negative) and monoderm (Gram-positive) bacteria is a perennial question in evolutionary microbiology (Gupta, 2011; Léonard et al., 2022; Megrian et al., 2020; Taib et al., 2020; Tocheva et al., 2016; Witwinowski et al., 2022), the physiological advantage of a dual membrane structure is uncontroversial and intuitive: an additional permeability barrier increases the resilience of bacteria against environmental threats, including antimicrobials. Thus, four of six listed species/genera in the highly-antibiotic resistant ESKAPE

(*Enterococcus faecium, Staphylococcus aureus, Klebsiella pneumoniae, Acinetobacter baumanii, Pseudomonas aeruginosa,* and *Enterobacter* spp.) group are Gram-negative (Rice, 2008). Accordingly, the updated 2024 edition of the World Health Organization's Bacterial Priority Pathogens List continues to stress the outsized influence of Gram-negative organisms to antibiotic resistance and global disease burden ("WHO bacterial priority pathogens list, 2024," 2024). But from a more basic perspective, the Gram-negative envelope is a unique and complicated structure (Figure 1-1), full of diverse biomolecules and sensory systems that function together to allow bacteria to exist and thrive in many contexts, not just clinical ones. Thus, understanding how Gram-negative bacteria build, monitor, and protect their envelopes remains a crucial question for microbiologists of every stripe.

Building the envelope

The Gram-negative envelope is a three-layered structure populated by proteins of diverse topology, structure, and function (Silhavy et al., 2010). The outermost layer is the outer membrane, an asymmetric bilayer of lipopolysaccharide (LPS) and phospholipids. Underneath this layer is a peptidoglycan cell wall that provides mechanical rigidity to the envelope (Höltje, 1998). The final layer is the inner membrane, a simpler phospholipid bilayer. An ATP (adenosine triphosphate)-devoid aqueous space known as the periplasm resides between the outer and inner membranes (Thanassi et al., 2005), housing molecules involved in transport, detoxification, and biogenesis (Miller and Salama, 2018). These layers, however, are not completely independent of each other but rather function together to protect bacterial cells. While the simplest phospholipid membranes form spontaneously and protein folding is usually energetically favourable (Alberts et al., 2002; Anfinsen and Scheraga, 1975), making and maintaining a bacterial cell envelope is far from a simple process and requires significant resource investment (Silhavy et al., 2010).

The inner membrane

The inner membrane is a phospholipid (PL) bilayer composed mostly of phosphatidylethanolamine (PE) with lower amounts of phosphatidylglycerol (PG), phosphatidylserine (PS), and cardiolipin (CL) (Yasuhiro et al., 1967). PE in both the inner and outer membranes feeds into the biosynthesis of other envelope constituents, for example, providing the acyl groups used by the apolipoprotein *N*-acyltransferase Lnt in the final acylation of lipoproteins (Gupta and Wu, 1991; Jackowski and Rock, 1986; Noland et al., 2017) and the acyltransferase PagP in acylation of LPS's lipid A (a notorious mechanism of defense against antimicrobial peptides) (Bishop, 2005). Interestingly, while the inner membrane is often thought of as a "symmetric" bilayer in contrast to the outer membrane, recent work suggests that the inner membrane also possesses regulated asymmetry in its lipid composition (Bogdanov et al., 2020).

Despite its seemingly simple lipid composition compared to the outer membrane, the inner membrane houses many critical metabolic processes. Every envelope-localized or secreted molecule must also pass through this layer. Much like their location at the inner mitochondrial membrane of eukaryotic cells, the complexes of the electron transport chain and ATP synthase reside at the inner membrane (Guo et al., 2018; Unden and Bongaerts, 1997). Because the periplasm lacks ATP, the cytoplasmic leaflet of the inner membrane serves as the interface for energized processes requiring ATP hydrolysis. Several inner membrane ATP-binding cassette (ABC) transporter proteins facilitate the movement of substrates into and out of the cytoplasm (Davidson et al., 2008). Secretion systems almost always possess an inner membrane base where cargo and adaptor proteins are loaded and ATP is hydrolyzed to energize transport (Costa et al., 2015; Green and Mecsas, 2016). Active transport can also be energized in an ATP-independent fashion through an electrochemical gradient of protons across

the inner membrane (the proton motive force (Maloney et al., 1974); for example, the transport of large molecules into the cell by TonB-dependent transporters is energized by proton motive force dissipation through the TonB-ExbBD complex (Celia et al., 2019; Noinaj et al., 2010). Finally, the inner membrane is also the site of almost all envelope biogenesis processes including unfolded and folded protein translocation by the Sec and Tat translocons, respectively, (Lycklama a Nijeholt and Driessen, 2012; Mori and Ito, 2001; Palmer and Berks, 2012), lipoprotein modification (Narita and Tokuda, 2017), LPS synthesis (Bertani and Ruiz, 2018; Wang and Quinn, 2010), peptidoglycan synthesis (Garde et al., 2021), and redox folding of proteins (Ito and Inaba, 2008). In these ways, the inner membrane serves as one of the cell's most critical organizing centres.

The cell wall

Gram-positive and -negative bacteria both possess a cell wall made up of peptidoglycan, chains of alternating sugars crosslinked together with short peptides. Together, strands of peptidoglycan form a polymeric unit surrounding the cell called the sacculus (Silhavy et al., 2010). The overall function of the cell wall is to resist changes in osmotic pressure and maintain cell shape (Cabeen and Jacobs-Wagner, 2005; Huang et al., 2008; Rojas and Huang, 2018; Vollmer and Bertsche, 2008). The main carbohydrate component of the cell wall consists of chains of alternating *N*-acetylglucosamine (Glc*N*Ac) and *N*-acetylmuramic acid (Mur*N*Ac) (Vollmer and Bertsche, 2008). In Gram-negatives, the Mur*N*Ac residue possesses a 4-5 amino acid peptide modification (Garde et al., 2021). Pentapeptidated Glc*N*Ac-Mur*N*Ac linked to undecaprenyl-phosphate (Und-P), which is referred to as lipid II, is synthesized in the cytoplasm and flipped across the inner membrane by the flippase MurJ (Sham et al., 2014). Lipid II is polymerized to form glycan strands by transglycosylation and peptide chains are crosslinked to other peptide chains by transpeptidation. These processes are mediated by transglycosylases

and transpeptidases (also known as penicillin binding proteins), respectively (Sauvage et al., 2008; Scheurwater et al., 2008). Crosslinks between glycan strands are hydrolyzed by endopeptidases, which allows for the incorporation of new disaccharides into glycan strands and, therefore, the growth of the sacculus (Vollmer et al., 2008). Two complexes, the elongasome and divisome, coordinate the growth and division of the cell wall respectively (Cameron and Margolin, 2024; Den Blaauwen et al., 2008; Du and Lutkenhaus, 2017; Szwedziak and Löwe, 2013). Peptidoglycan is also covalently linked to the outer membrane lipoprotein Lpp through L,D-transpeptidases LdtA, LdtB, and LdtC which bond a C-terminal lysine on Lpp with the mDAP[3] residue of peptidoglycan (Bahadur et al., 2021; Magnet et al., 2007; Winkle et al., 2021). Thus, peptidoglycan synthesis, incorporation, and turnover are highly choreographed processes that link to almost every other aspect of envelope structure and biogenesis.

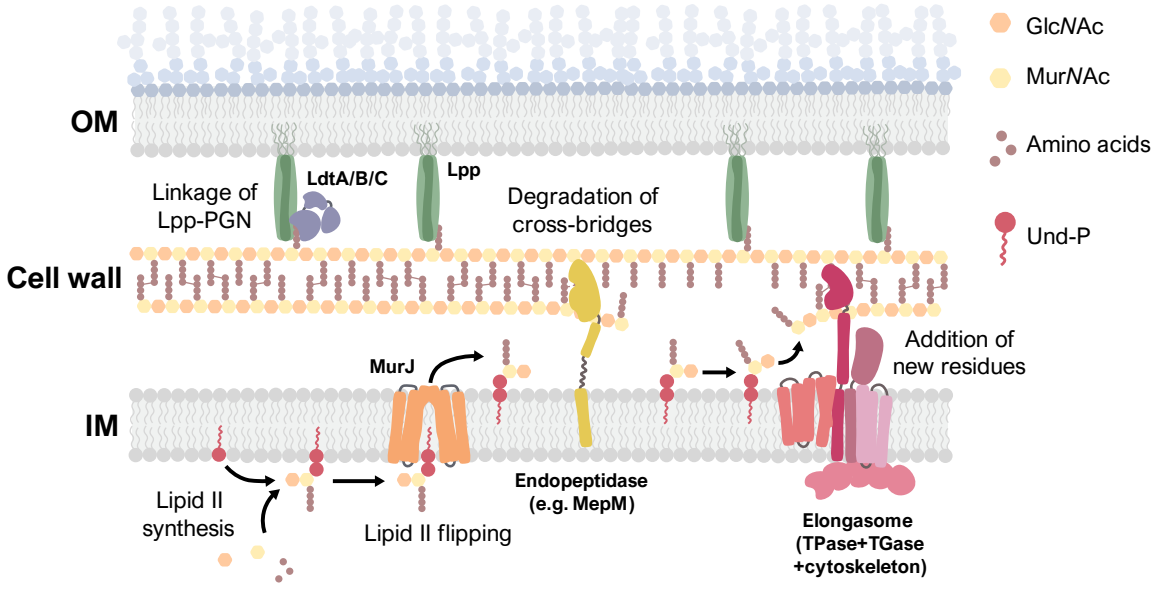

Figure 1-2. The cell wall and its synthesis.

Cell wall synthesis involves the production of peptidoglycan precursors, namely lipid II in the cytoplasm and the addition of lipid II to the existing sacculus. The main features of PGN synthesis are shown above in broad strokes. Abbreviations: Glc*N*Ac (*N*-acetylglucosamine), Mur*N*Ac (*N*-acetyl muramic acid), Und-P (undecaprenyl phosphate).

The outer membrane

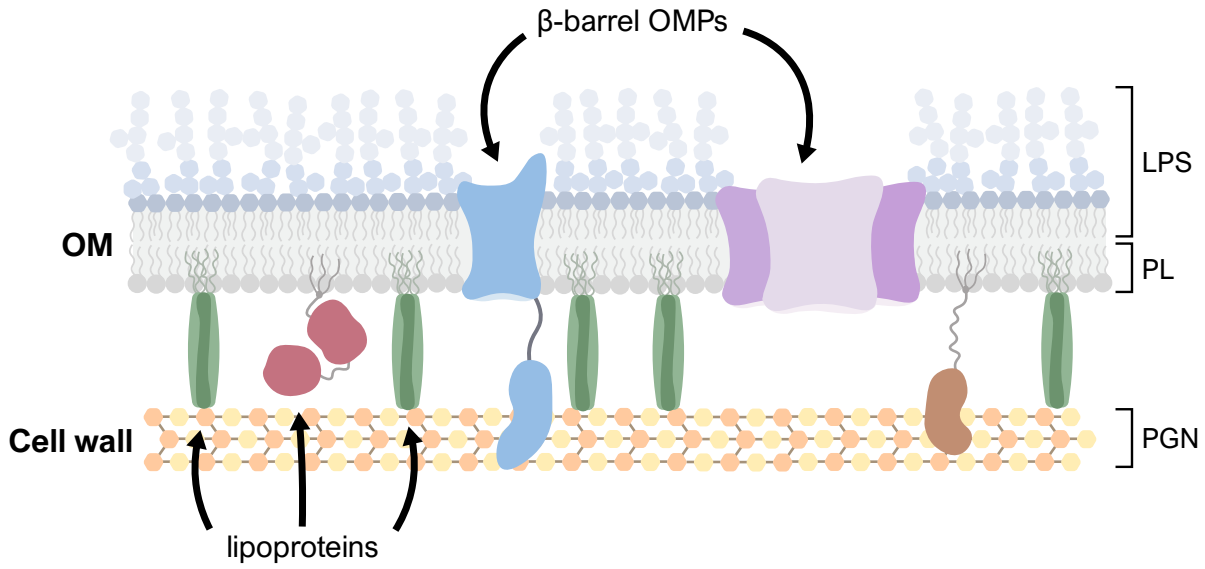

Figure 1-3. The outer membrane of Gram-negative bacteria.

The outer membrane is populated by a diverse set of proteins, lipids and carbohydrates. Abbreviations: OM (outer membrane), OMPs (outer membrane proteins) LPS (lipopolysaccharide), PL (phospholipid), PGN (peptidoglycan).

The outer membrane is the characteristic feature of Gram-negative bacteria (Figure 1-3). This layer acts as a selective permeability barrier that prevents the direct entry of most large and hydrophilic molecules and the efficient entry of many larger hydrophobic compounds (Maher and Hassan, 2023; Nikaido, 2003; Vaara, 1993). LPS is the main contributor to the decreased permeability of the Gram-negative envelope (Nikaido, 2003) and resides in the outer leaflet of the outer membrane. The inner (or periplasmic) leaflet of the outer membrane consists of phospholipids, predominantly PE (Bogdanov et al., 2020). The selectivity of the outer membrane is directly related to its structure; tightly packed LPS itself functions as an effective permeability barrier, and several porins form channels that allow for the facilitated diffusion of water and other

small molecules (Nikaido, 2003). Transport of larger molecules such as siderophores and vitamins is accomplished through several energized transporter complexes (Noinaj et al., 2010).

Recent work has shown that the outer membrane separates into “islands” rich in OMPs or LPS (Benn et al., 2021), highlighting its highly coordinated structure (Lithgow et al., 2023). LPS-PL asymmetry is strictly maintained by Gram-negative bacteria (Giacometti et al., 2022; Powers and Trent, 2019; Yeow and Chng, 2022), and its disruption occurs during envelope stress and greatly increases the susceptibility of Gram-negatives to antibiotics (Mikheyeva et al., 2023; Sutterlin et al., 2016; Vaara, 1993). While the outer membrane contains LPS in most characterized Gram-negatives, “simple” diderms without LPS (Thompson et al., 1982) and diderm-like organisms with distinct OM composition (such as the mycomembrane of *Mycobacteria* spp.) exist (Chiaradia et al., 2017), pointing to the diverse ways bacteria take advantage of a dual membrane envelope.

Furthermore, recent work challenges the paradigm that the cell wall is solely responsible for cell shape and stiffness, reporting a key role for the outer membrane in maintaining cell shape and resisting mechanical stress (Hummels et al., 2023; Mathelié-Guinlet et al., 2020; Rojas et al., 2018; Sun et al., 2022). Increases in alternative peptidoglycan crosslinks by the L,D-transpeptidase LdtD can compensate for defects in LPS biogenesis, pointing to an overlap in the mechanical function of these two layers (Bernal-Cabas et al., 2015; Delhaye et al., 2016; Morè et al., 2019). Outer membrane proteins also play a key role in stabilizing the envelope, particularly by forming links with the cell wall. In most Gram-negative bacteria, there are three proteins (OmpA, Lpp, and Pal) that form links between the cell wall and the outer membrane. Two of these proteins, the β-barrel transmembrane protein OmpA and the outer membrane lipoprotein Pal, form non-covalent interactions with peptidoglycan (Bouveret et al., 1999; Cascales et al., 2002; Park et al., 2017; Samsudin et al., 2017). OmpA is one of the most abundant OMPs in the

outer membrane and plays key roles in virulence and the surface properties of several Gram-negative species (Confer and Ayalew, 2013; Liao et al., 2022). Structurally, OmpA divides into an N-terminal outer membrane integral 8-stranded β-barrel and a C-terminal globular peptidoglycan binding domain (Marcoux et al., 2014). This cell wall binding fold is shared with the lipoprotein Pal, which coordinates the outer membrane and cell wall during division (Szczepaniak et al., 2020) and facilitates outer membrane lipid homeostasis (Shrivastava et al., 2017; Tan and Chng, 2024).

Lpp, also known as Braun's lipoprotein after its discoverer, forms the main covalent outer membrane-cell wall linkage and is also the most abundant envelope protein in *E. coli* (Braun and Rehn, 1969). Lpp controls two important aspects of envelope integrity: maintaining the outer membrane-cell wall linkage and the width of the periplasm itself (Asmar et al., 2017; Mandela et al., n.d.; Mathelié-Guinlet et al., 2020; Rojas et al., 2018). Strikingly, the need to maintain outer membrane-cell wall links is evolutionarily conserved, even if the proteins involved are not. Diderm Firmicutes possess no Pal or Lpp but instead express OmpM, a dual domain, trimeric protein that, in a fashion combining characteristics of OmpA and Lpp, inserts into the outer membrane and covalently links to peptidoglycan (Kalmokoff et al., 2009; Kojima et al., 2010; Silale et al., 2023; von Kügelgen et al., 2022; Witwinowski et al., 2022).

Lipopolysaccharide and phospholipids

LPS is a molecule unique to Gram-negative bacteria. It is essential in most species, although there are species that survive in its absence (Moffatt et al., 2010). Each LPS molecule consists of a lipid A molecule covalently attached to two regions of oligosaccharides: the core oligosaccharide and O-antigen (Bertani and Ruiz, 2018; Raetz and Whitfield, 2002). Gram-negative bacteria, however, possess significant diversity in the sugar composition of LPS (Silipo and Molinaro, 2010). The O-antigen is the outermost and most variable region of LPS (Bertani

and Ruiz, 2018; Samuel and Reeves, 2003; Whitfield et al., 2020). In just *E. coli* there are at least 170 O-antigen structures (Liu et al., 2019), this diversity being an important mechanism of antigenic variation and host immune evasion (Duerr et al., 2009).

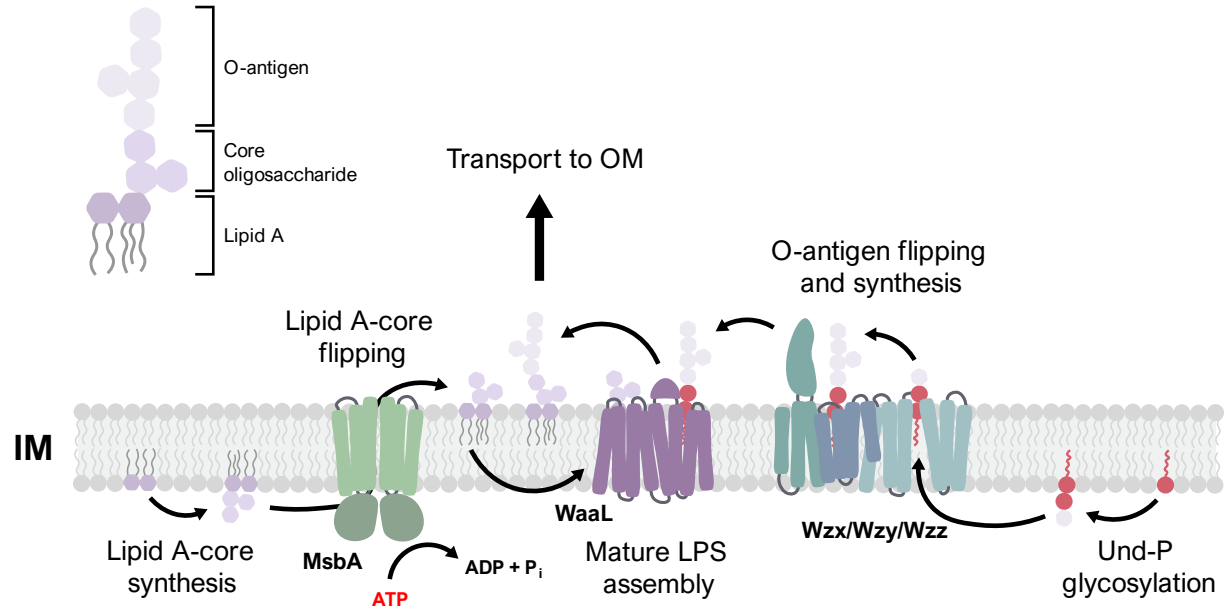

Figure 1-4. Summary of LPS biosynthesis.

The synthesis of LPS requires independent synthesis of two components (lipid A-core and O-antigen) that are combined to form mature LPS. The Wzx/Wzy/Wzz is shown as an example pathway of O-antigen synthesis. A simplified representation of the structure of LPS is shown in the top left corner.

Biosynthesis of LPS begins in the cytoplasm with the synthesis of the lipid A-core oligosaccharide molecule and the O-antigen separately (Figure 1-4). Briefly, acyl groups and sugars are added to form lipid A-core through the Raetz pathway (Bertani and Ruiz, 2018; Dowhan, 2011; Raetz and Whitfield, 2002), which is then flipped across the inner membrane by MsbA (Mi et al., 2017; Voss and Trent, 2018; Zhou et al., 1998). O-antigen is synthesized through the addition of sugars to Und-P through various pathways, such as the Wzz/Wzx/Wzy pathway,

which flips and synthesizes nascent O-antigen (Bertani and Ruiz, 2018; Islam and Lam, 2014; Whitfield et al., 2020). The final synthesis of mature LPS occurs at the periplasmic leaflet of the inner membrane through the transfer of O-antigen to lipid A-core by the ligase WaaL (Raetz and Whitfield, 2002).

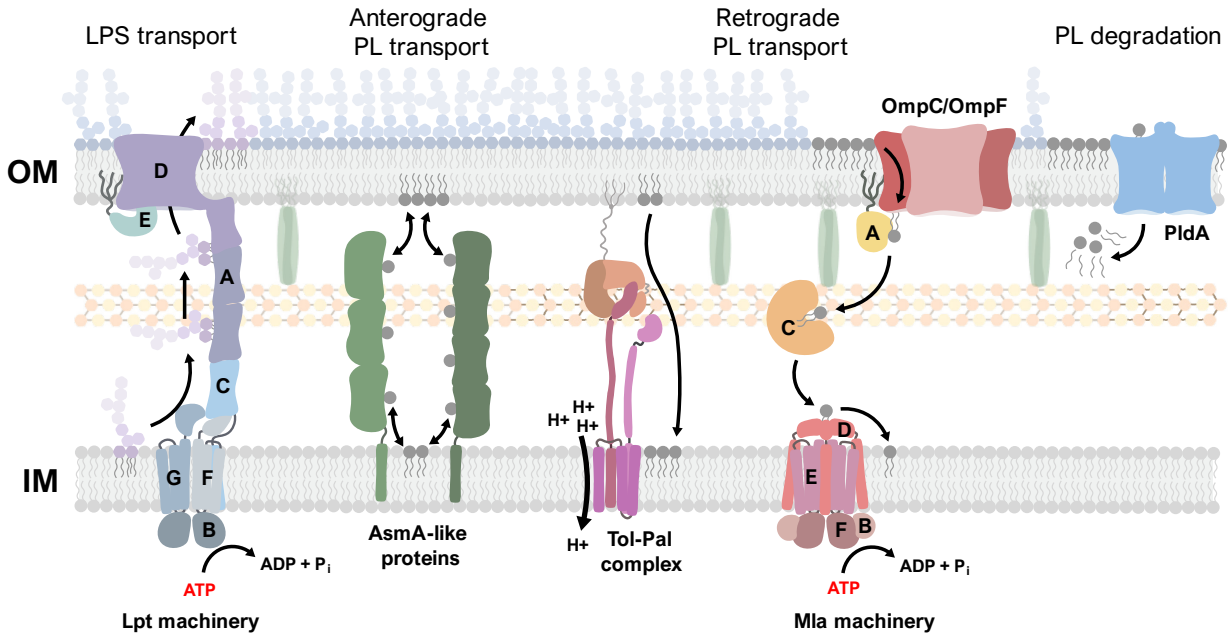

Figure 1-5. Phospholipid and lipopolysaccharide transport and homeostasis.

The asymmetry of the outer membrane, where LPS constitutes the outer leaflet and PLs the inner leaflet, is maintained through pathways that transport LPS to the outer membrane (the Lpt machinery, leftmost part of figure) and PLs between the inner and outer membranes.

The transport of PLs and LPS through the aqueous periplasm is challenging because of their hydrophobicity. Several transport pathways transport these molecules to and from the inner and outer membranes (Figure 1-5). Mature LPS is transported to the outer membrane through the Lpt pathway (Okuda et al., 2016). Periplasmic leaflet LPS is taken up by the $LptB_2FG$ ABC transporter. (Dong et al., 2017; Okuda et al., 2012; Tang et al., 2019). LPS is then transported through the hydrophobic cavity of the β-jellyroll fold found in LptC and LptA, which

shields it from the aqueous periplasm (Okuda et al., 2012; Schultz et al., 2017; Suits et al., 2008; Tran et al., 2010). LptA forms an oligomeric, envelope-spanning bridge, facilitating the direct movemnt of LPS from the inner to outer membrane (Chng et al., 2010; Freinkman et al., 2012; Okuda et al., 2016). The LPS transport is completed by a complex of the large β-barrel OMP LptD and the outer membrane lipoprotein LptE (Chimalakonda et al., 2011; Dong et al., 2014; Freinkman et al., 2011; Malojčić et al., 2014; Qiao et al., 2014). Recent work has also identified LptM (formerly YifL), a small lipoprotein that binds LptD and LptE to stabilize its structure by facilitating oxidative folding of LptD by mimicking the binding of LPS (Yang et al., 2023).

PLs undergo both anterograde (i.e. to the outer membrane) and retrograde (i.e. from the outer membrane) transport depending on the LPS-PL balance in the outer membrane (Kumar and Ruiz, 2023; Shrivastava and Chng, 2019; Yeow and Chng, 2022). Degradation of outer leaflet PLs is accomplished by the outer membrane phospholipase PldA (Bishop, 2008; Malinverni and Silhavy, 2009; Snijder et al., 1999). The acyl chains produced from PL degradation can then enter the cytoplasm to regulate the production of LPS through the regulatory enzyme LpxC (May and Silhavy, 2018). Retrograde transport of phospholipids is mostly accomplished by the Mla-OmpC system (Abellón-Ruiz et al., 2017; Chi et al., 2020; Coudray et al., 2020; Hughes et al., 2019, 2019; Malinverni and Silhavy, 2009; Yeow et al., 2023). Briefly, outer leaflet PLs are transported through a complex of the lipoprotein MlaA and the porin OmpC. PLs are then transferred to a soluble periplasmic chaperone, MlaC, which hands off PLs to an inner membrane complex of MlaFEDB (Isom et al., 2017). ATP hydrolysis then drives the transfer of PLs to the inner membrane (Low et al., 2021; Powers et al., 2020; Tang et al., 2021). Retrograde transport of PLs may also involve the Tol-Pal complex through a yet to be characterized mechanism (Shrivastava et al., 2017; Tan and Chng, 2024).

While evidence is still emerging, anterograde PL transport appears to be accomplished by the functionally redundant proteins in the AsmA superfamily (Kumar and Ruiz, 2023). AsmA-like proteins are predicted to possess a single transmembrane α-helix connected to a large periplasmic domain big enough to span the periplasm that possess a hydrophobic groove, forming a structure analogous to the transenvelope LPS bridge formed by Lpt proteins (Kumar and Ruiz, 2023). So far, three AsmA-like proteins, YhdP, TamB, and YdbH have been implicated in PL transport to the outer membrane (Douglass et al., 2022; Grimm et al., 2020; Ruiz et al., 2021), although other AsmA-like proteins exist whose functions have yet to be characterized (Kumar and Ruiz, 2023). Interestingly, many AsmA-like proteins were initially identified in relation to other components of the outer membrane, highlighting how connected OMP, LPS, and PL biogenesis are; AsmA was identified as a suppressor of OMP folding defects and decreases in LPS (Deng and Misra, 1996; Misra and Miao, 1995), and TamB was implicated in OMP assembly (Heinz et al., 2015; Stubenrauch et al., 2016).

Envelope proteins

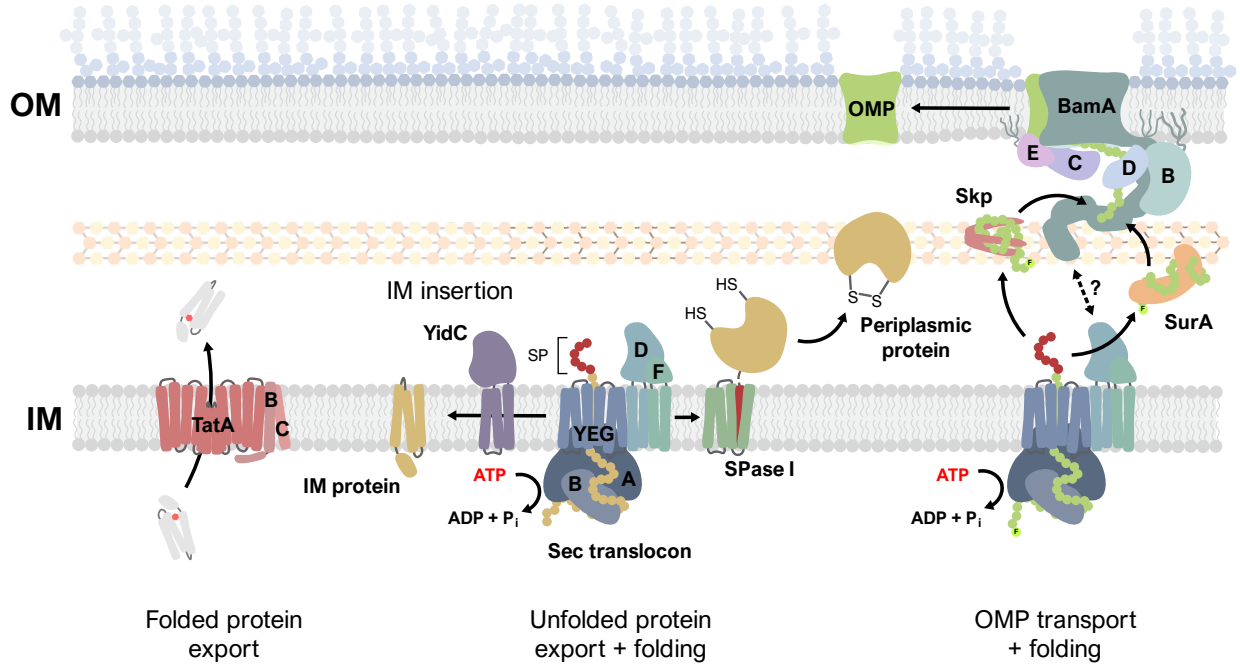

Figure 1-6. Protein secretion and assembly in the envelope.

Proteins are secreted folded or unfolded through the envelope through the Tat or Sec pathways, respectively. OMPs are inserted in the outer membrane by the BAM complex BamABCDE). The signal peptide of secreted proteins is highlighted in red (SP), and the C-terminal β-signal of OMPs is shown with a different shade of green and labelled with an F (for phenylalanine).

Most outer membrane proteins fall into two classes: membrane-integral β-barrel proteins and membrane-peripheral lipoproteins (Silhavy et al., 2010) (although membrane integral lipoproteins do exist (Dong et al., 2006; Epstein et al., 2009; Janssens et al., 2024)). Outer membrane β-barrel proteins (more generally referred to as OMPs) are characterized by a barrel-like structure composed of antiparallel β-strands (Fairman et al., 2011; Hermansen et al., 2022). OMPs often function as channels, including the abundant Enterobacterial porins OmpF and OmpC, which allow for the diffusion of hydrophilic molecules into the cell (Vergalli et al., 2020). In general, the barrel structure of OMPs allows them to accommodate a wide variety of

molecules in their lumen. For example, relatively large TonB-dependent transporters facilitate transport of larger molecules such as siderophores (e.g. the ferric enterobactin receptor FepA; (Buchanan et al., 1999)) or vitamins (e.g. the B12 receptor BtuB; (Chimento et al., 2003)). OMPs such as autotransporter proteins facilitate the movement of cargo out of cells (Leyton et al., 2012), and the central machinery for OMP and LPS insertion are both themselves β-barrel proteins (Dong et al., 2014; Leyton et al., 2015). OMPs also function as enzymes with various functions (Bishop, 2008; Hwang et al., 2002; Snijder et al., 2001; Vandeputte-Rutten et al., 2001), and facilitate virulence, for example, by promoting adhesion to host cells (Vogt and Schulz, 1999; Yamashita et al., 2011).

Envelope proteins are secreted through the inner membrane and either remain there, are released into the periplasm, or are transported to the outer membrane (Figure 1-6). Protein secretion through the inner membrane can occur while proteins are folded or unfolded. Secretion of folded proteins occurs with a relatively small subset of envelope proteins through the twin arginine translocation (Tat) pathway, named as such because of a twin arginine motif in their signal sequences (Frain et al., 2019; Palmer and Berks, 2012). In *E. coli*, the Tat pathway consists of three proteins, TatA, TatB, and TatC. The mechanism of translocation is not yet clear, with both membrane pore and membrane destabilization models proposed (Brüser and Sanders, 2003; Gohlke et al., 2005). The translocation of folded proteins across the inner membrane presents several advantages, for example, allowing cofactors to be incorporated into proteins in the cytoplasm rather than requiring additional mechanisms to transport and add them to proteins in the periplasm (Palmer and Berks, 2012).

Most proteins are secreted through the universally conserved, general secretory (Sec) pathway (Mori and Ito, 2001; Natale et al., 2008). Here, proteins are kept unfolded as they cross the inner membrane, after which they can be integrated into the inner membrane, released into

the periplasm, or be targeted to the outer membrane for final assembly. Protein export by the Sec translocon occurs either co-translationally or post-translationally. All translocated proteins possess an N-terminal signal peptide that is recognized by components of the Sec translocon (von Heijne, 1990). Co-translational translocation, typically used by proteins that are inserted into the inner membrane, is facilitated by the binding of the signal peptide of the nascent protein by the signal recognition particle (SRP) protein and subsequent formation of a complex between the Sec translocon and the ribosome, allowing for the secretion of the unfolded peptide as translation occurs (Hwang Fu et al., 2017). Post-translational secretion is facilitated by the chaperone SecB, which keeps proteins unfolded while targeting them to the ATPase SecA, which drives the active translocation of proteins through the Sec translocon (Hartl et al., 1990). In either case, translocation occurs through the SecYEG protein complex, forming the pore through which unfolded proteins are exported (Oswald et al., 2021). Translocation is powered by ATP hydrolysis but is also supported by harnessing the PMF through SecD and SecF (Tsukazaki et al., 2011). Insertion into the inner membrane is facilitated by the protein YidC (Kumazaki et al., 2014; Tsukazaki, 2019). For proteins that are targeted for the periplasm or outer membrane, the signal peptide is cleaved by signal peptidase I (SPase I) (Auclair et al., 2012).

Several systems ensure proper protein folding in the envelope (Miot and Betton, 2004). The proteins of the Dsb system promote the proper formation of disulfide bonds (Ito and Inaba, 2008); electrons are transferred to DsbA during the oxidation of cysteines on target proteins to create disulfide bonds. Electrons are then transferred to DsbB and the membrane quinone pool. Disulfide bonds can be isomerized through DsbC and DsbD, and unwanted disulfide bonds are reduced by DsbG (Depuydt et al., 2009). Periplasmic peptidylprolyl-cis-trans-isomerases (PPIases) such as FkpA further facilitate the isomerization of peptide bonds and assist in folding (Saul et al., 2004; Ünal and Steinert, 2014). Finally, several chaperones facilitate periplasmic

protein folding and the transport of unfolded OMPs (uOMPs) to the β-barrel assembly machinery (BAM) (De Geyter et al., 2016). Skp is a periplasmic chaperone that assists in the folding of several periplasmic proteins but is mostly involved in transporting unfolded OMPs to the outer membrane (Schiffrin et al., 2016). SurA appears to be the main chaperone involved in uOMP transport (Marx et al., 2020). DegP may possess both uOMP chaperone activity and protease activity (to degrade misfolded proteins), but recent studies indicate that the main role of DegP is as a protease under stress conditions (Chang, 2016). Several envelope stress responses also maintain protein folding integrity under stress (Mitchell and Silhavy, 2019).

uOMPs are delivered to the BAM complex, which is composed of a large β-barrel protein BamA and four associated lipoproteins, BamB, BamC, BamD, and BamE (Knowles et al., 2009; Konovalova et al., 2017). Of these, only BamA and BamD are essential, although the entire complex is required for full activity. The central component of the BAM complex is BamA, which comprises a large membrane-integral β-barrel protein attached to 5 polypeptide transport-associated (POTRA) domains (Albrecht et al., 2014). BamA is a highly dynamic protein (Doerner and Sousa, 2017; Doyle et al., 2022; Doyle and Bernstein, 2019). OMP folding appears to involve a BamA “gate” that allows for lateral movement of proteins and local distortions of the membrane (Konovalova et al., 2017). Several models have been proposed for BamA function. The two most prominent are the budding and assisted models, the former involving the formation of a temporary hybrid OMP-BamA that “buds” into the outer membrane, whereas the BamA-assisted model posits that BamA functions more as a chaperone-like protein. The essential lipoprotein BamD recognizes substrates for the BAM machinery (Hagan et al., 2015). uOMPs are targeted to the Bam complex via a C-terminal β-signal present on the uOMP itself. The other lipoproteins, while not essential, play various roles in ensuring efficient assembly of

OMPs and are often essential in combination with each other or other proteins involved in envelope biogenesis (Konovalova et al., 2017).

Lipoproteins

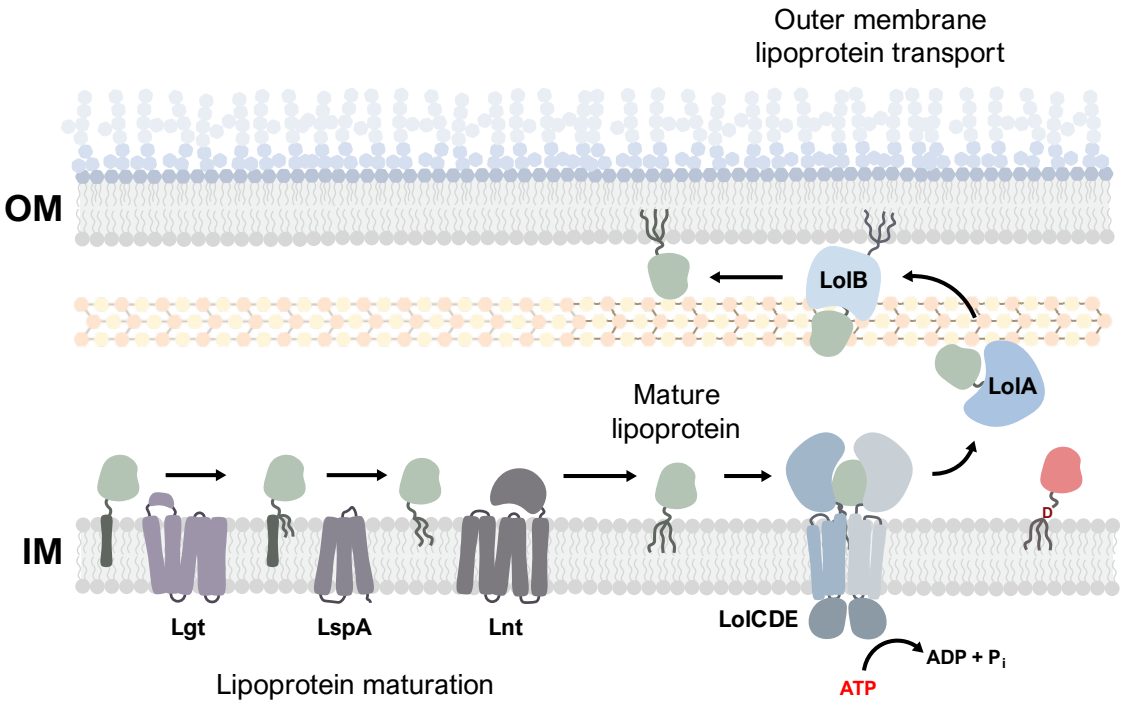

Figure 1-7. Lipoprotein maturation and transport in the envelope.

Lipoprotein biogenesis occurs through acylation of proteins through the inner membrane by Lgt, LspA, and Lnt. Outer membrane lipoproteins are then transported via the Lol pathway. An inner membrane lipoprotein with a Lol-avoidance signal is shown in red at the right side of the figure.

Lipoproteins possess a triacylated N-terminal cysteine residue that anchors them to either the inner or outer membranes (Narita and Tokuda, 2017). Lipoproteins play important roles in biogenesis, stress response, transport/metabolism, virulence, and structure (Braun and Hantke, 2019). Lipoproteins are mostly secreted through the Sec translocon, although Tat-secreted lipoproteins exist (Narita and Tokuda, 2017; Zückert, 2014). Immature lipoproteins are initially anchored to the inner membrane by their signal peptides. The C-terminus of the

lipoprotein's signal peptide contains a 4 amino acid lipobox which differentiates them from other envelope proteins (Zückert, 2014). The key residue in the lipobox is a universally conserved cysteine, which is the site of acylation. Lipoprotein maturation involves three enzymes (Figure 1-7). First, the preprolipoprotein diacylglyceryl transferase (Lgt) catalyzes a thioester linkage between (mostly) phosphotidylglycerol and the thiol group of the N-terminal cysteine (Sankaran and Wu, 1994). The signal peptide is then cleaved between the cysteine and the residue preceding it by the lipoprotein-specific signal peptidase LspA (or signal peptidase II) (Tokunaga et al., 1982). A third and final acyl chain is added by the *N*-acyl transferase Lnt at the amino group created by signal peptide cleavage (Jackowski and Rock, 1986).

For inner membrane lipoproteins, this final acylation is the terminal step. Outer membrane lipoproteins are trafficked to the outer membrane by the localization of lipoprotein (Lol) pathway (Grabowicz, 2019). A "Lol-avoidance" signal, which in *E. coli* consists of an aspartic acid at the +2 position (i.e. the residue immediately following the lipidated cysteine), ensures that inner membrane lipoproteins are not trafficked to the outer membrane (Hara et al., 2003). Recent work also suggests that outer membrane trafficking of lipoproteins depends on the presence of an almost universal, intrinsically disordered linker region at the N-terminus of the mature lipoprotein (El Rayes et al., 2021). Outer membrane lipoproteins are taken up by the LolCDE ABC transporter, primarily by interacting with LolE (Mizutani et al., 2013). The periplasmic chaperone LolA is recruited to and receives the lipoprotein from LolCDE (Kaplan et al., 2018; Lehman et al., 2024). As is the case with the hydrophobic moieties of LPS and PLs, the hydrophobic acyl modification of lipoproteins presents a challenge for transport. This acylated moiety is hidden with the hydrophobic cavity of LolA in a manner analogous to LPS transport by LptA (Takeda et al., 2003). However, unlike LptA, LolA does not form a continuous bridge from the inner to outer membrane to transport lipoproteins, but rather transports them as a soluble

chaperone through the periplasm. In this way, LolA functions more analogously to MlaC in PL transport (although in the opposite direction) (Shrivastava and Chng, 2019). After transit through the periplasm, lipoproteins are handed off to LolB, which is itself a lipoprotein and shares a similar lipoprotein binding fold as LolA (Takeda et al., 2003). While the mechanisms remain to be fully understood, LolB mediates the final insertion of lipoproteins to the outer membrane (Tsukahara et al., 2009).

Recent work underscores the complexity of outer membrane lipoprotein biogenesis. In *E. coli,* lipoproteins can get trafficked to the outer membrane in the absence of LolA or LolB, suggesting that Lol-independent pathways for trafficking of lipoproteins may exist (Grabowicz and Silhavy, 2017a). Several Gram-negative species lack homologues of LolB altogether (Okuda and Tokuda, 2011). Furthermore, many lipoproteins are exposed on the surface of cells (Konovalova and Silhavy, 2015). In some organisms, such as the spirochetes of *Borrelia*, most lipoproteins are surface exposed (Schulze and Zückert, 2006). Recent work has uncovered an outer membrane machine known as Slam specific for surface lipoproteins (SLPs) in *Neisseria* spp. (Hooda et al., 2017b, 2017a, 2016; Huynh et al., 2022). However, there is evidence for the surface exposure of lipoproteins even in lab strains of *E. coli* which do not possess Slam. One prominent example is RcsF, the stress sensor of the Rcs phosphorelay, which can become surface exposed in through the lumen of OMPs (Konovalova et al., 2016). Very novel (and not peer reviewed) evidence suggests the intriguing possibility that LptD or LptD-like proteins may receive at least a subset of lipoproteins as substrates and facilitate their surface exposure, although more work is required to verify this mechanism (He et al., 2022; Luo et al., 2022).

Envelope biogenesis as an interconnected system

No aspect of envelope biogenesis is truly independent of any other. This is well illustrated by recent advances in our understanding of OMP biogenesis. The BAM complex itself contains

four lipoproteins that mature at the inner membrane and are trafficked to the outer membrane by the Lol pathway (Narita and Tokuda, 2017). Recent evidence suggests that the Sec translocon and the BAM machinery come together to form a "super-complex" via interactions between SecDF and YidC at the inner membrane and almost all components of the BAM complex (Alvira et al., 2020). This finding suggests that uOMP transport may be analogous to LPS transport through the periplasm. Interestingly, Alvira, Watkins, and colleagues (2020) report that the lipid cardiolipid is required for complex formation, pointing to a regulatory role for lipids in OMP folding. Further evidence for the role of lipids in OMP folding comes from recent work reporting that the distribution of charge across asymmetric membranes controls OMP folding (Machin et al., 2023). Finally, recent work reports that BAM activity is synchronized to peptidoglycan maturation, making it clear that OMP biogenesis is intrinsically linked to the cell wall (Mamou et al., 2022).

Protecting the envelope

Several envelope stress responses (ESRs) monitor and maintain the integrity of the envelope. While each system tends to respond to a subset of different stressors, overlaps in the signals sensed and the regulons of these systems make it clear that protecting the envelope is accomplished by a network of cooperating systems (Grabowicz and Silhavy, 2017b). There are five stress responses that are traditionally considered to constitute the envelope stress response of Gram-negative bacteria, mostly based on studies in *E. coli* (Mitchell and Silhavy, 2019): the σ^E, Cpx, Rcs, Psp, and Bae systems (Figure 1-8).

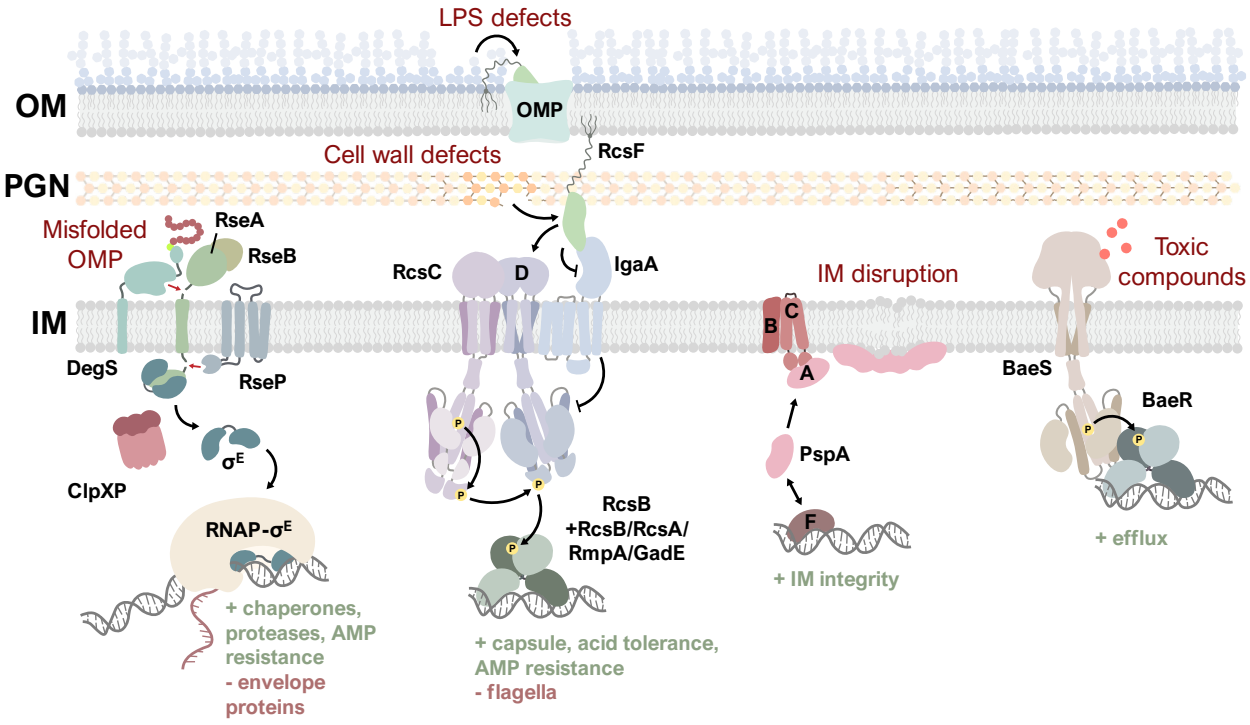

Figure 1-8. The classical envelope stress responses of Gram-negative bacteria.

From left to right: the σ^E response, Rcs phosphorelay, Psp response, Bae response. The Cpx response is not shown but will be elaborated on later. Processes shown in green (+) indicate those generally upregulated by these systems and those in red (-) are generally repressed.

The σ^E response

Sigma factor E (σ^E or σ^{24}) is an extracytoplasmic function (ECF) sigma factor that responds to unfolded OMPs in the periplasm (Ades et al., 1999; Hayden and Ades, 2008). Unfolded OMPs can result from several different stressors including OMP overexpression, LPS defects, heat, or mutations in proteins involved in folding OMPs (Brooks and Buchanan, 2008). As an alternative sigma factor, σ^E binds RNA polymerase to initiate the transcription of genes involved in the envelope stress response. The activity of σ^E is controlled by regulated intramembrane proteolysis (RIP) (Ades, 2008; Heinrich and Wiegert, 2009). σ^E, in the absence of envelope stress, is inhibited by the anti-sigma factor RseA, a membrane spanning protein that

binds σ^E in the cytoplasm (Campbell et al., 2003). A peptide containing the C-terminal OMP β-signal binds and activates the inner membrane protease DegS, which cleaves the periplasmic, C-terminal region of RseA, triggering further proteolysis by the inner membrane protease RseP (Ades, 2008; Walsh et al., 2003). The periplasmic protein RseB appears to increase the stability of RseA against DegS proteolysis (Cezairliyan and Sauer, 2007). Finally, the cytoplasmic region of RseA, which ultimately binds and sequesters σ^E, is degraded by the cytoplasmic protease ClpXP, releasing σ^E to bind RNAP and activate transcription of its regulon (Flynn et al., 2003).

When induced, the primary function of the σ^E response is to downregulate the expression of several OMPs and lipoproteins and promote the expression of envelope proteases and chaperones (Alba and Gross, 2004; Grabowicz and Silhavy, 2017b; Rhodius et al., 2005). Envelope protein folding factors and proteases include Skp, FkpA, and DegP, showing some overlap with factors also regulated by the Cpx envelope stress response (Danese and Silhavy, 1997; Pogliano et al., 1997). Proteins of the BAM complex are also themselves regulated by σ^E (Onufryk et al., 2005; Wu et al., 2005). OMPs and lipoprotein expression appears to be regulated by σ^E through several small RNAs (sRNAs). sRNAs MicA and RybB repress OMP expression (Gogol et al., 2011), and MicL represses expression of the abundant Lpp lipoprotein (Guo et al., 2014). The combined result of these efforts is a coherent response to envelope protein misfolding by downregulating expression of potential stress-causing proteins along with increasing expression of protein quality control factors.

The Rcs phosphorelay

The Rcs phosphorelay is a complex signal cascade, identified originally as a **r**egulator of colanic acid **c**apsule **s**ynthesis (Majdalani and Gottesman, 2005; Wall et al., 2018). Unlike a typical two-component system, which consists of a sensor kinase and its cognate response regulator, the Rcs system is a phosphorelay where a phosphate group is transferred through

several proteins before reaching a cytoplasmic response regulator. Briefly, the membrane bound sensor kinase RcsC autophosphorylates and transfers a phosphate group to a membrane bound phosphotransferase protein RcsD before final phosphorylation of the response regulator RcsB (Sato et al., 2017). Sensory signal transduction in the Rcs system is regulated by two envelope proteins: IgaA and RcsF. The inner membrane protein IgaA represses the response by inhibiting RcsD (Domínguez-Bernal et al., 2004; Wall et al., 2020). The outer membrane lipoprotein RcsF relieves this repression by IgaA in the presence of inducing cues, thus serving as the primary activator of the Rcs phosphorelay (Castanié-Cornet et al., 2006; Majdalani et al., 2005). Importantly, RcsF appears to sense most known inducing signals of the system, including LPS and peptidoglycan defects (Callewaert et al., 2009; Laubacher and Ades, 2008; Majdalani et al., 2005), and exposure to antimicrobial peptides (Farris et al., 2010).

A unique feature of the Rcs system is that RcsB can form dimers with several cytoplasmic proteins, each combination allowing for the regulation of a different set of genes (Wall et al., 2018). An RcsB-RcsB homodimer appears to regulate links between the Rcs response and σ^S, which is responsible for the general stress response (Majdalani et al., 2002). A heterodimer of RcsB-GadE helps mediate acid resistance (Krin et al., 2010). The RcsB-RcsA/RmpA heterodimer regulates the titular function of the Rcs response in capsule synthesis and downregulates flagellar motility (Francez-Charlot et al., 2003; Wall et al., 2018). RcsB-RcsA also helps regulate the expression of *ugd*, encoding the UDP-glucose dehydrogenase, important for lipid A modification and resistance to antimicrobial peptides such as polymyxin B (Mouslim and Groisman, 2003).

The Psp response

The **p**hage **s**hock **p**rotein (Psp) response was named after its initial characterization during filamentous phage infection (Joly et al., 2010; Mukhopadhyay and Kumar, 2023). Multiple

stressors at the inner membrane activate the Psp response (Flores-Kim and Darwin, 2016). These signals include treatment with PMF-dissipating agents and overexpression of outer membrane secretins (Flores-Kim and Darwin, 2016; Seo et al., 2007). Another possible inducing signal is higher levels of stress due to the curvature of the membrane itself (so called stored curvature elastic or SCE stress) (McDonald et al., 2015). While the precise molecular cue sensed by the Psp system is unclear, all inducing signals appear to influence/destabilize the inner membrane. Sensing and signal transduction in the Psp system is also unique from other envelope stress responses. Transcriptional changes due to Psp induction occurs through the action of PspF, a DNA-binding enhancer protein, which is normally inhibited by binding to PspA (Jovanovic et al., 2010). PspB and PspC (at least in *E. coli*) form an inner membrane complex that senses envelope stress and titrates PspA away from PspF (Flores-Kim and Darwin, 2016; Weiner et al., 1995). PspA plays both signaling and stress combative roles in the system, negatively regulating PspF and oligomerizing to protect the inner membrane, particularly by maintaining the proton motive force (Kobayashi et al., 2007). Indeed, the main regulatory consequence of Psp activation is induction of the *psp* operon itself, pointing to a highly self-contained system that both senses and ameliorates specific stressors to the inner membrane (Flores-Kim and Darwin, 2016).

The BaeRS system

The BaeRS two-component system was initially identified as the second regulatory system controlling expression of the periplasmic chaperone Spy (the other system being the CpxRA system) (Raffa and Raivio, 2002). The Bae response appears to sense various envelope-disturbing compounds such as zinc, ethanol, and indole through its sensor kinase BaeS (Bury-Moné et al., 2009; Lee et al., 2005; Raffa and Raivio, 2002). The main regulatory targets of the response regulator BaeR appear to be efflux pumps such as MdtABC and AcrD (Hirakawa et al.,

2004; Nagakubo et al., 2002). A recent study has also shown that the Bae system protects *E. coli* against a peptidoglycan-degrading type VI secretion system effector TseH, with at least some of the protection afforded by the periplasmic chaperone protein Spy (Hersch et al., 2020). However, as a whole, the precise niche of the BaeRS system remains far less comprehensively characterized compared to other regulatory systems given its overlap with other systems such as CpxRA, PhoBR, and CreAB (Nishino et al., 2005; Raffa and Raivio, 2002).

The CpxRA system

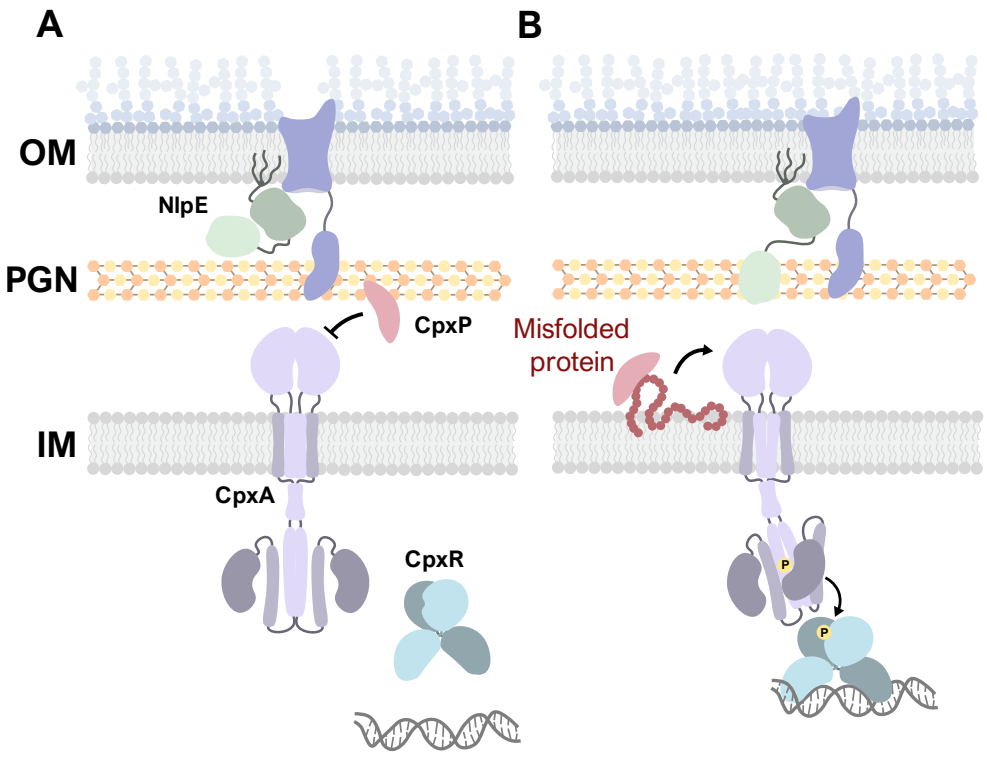

Figure 1-9. The Cpx envelope stress response.

The Cpx two-component system is a sensory system that consists of the sensor kinase CpxA and response regulator CpxR as well as accessory signaling proteins NlpE and CpxP. The Cpx response and its components are shown in their **(A)** basal and **(B)** induced state.

The Cpx envelope stress response is a two-component system comprising the sensor kinase CpxA and the response regulator CpxR (Figure 1-9) (Vogt and Raivio, 2012). Characterization of the Cpx response began with the isolation, mapping, and phenotypic analysis of several mutations. The name, Cpx, comes from early studies investigating two mutants (*cpxA* and *cpxB*) with defects in **c**onjugative **p**ilus e**x**pression (McEwen and Silverman, 1980a, 1980b). Genetic analyses established that *cpxA* mutations mapped to a single gene and could be complemented by expression of *cpxA* from a plasmid (Albin and Silverman, 1984a, 1984b). Early studies pointed to possible defects in other envelope associated enzymes as well as alterations in envelope protein content, indicating the involvement of *cpxA* in envelope homeostasis (McEwen et al., 1983; McEwen and Silverman, 1980c, 1982; Sambucetti et al., 1982; Sutton et al., 1982). Early biochemical characterization gave us our first clues into CpxA's classification as a sensor kinase due to its similarity to the sensor kinase EnvZ and chemosensory transducers, the presence of potential hydrophobic regions, and its inner membrane localization (Albin et al., 1986; Weber and Silverman, 1988). CpxR was identified as an OmpR-like gene encoded 5' to *cpxA* and its cognate response regulator (Dong et al., 1993). Further analysis showed that three other mutations, *ecfB* (**e**nergy **c**oupling **f**actor B)*, eup* (**e**nergy-**u**ncoupled **p**henotype)*,* and *ssd* (**s**uccinate non-utilizing, high **s**erine **d**eaminase activity) all mapped to *cpxA* and thus tied their phenotypes together, which included resistance to aminoglycosides, tolerance to colicins, defects in nutrient uptake, and impaired growth on succinate (Rainwater and Silverman, 1990).

How these disparate phenotypes are influenced by the *cpxRA* locus would become clearer through later work characterizing CpxR and CpxA as a stress response that combats envelope protein misfolding. Three papers published in 1995 from the Silhavy lab established that:

a) Gain of function alleles of *cpxA* (*cpxA**) can suppress the toxicity of mutated envelope proteins (LamBA23D) or fusion proteins that get stuck in the Sec translocon (LamB-LacZ-PhoA) (Cosma et al., 1995a).
b) Induction of the Cpx response upregulates factors that combat envelope stress, such as the protease DegP, and suppresses lethality through the degradation of toxic envelope proteins (Cosma et al., 1995a; Danese et al., 1995).
c) Overexpression of the outer membrane lipoprotein NlpE activates CpxA and alleviates fusion protein toxicity (Snyder et al., 1995).

Later studies in the 1990s would build on these findings to contribute to our current understanding of the Cpx response. Many *cpxA** mutations were characterized as constitutively activated and signal blind and mapped to the putative periplasmic domain of CpxA, leading to the identification of this region as the main sensory region of CpxA (Raivio and Silhavy, 1997). *cpxP* was identified as a highly upregulated gene during Cpx induction, encoding for a periplasmic protein that helps alleviate stress due to toxic envelope fusion proteins and negatively regulates the activity of CpxA (Danese and Silhavy, 1998; Raivio et al., 1999), establishing CpxP and NlpE as auxiliary regulators of the Cpx response with opposing functions. The discovery of envelope biogenesis and stress genes that are regulated by both the σ^E and Cpx responses contributed to an emerging picture of envelope stress responses in Gram-negative bacteria (Connolly et al., 1997; Danese and Silhavy, 1997; Pogliano et al., 1997). It has also become clear that the Cpx response is important for pathogenesis and colonization of hosts, suggesting that envelope stress responses do not only combat stress, but also ensure adaptation to different environmental niches (T. H. S. Cho et al., 2023a; Hews et al., 2019; Lasaro et al., 2014; Raivio, 2005; Thomassin et al., 2015).

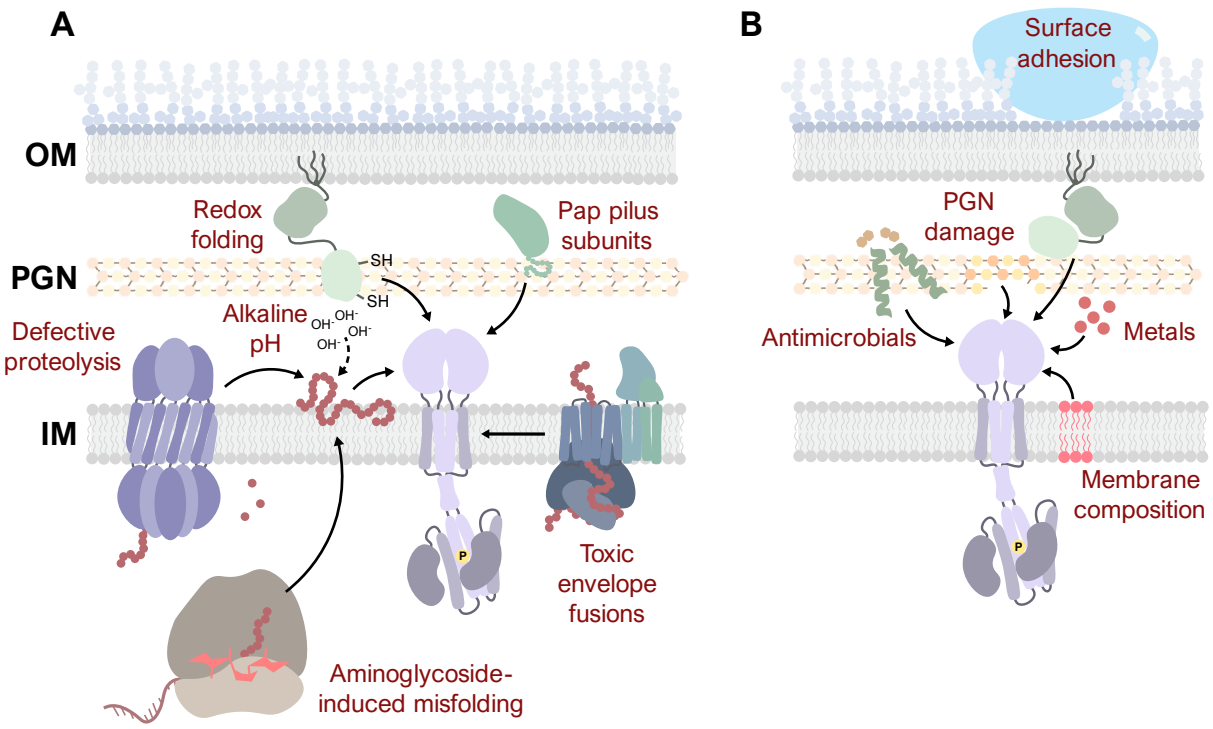

Figure 1-10. The Cpx response is induced in by a wide range of stimuli

(A) Many inducing signals of the Cpx response are related to misfolded protein in the envelope, particularly at the inner membrane. **(B)** However, the Cpx response also senses many signals not directly related to protein folding.

The Cpx response senses diverse inducing cues (Figure 1-10). These include alkaline pH (Danese and Silhavy, 1998), Pap pilus subunit overexpression (Jones, 1997), antimicrobial peptides and antibiotics (Audrain et al., 2013), and metals such as copper (Yamamoto and Ishihama, 2006). While the precise molecular cue sensed by CpxA is unknown, many Cpx inducing cues are thought to lead to protein misfolding at the inner membrane (Figure 1-10A) (Raivio, 2014). Heat shock and protein inclusion body formation can be resolved in a Cpx-dependent fashion (Hunke and Betton, 2003). The toxic proteins used in early Silhavy lab studies include LamB A23D, a processing deficient variant of the LamB OMP and the LamB-LacZ-PhoA tripartite fusion protein known to jam the Sec translocon (Cosma et al., 1995a;

Snyder and Silhavy, 1995). Induction of the Cpx response by Pap pilus subunit overexpression is due to the exposure of a specific C-terminal moiety present on the subunit itself, rather than general misfolding, suggesting that the Cpx response monitors the assembly of Pap pili (Hung, 2001; Jones, 1997; Lee et al., 2004). Part of the mechanism by which CpxA may become activated is titration of CpxP away from CpxA as it binds pilus subunits (Zhou et al., 2011). Accumulation of substrates of the inner membrane protease FtsH leads to activation of the Cpx response, suggesting that defective proteolysis of misfolded proteins is sensed by CpxA (Shimohata et al., 2002). Constitutively activated variants of CpxA are known to possess resistance to aminoglycoside antibiotics (Rainwater and Silverman, 1990), which inhibit translation and lead to the production of toxic, aberrant envelope proteins (Davis et al., 1986). Aminoglycoside antibiotics such as gentamicin are sensed by the Cpx response (Kashyap et al., 2011), and resistance to aminoglycosides may be mediated by Cpx-regulated protein YccA, a regulator of the FtsH protease (Kihara et al., 1995; van Stelten et al., 2009). The Cpx response also appears to use NlpE to sense periplasmic redox state, which is important for proper protein folding in the periplasm (Andrieu et al., 2023; Delhaye et al., 2016). Taken together, these studies establish envelope protein folding, particularly at the inner membrane, as a special area of concern for the Cpx response.

However, several other cues induce the Cpx response without being as directly tied to protein folding (Figure 1-10B). The outer membrane lipoprotein NlpE activates CpxA during adhesion to hydrophobic surfaces (Otto and Silhavy, 2002; Shimizu et al., 2016). The Cpx response is also induced in response to changes to the structure of phospholipid membranes and peptidoglycan. The Cpx response is activated in strains mutated in the genes responsible for PE synthesis, suggesting that the physical/chemical structure of membranes themselves is monitored by CpxA (Mileykovskaya and Dowhan, 1997). Accumulation of lipid II in the periplasm

also activates CpxA (Danese et al., 1998). Eliminating certain peptidoglycan synthases or transpeptidases induces the Cpx response, suggesting it also monitors the cell wall (Bernal-Cabas et al., 2015; Evans et al., 2013). Accordingly, the Cpx response is induced in the presence of antibiotics not known to cause protein folding stress, such as β-lactams (Masi et al., 2020). The Cpx response also senses other antimicrobials, including a wide range of antimicrobial peptides such as polymyxin B and melittin that cause a general disruption to the integrity of membranes (Audrain et al., 2013). Finally, metals such as copper and zinc are known inducers of the Cpx response (Yamamoto and Ishihama, 2005). Although the basis of activation remains unclear, recent and older evidence suggests that NlpE may sense metals (Gupta et al., 1995; May et al., 2019). Finally, the Cpx response is activated during growth in a CpxA-independent manner, suggesting that broader metabolic cues influence the activity of the system (De Wulf et al., 1999).

The Cpx regulon contains a set of genes that matches the diversity of its inducing cues (Price and Raivio, 2009; Raivio et al., 2013). In line with its induction by misfolded proteins, some of the most prominent members of the Cpx regulon are proteins involved in protein folding and degradation. DegP is a periplasmic protease that forms a multimeric complex (Šulskis et al., 2021). The inner membrane zinc-metalloprotease HtpX is also Cpx-regulated and appears to compensate for a loss in proteolysis by the major protease FtsH (Shimohata et al., 2002). The inner membrane protein YccA is a modulator of FtsH activity and appears to increase the stability of SecY during protein folding stress (van Stelten et al., 2009). Other proteins involved in protein folding are Cpx-regulated. The periplasmic chaperone Spy, which facilitates protein folding and prevents aggregation, is part of the Cpx regulon (Mitra et al., 2021; Price and Raivio, 2009). Notably, the oxidoreductase DsbA is Cpx regulated (Danese and Silhavy, 1997; Pogliano et al., 1997). A more novel mechanism of combating protein folding stress was recently

proposed; the sRNA CpxQ, encoded in the 3' untranslated region of the *cpxP* transcript, downregulates the expression of the periplasmic chaperone Skp to prevent it from folding OMPs aberrantly into the inner membrane (Grabowicz et al., 2016).

The Cpx response also directly regulates the expression of envelope protein complexes themselves, which is a mechanism for reducing potential sources of stress. For example, the Cpx response regulates the expression of proteins that form the electron transport chain. A microarray of transcripts enriched during Cpx induction found that genes encoding the proteins of the NADH dehydrogenase, succinate dehydrogenase, and cytochrome bo oxidase are downregulated by the Cpx response (Raivio et al., 2013). The Cpx response monitors and maintains the function of aerobic respiration, controlling the expression of the proteins in these complexes both transcriptionally and post-translationally (Guest et al., 2017; Tsviklist et al., 2022). The Cpx response also controls the synthesis of siderophores to ensure that iron is not aberrantly chelated from these respiratory proteins (Guest et al., 2019; Kunkle et al., 2017). Other large protein complexes are monitored and negatively regulated by the Cpx response, including Pap pili (Hung, 2001), type IV pili (Nevesinjac and Raivio, 2005; Vogt et al., 2010), flagella (De Wulf et al., 1999), and type III secretion systems (MacRitchie et al., 2012, 2008).

Several genes involved in cell wall modifications are upregulated by Cpx activation (Bernal-Cabas et al., 2015; Raivio et al., 2013). These include D-alanyl-D-alanine carboxypeptidase DacC (penicillin binding protein 6), L,D-transpeptidase LdtD, lytic transglycosylase Slt, and YgaU, a hypothetical protein with a LysM domain predicted to be involved in cell wall degradation (Buist et al., 2008). Activating the Cpx response increases diaminopimelic acid (DAP)-DAP crosslinks formed by LdtD, suggesting that Cpx activation directly modifies the structure of PGN (Bernal-Cabas et al., 2015). Deleting *cpxR* increases susceptibility to the β-lactam antibiotic mecillinam, but constitutive activation of the system leads

to defects in cell shape, growth, and division (Delhaye et al., 2016). Moreover, these defects were dependent on the expression of LdtD (Delhaye et al., 2016). Thus, the Cpx response not only monitors protein quality control in the envelope, but also helps maintain cell wall integrity. Other studies report that the Cpx response regulates amidases in *P. aeruginosa* and *S.* Typhimurium, suggesting that Cpx regulation of cell wall homeostasis is a conserved function across Gram-negative organisms (Weatherspoon-Griffin et al., 2011; Yakhnina et al., 2015).

Finally, the Cpx response regulates the activity of other stress responses through several regulatory proteins and sRNAs (Grabowicz and Silhavy, 2017b). Induction of the Cpx response represses expression of the components of the σ^E signal cascade (De Wulf et al., 1999; Pogliano et al., 1997; Raivio et al., 2013), suggesting that bacteria carefully coordinate these two overlapping but distinct stress responses. The Cpx-regulated periplasmic protein MzrA interacts with the osmotic stress sensor EnvZ and influences EnvZ signaling to OmpR, thus connecting CpxRA to the EnvZ-OmpR two-component system (Gerken et al., 2009; Gerken and Misra, 2010). In *Yersinia pseudotuberculosis*, Cpx activation strongly represses the Rcs phosphorelay to control expression of the Ysc-Yop type III secretion system (Fei et al., 2021). Finally, the Cpx regulated protein YdeH is a diguanylate cyclase, which are enzymes that produce cyclic di-GMP and influences biofilm production (Spangler et al., 2011). Taken together, these studies demonstrate that the Cpx response maintains key hierarchies in envelope stress signaling.

Other envelope stress responses

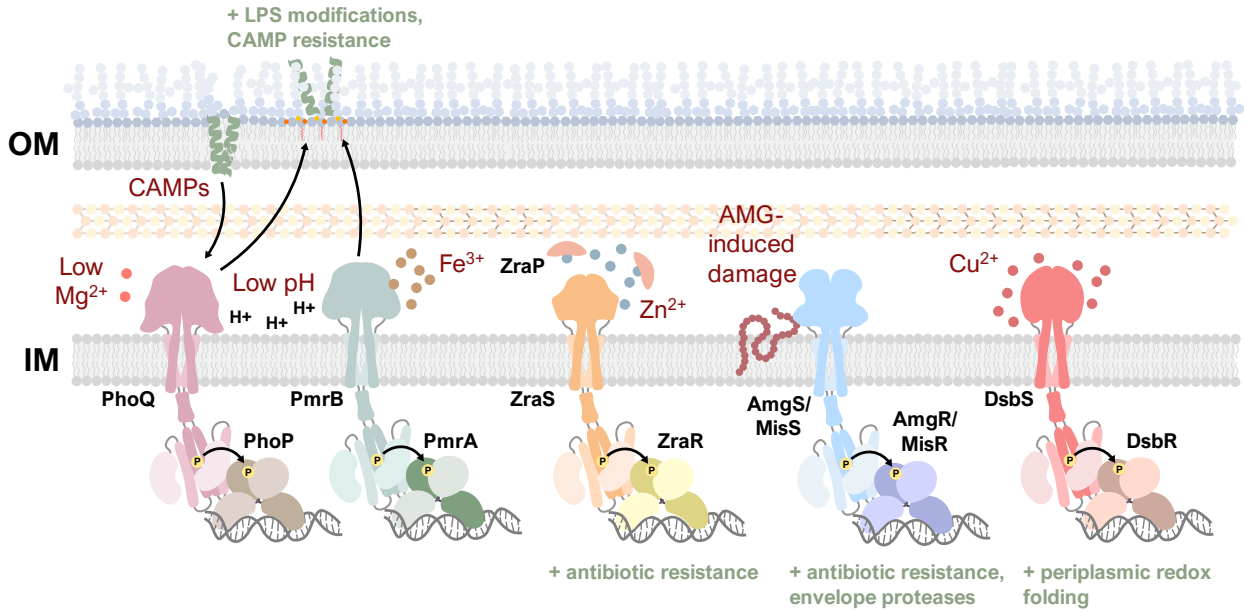

Figure 1-11. Other systems sense and respond to envelope stress.

A wide range of systems across Gram-negative bacteria sense many stimuli and mount protective responses. Abbreviations: CAMPs (cationic antimicrobial peptide), AMG (aminoglycoside).

While the systems outlined above constitute what can be considered the "classical" envelope stress responses, several other systems are activated by envelope stress and protect cells against it (Figure 1-11). Some of these systems have overlapping roles to systems in *E. coli*. For example, the MisRS system of *Neisseria* spp. and the AmgRS system of *P. aeruginosa* resemble the CpxRA system of *E. coli* based on the resistance to aminoglycoside antibiotics afforded by all three systems (Kandler et al., 2016; Lau et al., 2013; Poole et al., 2019). While expression of the Dsb system is controlled by the Cpx response in *E. coli*, expression of an analogous system in *P. aeruginosa* is controlled by a dedicated, copper-responsive two-component system DsbRS (Yu et al., 2022).

PmrAB and PhoPQ together form an intertwined network of stress sensitive systems that provide resistance to threats such as cationic antimicrobial peptides (CAMPs) via modifications of LPS (Chen and Groisman, 2013; Huang et al., 2020). The PhoQ sensor kinase is activated by the presence of CAMPs, acidic pH, or low Mg^{2+} concentration (Johnson et al., 2013; Perez et al., 2009; Prost et al., 2007; Zwir et al., 2005). The PmrB sensor kinase is induced by a distinct set of signals including the presence of metals such as Al^{3+} or Fe^{3+}, although both systems are induced by low pH (Chen and Groisman, 2013). The PhoP and PmrA regulons both include LPS modification genes, although somewhat distinct sets. The PhoPQ regulon is extensive, but one of its most important functions is the modification of lipid A of LPS by PagP and PagL (Guo et al., 1997; Murata et al., 2007). PmrA regulates the expression of a separate set of LPS modifying enzymes PmrC or Ugd and PbgP, which add PE or L-4-aminoarabinose to lipid A (Chen and Groisman, 2013; Gunn, 2008). Both the Pho and Pmr systems are also linked by a PhoPQ regulated protein PmrD, which allows for stimuli of the Pho system to indirectly induce PmrAB (Rubin et al., 2015), although this connection is not conserved across species (Chen and Groisman, 2013). Together, these two systems serve to fortify the outer membrane against insults such as polymyxins or other antimicrobial peptides; thus, both systems are important for the virulence of pathogens such as *Salmonella* spp. (Groisman et al., 2021; Gunn, 2008).

The ZraSRP two-component system is induced by zinc (Leonhartsberger et al., 2001; Petit-Härtlein et al., 2015); ZraP appears to act as a zinc-binding chaperone, and in a similar manner to CpxP for the Cpx response, represses the ZraRS system (Appia-Ayme et al., 2012; Petit-Härtlein et al., 2015). However, the relationship of the Zra system to zinc tolerance is unclear as deletions of *zraP, zraR,* or *zraS* do not increase sensitivity to zinc (Petit-Härtlein et al., 2015). A recent study has reported that the Zra system is required for full resistance to several classes of antimicrobials and regulates a wide regulon of genes involved in stress

response (Rome et al., 2018), raising the possibility that, besides responding to stresses caused by metals themselves, envelope stress responses may use metals as a signal for membrane damage to regulate adaptive responses such as antibiotic resistance. In line with this, ZraP, along with other ESR-regulated chaperones such as Spy and CpxP, contributes to polymyxin B resistance in *S.* Typhimurium (Appia-Ayme et al., 2012).

Signaling across the envelope

The envelope is a critical area for bacterial sensory signal transduction because it is the interface between the cell and the world around it. As discussed above, the envelope itself must be monitored in order to maintain its integrity. Bacteria possess a diverse array of envelope sensors (Galperin, 2004; Hoch, 2000). Envelope-localized chemoreceptors, which often possess periplasmic sensor domains that interact with substrate binding proteins, detect nutrients and direct bacteria to them (Bi and Lai, 2015). Two-component systems and phosphorelays form related signaling mechanisms that are explored in further detail below.

Two-component systems and phosphorelays

Two-component systems are the predominant mode of extracellular signal transduction in bacteria. Their distribution differs from organism to organism; *P. aeruginosa* possesses one of the most extensive arrays with over 60 systems (Gooderham and Hancock, 2009) while *E. coli* possesses around 30 (Yamamoto et al., 2005). As their name implies, two-component systems typically consist of two parts: a sensor histidine kinase (or just sensor kinase) and a cytoplasmic response regulator (Figure 1-12A) (Casino et al., 2010). However, more complex phosphorelay systems, which are based on two-component systems, often contain multiple proteins involved in phosphotransfer (Hoch, 2000). Regardless, signal transduction in these systems can be divided into a cascade of three events (Casino et al., 2010). First, a signal is sensed by the

sensor kinase. Second, this signal is transduced by phosphotransfer from the sensor kinase to the response regulator. Finally, the phosphorylated response regulator will use its effector domain to cause an adaptive response in the cell (Figure 1-12B).

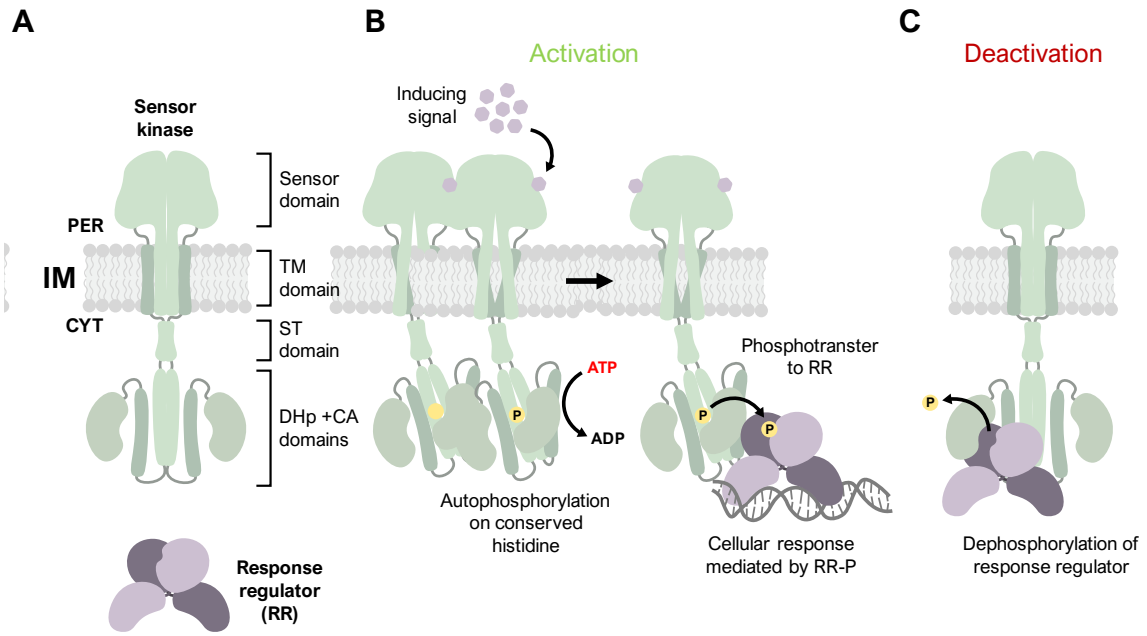

Figure 1-12. Two-component signal transduction.

(A) Components of a two-component system and basic structure of a typical sensor kinase. **(B)** General mechanism of activation of a sensor kinase and subsequent phosphorylation of its cognate response regulator. **(C)** Dephosphorylation of a response regulator as a mechanism of negative regulation by sensor kinases in the absence of inducing cues.

Most sensor kinases are homodimeric and membrane bound and contain periplasmic (or extracellular in the case of Gram-positives), transmembrane, and cytoplasmic regions. Precisely how these regions are arranged is variable across systems (Krell et al., 2010). However, exceptions in the natural world always exist, and histidine kinases are not always bound to membranes or dimeric, as is the case with the soluble and monomeric sensor kinase EL346 from *Erythrobacter litoralis* (Dikiy et al., 2019). Regardless, the fundamental workings of

sensor kinases are broadly conserved. The domains directly responsible for sensing signals are often extracytoplasmic (Cheung and Hendrickson, 2010). Extracytoplasmic sensor domains may comprise several different folds, although the most common are Per-ARNT-Sim (PAS) domains, which are universally distributed ligand-binding domains consisting of a conserved β-sheet surrounded by α-helical elements (Chang et al., 2010; Henry and Crosson, 2011). Other sensor kinases contain other folds, such as an all α-helical structure possessed by the nitrate sensor NarX (Cheung and Hendrickson, 2009). Regardless of the fold, each sensor kinase recognizes a specific set of signals, including ligands by direct binding. For example, the prototypical sensor domains of CitA and DcuS directly bind citrate and fumarate, respectively (Cheung and Hendrickson, 2008; Janausch et al., 2002; Reinelt et al., 2003; Sevvana et al., 2008).

A periplasmic signal must be transmitted through the inner membrane and to the cytoplasm. Transduction of this signal occurs through a four-helix transmembrane domain (two helices from each monomer) (Moukhametzianov et al., 2006). This transmembrane domain is attached to a cytoplasmic signal transduction domain that can adopt different folds (Bhate et al., 2015). In many histidine kinases, this signal transduction domain is a HAMP (**h**istidine kinase, **a**denylate cyclases, **m**ethyl-accepting proteins, and phosphatases) fold, comprising a four-helix bundle. Other signal transduction domains include PAS and GAF (c**G**MP-specific phosphodiesterases, **a**denylyl cyclases, and **f**ormate hydrogenases fold) domains (Ho et al., 2000).

Altogether, sensor domains, transmembrane domains, and signal transduction domains translate periplasmic stimuli into conformational changes that activate the kinase activity of catalytic (CA) domains. These domains transfer a phosphate group from ATP onto a conserved histidine residue on a dimerization and histidine phosphotransfer (DHp) domain (Bhate et al., 2015). For typical sensor kinases, the phosphate group is transferred from this residue to the

response regulator. However, in more complicated phosphorelay systems, the phosphate is transferred to an aspartate residue on a receiver domain that can be present on the sensor kinase itself (Appleby et al., 1996; Mitrophanov and Groisman, 2008). This phosphate is again transferred to a histidine residue, this time on a histidine phosphotransfer (HPt) domain containing protein (Kato et al., 1997; Mitrophanov and Groisman, 2008). These additional phosphorylation points allow for a less linear sequence of signaling and additional regulatory inputs (Appleby et al., 1996).

Response regulators consist of receiver and output/effector domains (Galperin, 2006; Gao et al., 2019, 2007). The receiver domain (as named) receives a phosphate group from its cognate sensor kinase on a conserved aspartate residue. The diversity in response regulator function is due to the variability of output domains (Galperin, 2006). The most well-known output domains are those that bind DNA, often winged-helix domains such as that of the prototypical OmpR (Itou and Tanaka, 2001) or helix-turn-helix motifs such as the one found in NarL (Baikalov et al., 1996). DNA-binding response regulators influence cell physiology by mediating transcriptional changes (Galperin, 2006). However, response regulators can also possess output domains with non-DNA binding functions. For example, the CheY response regulator, once phosphorylated, will directly bind to the flagella rotor complex to change its direction of rotation (Sarkar et al., 2010). Another chemotaxis related response regulator, CheB, is a methylesterase that modifies the methylation of methyl-accepting chemotaxis proteins (MCPs) to directly influence signal transduction (Kehry and Dahlquist, 1982).

Signaling across the envelope

While some signals (such as small molecules) readily diffuse across aqueous spaces, other signals (such as defects in LPS or OMPs) do not. The lack of ATP in the envelope poses another challenge, as it rules out phosphorylation or other ATP-dependent processes as a direct

mechanism of signaling. Finally, if the cell wall is a single, continuous mesh-like structure that surrounds the inner membrane, a signal from the outer membrane must reach the inner membrane through this layer, suggesting some level of coordination between signal transduction systems and the cell wall. Thus, a key question of signaling in the envelope is how signals *cross* the envelope to reach sensory systems located in the inner membrane or cytoplasm. One recently reported mechanism is the use of anti-sigma factors that possess domains that integrate into the outer membrane, span across the periplasm, cross the inner membrane, and bind cytoplasmic sigma factors, recently described in *Bacteroides thetaiotamicron* (Pardue et al., 2024). In the presence of an extracellular signal, presumptive proteolysis of this membrane spanning anti-sigma factor leads to the release of the cytoplasmic sigma factor, modulating expression of genes involved in outer membrane vesiculation. However interesting, such a mechanism is only one of the creative ways that Gram-negative bacteria sense and transduce signals across multiple membranes.

Sensing surfaces across the envelope

Signal transduction across the envelope is especially critical in sensing adhesion to surfaces, an essential step in biofilm formation (O'Toole et al., 2000). A signal at the cell surface necessarily crosses both the outer and inner membranes to reach cytoplasmic effectors. There are several mechanisms for surface sensing in Gram-negative bacteria that allow for this, responding to chemical, mechanical, and stress-based cues (Kimkes and Heinemann, 2019; Laventie and Jenal, 2020; O'Toole and Wong, 2016). Flagella and pili, structures that span the inner and outer membranes, physically attach to surfaces, a mechanical signal which can be transferred through these structures themselves to communicate to the cell that they are attached to a surface. While primarily thought to promote planktonic motility, initial flagellar attachment to surfaces is critical for surface sensing, and this signal is dependent on the stator

proteins MotAB mediating a subsequent increase in cyclic di-GMP signaling (Belas, 2014; Laventie et al., 2019). Similarly, increased tensile force experienced by type IV pili during adhesion serves as a mechanical signal of surface adhesion (Persat, 2017). In *P. aeruginosa*, this mechanical signal results in an increase in intracellular cAMP and c-di-GMP through the Chp two-component system (the Pil-Chp axis), ultimately regulating the expression of several virulence factors (Persat et al., 2015).

Envelope stress appears to be an integral part of how bacteria sense surface adhesion. The Rcs phosphorelay is activated in surface adhered cells (Kimkes and Heinemann, 2018) and regulates genes related to biofilm formation and motility (Majdalani and Gottesman, 2005; Morgenstein and Rather, 2012). The Cpx response has been implicated in sensing adhesion through the outer membrane lipoprotein NlpE (Otto and Silhavy, 2002; Shimizu et al., 2016), and many authors have noted the overlap between the genes of the Cpx regulon and genes induced in biofilms (Dorel et al., 2006; Prigent-Combaret et al., 2001). Recent work has also shown that envelope stress is a key inducer of the WspRS system of *P. aeruginosa*, which leads to the production of c-di-GMP and biofilm components (O'Neal et al., 2022). Indeed, this study and others have shown that surface adhesion itself can lead to envelope stress that is sensed by envelope stress responses (Harper et al., 2023; Laventie and Jenal, 2020).

Lipoproteins as trans-envelope communication molecules

Cross-envelope communication, however, is critical in many other contexts, not just surface sensing. As a class of proteins, lipoproteins often function as signaling molecules in both Gram-negative and -positive species. In particular, lipoproteins are commonly connected to two-component signaling. For example, in *Mycobacterium* spp., the lipoproteins LprJ and LprF are thought to sense extracytoplasmic potassium levels that are communicated to the KdpD sensor kinase (Brülle et al., 2010; Steyn et al., 2003; Sutcliffe and Harrington, 2004). The sporulation

kinase KinB of the Gram-positive *Bacillus subtilis* requires a lipoprotein KapB for activation (Dartois et al., 1997).

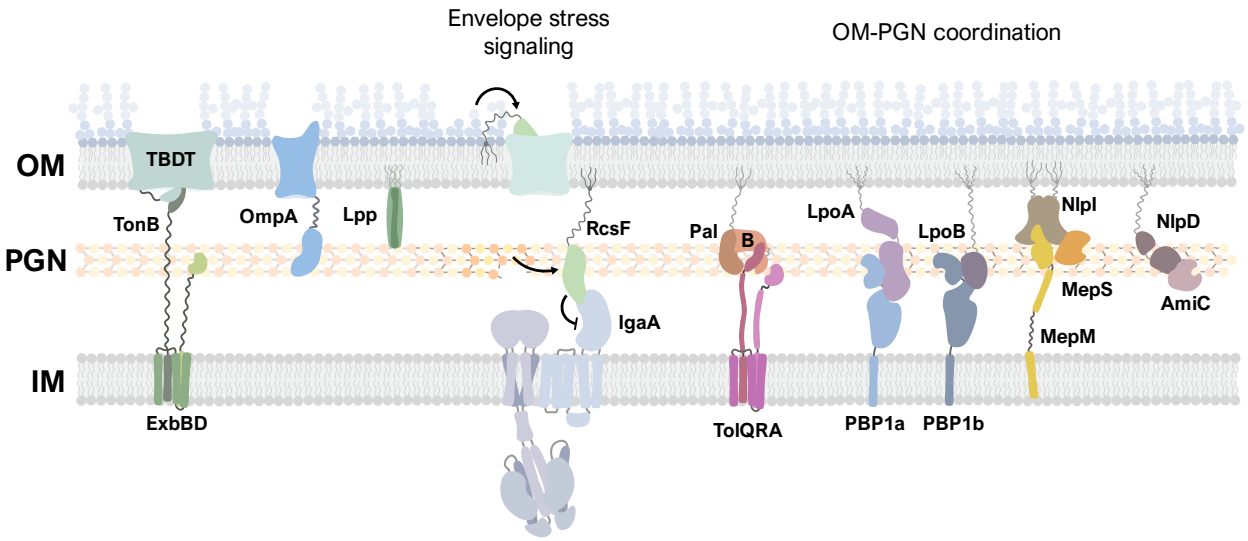

Figure 1-13. Trans-envelope communication by outer membrane lipoproteins.
The structure of outer membrane lipoproteins makes them useful molecules for linking the outer membrane to the inner membrane in various processes.

In Gram-negative bacteria, outer membrane lipoproteins serve as a physical link between the inner and outer membranes, with roles in cell wall synthesis, division, and envelope stress signaling (Figure 1-13). Several structural features of lipoproteins make them suitable for this role. The acylated cysteine of lipoproteins allows for membrane anchoring via a relatively modest moiety, letting lipoproteins localize relatively freely across the envelope. Furthermore, many outer membrane lipoproteins possess an intrinsically disordered “tether” region between their N-terminal lipidated cysteine and the first globular domain (El Rayes et al., 2021; Zückert, 2014). This region varies in length but is essential for outer membrane trafficking (El Rayes et al., 2021) and may afford lipoproteins a degree of flexibility in reaching across the periplasm to interact with partner proteins. Interestingly, this linker resembles regions in other envelope spanning

proteins. The inner membrane-anchored TonB protein possesses a long, flexible, proline-rich linker that connects an N-terminal transmembrane domain to a C-terminal globular domain that interacts with the TonB box of TonB-dependent transporters (Brewer et al., 1990; Sean Peacock et al., 2005). This region, corresponding to about 70 amino acids, is intrinsically disordered and thought to span the periplasm to connect the inner membrane PMF-harnessing complex of TonB-ExbBD with outer membrane transporters. The outer membrane protein OmpA also possesses a shorter proline-rich region that connects its membrane integral β-barrel with its C-terminal peptidoglycan binding domain (Marcoux et al., 2014), providing another example of a disordered linker connecting layers in the envelope.

Several outer membrane lipoproteins connect the outer membrane to inner membrane complexes involved in cell wall synthesis or remodeling. The peptidoglycan associated outer membrane lipoprotein Pal associated with the periplasmic TolB protein and the inner membrane complex of TolQRA forms a trans-envelope complex that coordinates the outer membrane and cell wall during division (Szczepaniak et al., 2020; Tsang et al., 2017; Webby et al., 2022; Yakhnina and Bernhardt, 2020). Recent work suggests that Pal possesses different levels of mobility through the envelope depending on its association with peptidoglycan or the periplasmic protein TolB; Pal-PGN is more limited in its mobility, while Pal-TolB diffuses more freely (Szczepaniak et al., 2020). In this model, Pal-TolB is captured by TolQRA at the divisome and Pal is “offloaded” to the cell wall at the midcell, highlighting the ability of lipoproteins to both coordinate inner and outer membrane structures and move around the envelope freely when need be.

Other lipoproteins are crucial regulators of cell wall synthesis and remodelling. The outer membrane lipoproteins LpoA and LpoB activate peptidoglycan synthesis by spanning the periplasm and interacting with the inner membrane enzymes PBP1a and PBP1b, respectively

(Egan et al., 2014; Sardis et al., 2021). Endopeptidase activity is similarly controlled by the dimeric outer membrane lipoprotein NlpI, which interacts directly with endopeptidases such as MepS and MepM (Banzhaf et al., 2020; Wang et al., 2024). Peptidoglycan amidases such as AmiC, enzymes essential for the breakdown of the cell wall during cell division, are controlled by the outer membrane lipoprotein NlpD (Chan et al., 2022; Tsang et al., 2017). These lipoproteins possess different lengths of N-terminal linkers that allow them to span the periplasm; some, such as LpoB and NlpD possess long, unstructured linkers (Egan et al., 2014; El Rayes et al., 2021), whereas LpoA and NlpI possess linkers of more modest length. Regardless, these findings make it clear that lipoproteins are an effective tool for inter-membrane coordination.

The stress sensor RcsF plays a direct role in signal transduction. RcsF is the primary sensor of the Rcs phosphorelay and is required for sensing many if not most Rcs inducing cues (Majdalani et al., 2005). Like many other lipoproteins discussed here, RcsF possesses a long unstructured linker at its N-terminus, which is attached to a small, globular C-terminal domain (El Rayes et al., 2021; Leverrier et al., 2011). However, the precise signal sensed by RcsF is controversial (S.-H. Cho et al., 2023). One model is that RcsF is primarily a sensor of BAM complex function (Figure 1-14) (Cho et al., 2014; S.-H. Cho et al., 2023; Dekoninck et al., 2020; Rodríguez-Alonso et al., 2020). Here, RcsF is anchored to the periplasmic leaflet of the outer membrane and complexes with OMPs with its linker facing the periplasm (Cho et al., 2014; Rodríguez-Alonso et al., 2020). In this model, OMPs play a passive role, sequestering RcsF away from inner membrane signaling factors, namely the repressor IgaA. When BamA function is compromised, RcsF-OMP complexes do not form, releasing the globular domain of RcsF into the periplasm where it can interact with the IgaA (Cho et al., 2014). Similarly, RcsF is proposed to interact with the periplasmic C-terminal domain of OmpA, which may act as a sort of “buffer” that sequesters RcsF from IgaA in the absence of envelope stress (Dekoninck et al., 2020).

Strong structural support for this model comes from the structure of the RcsF-BamA complex, which places RcsF in a conformation more in line with a periplasmic-leaflet anchored RcsF (Rodríguez-Alonso et al., 2020).

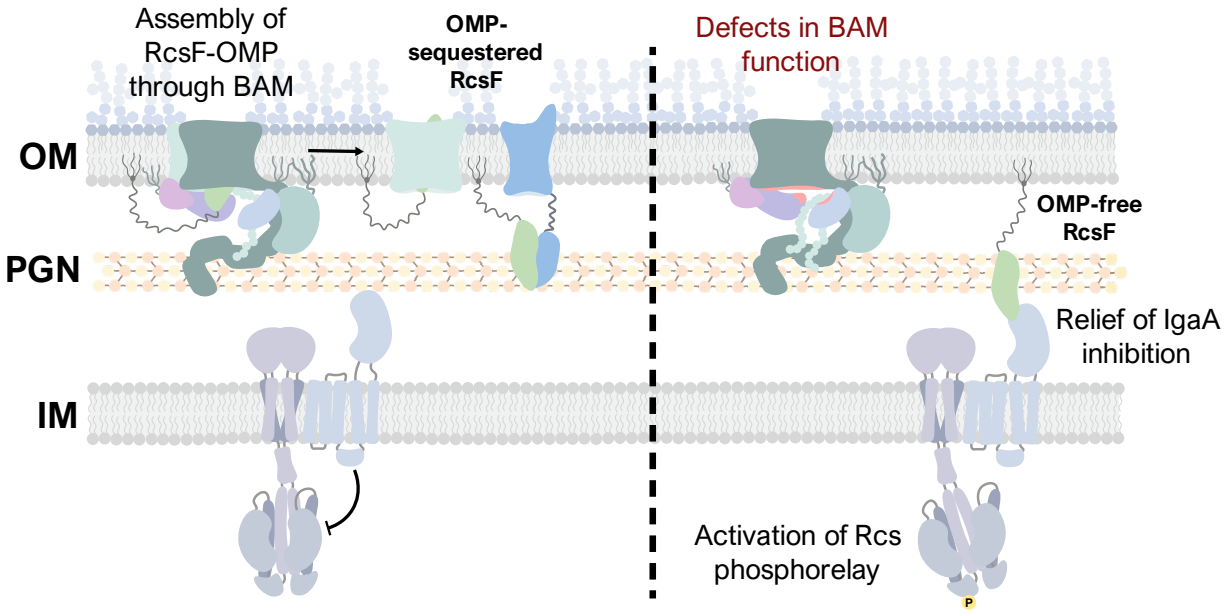

Figure 1-14. The BAM sensor model of RcsF signaling.

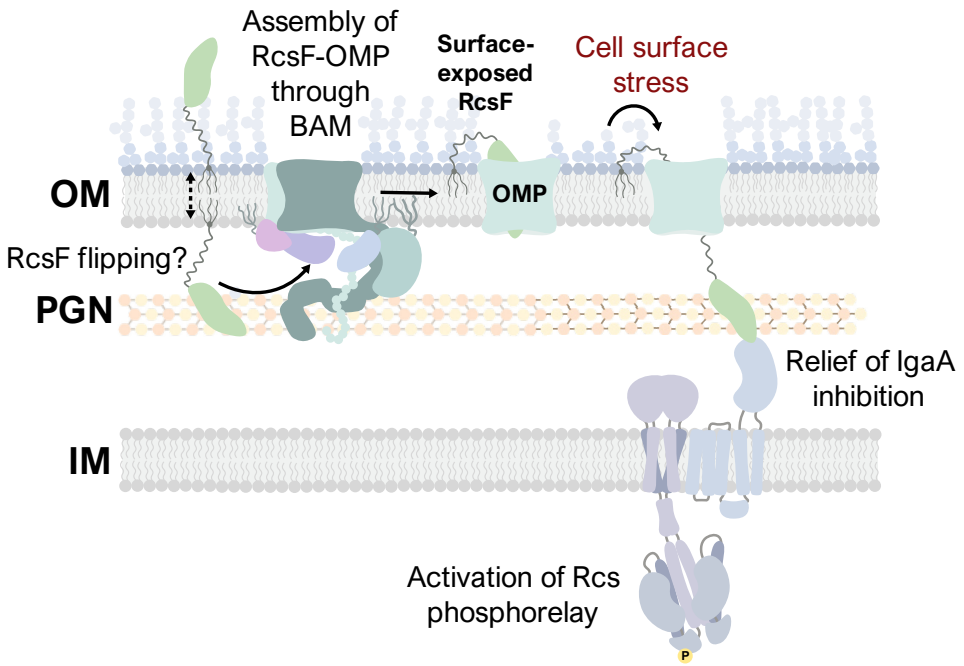

Figure 1-15. The RcsF-OMP stress sensing model.

An alternative model posits that RcsF-OMP complex is required for sensing defects in lipopolysaccharide not BAM complex function (Figure 1-15) (Konovalova et al., 2016; Lach et al., 2023; Tata et al., 2021). RcsF is one of the few known *E. coli* lipoproteins that can become surface exposed, which it does by threading through the lumen of OMPs such as OmpC and OmpF (Konovalova et al., 2014). Here, the acylated cysteine and N-terminal linker of RcsF are surface exposed and directly involved in sensing LPS defects (Konovalova et al., 2016, 2014). In this model, OMPs are an active participant in RcsF surface signaling, rather than simply sequestering RcsF away from inner membrane signaling components (Konovalova et al., 2016; Lach et al., 2023). How exactly RcsF becomes surface exposed on the outer leaflet is unknown and would require additional (unknown) mechanisms for the flipping of RcsF's acylated cysteine. Nonetheless, recent studies from the Konovalova lab dispute that RcsF monitors BamA function (Tata et al., 2021). Tata and colleagues report that mutations in RcsF that prevent the formation of an RcsF-BamA complex do not by itself lead to Rcs activation. Furthermore, RcsF associates equally with mutant alleles of BamA with varying functionality, suggesting it does not discriminate between functional and non-functional BamA.

More work will be required to tease out the precise molecular cue sensed by RcsF. Regardless, aspects of cross-periplasm signaling by RcsF are firmly established. Both models agree in that RcsF interacts with OMPs and the RcsF-OMP complex is formed during OMP assembly, facilitated by the BAM lipoprotein BamE (Cho et al., 2014; Konovalova et al., 2014; Rodríguez-Alonso et al., 2020; Tata and Konovalova, 2019). It's uncontroversial that RcsF signals across the periplasm and activates the Rcs phosphorelay by relieving inhibition by the inner membrane protein IgaA (Hussein et al., 2018). The globular C-terminal domain of RcsF interacts with the periplasmic C-terminal domain of IgaA; the structure of this complex was recently solved (Watanabe and Savchenko, 2024). Unsurprisingly, mislocalization of RcsF to the inner

membrane is able to overcome IgaA inhibition and activates the system, and although mislocalized RcsF is able to sense some Rcs inducing cues, it is unable to sense LPS defects (Shiba et al., 2012). Further evidence that RcsF spans the periplasm to communicate with IgaA comes from a creative study manipulating the length of the periplasm by introducing variants of longer-than-WT Lpp; increasing the length of Lpp (and therefore the width of the periplasm) abolishes RcsF signaling, which can be restored by commensurately lengthening the linker region of RcsF (Asmar et al., 2017). In sum, RcsF provides us with a model for understanding how lipoproteins transduce signals across the envelope, which may be applied to other stress sensitive lipoproteins such as NlpE of the Cpx envelope stress response.

Signaling in the Cpx response

CpxA and CpxR form the core signaling unit

While CpxP and NlpE allow for negative and positive regulatory inputs to the Cpx system, neither is required for sensing many if not most Cpx inducing cues (DiGiuseppe and Silhavy, 2003). Thus, the core of signaling in the Cpx response is mediated by interactions between the sensor kinase CpxA and response regulator CpxR. CpxA is a homodimer comprising a fairly standard sensor kinase. Structures of the cytoplasmic regions of CpxA provide a clear picture of phosphotransfer from CpxA to CpxR (Mechaly et al., 2017, 2014). A symmetric four helix HAMP domain immediately follows the transmembrane region of CpxA, which is linked to the dimer DHp and catalytic domains and transfers a signal from the membrane as a disruption of dimer symmetry, which is communicated to the DHp+CA domains (Mechaly et al., 2014). Crystal structures of the cytoplasmic domains of kinase active CpxA reveal a highly asymmetric structure where only one CA subunit is active, leading to phosphorylation on only one monomer of CpxA (despite homodimerization) (Mechaly et al., 2014). This active CA subunit binds ATP and catalyzes phosphorylation of His248. A hemiphosphorylated structure of CpxA's cytoplasmic

domains suggests that one histidine residue on CpxA is phosphorylated, while the other is "primed" for phosphorylation (Mechaly et al., 2017). CpxR binding to CpxA promotes phosphotransfer from the phosphorylated histidine to CpxR, but simultaneously stimulates autophosphorylation on the other protomer, creating a dynamic cycle of phosphorylation and phosphotransferase reactions that ultimately maximizes the efficiency of signal transduction from CpxA to CpxR (Mechaly et al., 2017).

The upstream reactions leading to autophosphorylation and phosphotransfer remain significantly more mysterious. Early studies of CpxA isolated several mutations to CpxA's periplasmic region with hyper-activated and signal blind phenotypes (Cosma et al., 1995a; Raivio and Silhavy, 1997). Almost all mutations to CpxA in this region are hyperactivating, suggesting that this region might normally control CpxA activation by preventing activation. In line with this, CpxA variants without a periplasmic domain are constitutively kinase active (Mechaly et al., 2014). The periplasmic sensor domain (at least in *Vibrio parahaemolyticus*) was solved as a PAS fold, similar to those possessed by other sensor kinases (Kwon et al., 2012a). This PAS domain possessed several charged regions, but unlike other histidine kinases, did not have a ligand bound to it. The solved dimer structure was also deemed to be a crystallographic artifact because the locations of the N- and C-termini of the structure cannot form the canonical transmembrane helix bundle found in other sensor kinases, thus leaving many questions about the precise mode of signal detection by CpxA.

CpxR is an OmpR/PhoB-like response regulator with both a receiver domain that gets phosphorylated and a DNA binding effector domain; these regions are connected by a flexible linker region (Gao and Stock, 2009; Mechaly et al., 2018). Structural studies of CpxR show that it functions as a highly dynamic protein that adopts different dimer structures corresponding to its phosphorylation state. When unphosphorylated, CpxR, exists in an equilibrium of non-DNA

binding monomers and dimers; upon phosphorylation, CpxR shifts exclusively into a DNA binding dimer conformation (Mechaly et al., 2018), interacting with a consensus sequence of 5'-GTAAN$_{6-7}$GTAA-3' (De Wulf et al., 1999; Pogliano et al., 1997) and mediating the changes in transcription outlined above.

CpxP is a negative regulator of signaling

The periplasmic chaperone protein CpxP is thought to act as a negative regulator of the system while also being one of the most highly expressed members of the Cpx regulon (Danese and Silhavy, 1998; Raivio et al., 2000, 1999). CpxP is a member of a family of periplasmic chaperones including Spy and ZraP that form higher order multimeric structures possessing a conserved LTxxQ motif (Appia-Ayme et al., 2012; Kwon et al., 2010; Thede et al., 2011; Zhou et al., 2011). CpxP is thought to bind certain misfolded protein substrates, such as overexpressed P-pilus subunits, in the envelope, which titrates it away from CpxA, relieving inhibition (Buelow and Raivio, 2005; Isaac et al., 2005; Zhou et al., 2011). CpxP is also the target of proteolysis by the Cpx-regulated protease DegP (Isaac et al., 2005). Thus, the Cpx response appears to be regulated by a negative feedback mechanism where CpxA activation leads to the production of a factor that is both stress combative and dampens CpxA activation, perhaps to prevent overactivation (Raivio et al., 1999). While the structure of CpxP has been solved (Thede et al., 2011; Zhou et al., 2011), the precise molecular basis for how it interacts with the Cpx response is not fully understood, although current hypotheses posit a direct CpxP-CpxA interaction that inhibits activation of CpxA (Tschauner et al., 2014). The precise role of CpxP in sensing Cpx inducing cues is also unclear. A recent study proposed that muropeptides formed upon treatment with a β-lactam antibiotic may interact with CpxP to titrate it away from CpxA (Masi et al., 2020). However, CpxP is not required for sensing almost all Cpx inducing cues, suggesting

that it is not integral to detecting most activating signals of the Cpx response (DiGiuseppe and Silhavy, 2003).

NlpE is an activator that senses diverse signals

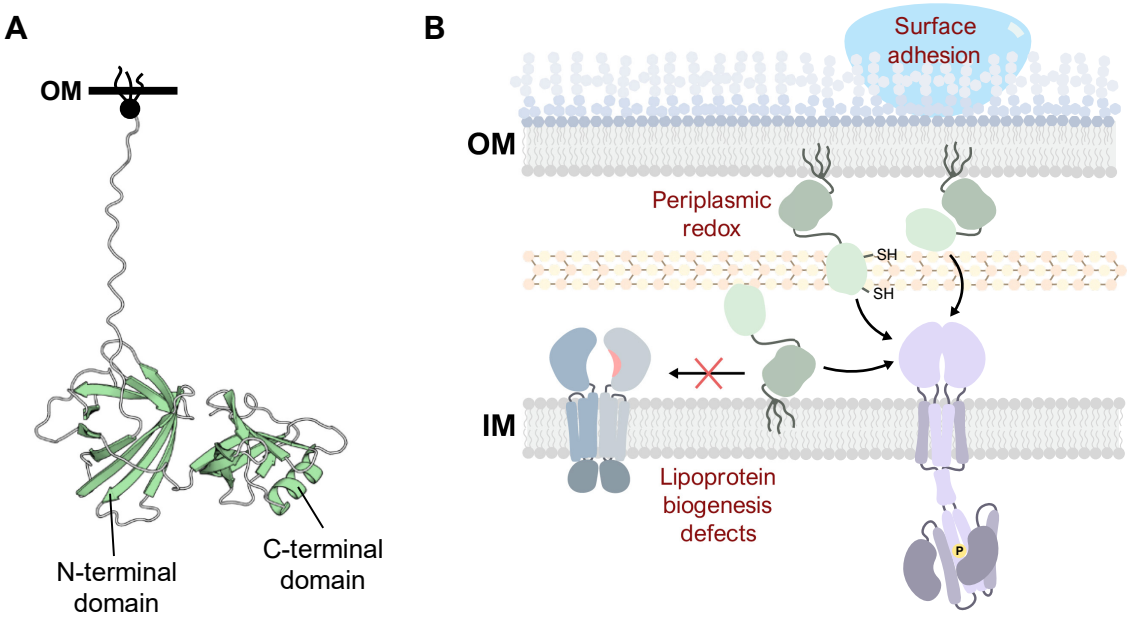

Figure 1-16. NlpE is an activator that senses diverse signals.

(A) Structure of NlpE according to AlphaFold2 (from the AlphaFold database https://alphafold.ebi.ac.uk/), which matches well with the hypothetical monomer model of (Hirano et al., 2007). **(B)** Signaling functions of NlpE for the Cpx response.

NlpE was identified by two independent studies in 1995 with Snyder and colleagues finding that overexpression of NlpE activates the Cpx response and Gupta and colleagues identifying it as a factor required for resistance to copper (Gupta et al., 1995; Snyder et al., 1995). The structure of NlpE was later solved as a unique domain-swapped dimer (Hirano et al., 2007, 2006). Each monomer consists of independently folding N- and C-terminal domains (Figure 1-16A). The N-terminal domain is a β-barrel that resembles the bacterial lipocalin while the C-terminal domain was found to possess an oligosaccharide/oligonucleotide binding (OB)

fold. However, none of these potential functions have been experimentally investigated. NlpE was also found to possess two pairs of conserved disulfide bonds; the disulfide on the N-terminal domain is found in a CXXC motif and was proposed to bind metals, whereas the C-terminal domain disulfide bond forms between Cys145 and Cys211. Hirano and colleagues also highlight a putative protease inhibitor signal in the N-terminal domain (Hirano et al., 2007, 2006), which was also noted in earlier studies (Snyder et al., 1995). Taken together, the structural study of NlpE proposed a mechanism of signaling where partial unfolding of NlpE would allow its C-terminal domain to extend from the N-terminal domain (anchored to the outer membrane by its acylated cysteine) to interact with inner membrane CpxA (Hirano et al., 2007).

NlpE appears to have many signaling roles (Figure1-16B). Gupta and colleagues (1995) found that the mutants of the *cutF* gene (confirmed to be the same as *nlpE*) displayed increased sensitivity to copper. Snyder and colleagues (1995) found that multicopy expression of NlpE could suppress envelope fusion protein toxicity through activation of CpxA. A later study found that mislocalization of NlpE to the inner membrane activates the Cpx response, analogously to RcsF in the Rcs phosphorelay (Miyadai et al., 2004). How all these findings tie to a physiological stressor would not become clear until Grabowicz and Silhavy found that the Cpx response is activated through NlpE in strains where *lolB* and/or *lolA* are knocked out, suggesting that mislocalized NlpE activates the Cpx response in the presence of a stressor that causes lipoproteins to not be properly trafficked to the outer membrane, (Grabowicz and Silhavy, 2017a). Since then, other studies have reported the details of NlpE's function as a monitor of lipoprotein health (Delhaye et al., 2019; Marotta et al., 2023a; May et al., 2019). These studies report that the N-terminal domain of NlpE physically interacts with CpxA at the inner membrane (Delhaye et al., 2019; Marotta et al., 2023b). NlpE is required to sense compounds that disrupt lipoprotein maturation or trafficking and NlpE must continuously be synthesized for this induction

to occur (May et al., 2019). Interestingly, these recent findings provide insight into the involvement of NlpE in copper resistance (Gupta et al., 1995). May and colleagues report that *nlpE* deletion mutants are sensitive to copper, similar to (Gupta et al., 1995) and that copper leads to the accumulation of aberrantly processed Lpp, suggesting that copper might induce the Cpx response through NlpE by interfering with its maturation.

However, NlpE also acts as a sensor of surface adhesion. Otto and Silhavy (2002) report that the Cpx response is induced in cells adhered to hydrophobic glass beads through NlpE. This induction does not occur in on hydrophilic glass beads, and attachment to hydrophobic surfaces is impaired in *cpxR::spc* and *nlpE::spc* mutants. Thus, NlpE and the Cpx response appear to play a critical role in the transition from planktonic to surface-adhered lifestyles. A later study reported that NlpE plays a similar role in enterohemorrhagic *E. coli* (EHEC) (Shimizu et al., 2016). Shimizu and colleagues confirm that NlpE senses hydrophobic surfaces but also report that NlpE may sense adhesion to living cells (namely, Caco-2 cells). NlpE sensing led to an upregulation of locus of enterocyte effacement genes, thus promoting the virulence of EHEC. Somewhat surprisingly, a recent study described almost exactly the same finding except that NlpE sensing of surfaces led to activation of the BaeRS system and induction of virulence through a separate regulatory pathway (Feng et al., 2022).

NlpE's signaling roles are not limited to sensing lipoprotein trafficking and surface adhesion. Recent studies propose that the C-terminal disulfide bonds on NlpE are involved in sensing periplasmic redox state (Andrieu et al., 2023; Delhaye et al., 2019). Delhaye and colleagues report that NlpE is a substrate of the oxidoreductase DsbA. Deletion of *dsbA* leads to Cpx induction through NlpE in a manner dependent on its C-terminal disulfide bonds. Similarly, Andrieu and colleagues report that the reactive chlorine species *N*-chlorotaurine activates the Cpx response through NlpE. Taken together, these studies make clear that NlpE is a versatile

sensor that is linked to the Cpx response in several roles, even while not being required for basal CpxA activity (DiGiuseppe and Silhavy, 2003). Thus, NlpE's role in the Cpx response is best thought of as an accessory activator that greatly expands the repertoire of stimuli that activate CpxA.

Thesis objectives & overview

While the Cpx regulon and its implications for envelope stress response are well-understood, the molecular basis for signal detection and transduction in this system is not as completely characterized. We study this system in *E. coli* because of its widespread use as a model Gram-negative organism for genetics and envelope biogenesis (Blount, 2015) and because of how important this organism has been for the study of the CpxRA system (Cosma et al., 1995a; Danese et al., 1995; McEwen and Silverman, 1980a, 1980c).

Early studies have isolated several gain of function mutations of *cpxA* (for example (Cosma et al., 1995a; Keller et al., 2011; Raivio and Silhavy, 1997)); however, the molecular basis for the phenotypes of these mutations remains unclear. A structure of *Vibrio parahaemolyticus* CpxA has been published (Kwon et al., 2012a), but applying this structure to the genetic data from previous studies is difficult because most of the work characterizing CpxA is not in this organism. Thus, exactly how CpxA becomes activated in the response to envelope cues is unclear. In Chapter 2, we (in collaboration with the Glover lab, University of Alberta, Department of Biochemistry) determine how CpxA's sensor domains regulate its activation. Our collaborators purified and solved the structure of CpxA by X-ray crystallography as a Per-ARNT-Sim (PAS) domain. However, because this structure did not provide a strong model for the dimer of CpxA, we used AlphaFold2 to predict the dimer structure of CpxA's sensor domains as a dimer. We then used mutagenesis to test the AlphaFold2 model to determine how the dimer of CpxA's

sensor domain regulates its signaling. Comparative studies of CpxA and other PAS domain containing proteins were used to examine the diversity of PAS domains in sensor kinases.

Studies implicate the outer membrane lipoprotein NlpE, seemingly, in two roles, one as a sensor for surface adhesion at the outer membrane (Otto and Silhavy, 2002; Shimizu et al., 2016) and the other as an indicator of lipoprotein health at the inner membrane (Delhaye et al., 2019; Grabowicz and Silhavy, 2017a; May et al., 2019). How these two functions are integrated into a single protein remains to be fully answered.

In Chapters 3 and 4, we investigate this question by examining NlpE in two distinct signaling roles: NlpE overexpression and mislocalization (Chapter 3) and NlpE signaling from the outer membrane (Chapter 4). We constructed expression vectors of NlpE to determine the domains necessary for activating CpxA during NlpE overexpression and mislocalization to the inner membrane. Bacterial two-hybrid assays were used to test for interactions between CpxA and NlpE. Mutagenesis based on the structure of NlpE and CpxA was then used to determine the molecular details of the NlpE-CpxA interaction at the inner membrane. Finally, we explored the proteolysis of NlpE, especially as influenced by the Cpx-regulated proteins CpxP and DegP.

In Chapter 4, we explore how NlpE functions as an outer membrane sensor that cooperates with OmpA to signal from the outer membrane. We confirm previous results from the Raivio lab that NlpE interacts with the major OMP OmpA and use mutagenesis and crosslinking to determine the details of this interaction. We then studied NlpE-OmpA signaling by using a phenotype reported by Junshu Wang in the Raivio lab that NlpE senses OmpA overexpression. We used mutagenesis of both NlpE and OmpA in this context to determine how NlpE signals from the outer membrane. Dot blot assays and surface crosslinking were used to test for NlpE surface exposure.

Finally, the Appendix to this thesis explores emerging findings regarding NlpE homologs across bacterial species and the implications of NlpE evolution for our understanding of its signaling role in Gram-negative bacteria. Taken together, this thesis aims to greatly expand our understanding of how bacteria sense signals within and through their envelopes.

Chapter 2 – The sensor of the bacterial histidine kinase CpxA is a novel dimer of extracytoplasmic Per-ARNT-Sim domains[†]

[†] Published as Cho, T.H.S., Murray, C., Malpica, R., Margain-Quevedo, R., Thede, G.L., Lu, J., Edwards, R.A., Glover, J.N.M., Raivio, T.L., 2024. The sensor of the bacterial histidine kinase CpxA is a novel dimer of extracytoplasmic Per-ARNT-Sim domains. Journal of Biological Chemistry 300. https://doi.org/10.1016/j.jbc.2024.107265

Cameron Murray and I conceptualized most of the work presented in this chapter and co-wrote the manuscript. I was responsible for Figures 2-2A,B,C; 2-3; 2-7; 2-8; 2-10; 2-11; and 2-18. Cameron Murray was responsible for figures 2-1B; 2-5B,C; 2-6; 2-13; 2-14; 2-16; and 2-17. Drs. Gina L. Thede, Ross A. Edwards, and Jun Lu all worked to generate the crystal structure of CpxA shown in Figure 2-1A and 2-4A. Gina Thede was responsible for purifying the sensor domain of CpxA and crystallization; Ross Edwards assisted with the refinement of the crystallographic data; and Jun Lu contributed to biochemical work on CpxA. Roxana Malpica generated the data shown in Figure 2-2D,E. Rodrigo Margain-Quevedo provided the data used in Figures 2-4B,C, 2-9, 2-12, 2-15. Drs. Tracy Raivio and Mark Glover provided feedback on and reviewed the manuscript.

Abstract

Histidine kinases are key bacterial sensors that recognize diverse environmental stimuli. While mechanisms of phosphorylation and phosphotransfer by cytoplasmic kinase domains are relatively well-characterized, the ways in which extracytoplasmic sensor domains regulate activation remain mysterious. The Cpx envelope stress response is a conserved Gram-negative two-component system which is controlled by the sensor kinase CpxA. We report the structure of the *Escherichia coli* CpxA sensor domain (CpxA-SD) as a globular Per-ARNT-Sim (PAS)-like fold highly similar to that of *Vibrio parahaemolyticus* CpxA as determined by X-ray crystallography. Because sensor kinase dimerization is important for signaling, we used AlphaFold2 to model CpxA-SD in the context of its connected transmembrane domains, which yielded a novel dimer of PAS domains possessing a distinct dimer organization compared to previously characterized sensor domains. Gain of function *cpxA** alleles map to the dimer interface, and mutation of other residues in this region also leads to constitutive activation. CpxA activation can be suppressed by mutations that restore inter-monomer interactions, suggesting that inhibitory interactions between CpxA-SD monomers are the major point of control for CpxA activation and signaling. Searching through hundreds of structural homologues revealed the sensor domain of *Pseudomonas aeruginosa* sensor kinase PfeS as the only PAS structure in the same novel dimer orientation as CpxA, suggesting that our dimer orientation may be utilized by other extracytoplasmic PAS domains. Overall, our findings provide insight into the diversity of the organization of PAS sensory domains and how they regulate sensor kinase activation.

Introduction

Two-component systems (TCS) are ubiquitous bacterial sensory systems that recognize diverse environmental and cellular signals. Here, sensor histidine kinases sense stimuli and phosphorylate a cytoplasmic response regulator, which are usually transcription factors modulating the expression of target genes. Sensor kinases possess diverse and modular organizations (Bhate et al., 2015; Krell et al., 2010; Raivio, 2019). Upon receiving a signal by sensory domains, conformational changes in these domains trigger downstream signaling events through common signal transduction domains, ultimately leading to autophosphorylation and phosphotransfer mediated by conserved kinase domains. While the structure and activity of cytoplasmic kinase domains are conserved and well-characterized, extracellular/periplasmic sensor domains and the mechanisms by which they sense and transduce signals are relatively more diverse (Gao and Stock, 2009; Mascher et al., 2006). Thus, the molecular basis for sensing and signal transduction by these domains remains more difficult to precisely characterize.

While extracytoplasmic sensor domains adopt a variety of folds, many sensor kinases (and other sensory proteins such as chemotaxis proteins) possess Per-ARNT-Sim (PAS)-like domains in this region (Cheung and Hendrickson, 2010). Like other PAS domains, these extracytoplasmic PAS domains are characterized by a 5-stranded β-sheet with a 2-5-1-4-3 topology (Hefti et al., 2004; Henry and Crosson, 2011; Möglich et al., 2009). While often adopting highly similar folds, these domains tend to share low sequence homology (Vreede et al., 2003). Largely unique to extracytoplasmic PAS domains is the presence of a long N-terminal helix, sometimes termed the periplasmic helix (or p helix) (Bhate et al., 2015), which is continuous with the first transmembrane domain. These helices are thought to play a key role in transducing signals to downstream elements of sensor kinases (reviewed in (Bhate et al., 2015; Jacob-Dubuisson et al., 2018)), which largely exist and function as homodimers. Importantly, this helix

forms the dimer interface in the prototypical periplasmic sensor domains of PhoQ (Cheung et al., 2008), DcuS (Cheung and Hendrickson, 2008), and CitA (Sevvana et al., 2008). Some authors have proposed that extracytoplasmic PAS-like domains be classed into a separate family based on these representative members called PhoQ-DcuS-CitA (PDC) domains due to common differences between intracellular and extracellular/periplasmic PAS domains (Cheung et al., 2008). However, the exact classification of these domains remains somewhat controversial. Recently, Upadhyay and colleagues proposed that extracytoplasmic PAS domains belong to a homologous but distinct family of domains known as Cache domains according to computational modelling (Upadhyay et al., 2016). Others have disputed whether extracytoplasmic PAS domains belong to a separate class of PAS domains because of the high level of sequence diversity between PAS domains and the high degree of structural similarity of the central β-sheets of intra- and extracellular PAS domains (Chang et al., 2010; Möglich et al., 2009). This diversity in nomenclature not only reflects a need for consensus in classification but also underscores the need for further study of these ubiquitous sensor domains.

CpxA is the sensor kinase of the CpxRA system, a conserved Gram-negative envelope stress response that responds to perturbations to envelope protein homeostasis (Raivio, 2014; Vogt and Raivio, 2012). Early studies of the Cpx response identified several alleles of *cpxA* (*cpxA**) which possess constitutively activated phenotypes (Cosma et al., 1995b; Danese et al., 1995; Rainwater and Silverman, 1990). These *cpxA** mutations were later sequenced and found to map to all regions of the protein (Raivio and Silhavy, 1997). Mutations from these studies mapping to the periplasmic portion of CpxA resulted in both hyper-activated and signal blind phenotypes, which led to the identification of this region as the main sensory domain. The periplasmic domain of CpxA in *Vibrio parahaemolyticus* was solved by X-ray crystallography as a globular PAS fold (Kwon et al., 2012b). Like other extracytoplasmic PAS domains, the

periplasmic domain of *V. parahaemolyticus'* CpxA contains a long α-helix at its N-terminus and a five-stranded β-sheet with the canonical 2-5-1-4-3 strand order. However, unlike most other sensor kinases, no known small molecule ligands have been found to bind CpxA. Instead, CpxA senses a wide variety of cues that result from envelope stress, especially those arising from misfolded proteins that affect inner membrane integrity (Danese and Silhavy, 1997; Pogliano et al., 1997; Raivio, 2014; Vogt and Raivio, 2012). CpxA also integrates signals from other envelope proteins such as the periplasmic chaperone-like protein CpxP (Danese and Silhavy, 1998; Raivio et al., 1999; Tschauner et al., 2014) and the outer membrane lipoprotein NlpE (Otto and Silhavy, 2002; Snyder et al., 1995). These factors help CpxA sense cues such as copper exposure and surface adhesion in the case of NlpE (T. H. S. Cho et al., 2023b; May et al., 2019; Otto and Silhavy, 2002; Shimizu et al., 2016) or the presence of misfolded pilus subunits in the case of CpxP (Buelow and Raivio, 2005; Isaac et al., 2005; Zhou et al., 2011). However, NlpE and CpxP are not required for sensing many, if not most, Cpx inducing cues (DiGiuseppe and Silhavy, 2003), suggesting that they are not integral to CpxA's inherent mechanism of sensing and activation.

While the structure of the *V. parahaemolyticus* CpxA periplasmic domain has been solved (Kwon et al., 2012b), the structural and molecular basis for CpxA sensing and activation remains elusive. In addition, the Cpx response of *Vibrio* spp. remains relatively poorly characterized compared to studies of the system in *Escherichia coli* and related Enterobacteriaceae, and significant differences exist between signals sensed by CpxA in *Vibrio cholerae* and *E. coli* (Acosta et al., 2015; Slamti and Waldor, 2009). We report the structure of the *E. coli* CpxA periplasmic sensor domain (CpxA-SD_{EC}) as determined by X-ray crystallography. CpxA-SD_{EC} adopts a globular PAS fold like the previously reported structure. To better understand CpxA-SD in its dimeric context, we used AlphaFold2 to model CpxA-SD. The

resulting model predicted a novel organization of PAS domains in sensor kinases. Previously identified hyper-activated *cpxA** alleles map to the modelled dimer interface, and mutation of conserved residues in this region also possess constitutively active and signal-blind phenotypes. The hyperactivation of these mutations can be completely or largely suppressed by introducing mutations predicted to restore interactions between CpxA-SD monomers, suggesting that CpxA kinase activity is controlled by inhibitory interactions between sensor domain monomers in the absence of inducing cues. Finally, the previously solved structure of PfeS (PDB 3KYZ), an enterobactin sensor from *Pseudomonas aeruginosa*, adopts highly similar characteristics to CpxA-SD. Taken together, we suggest that CpxA-SD represents a novel class of PAS domains that evolved to sense signals using a distinct dimer orientation from other PAS domains.

Results

CpxA-SD adopts a PAS fold

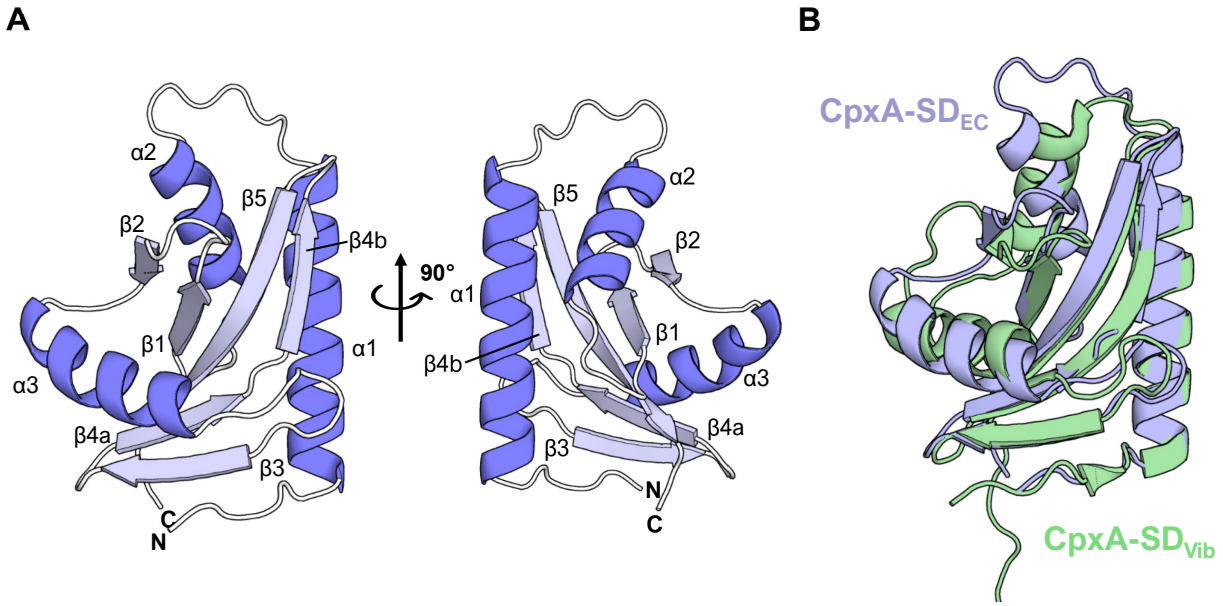

Figure 2-1. The sensor domain of CpxA adopts a PAS fold.

(A) The resolved structure of CpxA-SD (aa 31-163) is shown as ribbon diagrams with secondary structure elements labelled α for helices and β for strands of β-sheets. Two views at a 90° rotation are shown. Shown is Chain B of the asymmetric unit. **(B)** Overlay of *E. coli* CpxA-SD (this study; blue) and CpxA$_{Vib}$ (PDB 3V67; green).

We purified and crystallized the *E. coli* CpxA sensor domain corresponding to residues 31-163 (CpxA-SD) and determined its structure to a final resolution of 1.8 Å (see supplemental methods and Table 2-1 for a full list of refinement statistics). Like CpxA in *Vibrio parahaemolyticus* (CpxA-SD$_{Vib}$), *E. coli* CpxA-SD (CpxA-SD$_{EC}$) adopts a PAS-like fold with each globular domain consisting of three α-helices surrounding a five-stranded antiparallel β-sheet in the canonical 2-5-1-4-3 topology (Figure 2-1A). Like other extracytoplasmic PAS domains, CpxA-SD, contains a long N-terminal helix (α1). However, this helix does not form the extreme

N-terminus of the structure, instead containing an N-cap motif at its N-terminus and an extended tail region that folds against the β3 strand of the main PAS β-sheet (see later in Results for further discussion of this region). Overall, the monomer structure of CpxA-SD_{EC} is similar to that of the CpxA-SD_{Vib}, with a root-mean-square deviation (RMSD) of 2.9 Å over 108 atoms (Figure 2-1B). As seen with other PAS domains (Vreede et al., 2003), CpxA-SD_{EC} and CpxA-SD_{Vib} secondary structure bears significant similarity despite a low sequence identity of 20% between residues 35-150. The regions around the α2 helix and the N-terminus of the α3 helix appear to be slightly different between these two structures, however, the physiological relevance of this difference is uncertain. Between the α2 and α3 helices (*E. coli* region: M33-A79, *V. parahaemolyticus* region: D71-I123) close crystal contacts bury 48.5% and 57.1% of the total solvent accessible area of CpxA-SD_{EC} and CpxA-SD_{Vib}, respectively. Taken together with the placement of the flexible C-terminal tail of CpxA-SD_{Vib} along the α1 helix, crystal packing artifacts may explain the differences between the two structures, but a definite conclusion cannot be reached without further experiments.

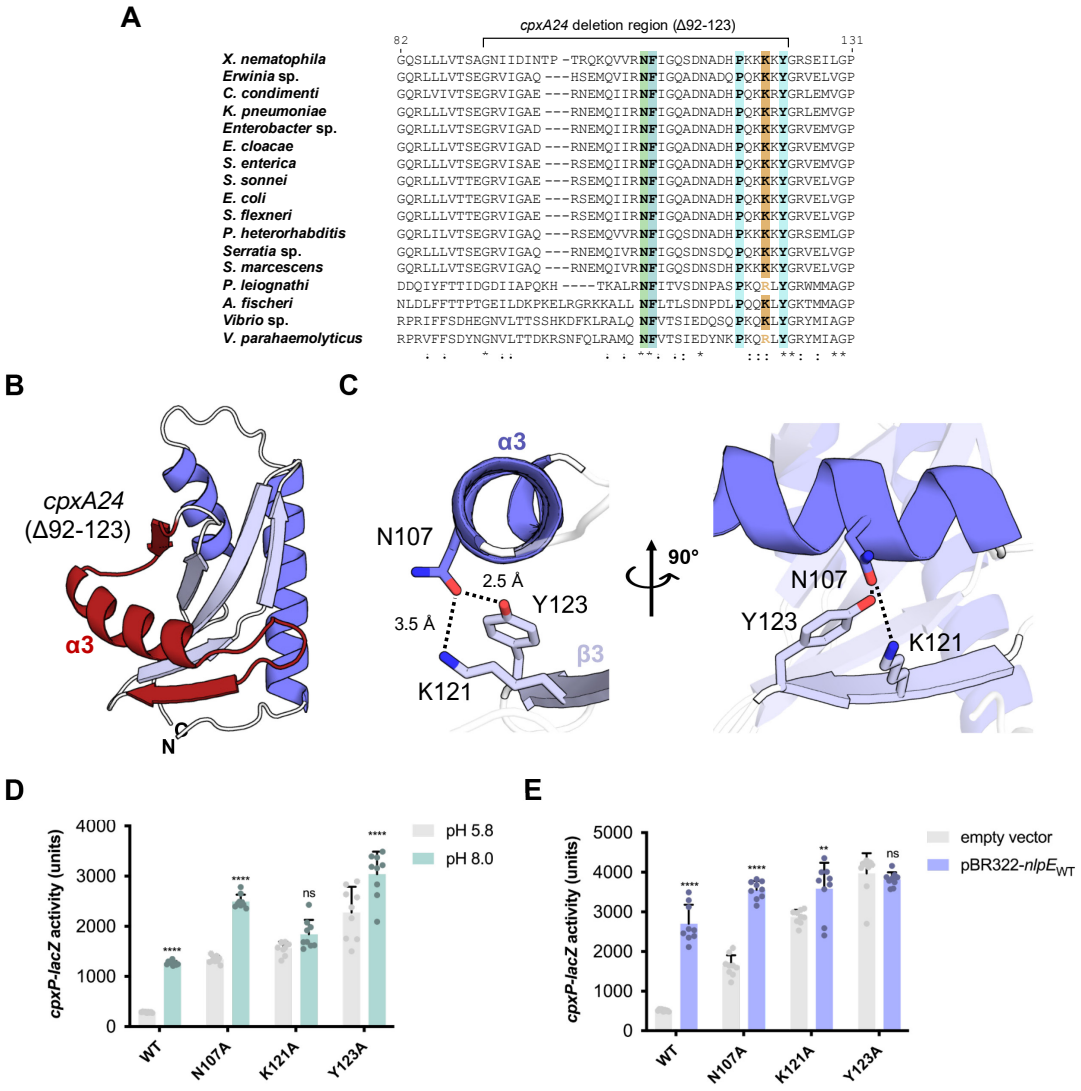

Figure 2-2. Conserved residues in CpxA-SD impact activation.

(A) Multiple sequence alignment of CpxA-SD sequences from multiple organisms shows the conservation of several key residues in the *cpxA24* deletion region (Δ92-123), which is shown on the crystal structure of CpxA-SD in **(B)**. The hydrogen bond network formed by conserved residues N107, K121, and Y123 are shown in **(C)** in two views. Strains expressing chromosomal *cpxA* mutants (N107A, K121A, and Y123A) were tested for their ability to sense alkaline pH **(D)** and NlpE overexpression **(E)**, as measured by the activity of a chromosomal *cpxP-lacZ* reporter. Reporter activity was quantified by measuring β-galactosidase assay. Shown are mean and standard deviation from the pooled data from three independent experiments with three

replicates in each experiment. Significance indicates the results of a two-way ANOVA with post hoc Tukey HSD test that were conducted between induced treatments (pH 8.0 and pBR322-*nlpE*$_{WT}$) compared to either pH 5.8 or empty vector treatments of the same genetic background (** p<0.01, **** p<0.0001, ns = non-significant).

Several residues in the CpxA-SD appear to be conserved across hundreds of organisms. While most of these are hydrophobes buried within the PAS domain, asparagine 107 (N107), lysine 121 (K121), and tyrosine 123 (Y123) are notable exceptions (Figure 2-2A). These residues are also located within the deleted region of the constitutively activated and signal blind *cpxA24* allele (Δ92-123) (Raivio and Silhavy, 1997) (Figure 2-2B) and form a hydrogen bond network connecting the α3 helix and β3 strand in our crystal structure (Figure 2-2C). We hypothesized that this coordination may be important for CpxA activation. To investigate this, we introduced alanine swaps of these residues in the chromosomal copy of *cpxA* and tested the ability of these mutants to sense known Cpx activating signals, alkaline pH and NlpE overexpression (Figure 2-2D,E). Mutating these residues led to higher levels of basal activation of the Cpx response. The K121A and Y123A mutations also reduced sensitivity to alkaline pH and NlpE overexpression, reminiscent of previously identified *cpxA** alleles (Raivio and Silhavy, 1997). CpxA N107A was still activated by these cues, albeit relatively more weakly compared to WT CpxA. Overall, protein levels of CpxA N107A, K121A, and Y123A were comparable to WT CpxA (Figure 2-3). We thus think it is unlikely that the phenotype conferred by these mutations is due to misfolding. Together, these results indicate that these residues are important for regulating CpxA activation, and by extension that interactions affecting α3 positioning play a key role here.

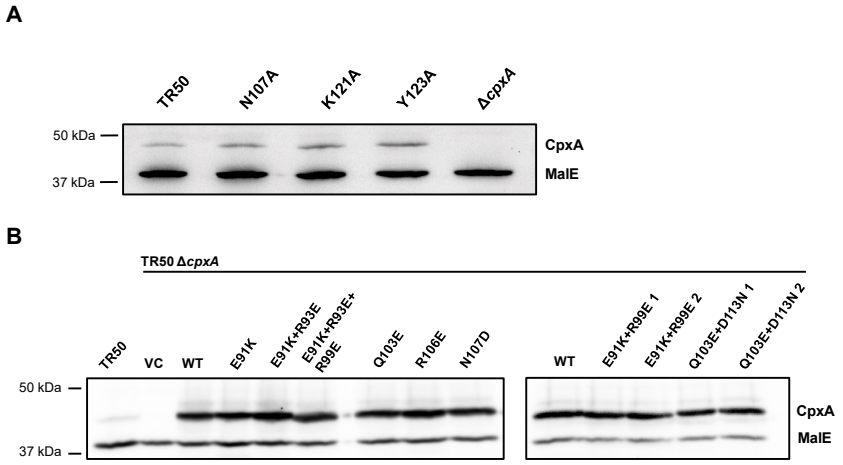

Figure 2-3. Expression levels of CpxA variants.

Expression levels of **(A)** *cpxA* chromosomal mutants and **(B)** plasmid-based mutations of CpxA were determined via Western blots using an anti-CpxA-MBP antibody probing for CpxA from whole-cell lysate.

We wondered if the dimer structure of CpxA-SD would provide further insight into CpxA signaling as dimerization is important for sensor kinase structure and function (Affandi et al., 2016; Bhate et al., 2015; Cheung et al., 2008). The asymmetric unit of the crystal provided a dimer structure of CpxA-SD where the main dimer interface centres around its α1 helices, which cross each other roughly perpendicularly (Figure 2-4A). This structure is somewhat reminiscent of an early structure of the *Salmonella enterica* PhoQ sensor domain dimer possessing similar crossed α1 helices (PDB 1YAX) (Cho et al., 2006), which appears to not be physiologically relevant (Cheung et al., 2008; Goldberg et al., 2008). In line with this, mutation of the M48 residue (M48K), which lies at the main dimer interface of this structure, did not lead to significant changes in activation of CpxA or its ability to sense alkaline pH (Figure 2-4B) or NlpE overexpression (Figure 2-4C), and CpxA M48K was expressed to similar levels as WT CpxA (Figure 2-4D). This was surprising given the importance of sensor kinase dimerization and led us to conclude that this dimer orientation was likely a crystallographic artifact.

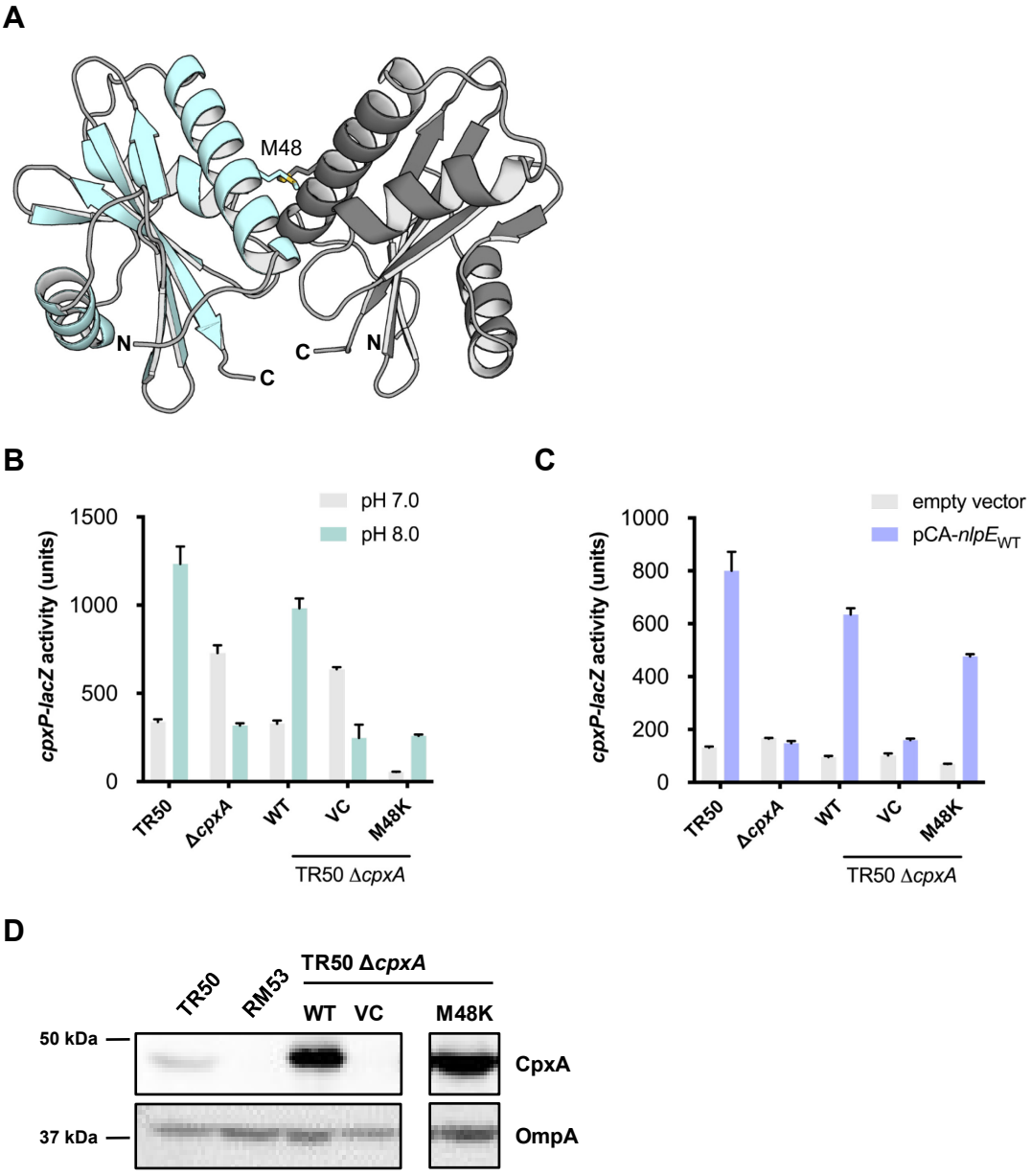

Figure 2-4. Crystal dimer structure of CpxA.

(A) Ribbon cartoon diagram of the dimer with each monomer shown in a different color. The main dimer interface residue M48 is highlighted. The ability of the M48K mutation to sense **(B)** alkaline pH and **(C)** NlpE overexpression, as seen in the activity of a *cpxP-lacZ* transcriptional reporter. Shown are mean with standard deviation of three replicates from three independent experiments. **(D)** shows the expression levels of CpxA in relevant strains as determined by Western blotting with anti-CpxA-MBP antibody. An unrelated protein (OmpA) was used as a loading control.

AlphaFold2 predicts a novel PAS domain dimer organization for CpxA-SD

While sensor kinases are extensively dimerized proteins, the presence of distinct domains in extracytoplasmic, membrane-integral, and cytoplasmic regions of the cell presents significant challenges to studying sensor kinases holistically. To investigate the dimeric structure of CpxA, we used the ColabFold implementation of AlphaFold2 (Jumper et al., 2021; Mirdita et al., 2022) using custom multiple sequence alignments (MSA; see Methods) to model CpxA homodimers. Full length CpxA dimer models were initially generated (data not shown); however, monomers were rotationally symmetric and identical due to limitations in AlphaFold2. This artifactual symmetry resulted in poor alignments between the model and previously crystallized CpxA kinase domains, which possess significant asymmetry (Mechaly et al., 2014) (data not shown). Additionally, any single model AlphaFold2 generates is an average of multiple potential states of CpxA (e.g. active and inactive) (Jumper et al., 2021). This averaging is exacerbated when the difference between the states is greatest, as is seen in the active and inactive states of cytoplasmic kinase domains (Mechaly et al., 2014). To mitigate these issues, we excluded the histidine phosphotransfer (DHp) and catalytic (CA) domains from our modeled complexes, limiting our models to the region encompassing transmembrane helix 1 (TM1), the PAS domain, transmembrane helix 2 (TM2), and the HAMP domain (Figure 2-5A). These smaller models had higher local (pLDDT) and global (pTm) confidence than the full length models, which indicated that these models better represent a single state of CpxA (Figure 2-6) (Jumper et al., 2021). Both *E. coli* and *V. parahaemolyticus* CpxA models were created either terminating at the end of TM2 or the HAMP domain. The top dimer structures were similar for both the *E. coli* and *V. parahaemolyticus* structures, and the inclusion of the HAMP domain did not significantly influence the overall dimer arrangement (Figure 2-5B,C). Notably, the sensor PAS domain

modelled by AlphaFold2 was virtually identical to the structure we solved by X-ray crystallography (Figure 2-7).

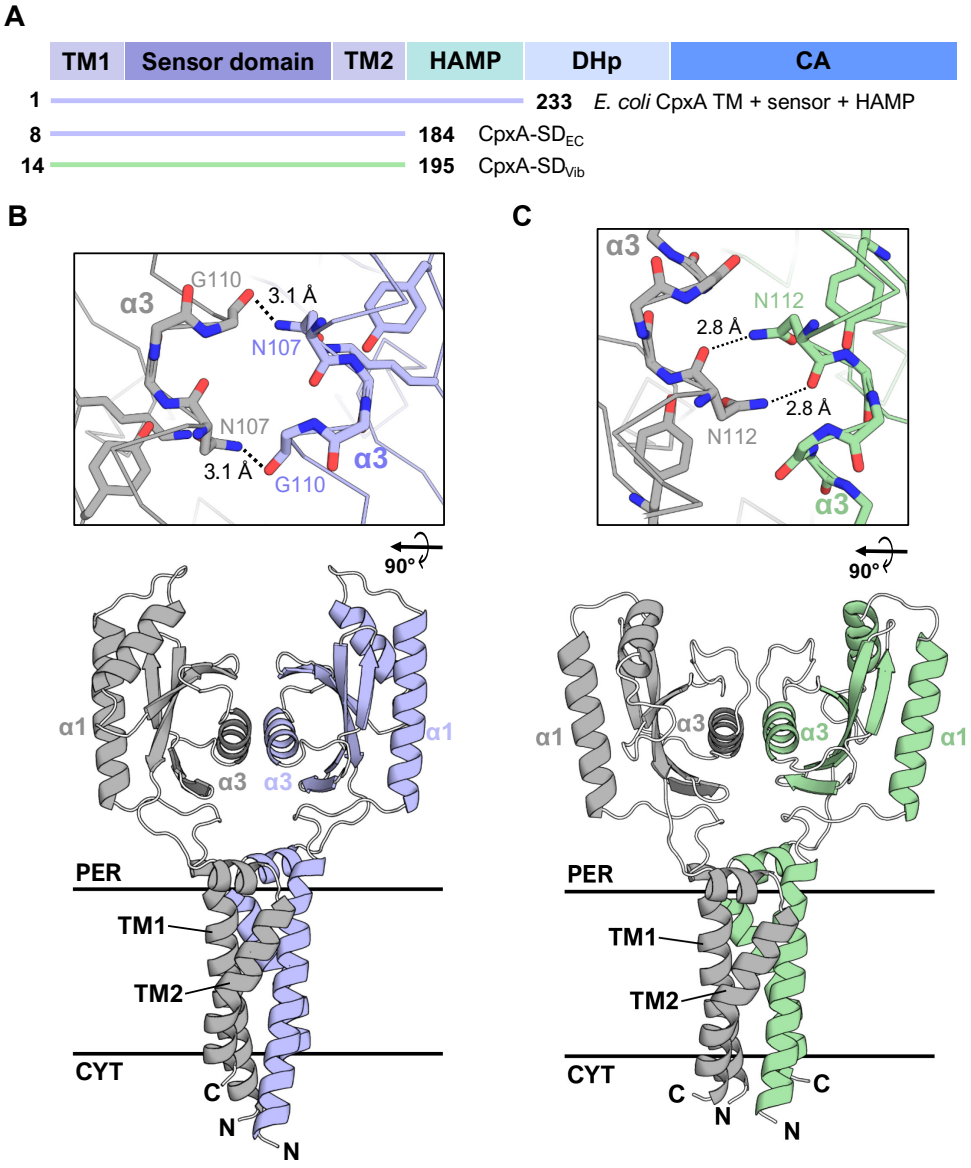

Figure 2-5. AlphaFold2 models of CpxA sensor and transmembrane domain dimers.

(A) Domain architecture of CpxA with the AlphaFold2-modeled portions of each CpxA sequence from *E. coli* (*E. coli* CpxA TM + sensor + HAMP, CpxA-SD_{EC}) and *V. parahaemolyticus* (CpxA-SD_{Vib}). Modelled amino acids numbers are shown alongside each schematic of the modeled region of CpxA. AlphaFold2 models of the sensor and transmembrane (TM1 and TM2) domains of **(B)** *E. coli* and **(C)** *V. parahaemolyticus* CpxA. The α3-α3 dimer interface of both proteins (from a top-down view) is shown in the insets above each of the structures.

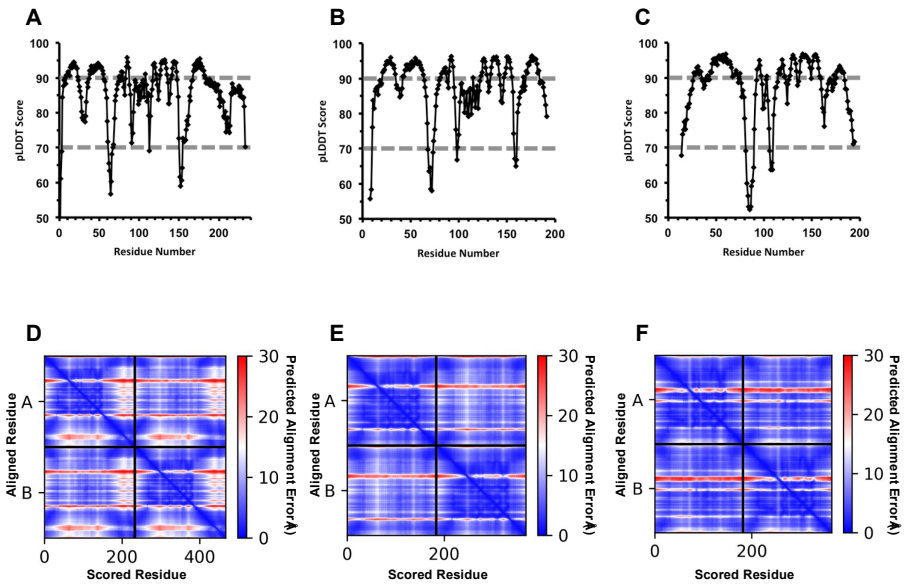

Figure 2-6. AlphaFold2 confidence metrics for *E. coli* and *V. parahaemolyticus* models.

Predicted local distance difference test (pLDDT) scores per residue for CpxA-EC TM1-HAMP **(A)**, CpxA-SD_{EC} **(B)**, CpxA-SD_{Vib} **(C)**. Dashed lines indicate cut offs for very high confidence (pLDDT > 90) and high confidence (pLDDT > 70). **D-F** Predicted alignment error (pAE) within monomers (Top Left and Bottom Right sub-panels) and between monomers (Top Right and Bottom Left sub-panels) for CpxA-EC TM1-HAMP **(D)**, CpxA-SD_{EC} **(E)**, CpxA-SD_{Vib} **(F)**.

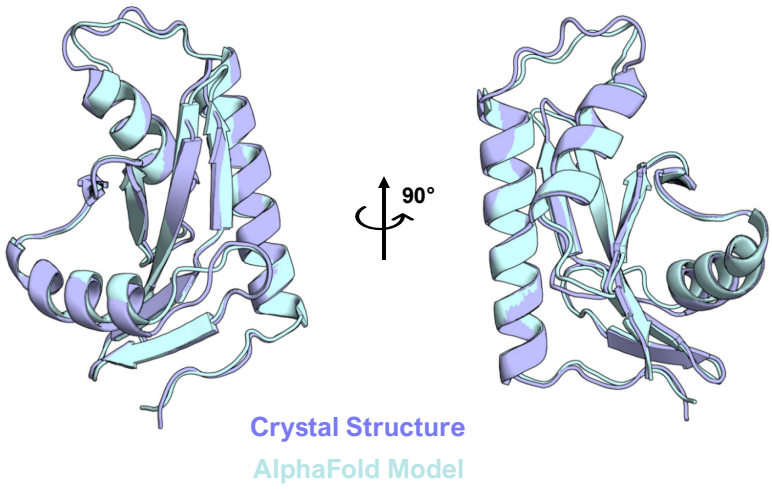

Figure 2-7. Alignment of the crystal structure and AlphaFold2 model monomer of E. coli CpxA-SD.

Structures of the experimentally determined CpxA sensor domain structure and the AlphaFold2 predicted structure were aligned using PyMOL's alignment function.

Both CpxA-SD_{EC} and CpxA-SD_{Vib} were modeled as homodimers with their TM domains in a tight four helix bundle, similar to other histidine kinases (Figure 2-5B,C) (Gordeliy et al., 2002; Moukhametzianov et al., 2006). However, their PAS domains were oriented opposite to those found in most histidine kinases, which are oriented such that the α1 helices form the dimer interface, while the α3 helices are exposed and (usually) involved in ligand binding(Henry and Crosson, 2011). In contrast, the CpxA-SD PAS domains were modelled with the α3 helices forming the dimer interface, placing N107, K121, and Y123 at the interacting surface. The aforementioned *cpxA24* mutation encompasses nearly the entirety of the α3 helix and β3 strand, which comprises the majority of the CpxA-SD dimer interface in the AlphaFold2 model. Importantly, the previously identified N107 residue lies at the dimer interface in the AlphaFold2 models. N107, K121, and Y123 are structurally conserved in both *E. coli* and *V. parahaemolyticus.* K121 and Y123 form a hydrogen bond network with N107 (Figure 2-2C), which has the effect of precisely positioning N107 such that its amine group protrudes towards the other monomer (top inset of Figure 2-5B). In both *E. coli* and *V. parahaemolyticus* models, this central asparagine (N107 and N112, respectively) forms hydrogen bonds with a main chain carbonyl group of the other monomer (top insets of Figure 2-5B,C). While the exact positioning of these hydrogen bonds is modeled differently between CpxA-SD in *E. coli* and *V. parahaemolyticus*, these bounds could limit the inter-monomer flexibility of this dimer orientation in both models. Thus, we reasoned that disrupting these interactions would destabilize the CpxA-SD dimer and impact CpxA activation.

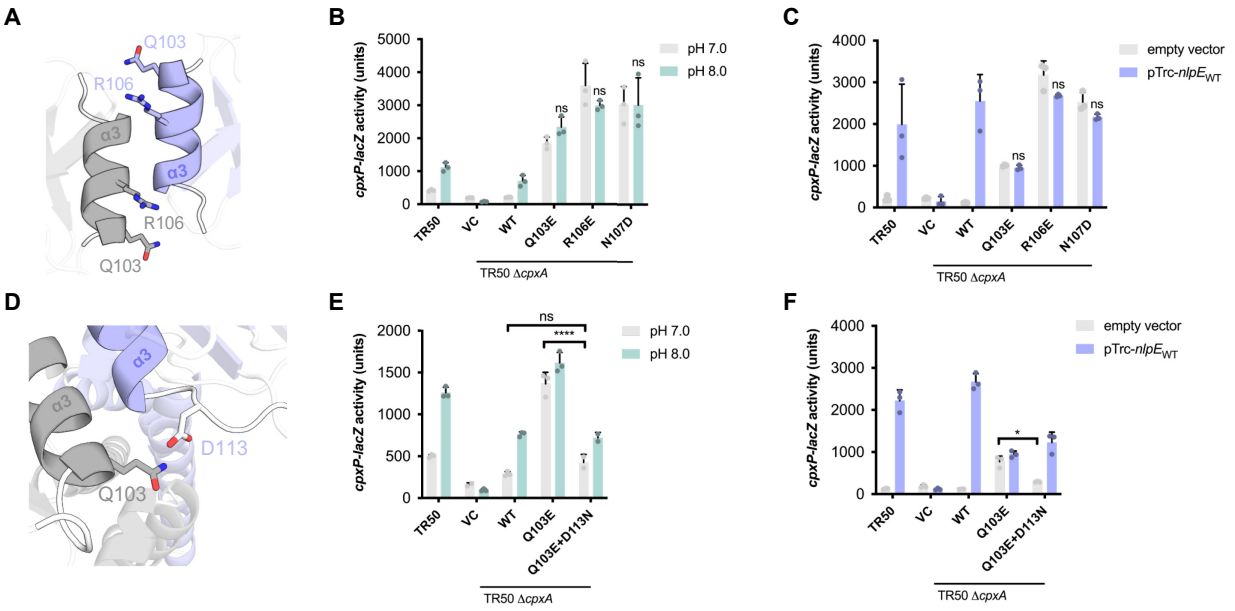

Figure 2-8. Mutations in the dimer interface of CpxA-SD lead to activation.

(A) Other residues on the α3 helix. Residues Q103 and R106 are shown on the AlphaFold2 model of *E. coli* CpxA-SD. The ability of mutants of CpxA Q103, R106, and N107 in *E. coli* to sense alkaline pH and NlpE overexpression are shown in **(B)** and **(C),** respectively. TR50 refers to the WT strain of *E. coli* MC4100 encoding a chromosomal *cpxP-lacZ* reporter. Variants of CpxA were expressed from plasmids in a TR50 Δ*cpxA* background and tested for activation of a *cpxP-lacZ* reporter. **(D)** The position of Q103 and D113 on opposing monomers are shown. The ability of the rescued CpxA Q103E+D113K mutant to sense these signals are shown in **(E)** and **(F)**. Shown are a mean of three independent replicates. Significance indicates the results of a two-way ANOVA with post hoc Tukey HSD test that were conducted between the bars shown in brackets or, in the case that no brackets are shown, compared to either pH 7.0 or empty vector treatments of the same genetic background (* $p<0.05$, **** $p<0.0001$, ns = non-significant).

We further tested the roles of the conserved N107, K121 and Y123 residues and their predicted interactions in *E. coli* CpxA. To facilitate further testing of *cpxA* mutants, we cloned *cpxA* into plasmid pK184 and introduced it into a strain lacking chromosomal *cpxA* and possessing a chromosomal CpxA-regulated *cpxP-lacZ* reporter (TR50). We confirmed that this plasmid-based system complements the phenotype of the Δ*cpxA* mutant as it restored the ability

of the mutant to sense alkaline pH and NlpE overexpression (compare the WT reporter strain TR50 vs the Δ*cpxA* strain expressing CpxA [WT] in Figure 2-8). This was despite the fact that expression from the plasmid was significantly higher than native levels of CpxA (Figure 2-3B). Using this system, we again looked at the function of N107. The higher activation of CpxA N107A suggests the AlphaFold2-predicted dimer interface was physiologically relevant. However, its phenotype could be explained by the alanine substitution disrupting the intra-monomer hydrogen bonding network (Figure 2-2C). Based on the model (Figure 2-5B), we predicted that replacing N107 with an aspartate (N107D) would yield a phenotype specific to interactions between CpxA-SD by introducing repulsion at the interface between monomers while maintaining the hydrogen bonding network between α3 and β2 within the monomer (Figure 2-2C). We also introduced mutations into neighbouring residues Gln103 and Arg106 which reside on the α3 helix and face towards the other CpxA-SD monomer in the AlphaFold2 model (Figure 2-8A). We found that CpxA N107D was hyper-activated in the absence of inducing cues and no longer sensed alkaline pH and NlpE overexpression, resulting in a signal blind phenotype (Figure 2-8B,C). Similarly, CpxA Q103E and R106E showed high levels of activation in the absence of inducing signal compared to WT CpxA and were insensitive to inducing cues (Figure 2-8B,C).

Charge swap mutations at the predicted dimer interface restore signaling

AlphaFold2 modelling predicted that Q103 could hydrogen bond to D113 on the opposing CpxA-SD monomer (Figure 2-8D), leading us to hypothesize that the Q103E mutation results in a charge repulsion between monomers that leads to aberrant CpxA activation. We tested if the hyper-activation of this mutant could be suppressed by re-introducing a hydrogen bond at this position via an asparagine substitution at D113. Strikingly, we observed that Q103E and D113N mutations together suppress the hyper-activation of CpxA Q103E in the absence of

inducing cues (pH 7.0 or empty vector in Figure 2-8E,F). Further, CpxA Q103E+D113N was activated to a similar extent as WT CpxA in the presence of alkaline pH (pH 8.0). As expected, introducing a D113K mutation into CpxA also confers a hyper-activated and signal blind phenotype (Figure 2-9), supporting our hypothesis that disrupting interactions between CpxA-SD monomers leads to inappropriate CpxA activation.

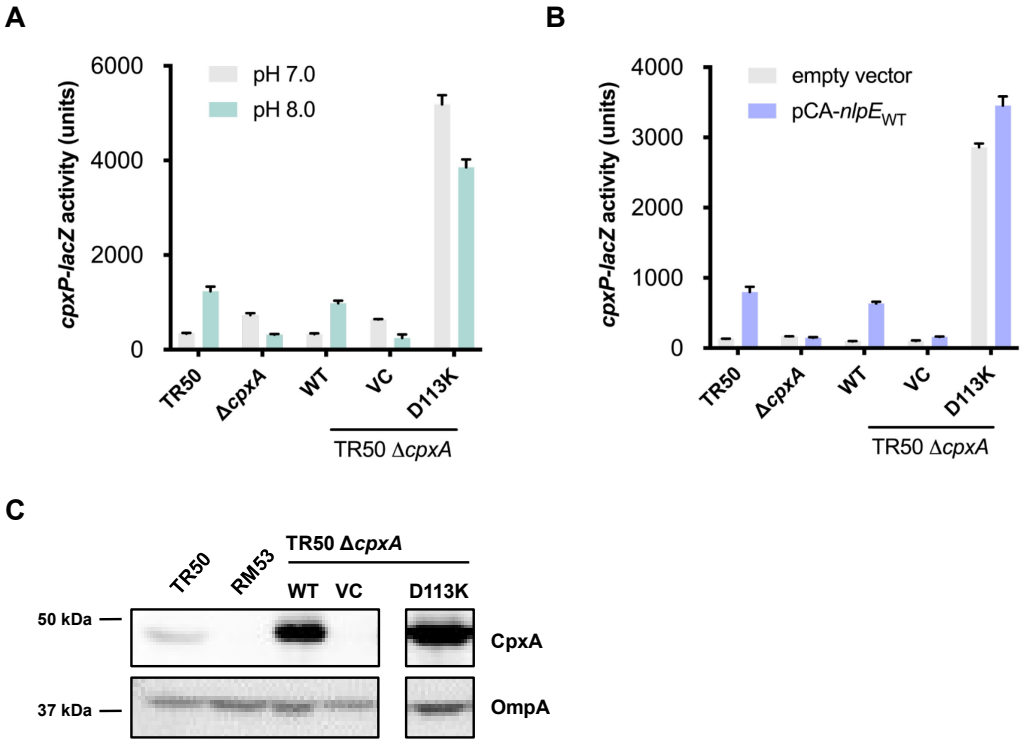

Figure 2-9. CpxA D113K is hyper-activated.

Ability of plasmid-borne CpxA D113K variant to sense **(A)** alkaline pH and **(B)** NlpE overexpression. Shown are mean with standard deviation of three replicates from three independent experiments. **(C)** shows the expression level of D113K compared to WT CpxA by Western blotting. Expression levels of an unrelated protein (OmpA) was used as a loading control.

We observed that strains expressing CpxA Q103E+D113N were induced during NlpE expression but not to the same extent as WT CpxA. However, NlpE expression levels were

greatly reduced in CpxA Q103E+D113N compared to strains expressing WT CpxA (Figure 2-10A). Furthermore, and surprisingly, NlpE expression was abolished in strains expressing CpxA Q103E, explaining the lack of induction seen in this strain and suggesting that post-transcriptional regulation of NlpE may occur and be influenced by certain activated states of CpxA. We note, however, that hyper-activation of CpxA by itself does not appear to lead to this phenotype as NlpE levels were unaffected in the hyper-activated CpxA N107D strain (Figure 2-10B). Together, these results suggest a previously undocumented level of Cpx envelope stress response regulation in which specific states of CpxA may influence the levels of its signaling partner NlpE. This will be an exciting area of further study.

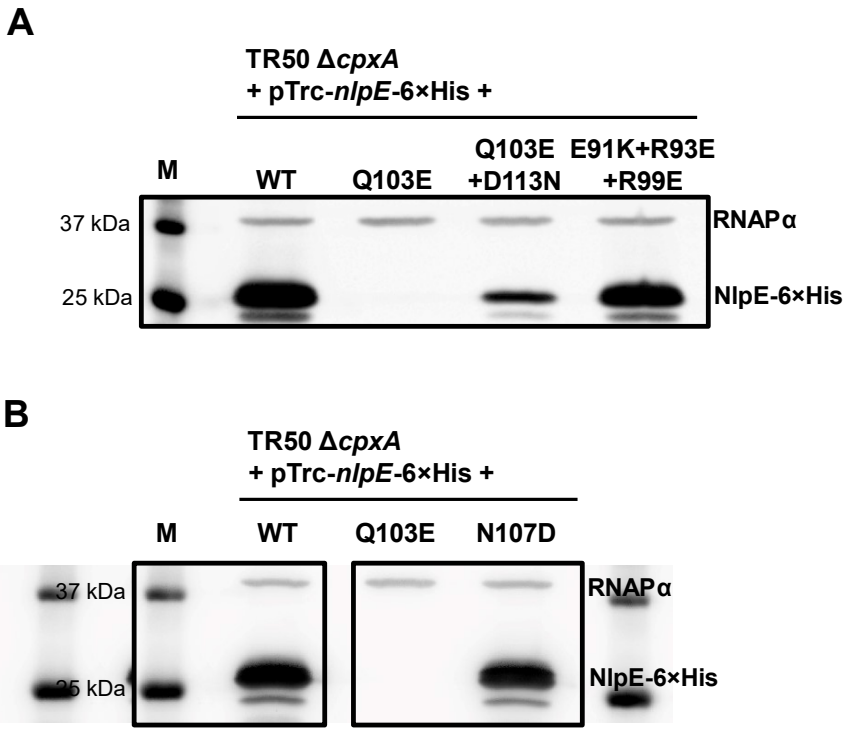

Figure 2-10. Expression levels of NlpE in hyper-activated CpxA strains.

Western blots showing expression levels of His-tagged NlpE in strains expressing CpxA mutants. Strains cultured in identical conditions to reporter assay experiments were harvested, lysed and prepared for SDS-PAGE. After transfer, membranes were probed with antibody raised against RNAP α subunit (loading control) and His×6 (NlpE).

To further test the role of the predicted dimer interface in signaling, we used the AlphaFold2 model to investigate previously identified *cpxA** alleles which map to the sensor domain. *cpxA102* is a single amino acid substitution of a lysine at E91(Raivio and Silhavy, 1997), which maps to the β2 strand that is located towards the top of the dimer interface in the AlphaFold2 model. Further examination of the residues surrounding this allele revealed several nearby positively charged arginines (R93 and R99) at the dimerization interface (Figure 2-11A). While none of these residues are predicted to form hydrogen bonds with E91, we hypothesized that the introduction of a positive charge in this region may introduce repulsion between CpxA-SD monomers, leading to the observed constitutive activation. Based on this hypothesis, we attempted to rescue the hyper-activation of CpxA E91K by introducing negatively charged residues at R93 and/or R99.

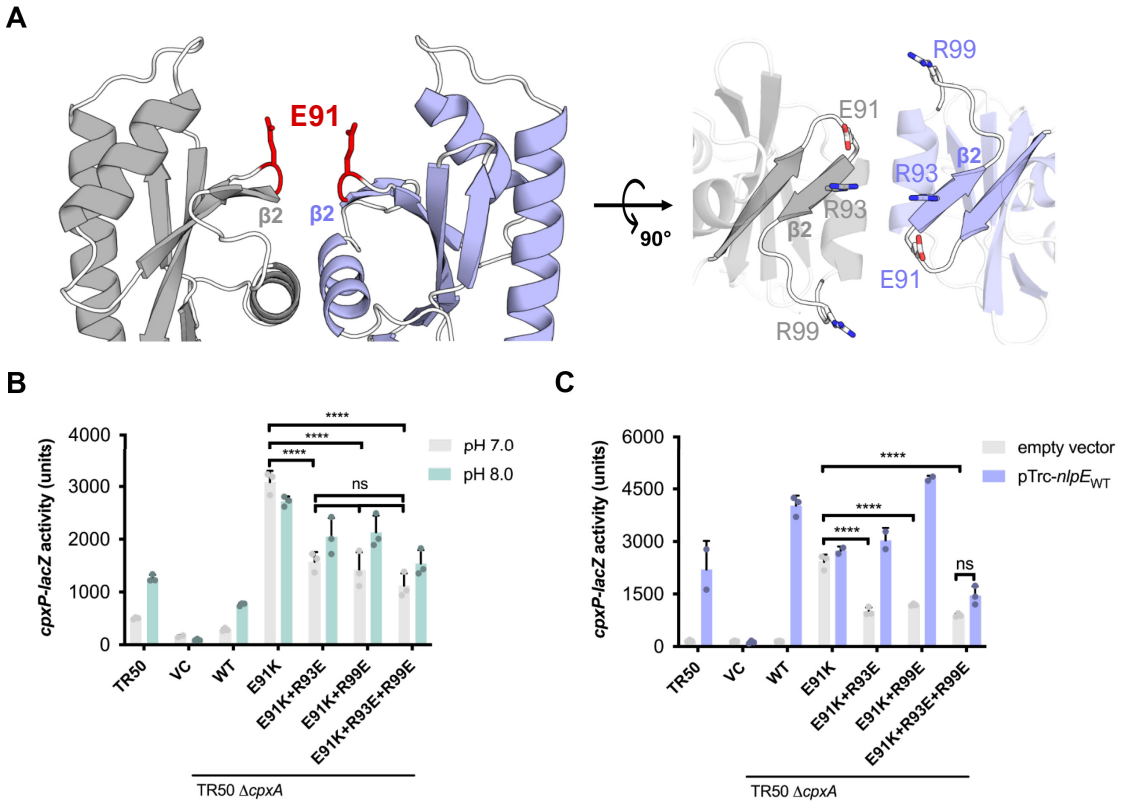

Figure 2-11. Other mutations of CpxA-SD lead to hyper-activation.

(A) shows the location of E91, the residue mutated in the *cpxA102* allele (CpxA E91K). Two views are shown, with surrounding basic residues R93 and R99 shown in the right panel. The ability of E91K-containing mutations expressed from plasmid in a Δ*cpxA* strain to sense **(B)** alkaline pH and **(C)** NlpE overexpression was tested in by assaying the activity of a *cpxP-lacZ* reporter. Shown are a mean of three independent replicates (Tukey HSD post hoc test with two-way ANOVA **** $p<0.0001$, ns = non-significant).

We introduced the E91K mutation singly as well as in combination with mutations predicted to restore wild-type charge to the dimer interface (R93E and R99E) into our CpxA expression vector and measured both the basal activity of these variants and their ability to respond to alkaline pH and NlpE overexpression (Figure 2-11B,C). Consistent with previous studies (Raivio and Silhavy, 1997), we found that CpxA E91K was hyper-activated basally at pH 7 (Figure 2-11B) and in the absence of NlpE overexpression (Figure 2-11C). CpxA E91K was also

insensitive to alkaline pH and NlpE overexpression (Figure 2-11B,C**)**. In line with our hypothesis, the introduction of either R93E or R99E in combination with E91K into CpxA was significantly reduced basal activation, although not completely to wildtype levels. Interestingly both mutations reduced activation to similar extents and there was no additive effect of introducing these mutations in tandem, as the triple mutant (CpxA E91K+R93E+R99E) possessed similar levels of basal activation to the double mutations. These rescued mutations slightly restored the ability of CpxA to sense alkaline pH, as shown by slightly higher activity at pH 8; however, they were significantly less sensitive to pH than WT CpxA. CpxA E91K+R93E and E91K+R99E were sensitive to NlpE overexpression. In contrast, the triple mutant was largely insensitive despite similar levels of NlpE expression to strains with WT CpxA (Figure 2-10A), suggesting this mutant is genuinely blind to NlpE.

Unlike Q103 and D113, these residues are near the previously reported NlpE binding interface (Marotta et al., 2023a) so they could interfere with the binding of NlpE to CpxA; however, this requires further investigation. CpxA expression levels are unlikely to account for any of the observed phenotypes since all of these mutants are expressed at similar levels to WT CpxA from our plasmid (Figure 2-3B). Further, introducing an E91A mutation into CpxA, while leading to higher activation, did not lead to the same level of hyper-activation and signal-blindness as the CpxA E91K charge swap (Figure 2-12). Thus, constitutive activation of *cpxA102* (CpxA E91K) is likely caused by the repulsion introduced by the lysine residue with neighbouring positive residues between CpxA-SD monomers.

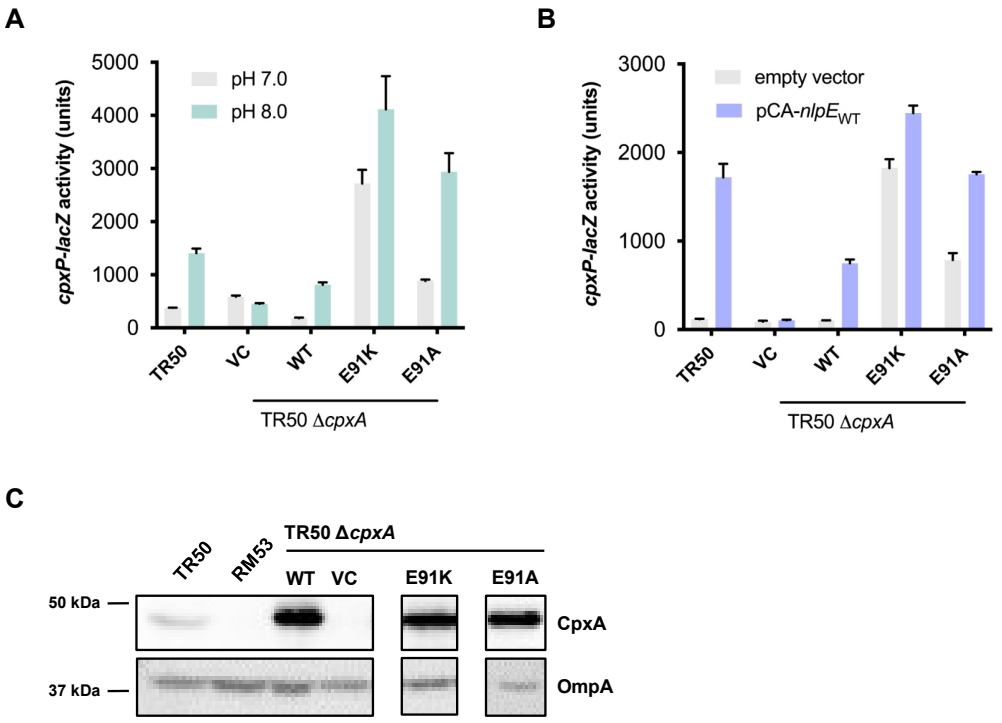

Figure 2-12. Hyperactivation of CpxA E91K depends on its charge swap.

Ability of plasmid-borne CpxA E91K and E91A variants to sense **(A)** alkaline pH and **(B)** NlpE overexpression. **(C)** shows the expression level of D113K compared to WT CpxA by Western blotting. Shown are mean with standard deviation of three replicates from three independent experiments. A blot for an unrelated protein (OmpA) was used as a loading control.

CpxA-SD is a novel dimer of extracytoplasmic PAS domains

These findings suggest that, like the AlphaFold2 model, the α3 helix of the CpxA-SD PAS domain is proximal to the dimer interface while CpxA's α1 helix is distal to the dimer interface. As mentioned previously, this dimer orientation is unusual and, to our knowledge, has not been reported. We verified this by performing a structural homology search using the web server Dali (Holm and Sander, 1995) and the crystal structure of CpxA-SD as a query. This search yielded 700 non-unique molecules with a Z-score greater than two. Among the top hits were the prototypical extracytoplasmic PAS domains of the sensor kinases PhoQ, CitA, and DcuS (Figure 2-13A-C), and other PAS domain sensors (Figure 2-14). While these structures also feature long

α1 helices, their α1 helices are at the dimer interface and are likely continuous with their respective transmembrane domains (Cheung and Hendrickson, 2010). A custom python script was used to search the homologous structures to find any that exhibit a similar dimer orientation to that found in the CpxA AlphaFold2 model. For each PDB entry, each pair of nearby chains in that entry were evaluated to find parallel dimers where the α3 helices are facing each other.

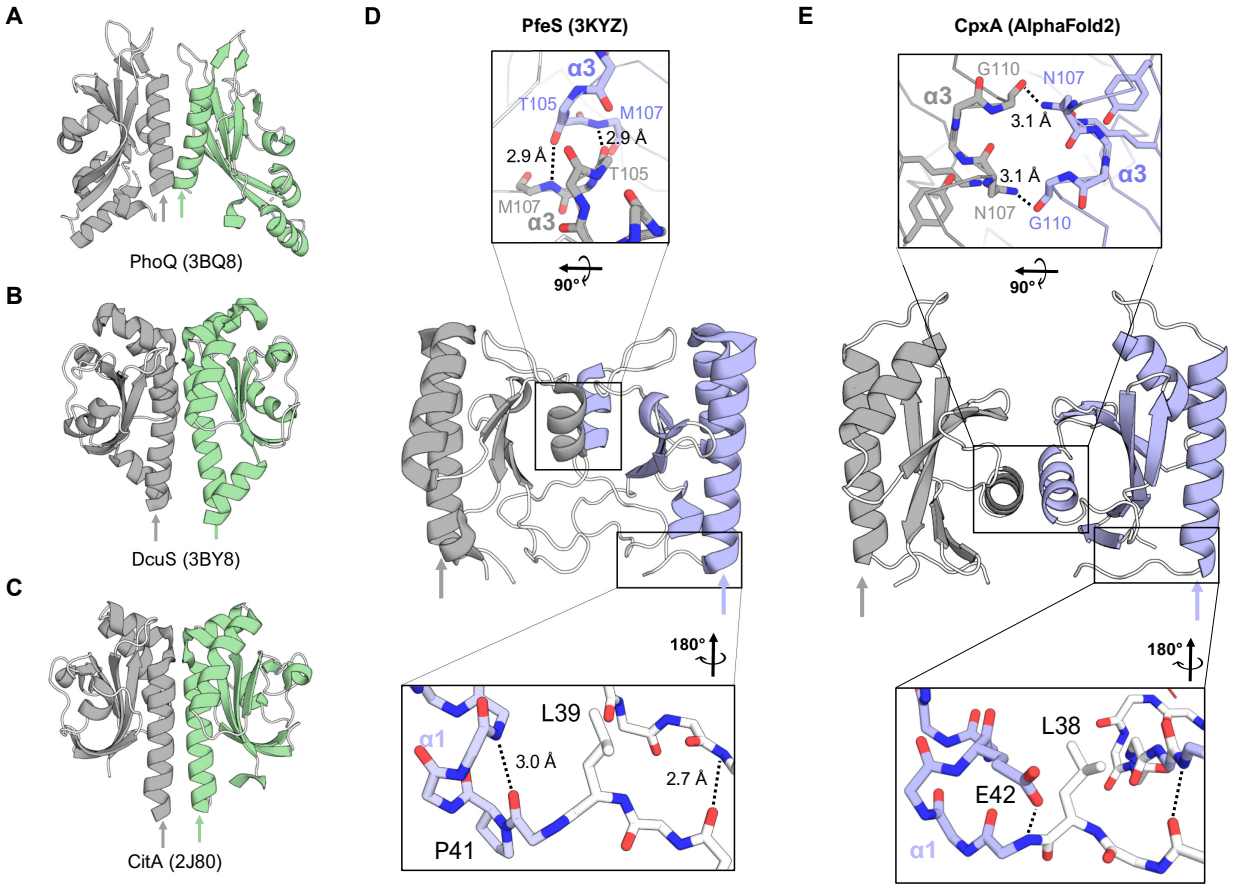

Figure 2-13. The PAS domains of CpxA adopt a novel orientation.

The structures of the representative PAS domains of histidine kinases: **(A)** *E. coli* PhoQ (PDB 3BQ8), **(B)** *Klebsiella pneumoniae* CitA (PDB 2J80), **(C)** *E. coli* DcuS (PDB 3BY8). The crystal structure of the periplasmic domain of enterobactin sensor PfeS (PDB 3KYZ) from *Pseudomonas aeruginosa* is shown in **(D)** with key areas shown as insets above (dimer interface) and below ("bridge") the structure. A parallel comparison to the AlphaFold2 model of *E. coli* CpxA-SD is shown in **(E)**, with corresponding regions also shown in insets.

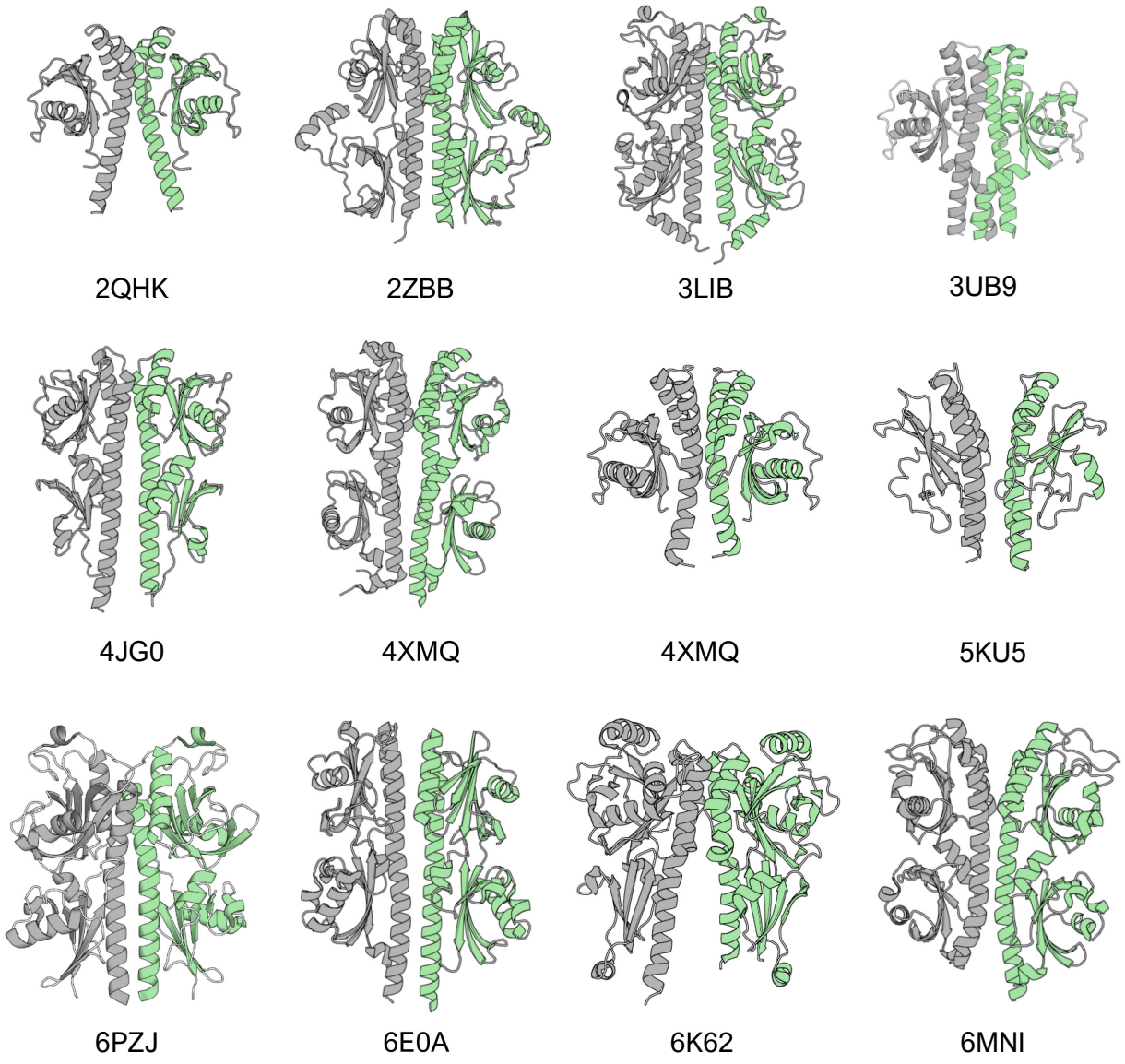

Figure 2-14. More PAS domain dimer hits of CpxA-SD.

Each monomer is represented as a different colored chain (grey vs green). Protein Database (PDB) codes for each structure are listed below.

One hit from our search had striking similarity to CpxA-SD_{EC}: the crystal structure of the periplasmic sensor domain of PfeS (PDB 3KYZ), a sensor of enterobactin from *Pseudomonas aeruginosa* (Figure 2-13D) (Dean et al., 1996; Dean and Poole, 1993). The PfeS dimer interface also centres on its α3 helix while its α1 helix is oriented towards the outside of the protein. At the

dimer interface, symmetrical hydrogen bonds between the α3 helices (T105-M107 in the case of PfeS, N107 in CpxA; top insets of Figure 2-13D and E) are present near the axis of rotation, and the N-terminus of the PfeS α1 helix possesses a proline containing N-cap preceded by a leucine in the same orientation as CpxA-SD_{Vib} and CpxA-SD_{EC} (compare bottom insets of Figure 2-13D and E). Since an N-cap at the α1 helix appeared to be characteristic of this dimer form, a second search of the Dali hits was performed to find monomers that possessed such an N-cap. This search revealed many α1 N-cap containing PAS structures, including soluble and membrane-bound histidine kinases. While most of the histidine kinases were crystallized as α1-helix dimers, one structure of the complex carbohydrate sensor AbfS from *Cellvibrio japonicus* (PDB 2VA0) (Emami et al., 2009) was not and represents another potential α3-helix-dimer candidate, suggesting novel CpxA-like PAS dimers may be more prevalent across histidine kinases.

We propose that the extracytoplasmic PAS domains of CpxA, while adopting essentially the same overall fold as other PAS domains, has evolved to adopt a distinct dimer conformation which may be present in other PAS domain-containing histidine kinases. Interestingly, CpxA, like PfeS, has been implicated in sensing enterobactin or enterobactin-related signals; periplasmic accumulation of enterobactin or vibriobactin is thought to strip iron from membrane-integral iron-sulfur cluster-containing proteins, disrupting protein folding and activating CpxA (Guest et al., 2019; Kunkle et al., 2017). While PfeS appears to sense enterobactin to combat iron starvation (Dean et al., 1996; Dean and Poole, 1993), the structural and sensory parallels between these proteins may point to a signaling mechanism unique to this dimeric arrangement of PAS domains.

Discussion

The extracytoplasmic PAS domains of histidine kinases play a key role in signal sensing and controlling kinase activity. In this study, we report the crystal structure of CpxA's PAS domain and use AlphaFold2 to investigate how this domain regulates CpxA activation. Our results suggest that interactions between residues at the novel CpxA-SD PAS dimer interface regulate CpxA's kinase activity. Because disturbance of this interface almost invariably results in aberrant CpxA activation, the basal state of the CpxA kinase domains is likely kept OFF by inhibitory interactions between CpxA-SD monomers. This is reminiscent of findings in other sensor kinases and sensory proteins. Lee and colleagues propose that the N-terminal PAS (PAS-A) domain of the sporulation regulator KinA of *Bacillus subtilis* regulates kinase activation by its dimerization state (Lee et al., 2008). In a model with many parallels to our own, dimeric PAS-A represents a basal or kinase off state of KinA, while monomeric PAS-A corresponds to activation of KinA. This model was based on studies of bacterial phytochromes which found that in activated proteins, N-terminal sensor domains are distal, while being dimeric in inactive conformations (Evans et al., 2006). Despite the fact that both of these proteins are cytoplasmic, soluble histidine kinases, their extensive dimerization is shared with membrane-bound histidine kinases. While there appears to be some controversy about the exact contribution of the PAS-A domain to KinA function (Kiehler et al., 2017), this model nonetheless provides an interesting parallel to our own model of how PAS sensor domain dimerization regulates activation in the context of a highly dimerized protein.

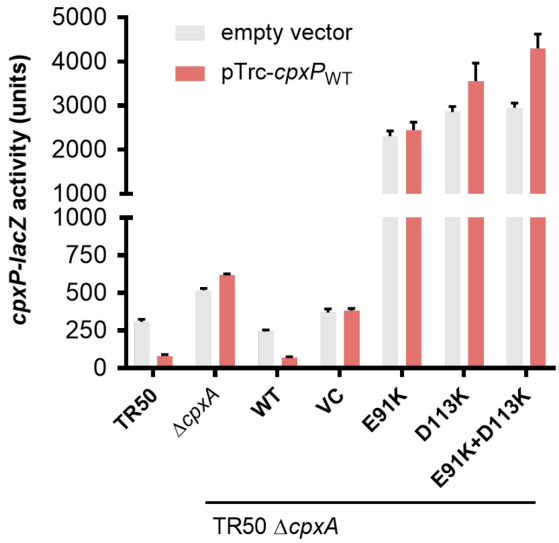

Figure 2-15. The ability of hyperactivated CpxA variants to sense CpxP overexpression. CpxP was induced from plasmid pTrc-*cpxP* with 0.1 mM IPTG for 2 hours after cells reached mid-log phase. The activity of a *cpxP-lacZ* reporter was used to measure activation of CpxA. Indicated CpxA variants were expressed from plasmid pK184. Shown are mean with standard deviation of three replicates from three independent experiments.

Previous studies have suggested that CpxA is biased towards an OFF state by interaction with the periplasmic chaperone-like protein CpxP. Evidence supports a model where CpxA is shifted towards the active state by sequestration of CpxP through its interaction with misfolded protein substrates (Tschauner et al., 2014). However, deletion of *cpxP* does not lead to full activation of the Cpx response, and inhibition of CpxA by CpxP overexpression does not occur in *cpxA** strains (Raivio et al., 1999). In line with these results, we found that hyper activating mutations in the sensor domain, such as CpxA E91K and D113K, are insensitive to CpxP overexpression (Figure 2-15). Further, ratio of CpxA to CpxP present in the periplasm is unlikely to be one to one. While CpxP and CpxA appear to be translated at similar levels (Li et al., 2014), the protein levels of CpxP are heavily regulated by proteolysis such that CpxP is only detectable by Western blot when DegP, the protease responsible for CpxP degradation, is deleted or if the

Cpx response is strongly activated (Isaac et al., 2005). Because it is unlikely that there is a CpxP molecule for every CpxA molecule present in the envelope, it is unlikely that CpxP is fully responsible for maintaining CpxA in an OFF state, suggesting additional, CpxA-inherent mechanisms control the activation of CpxA in the absence of inducing cues.

The behaviour of our dimer interface mutants also warrants a contrasting comparison to the sensor domain of PhoQ. Dimerization of the sensor domain of PhoQ has been extensively characterized (Cheung et al., 2008; Goldberg et al., 2008); monomer-monomer interactions in the sensor domain of PhoQ appear to control PhoQ activation, as disrupting the dimer interface abrogates low magnesium sensing. However, it does not lead to constitutive activation like mutating CpxA's dimer interface (Cheung et al., 2008). Thus, the dimer interface of PhoQ may play an important role in facilitating activation. In line with this, Mensa and colleagues observed that the PhoQ sensor domain appears to favour an "ON" state, as seen in experiments mutationally decoupling sensor, HAMP, and catalytic domains (Mensa et al., 2021). Because the dimer interface of CpxA-SD is sensitive to mutations, which tend to have activating effects, relatively modest dimer interface of CpxA-SD may increase sensitivity to signals present in the periplasm, such as the presence of a broad range of misfolded proteins or small changes in the levels of interacting partner proteins such as CpxP or NlpE. This sensitivity may also be linked to sensing deformations in the membrane such as defects in translocation through the Sec pathway (Shimohata et al., 2002), respiratory complex assembly (Guest et al., 2017; Tsviklist et al., 2022), or changes in membrane composition (Danese et al., 1998; Mileykovskaya and Dowhan, 1997). However, the molecular basis for how CpxA senses misfolded proteins in the periplasm remains unclear. In comparison to other PAS domain containing sensor kinases, studies of CpxA may be hampered by the lack of known small molecule ligands for CpxA. Thus, future studies should focus on CpxA's known protein partners, as direct binding of NlpE to CpxA

appears to activate CpxA (Delhaye et al., 2019; Marotta et al., 2023a; May et al., 2019). CpxP overexpression and interaction inhibits basal kinase activity of CpxA (Raivio et al., 2000, 1999; Raivio and Silhavy, 1997), suggesting that CpxP may act predominantly as a factor to stabilize CpxA sensor domains to dull activation of CpxA in a negative feedback mechanism. Further structural studies of the sensor domain of CpxA in these contexts may shed more light on how the non-typical PAS orientation of CpxA regulates kinase activation.

Our work shows that previously characterized and structure-guided *cpxA** mutations are likely to alter signaling by impacting folding within monomers (Figure 2-2) and/or those between monomers at a novel dimer interface (Figures 1-8, 1-11). We therefore further investigated how other previously isolated *cpxA** mutations might affect the structure of CpxA, potentially providing insight into how CpxA transmits signals from the periplasm. Interestingly, we identified two domain-domain interface regions where clusters of *cpxA** alleles have been found to map, namely, the PAS-TM interface and the TM-HAMP interface.

The crystal structures of CpxA-SD_{EC}, CpxA-SD_{Vib}, and PfeS all possess an α1 helix that is preceded by a seemingly unstructured tail (Figure 2-5B,C). The existence of this region does not seem to be a coincidence since such a region would be required to accommodate the novel dimer orientation of CpxA while maintaining both the overall domain organization and tightly packed TM bundle exhibited in histidine kinases (Bhate et al., 2015). In the AlphaFold2 models, we see exactly that; this region links α1 to TM1 and forms the PAS-TM interface. The most notable similarity in the three crystal structures was an N-cap motif at the N-termini of the α1 helix. N-cap motifs are diverse in sequence and stabilize exposed N-terminal main chain amines of the helix (Figure 2-13D,E lower inset) (Newell, 2015). These motifs are seen in 92.2% (296/321) of analyzed CpxA homologues, with the other 7.8% (25/321) possessing motifs that are found in known N-caps but are not traditional capping box motifs (Figure 2-16). The N-cap

motif in all three structures is preceded by a leucine or isoleucine, which is present in 89.4% (287/321) of analyzed CpxA homologues with other branched hydrophobes (methionine and valine) making up a further 8.4% (27/321).

A

	...[EQH]	...[DN]	Other	Total
P...	93	6	56	155
[STDN]...	42	9	21	72
[QE]...	24	4	7	35
Other	45	14	0	59
Total	204	33	84	321

B

	...[EQH]	...[DN]	Other	Total
P...	0	0	0	0
[STDN]...	3	0	63	65
[QE]...	1	0	109	110
Other	16	2	128	146
Total	20	2	299	321

Figure 2-16. Conservation of N-capping motifs in *cpxA* sequences.

(A) shows sequence motifs that are present at the N-cap site. **(B)** shows the lack of the presence of N-capping motifs in sequences immediately following the N-cap position in CpxA-SD_{EC} and CpxA-SD_{Vib}.

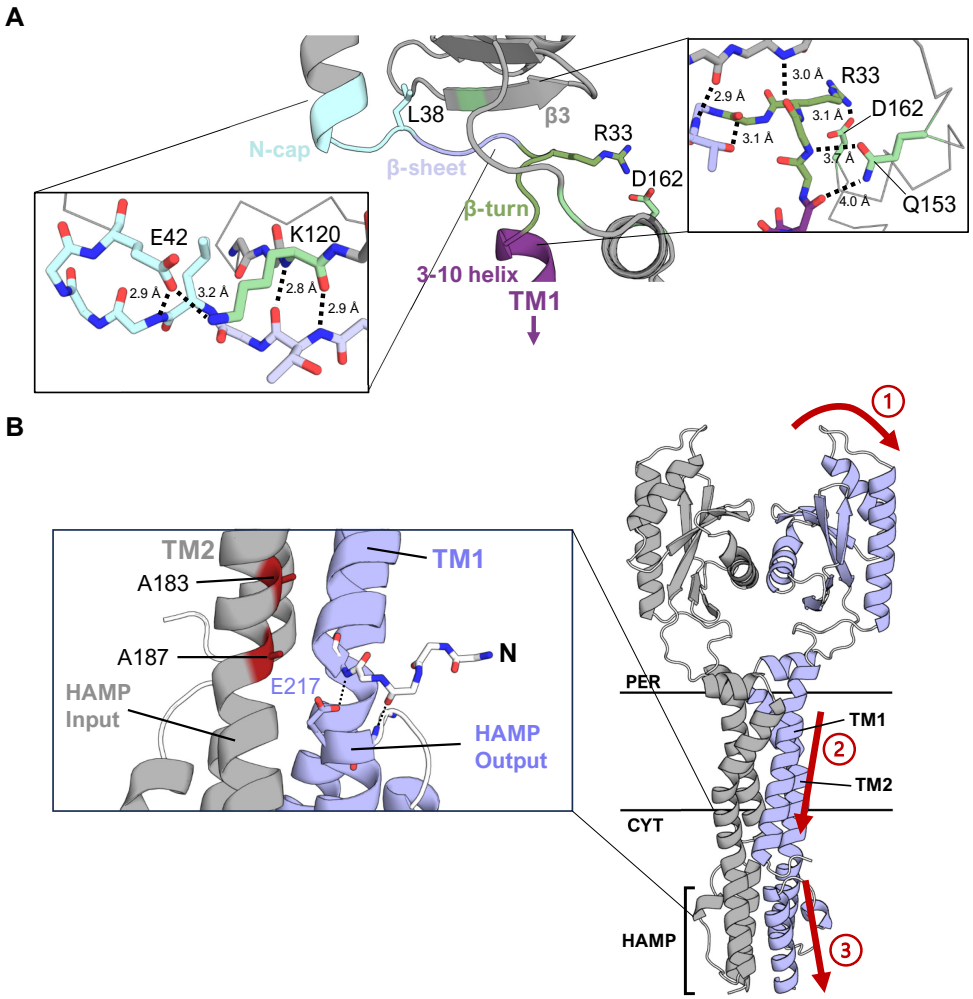

Figure 2-17. The AlphaFold2 model explains the phenotypes of mutants in other regions of CpxA.

(A) The bridge region from the AlphaFold2 model of CpxA-SD_{EC} is shown with key elements colour coded. Insets show rotated and zoomed in stick models of those regions with pertinent predicted interactions shown with distance measurements. A 3-10 helix is a helix where the i-th residue hydrogen bonds to the i+3 residue instead of α helical i to i+4 hydrogen bonding. **(B)** The AlphaFold2 model of CpxA including the HAMP domain. Inset shows previously identified mutations neighbouring the HAMP domain which lead to activation of CpxA. Red arrows show a tentative mechanism of how signals are transduced from the sensor domain to the HAMP domains based on data presented in this paper as well as historical data.

The level of structural and sequence conservation suggests this is a critical region for protein function. Indeed, an L38P (*cpxA9*) mutation was reported to strongly activate CpxA

kinase activity (Keller et al., 2011; Rainwater and Silverman, 1990), despite prolines being common in *cpxA* sequences at flanking residues 37 and 39. Based on structures of N-caps with proline at this position, it's likely that this mutation promotes backbone conformers other than those seen in the crystal structure (Newell, 2015), possibly decoupling the main PAS fold of CpxA from the first TM domain. Other small secondary structure elements exist N-terminal to the N-cap that bridge the PAS and TM1 domains in the AlphaFold2 models (Figure 2-17A). In CpxA-SD_{EC}, these elements are tethered to TM2 via Q153 and the salt bridge between R33 and D162, which appears to be highly conserved (Figure 2-17A). Two other *cpxA** alleles (Raivio and Silhavy, 1997), *cpxA104* (CpxA R33C) and *cpxA103* (CpxA R163P) likely act by disrupting this salt bridge either directly, in the case of *cpxA104* (CpxA R33C), or indirectly by significantly altering the position of D162 (CpxA R163P, *cpxA103*) (Cosma et al., 1995b; Raivio and Silhavy, 1997). Similar to our observations of the CpxA PAS domain dimer, our model suggests that interactions in this bridge region stabilize an OFF state. The fact that all of these mutations lead to aberrant activation of CpxA suggests that activation of CpxA likely involves signals being transduced from the PAS domain through this linker either directly to TM1 or indirectly to TM2.

Further insights into signal transduction by CpxA can be gleaned from mapping other *cpxA** mutations onto the AlphaFold2 model including the cytoplasmic HAMP domains directly following the TM domains (Figure 2-17B). In this model, the N-terminus of the first TM domain packs against the top of the output helix of the HAMP domain. At the cytosolic end of the TM bundle, A183 and A187 are modeled to pack against TM1 of the opposing dimer close to where TM1 contacts the output helix of the HAMP domain (Figure 2-17B). These positions show strong selection for small residues such as Ala, Gly, Ser and Thr, resembling GxxxG motifs (Teese and Langosch, 2015). Previous studies have identified activating *cpxA** mutations *cpxA711* (CpxA A183T) and *cpxA17* (CpxA A187E) in this region (Cosma et al., 1995b; Raivio and Silhavy,

1997). Disruption of this tight packing through mutations of A183T or A187E would perturb the modeled interaction between the highly conserved glutamate (E217) on the output helix of the HAMP domain and the N-cap of TM1. Breaking this conserved interface between signal transduction domains is likely to affect CpxA's activity and would represent a large change from the AlphaFold2 model, which appears to represent a basal state of CpxA, implying that TM1 mobility is important for signal transduction from the periplasmic PAS domain. The AlphaFold2 models of $CpxA_{EC}$ along with our, and previously published, mutation data suggest an overall signal path for CpxA. Disruption of interactions between the PAS domains causes signal to be transmitted through the PAS-TM1 linker to TM1, which carries the signal through the membrane. The N-terminus of TM1 interacts with the output helix of the HAMP domain which passes signal to the kinase domains (Figure 2-17B). This model will be a useful generalization to guide further study of signal transduction in CpxA and other histidine kinases.

Conclusion

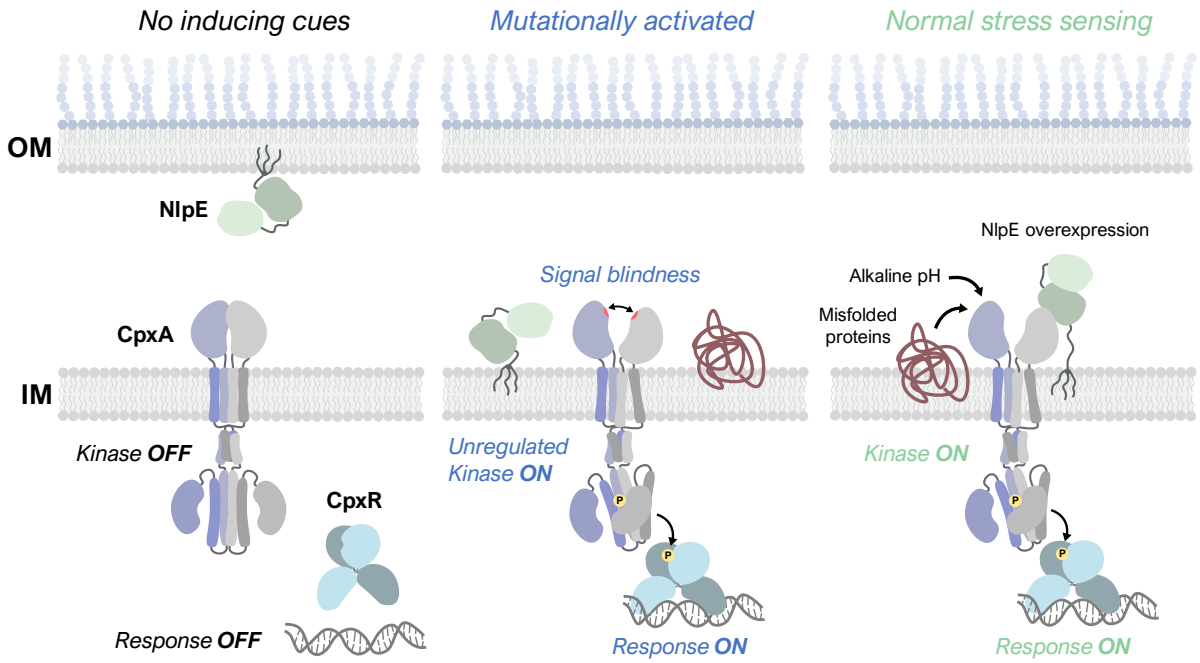

Figure 2-18. The novel organization of PAS domain dimers in CpxA regulates its activity.

In the absence of inducing cues, CpxA is kept off by interactions between its PAS domains. Aberrant activation by mutations disrupting monomer-monomer interactions alter the structural relationship between the PAS and transmembrane domains. Thus, normal sensing CpxA likely involves relief of this auto-inhibition and transduction of signals through the PAS-TM interface.

Despite the crucial role of sensor domains of histidine kinases in initiating kinase activation, considerable mystery remains as to how these sensor domains function due to both the diversity of the signals sensed by these proteins and the structures of their sensor domains (Gao and Stock, 2009; Mascher et al., 2006). While CpxA contains a PAS domain that is largely similar to the PAS folds of other sensor kinases, CpxA's "non-canonical" dimer structure regulates its ability to sense periplasmic triggers (Figure 2-18); diverse inputs that disrupt the stability of the CpxA-SD dimer appear to activate CpxA kinase activity. This is clearly indicated by mutations that disrupt dimerization leading to activation, whereas mutations restoring dimer

stability rescue CpxA's basal OFF state. We hypothesize that activating signals might work by a similar mechanism of destabilizing the CpxA-SD dimer. Further work is required to test this model in the context of known CpxA inducing signals, such as the presence of unfolded proteins, high pH, and NlpE binding.

Structural studies of histidine kinases have tended to focus on domains in isolation because of the modular organization of these proteins. The AlphaFold2 model of CpxA homodimers provides a basis to explain the phenotypes of previously described and novel mutations using a model of CpxA-SD in the context of its transmembrane and cytoplasmic domains. While experimentally determined, full-length structures of sensor kinases remain elusive, studies incorporating machine-learning based protein structure prediction tools and experimental approaches may provide a more holistic picture of how these proteins function and shed light on both the unity and diversity present in the broadly distributed family of PAS sensory folds.

Materials and Methods

Strains and growth conditions

All strains used in this study are listed in Table 2-2. Strains were cultured in lysogeny broth (LB; 10 g/L Bacto-Tryptone, 5 g/L Bacto-Yeast Extract, 5 g/L sodium chloride) with appropriate antibiotics (50 µg/ml kanamycin; 100 µg/ml ampicillin). Experiments involved in alkaline pH sensing used LB media containing 100 mM 3-(*N*-morpholino)propanesulfonic acid (MOPS) with pH adjusted with sodium hydroxide to pH 7.0 or 8.0 or LB media buffered with 100 mM sodium phosphate with pH adjusted to 5.8 (non-inducing) or 8.0 (inducing). A final concentration of 0.1 mM IPTG was used in experiments to induce NlpE or CpxA expression from plasmids. All cultures were grown at 37°C with shaking at 225 RPM.

Strain construction

A list of primers used in this study are listed in Table 2-3. RM53 (TR50 Δ*cpxA*) was created by P1 generalized transduction using lysates generated from the Keio collection of mutants as previously described (Baba et al., 2006). Kanamycin resistance cassettes were removed using plasmid-based expression of the Flp recombinase as previously described (Hoang et al., 1998). Strains encoding for *cpxA* chromosomal mutants N107A, K121A, and Y123A were generated by using site-directed mutagenesis and λRed recombination(Datsenko and Wanner, 2000). The native *cpxA* chromosomal locus was replaced with a counter-selectable *cat-sacB* cassette(Thomason et al., 2014), which was amplified with 50 bp of homology to the 5' and 3' ends of *cpxA* using the primers in Table 2-3**,** by an initial round of λRed recombination. Successful recombination was confirmed by chloramphenicol resistance and sucrose sensitivity.

A plasmid encoding *cpxA* with each of the aforementioned mutations were generated by replacing the *cpxA* locus of plasmid pCA-*cpxA* from the ASKA library in the pCA24N plasmid backbone (Kitagawa et al., 2006). Site-directed mutagenesis was conducted as described by Ko and Ma (Ko and Ma, 2005). Briefly, the regions upstream and downstream of the codon to be mutated were amplified separately by PCR. Each product was amplified with one primer containing an SfiI site for cloning into pCA24N and the other being a mutagenic primer containing an EarI site (Table 2-3). Both products were digested with EarI and ligated to yield an SfiI-flanked product with the desired alanine substitution. This product was purified with a QIAquick PCR purification kit (QIAGEN), digested with SfiI, and ligated into SfiI-digested pCA-*cpxA* to yield pCA24N-based vectors with *cpxA* harbouring the desired mutations.

These plasmids were then used as templates to generate PCR fragments containing each *cpxA* variant flanked by about 40 bp to the 5' and 3' ends of the *cpxA*::*cat-sacB* region for a second round of λRed recombination. These fragments were then electroporated into MC4100 *cpxA*::*cat-sacB* containing the λRed system, and successful recombinants were selected by screening for growth on sucrose and sensitivity to chloramphenicol, and mutations were confirmed by sequencing. Finally, a *cpxP-lacZ* reporter carried on a recombinant λ phage was moved into all mutant strain backgrounds using two P1 transductions. First, a *nadA*::Tn10 allele tightly linked to the λ attachment site which confers resistance to tetracycline and the inability to grow on minimal media (MM) was transduced into the mutant strains. Tet^R and MM^- transductants were used in a second transduction with P1 lysate prepared from TR50 (IRS88 *cpxP-lacZ*) (Raivio and Silhavy, 1997). Lac^+ transductants were selected on minimal media containing X-gal, and these transductants were screened for sensitivity to tetracycline to yield the strains used in experiments.

Plasmid construction

A list of plasmids used in this study are listed in Table 2-4. Expression vectors for CpxA were created through standard molecular biology techniques. For the crystallization construct, the predicted periplasmic domain of CpxA (amino acids 31-163) was amplified from *E. coli* MC4100 using primers 5'-31 and 3'-163 (Table 2-3) with BamHI and EcoRI restriction sites. Amplified $cpxA_{31\text{-}163}$ was cloned into BamHI/EcoRI-digested pGEX-6P-1 expression vector (GE Healthcare), which encodes for an N-terminal glutathione S-transferase (GST) tag and PreScission™ Protease cleavage sites.

The pK184-*cpxA* vectors used in reporter experiments was generated using restriction digest cloning procedures. Because *cpxA* contains an internal EcoRI cut site, plasmid pK184 was digested with EcoRI, treated with the Klenow fragment and religated to eliminate this site. *cpxA* coding sequence was amplified from pCA-*cpxA* (Kitagawa et al., 2006) with flanking BamHI-HindIII sites added using primers listed in Table 2-3. After PCR amplification, BamHI and HindIII (Invitrogen) digested *cpxA* PCR product was ligated into BamHI and HindIII digested pK184. *cpxA* ligation was confirmed by restriction digest analysis and Sanger sequencing (Molecular Biology Services Unit, University of Alberta).

Mutations were introduced into pK184-*cpxA* (except M48K and D113K, see below) by site-directed mutagenesis using the Q5 site-directed mutagenesis kit (New England Biolabs) according to manufacturer instructions. Mutagenesis primers were generated using NEBaseChanger (New England Biolabs) and PCR conditions were determined using recommended annealing temperatures. Plasmids pK184-$cpxA_{M48K}$ and pK184-$cpxA_{D113K}$ were generated by overlap extension PCR using standard molecular techniques using the primers listed in Table 2-3. All mutations were confirmed by Sanger sequencing (Molecular Biology Services Unit, University of Alberta).

CpxA expression and purification

Plasmid pGEX-*cpxA* was transformed into *E. coli* BL21(DE3). Cells were cultured at 30°C in LB with ampicillin until the culture reached an optical density of 0.8-0.9 at 600 nm. Cultures were then induced with 0.05 mM IPTG and grown at 22°C for 21 hours. $CpxA_{31-163}$-GST was purified at 4°C using a protocol modified from the GST Gene Fusion System Handbook (GE Healthcare). Briefly, cells were harvested by centrifugation, and pellets were resuspended in buffer (50 mM Tris-HCl pH 7.5, 400 mM NaCl, and protease inhibitors leupeptin, pepstatin, and phenylmethylsulfonyl fluoride). Cells were lysed using chicken egg white lysozyme treatment and sonication. Lysates were centrifuged and clarified; clarified lysate was mixed with Glutathione Sepharose 4B resin (GE Healthcare) which was pre-equilibrated in resuspension buffer. The binding reaction was incubated with nutation for 1.5 hrs. The resin was then washed with 10 volumes of resuspension buffer, and the bound CpxA-GST was eluted using resuspension buffer containing 20 mM reduced glutathione at pH 7.5.

The elutions were then pooled, buffer exchanged into resuspension buffer, and concentrated using a 10,000 MWCO centrifugal filter device (Millipore, Fisher Scientific). The GST tag was cleaved by PreScission Protease (GE Healthcare) treatment over 12 hrs at 4°C with the progress of reaction monitored by SDS-PAGE. The cleavage reaction was then applied to a second and third affinity column to remove resilient proteolyzed GST and any remaining fusion proteins. The column flow-through and washes containing $CpxA_{31-163}$ were pooled and concentrated using a 3,000 MWCO spin concentrator (Millipore, Fisher Scientific). As a final purification step, $CpxA_{31-163}$ was passed over a HiLoad Superdex 75 26/60 size-exclusion column equilibrated with resuspension buffer on an ÄKTA purifier (GE Healthcare). The $CpxA_{31-163}$ elution peak fractions were pooled and concentrated using a 3,000 MWCO spin concentrator.

Crystallization and data collection

Purified $CpxA_{31-163}$ was dialyzed into crystallization buffer (50 mM HEPES pH 7.0, 350 mM NaCl) using 3000 MWCO spin concentrator. The concentration was estimated to be 21.1 mg/ml based on absorbance at 280 nm, using the theoretical extinction coefficient of 26,470 $M^{-1}cm^{-1}$ derived from the amino acid sequence of $CpxA_{31-163}$ plus extra residues using ProtParam(Gasteiger et al., 2005). Initial crystallization conditions for $CpxA_{31-163}$ were identified from the NeXtal JCSG+ ProComplex Suite, F3 (Qiagen) and were further optimized. $CpxA_{31-163}$ was crystallized by hanging drop vapour diffusion at room temperature (~21°C) by mixing 1 µl of protein at 21.1 mg/ml in crystallization buffer with 1 µl of reservoir solution (100 mM Tris-HCl pH 7.5, 20% v/v 2-methyl-2,4-pentanediol).

The crystals were harvested and flash frozen in liquid nitrogen without any additional cryoprotectant. Diffraction data were collected at the Advanced Light Source, SIBYLS beamline 12.3.1 (Berkeley, CA) and Canadian Light Source, beamline CMCF-BM 08b1-1 (Saskatoon, Canada). CpxA crystallized in the space group P212121 and diffraction data data was collected to a resolution of 1.8 or 2.0 Å.

Structure solution and refinement

The periplasmic domain of *V. parahaemolyticus* CpxA (PDB 3V67)(Kwon et al., 2012b) was used as a search model for molecular replacement. A single domain (Chain A, residues 45-159) was mutated to the corresponding *E. coli* sequence based on sequence alignment and further modified using Sculptor (Bunkóczi and Read, 2011) in PHENIX (Liebschner et al., 2019) by pruning sidechains using the Schwarzenbacher method (Schwarzenbacher et al., 2004). Molecular replacement with PHASER (McCoy et al., 2007) using the 2.0 Å data set placed two copies with a TFZ sore of 8.0. A model of the same domain was generated using SWISSMODEL

(Biasini et al., 2014; Waterhouse et al., 2018), superimposed on the molecular replacement solution and improved with iterative model building in PHENIX AutoBuild (Terwilliger et al., 2008) followed by refinement in phenix.refine (Afonine et al., 2012) resulting in an R-free of 0.323. One of the monomers was then used as the search model to phase the 1.8 Å data set placing two copies with a PHASER TFZ sore of 52.1. Subsequent iterative manual model building in COOT (Emsley and Cowtan, 2004) and refinement in PHENIX yielded a final model with R-free 0.247. The model derived from the 1.8 Å data set was used for all further experiments and figures.

Generation of multiple sequence alignments (MSA) of cpxA for AlphaFold2 modelling

The query sequence, residues 1-184 of *E. coli* CpxA (Uniprot P0AE82), was input into pHMMER (https://www.ebi.ac.uk/Tools/hmmer/search/phmmer) and searched against the uniprotKB database with default search settings, except BLOSUM45 was used, yielding an MSA of 2379 sequences. Jalview was used to remove all sequences with 98% or 96% redundancy resulting in MSAs of 580 and 321 sequences, respectively. The 98% redundant MSA was made gapless for the *E. coli* CpxA sequence and used for AlphaFold2 modeling (pHMMER_98%_non-redundant). The 96% redundant MSA was realigned in Jalview using the MAFFT E-INS-i preset, since the middle (PAS) sequence was known to have low sequence homology (Vreede et al., 2003). This realigned MSA was used for all analysis.

AlphaFold2 modeling of CpxA-SD

CpxA structural modeling was performed using the Colab-Fold implementation of AlphaFold2 (Jumper et al., 2021; Mirdita et al., 2022). Sequences of either *E. coli* or *V. parahaemolyticus* CpxA were input into the AlphaFold2_MMseqs2 Google Colab notebook (v 1.3.0), and multiple sequence alignments were generated using only the MMseqs2 algorithm or

were supplemented with a pHMMER MSA (see MSA generation). All runs used the mulitmer_V2 weights, 48 recycles and generated five models; full input parameters are listed in Table 2-5. The models were ranked by pTM score, and the highest scoring model was used for analysis. Pymol (Version 2.4.0, Schrödinger, LLC) was used for analyzing the AlphaFold2 models and for creating images. Confidence metrics were analyzed using python3 scripts and plotted with Gnuplot (Version 5.4, http://www.gnuplot.info/).

β-galactosidase assays

Activation of the Cpx response was measured by quantifying the activity of a chromosomal *cpxP-lacZ* reporter. Strains prepared in biological triplicate were subcultured into LB with kanamycin (and ampicillin for NlpE overexpression experiments) from overnight cultures for 2 hours. For alkaline pH experiments, cells were pelleted by centrifugation at 4000 RPM for 10 minutes and resuspended in LB+100mM MOPS pH 7.0 or 8.0 and grown for a further 2 hours. For NlpE overexpression experiments, cells were induced with 0.1 mM IPTG and grown for a further 3 hours with shaking. β-galactosidase assays were conducted as previously described (Buelow and Raivio, 2005; Slauch and Silhavy, 1991). Briefly, cultures were centrifuged at 4000 RPM for 10 minutes, and pellets were resuspended in Z-buffer (Miller, 1972). Optical density (absorbance at 600nm) was measured from an aliquot of resuspended culture for standardization. Each culture was treated with chloroform and sodium dodecyl sulfate (SDS) and vortexed to permeabilize cells. Absorbance at 420nm (A_{420}) was measured in a plate reader for each culture at 30 second intervals after the addition of 10 mg/ml ONPG. β-galactosidase activity (*cpxP-lacZ* reporter) activity was quantified by calculating the maximum slope of the A_{420} measures standardized to that of the respective culture's optical density as previously described. Statistical significance was using unpaired *t*-tests (Prism, GraphPad).

SDS-PAGE and Western blotting

SDS-PAGE and Western blotting was used to confirm expression of CpxA from our plasmids according to standard procedures. Cultures were grown in the same conditions as for other experiments. The optical density of each culture was measured and the equivalent of OD 4.0 cells in 100 µl was collected. Cells were washed twice in phosphate buffered saline (PBS) and resuspended in water and 2× Laemmli buffer (Sigma). Samples were heated at 95°C for 5 minutes and cooled to room temperature before being separated on an 8% tris-glycine SDS-PAGE gel and transferred to a nitrocellulose membrane using a semi-dry transfer machine (Bio-Rad). Membranes were blocked in 5% skim milk dissolved in Tris-buffered saline with 0.1% Tween-20 (TBST) for 1-3 hours and incubated with rabbit anti-CpxA-MBP(Raivio and Silhavy, 1997), rabbit anti-His×6 (Thermo-Fischer), and/or mouse anti-RNAPα (BioLegend) antibodies in 2% bovine serum albumin (BSA) in TBST overnight. The specificities of antibodies were confirmed in Western blots with lysates from strains lacking *cpxA* or a His×6-tagged protein (data not shown). The next day, membranes were washed four times with TBST and incubated with fluorescent IRDye680RD (goat anti-mouse) and or IRDye800 (goat anti-rabbit) secondary antibodies in 5% milk in TBST for 1 hour and imaged using a Bio-Rad ChemiDoc imager.

Acknowledgements

Diffraction data were collected at the Advanced Light Source, SIBYLS beamline 12.3.1 (Berkeley, CA) and Canadian Light Source, beamline CMCF-BM 08b1-1 (Saskatoon, Canada). This work was supported by operating grants from the Natural Sciences and Engineering Research Council (NSERC RGPIN-2021-02710 to T.L.R. and NSERC Discovery Grant RGPIN-2016-05163 to J.N.M.G.) and the Canadian Institutes of Health Research (CIHR MOP 142347 to T.L.R. and CIHR168972 to J.N.M.G.). T.H.S.C. is supported by the NSERC Postgraduate

Scholarship (PGS-D) award. G.L.T. is supported by an AHFMR Studentship Award and a recipient of the CIHR Frederick Banting and Charles Best CGS Doctoral Award.

Tables

Table 2-1. Data collection and refinement statistics.

	CpxA (31-163)	CpxA (31-163) †
Wavelength	1.03316	0.97950
Resolution range	39.2-1.8 (1.86-1.8)	39.6-2.0 (2.07-2.0)
Space group	P 21 21 21	P 21 21 21
Unit cell	37.16 43.16 186.98 90 90 90	37.05 43.77 186.34 90 90 90
Total reflections	227024 (21825)	170877 (5615)
Unique reflections	28482 (2769)	21058 (1864)
Multiplicity	8.0 (7.9)	8.1 (3.0)
Completeness (%)	98.1 (96.6)	98.4 (89.0)
Mean I/sigma(I)	13.75 (2.68)	13.83 (1.37)
Wilson B-factor	34.85	34.28
R-merge	0.070 (1.09)	0.078 (0.800)
R-meas	0.076 (1.16)	0.083 (0.926)
R-pim	0.028 (0.408)	0.027 (0.488)
CC 1/2	0.997 (0.958)	0.999 (0.741)
CC*	0.999 (0.989)	1 (0.923)
Reflections used in refinement	28337 (2735)	21045 (1861)
Reflections used for R-free	1345 (133)	969 (86)
R-work	0.204 (0.303)	
R-free	0.247 (0.348)	
CC(work)	0.955 (0.919)	
CC(free)	0.954 (0.856)	
Number of non-hydrogen atoms	2032	
macromolecules	1943	
solvent	89	
Protein residues	233	
RMS(bonds)	0.013	
RMS(angles)	1.15	
Ramachandran favored (%)	97.82	
Ramachandran allowed (%)	2.18	
Ramachandran outliers (%)	0.00	
Rotamer outliers (%)	2.91	
Clashscore	3.10	
Average B-factor	56.92	
macromolecules	57.16	
solvent	51.77	
Number of TLS groups	16	

Statistics for the highest-resolution shell are shown in parentheses.

† Used for phasing.

Table 2-2. Strains used in this study.

Strain	Description	Source
MC4100	F_ *araD139* (*argF-lac*)*U169 rpsL150* (Strr) *relA1 flbB5301 decC1 ptsF25 rbsR*	(1)
TR50	MC4100 λRS88[*cpxP'-lacZ*$^+$]	(2)
RM53	TR50 Δ*cpxA*	This study
GLT100	BL21(DE3) + pGEX-*cpxA*$_{31\text{-}163}$	This study
RM336	MC4100 *cpxA*$_{N107A}$	This study
RM367	MC4100 *cpxA*$_{K121A}$	This study
RM338	MC4100 *cpxA*$_{Y123A}$	This study
RM441	MC4100 lRS88[*cpxP-lacZ*] *cpxA*$_{N107A}$	This study
RM448	MC4100 lRS88[*cpxP-lacZ*] *cpxA*$_{K121A}$	This study
RM444	MC4100 lRS88[*cpxP-lacZ*] *cpxA*$_{Y123A}$	This study
RM477	RM441 + pBR322	This study
RM478	RM441 + pLD404	This study
RM481	RM448 + pBR322	This study
RM482	RM448 + pLD404	This study
RM483	RM444 + pBR322	This study
RM484	RM444 + pLD404	This study
TC636	RM53 + pK184	This study
RMQ2	RM53 + pK184-*cpxA*$_{WT}$	This study
RMQ6	RM53 + pK184-*cpxA*$_{M48K}$	This study
RMQ7	RM53 + pK184-*cpxA*$_{D113K}$	This study
RMQ21	RM53 + pK184-*cpxA*$_{WT}$ + pCA24N	This study
RMQ22	RM53 + pK184-*cpxA*$_{WT}$ + pCA-*nlpE*	This study
RMQ23	RM53 + pK184-*traJ* + pCA24N	This study
RMQ24	RM53 + pK184-*traJ* + pCA-*nlpE*	This study
RMQ27	RM53 + pK184-*cpxA*$_{M48K}$ + pCA24N	This study
RMQ28	RM53 + pK184-*cpxA*$_{M48K}$ + pCA-*nlpE*	This study
RMQ29	RM53 + pK184-*cpxA*$_{D113K}$ + pCA24N	This study
RMQ30	RM53 + pK184-*cpxA*$_{D113K}$ + pCA-*nlpE*	This study
RMQ34	RM53 + pK184-*cpxA*$_{E91A}$	This study
RMQ52	RM53 + pK184-*cpxA*$_{E91A}$ + pCA24N	This study
RMQ53	RM53 + pK184-*cpxA*$_{E91A}$ + pCA-*nlpE*	This study
TC643	RM53 + pK184-*cpxA*$_{E91K}$	This study
TC644	RM53 + pK184-*cpxA*$_{E91K+R93E}$	This study
TC646	RM53 + pK184 + pTrc99A	This study
TC647	RM53 + pK184 + pTrc-*nlpE*	This study
TC648	RM53 + pK184-*cpxA* + pTrc99A	This study
TC649	RM53 + pK184-*cpxA* + pTrc-*nlpE*	This study
TC650	RM53 + pK184-*cpxA*$_{E91K}$ + pTrc99A	This study
TC651	RM53 + pK184-*cpxA*$_{E91K}$ + pTrc-*nlpE*	This study
TC652	RM53 + pK184-*cpxA*$_{E91K+R93E}$ + pTrc99A	This study
TC653	RM53 + pK184-*cpxA*$_{E91K+R93E}$ + pTrc-*nlpE*	This study
TC726	RM53 + pK184-*cpxA*$_{N107D}$	This study

TC719	RM53 + pK184-*cpxA*$_{Q103E}$	This study
TC721	RM53 + pK184-*cpxA*$_{R106E}$	This study
TC758	RM53 + pK184-*cpxA*$_{N107D}$ + pTrc99A	This study
TC761	RM53 + pK184-*cpxA*$_{N107D}$ + pTrc-*nlpE*	This study
TC763	RM53 + pK184-*cpxA*$_{Q103E+D113N}$	This study
TC756	RM53 + pK184-*cpxA*$_{Q103E}$ + pTrc99A	This study
TC759	RM53 + pK184-*cpxA*$_{Q103E}$ + pTrc-*nlpE*	This study
TC757	RM53 + pK184-*cpxA*$_{R106E}$ + pTrc99A	This study
TC760	RM53 + pK184-*cpxA*$_{R106E}$ + pTrc-*nlpE*	This study
TC724	RM53 + pK184-*cpxA*$_{E91K+R99E}$	This study
TC725	RM53 + pK184-*cpxA*$_{E91K+R93E+R99E}$	This study
TC796	RM53 + pK184-*cpxA*$_{E91K+R99E}$ + pTrc99A	This study
TC797	RM53 + pK184-*cpxA*$_{E91K+R99E}$ + pTrc-*nlpE*	This study
TC798	RM53 + pK184-*cpxA*$_{E91K+R93E+R99E}$ + pTrc99A	This study
TC799	RM53 + pK184-*cpxA*$_{E91K+R93E+R99E}$ + pTrc-*nlpE*	This study

Table 2-3. Primers used in this study.

Primer Name	Sequence (5'-3')	Notes
For generation of cpxA *chromosomal mutants*		
pCAF8	CGTCTTCACCTCGAGAAATC	Anchor primer to pCA24N encoding SfiI sites
pCAR4	TTGCATCACCTTCACCCTCTCCACTGACAG	Anchor primer to pCA24N encoding SfiI sites
CpxAN$_{107}$AFw	AACTCTTCAGCTTTTATTGGTCAGGCCGA	Mutagenic primer to generate N107A fragment with EarI site
CpxAN$_{107}$ARv	AACTCTTCAAGCACGAATGATCTGCATTTCG	Mutagenic primer to generate N107A fragment with EarI site
CpxAK$_{121}$AFw	AACTCTTCAGCTAAGTATGGCCGCGTGGA	Mutagenic primer to generate K121A fragment with EarI site
CpxAK$_{121}$ARv	AACTCTTCAAGCCTTCTGCGGATGATCGG	Mutagenic primer to generate K121A fragment with EarI site
CpxAY$_{123}$AFw	AACTCTTCAGCAGGCCGCGTGGAACTGGT	Mutagenic primer to generate Y123A fragment with EarI site
CpxAY$_{123}$ARv	AACTCTTCATGCCTTTTTCTTCTGCGGAT	Mutagenic primer to generate Y123A fragment with EarI site
cpxA-cat	ATTTAATGTGGTGGCGGCGTCTGTTCCGGGCGATTGATAAGTGGGCACCGTGTGACGGAAGATCACTTCGCAG	For amplification of *cat-sacB* cassette
sacB-cpxA	GGTCAAACAGTAAGTTAATGAAATCGGATTGAGAACTGCTGGCCGGATCAAAGGGAAAACTGTCCATAT	For amplification of *cat-sacB* cassette
*cpxA*181Fw	TCCGCCCAACGATTTAATG	For amplification of *cpxA* variants from pCA24N expression vector
*cpxA*503Rv	AGCAGTAATAGCGGGCGGT	For amplification of *cpxA* variants from pCA24N expression vector
For generation of CpxA$_{31-163}$ expression vector		
5'-31	CGCGGATCCGATTCACGCCAGATGACCGA	For amplification of *cpxA*$_{31-163}$ from genome
3'-163	GCGAATTCCTAGCGGTCAAACAGTAAGTT	For amplification of *cpxA*$_{31-163}$ from genome
*For generation of pK184-*cpxA		
XA-1 fw	ATAGGATCCGTGAGGAGGTTCCTATGATAGGCAGCTTAACCGCGC	For amplification of *cpxA* with EcoRI site (and for creation of overlap fragments, see below)
XA-2c rv	TATATAAGCTTCTGCAGTTATGACCGCTTATACAGCGGCAACCAAATCACC	For amplification of *cpxA* with BamHI site
pK184_F	CGTATGTTGTGTGGAATTGTG	For sequencing of inserts into pK184

pK184_R	CAAGGCGATTAAGTTGGGTAA	For sequencing of inserts into pK184
For generation of mutations in pK184-cpxA		
XA-2b rv	GGCAAGGAATTCCTGTGGCCC	For generation of downstream fragment for all mutations
XA-5 fw	AGATTGAGCAGCATGTCGAAGCG	For generation of downstream fragment (with XA-2b) to create M48K mutation by overlap extension PCR
XA-6 rv	CGCTTCGACATGCTGCTCAATCTTCAGACCCTGACGCTGTTCGCT	For generation of upstream fragment (with XA-1) to create M48K mutation by overlap extension PCR
XA-7 fw	AAAAACGCCGATCATCCGCAGAAG	For generation of downstream fragment (with XA-2b) to create D113K mutation by overlap extension PCR
XA-8 rv	CTTCTGCGATGATCGGCGTTTTTGGCCTGACCAATAAAGTTACGAATGATCTGC	For generation of upstream fragment (with XA-1) to create D113K mutation by overlap extension PCR
CpxA E91A-fw	GGTGACCACCGCTGGCCGCGTGA	For generation of E91A by Q5 site-directed mutagenesis
CpxA E91A-rv	AATAACAAACGCTGTCCTGGC	For generation of E91A by Q5 site-directed mutagenesis
CpxA E91K-fw	GGTGACCACCAAAGGCCGCGTGA	For generation of E91K by Q5 site-directed mutagenesis
CpxA E91K-rv	AATAACAAACGCTGTCCTGGCGG	For generation of E91K by Q5 site-directed mutagenesis
Q5SDM_E91K_R93E_F	CGAAGTGATCGGCGCTGAACGC	For generation of E91K+R93E by Q5 site-directed mutagenesis
Q5SDM_E91K_R93E_R	CCTTTGGTGGTCACCAATAACAAACGC	For generation of E91K+R93E by Q5 site-directed mutagenesis
Q5SDM_99+91_F	CGGCGCTGAAGAAAGCGAAATGCAGATCATTC	For generation of E91K+R99E by Q5 site-directed mutagenesis
Q5SDM_99+91_R	ATCACGCGGCCTTTGGTG	For generation of E91K+R99E by Q5 site-directed mutagenesis
Q5SDM_91 93 99_F	CGGCGCTGAAGAAAGCGAAATGC	For generation of E91K+R93E+R99E by Q5 site-directed mutagenesis
Q5SDM_91 93 99_R	ATCACTTCGCCTTTGGTG	For generation of E91K+R93E+R99E by Q5 site-directed mutagenesis
Q5SDM_Q103E_F	CAGCGAAATGGAAATCATTCGTAACTTTATTG	For generation of Q103E by Q5 site-directed mutagenesis
Q5SDM_Q103E_R	CGTTCAGCGCCGATCACG	For generation of Q103E by Q5 site-directed mutagenesis
Q5SDM_R106E_F	GCAGATCATTGAAAACTTTATTGGTCAGGCC	For generation of R106E by Q5 site-directed mutagenesis
Q5SDM_R106E_R	ATTTCGCTGCGTTCAGCG	For generation of R106E by Q5 site-directed mutagenesis

Q5SDM_N107D_F	GATCATTCGTGATTTTATTGGTCAGGCC	For generation of N107D by Q5 site-directed mutagenesis
Q5SDM_N107D_R	TGCATTTCGCTGCGTTCA	For generation of N107D by Q5 site-directed mutagenesis
Q5SDM_D113N_F	TGGTCAGGCCAATAACGCCGATC	For generation of Q103E+D113N by Q5 site-directed mutagenesis
Q5SDM_103+113_R	ATAAAGTTACGAATGATTTCCATTTCGC	For generation of Q103E+D113N by Q5 site-directed mutagenesis

Table 2-4. Plasmids used in this study.

Plasmid	Description	Source
pCA24N	Empty ASKA library vector, Cam^R	(Kitagawa et al., 2006)
pCA-*cpxA*	CpxA expression from pCA24N backbone, IPTG-inducible, ASKA library (GFP-), Cam^R	(Kitagawa et al., 2006)
pTrc99A	Empty expression vector, IPTG-inducible from *trc* promoter, Amp^R	(Amann et al., 1988)
pTrc-$nlpE_{WT}$	His-tagged NlpE expression from pTrc99A backbone, IPTG-inducible, Amp^R	This study
pBR322	Cloning vector, Amp^R	(Balbás et al., 1986)
pLD404	NlpE expression from the pBR322 backbone, Amp^R	(Snyder et al., 1995)
pK184	Empty expression vector, Kan^R	(Jobling and Holmes, 1990)
pK184-*traJ*	pK184 encoding for the *traJ* locus which was used as a less toxic vector control in some experiments as it has no impact on activation of the Cpx response, Kan^R	(Lu et al., 2018)
pK184-$cpxA_{WT}$	WT *cpxA* cloned into pK184, Kan^R	This study
pK184-$cpxA_{M48K}$	*cpxA* M48K cloned into pK184, Kan^R	This study
pK184-$cpxA_{D113K}$	*cpxA* D113K cloned into pK184, Kan^R	This study
pK184-$cpxA_{E91A}$	*cpxA* E91A cloned into pK184, Kan^R	This study
pK184-$cpxA_{E91K}$	*cpxA* E91K cloned into pK184, Kan^R	This study
pK184-$cpxA_{E91K+R93E}$	*cpxA* E91K+R93E cloned into pK184, Kan^R	This study
pK184-$cpxA_{N107D}$	*cpxA* N107D cloned into pK184, Kan^R	This study
pK184-$cpxA_{Q103E}$	*cpxA* Q103E cloned into pK184, Kan^R	This study
pK184-$cpxA_{R106E}$	*cpxA* R106E cloned into pK184, Kan^R	This study
pK184-$cpxA_{Q103E+D113N}$	*cpxA* Q103E+D113N cloned into pK184, Kan^R	This study
pK184-$cpxA_{E91K+R99E}$	*cpxA* E91K+R99E cloned into pK184, Kan^R	This study
pK184-$cpxA_{E91K+R93E+R99E}$	*cpxA* E91K+R93E+R99E cloned into pK184, Kan^R	This study
pFLP2	Plasmid encoding for Flp recombinase, Amp^R	
pKD46	Plasmid encoding for λRed functions, Amp^R	
pRM24	pCA-$cpxA_{N107A}$, pCA24N vector harbouring *cpxA* N107A	This study
pRM12	pCA-$cpxA_{K121A}$, pCA24N vector harbouring *cpxA* K121A	This study
pRM13	pCA-$cpxA_{Y123A}$, pCA24N vector harbouring *cpxA* Y123A	This study

Table 2-5. Modeling parameters and outputs of ColabFold.

Model	Avg pLDDT	pTm	Sequences used	# Sequences	Start Res	End Res
CpxA ecoli Dimer_10	87.65	0.76	mmSeqs2 + pHMMER_98%_non-redundant	1214	8	184
CpxA vib	87.09	0.82	mmSeqs2	484	14	195
CpxA ecoli PAS-TM-HAMP	85.69	0.76	mmSeqs2	3647	1	233

Chapter 3 – Characterization of NlpE and its inner membrane signaling role

Abstract

The CpxRA system senses and responds to envelope stresses such as those that lead to protein misfolding. The envelope, however, presents a complex environment for signaling. One of the ways that the sensor kinase CpxA increases the number of signals it can sense is through its association with the outer membrane lipoprotein NlpE. NlpE is associated with sensing surface adhesion for the Cpx response but is also known to activate the Cpx response when overexpressed and mislocalized. Recent work suggests that mislocalized NlpE is used by the Cpx response to sense defects in lipoprotein biogenesis. However, the molecular details of signaling by NlpE at the inner membrane are still emerging. In this chapter, I explore the structural features of NlpE based on its published structure and examine their contribution to activating CpxA at the inner membrane. Overexpression of NlpE leads to increased accumulation of NlpE at the inner membrane, a stress that can be relieved both by the degradation of NlpE or through increased trafficking of NlpE to the outer membrane. Interactions between NlpE and CpxA are mediated by electrostatic interactions between basic patches on NlpE's N-terminal domain and acidic residues on the sensor domain of CpxA. DegP and CpxP both appear to influence the stability of NlpE, although these proteins accomplish this in different signaling contexts, suggesting mechanisms by which Cpx-regulated factors influence signaling through NlpE. Overall, this chapter supports the developing picture for NlpE as an inner membrane stress sensor and provides experimental evidence for NlpE's mode of signaling at the inner membrane.

Introduction

The bacterial envelope is a complicated structure composed of diverse biomolecules with equally diverse functions (Silhavy et al., 2010). Lipoproteins are an essential part of the Gram-negative envelope, playing roles in pathogenesis, biogenesis, transport, and metabolism (Braun and Hantke, 2019). Lipoproteins such as Lpp and Pal play a critical role in coordinating the outer membrane with the cell wall, stabilizing the envelope as a whole (Bouveret et al., 1999; Braun and Rehn, 1969; Cascales et al., 2002; Park et al., 2017; Samsudin et al., 2017). Lipoproteins are also emerging as important signaling molecules in the envelope (El Rayes et al., 2021). For example, the outer membrane lipoprotein RcsF is an essential sensor for the Rcs envelope stress response, sensing defects in lipopolysaccharide and the cell wall (Castanié-Cornet et al., 2006). Thus, lipoproteins not only help build and stabilize the envelope, but are also key sentinels of envelope health.

Like RcsF, the outer membrane lipoprotein NlpE is an envelope stress sensor. NlpE is an activator of the Cpx envelope stress response initially discovered as both a copper resistance factor (Gupta et al., 1995) and a suppressor of envelope protein toxicity (Snyder et al., 1995). However, NlpE also is implicated in sensing adhesion to surfaces (Feng et al., 2022; Otto and Silhavy, 2002; Shimizu et al., 2016) and sensing disturbances to periplasmic redox state (Andrieu et al., 2023; Delhaye et al., 2019). NlpE's diverse signaling roles can in part be explained by its structure. NlpE crystallizes as a unique domain swapped dimer with independently folding N- and C-terminal domains (Hirano et al., 2007). While this structural study found some resemblances between NlpE and other lipoproteins, such as bacterial lipocalin and oligonucleotide/oligosaccharide binding folds, a signaling mechanism remained elusive. Furthermore, it's unclear from this structure how NlpE senses such a diverse array of signals.

As with other outer membrane lipoproteins, NlpE undergoes modification after secretion across the inner membrane. After secretion through the Tat or Sec translocon, nascent lipoproteins are diacylated by the preprolipoprotein diacylglyceryl transferase Lgt at a universally present N-terminal cysteine residue (Sankaran and Wu, 1994). The nascent lipoprotein signal peptide is then cleaved by a lipoprotein-specific signal peptidase LspA (or signal peptidase II) (Tokunaga et al., 1982) before a final acyl chain is added to the now free amino group of the N-terminal cysteine by the *N*-acyl transferase Lnt (Jackowski and Rock, 1986). Outer membrane lipoproteins are then trafficked to the outer membrane by the Lol (**l**ocalization **o**f **l**ipoproteins) pathway (Grabowicz, 2019); inner membrane lipoproteins are extracted by the LolCDE ATP-binding cassette (ABC) transporter and transferred to the periplasmic chaperone LolA. LolA shields the hydrophobic acyl moiety of lipoproteins and hands off lipoproteins to the outer membrane lipoprotein insertase LolB. Inner membrane lipoproteins possess a Lol-avoidance signal that allows for them to remain in the inner membrane (Hara et al., 2003).

Recent works have linked NlpE to sensing the integrity of these maturation and trafficking pathways (Delhaye et al., 2019; Grabowicz and Silhavy, 2017a; Marotta et al., 2023a; May et al., 2019). An earlier study reported that NlpE activates the Cpx response when forced to localize to the inner membrane (Miyadai et al., 2004). A study from the Tokuda lab in 2010 reported that a lethal LolA variant induces the Cpx response (Tao et al., 2010). Later, Grabowicz and Silhavy (2017) reported that the Cpx response, and NlpE specifically, are required for survival in backgrounds with deficient lipoprotein trafficking. Subsequent studies reported direct interactions between the N-terminal domain of NlpE with the sensor domain of CpxA (Delhaye et al., 2019; Marotta et al., 2023a). Further work from the Grabowicz lab reported that NlpE is required for activating the Cpx response in the presence of compounds that disrupt lipoprotein biogenesis and high concentrations of copper (May et al., 2019), suggesting that inner

membrane localized NlpE alerts the cell to this stress by activating the Cpx response. Interestingly, a recent study found that the synthetic lethality of the deletion of genes encoding two envelope proteins, *yciB* and *dcrB*, is due to defects in Lgt activity (Mychack et al., 2019; Mychack and Janakiraman, 2021). Δ*yciB*Δ*dcrB* strains have pleiotropic envelope defects but much of the toxicity appears to be from aberrant crosslinks between inner membrane localized Lpp and the cell wall. This is strongly reminiscent of the findings of Grabowicz and Silhavy (2017). However, while, the Cpx response is induced in the Δ*yciB*Δ*dcrB* background and promotes survival in this strain, NlpE is not required for Cpx induction or survival. Thus, the precise context in which NlpE acts as a sentinel for lipoprotein trafficking remains to be fully characterized.

Despite several recent studies, the details around NlpE activation of CpxA at the inner membrane are still emerging. Furthermore, many questions remain about the relevance of the structural features of NlpE based on the published structure (Hirano et al., 2007). This chapter investigates the molecular mechanisms of NlpE signaling at the inner membrane. Here, we provide experimental evidence for the dimer model proposed by Hirano and colleagues (2007) and show that the dimer of NlpE may be important for signaling and NlpE stability. We experimentally link the novel lipoprotein sentinel role of NlpE with activation of the Cpx response during overexpression by showing that overexpression of NlpE leads to mislocalization due to overloaded lipoprotein trafficking. We also show that the N-terminal domain of NlpE physically interacts with CpxA's sensor domain and basic residues on the N-terminal domain of NlpE mediate this interaction. Furthermore, we show that NlpE is regulated both by proteolysis and by being stabilized by the Cpx-regulated factors CpxP and DegP under certain conditions, suggesting a novel axis of NlpE regulation. Taken together, this chapter contributes to the

growing body of work on NlpE as a sensor of lipoprotein health and provides new insights into the mode of NlpE signaling at the inner membrane.

Results

Truncation mutants of NlpE

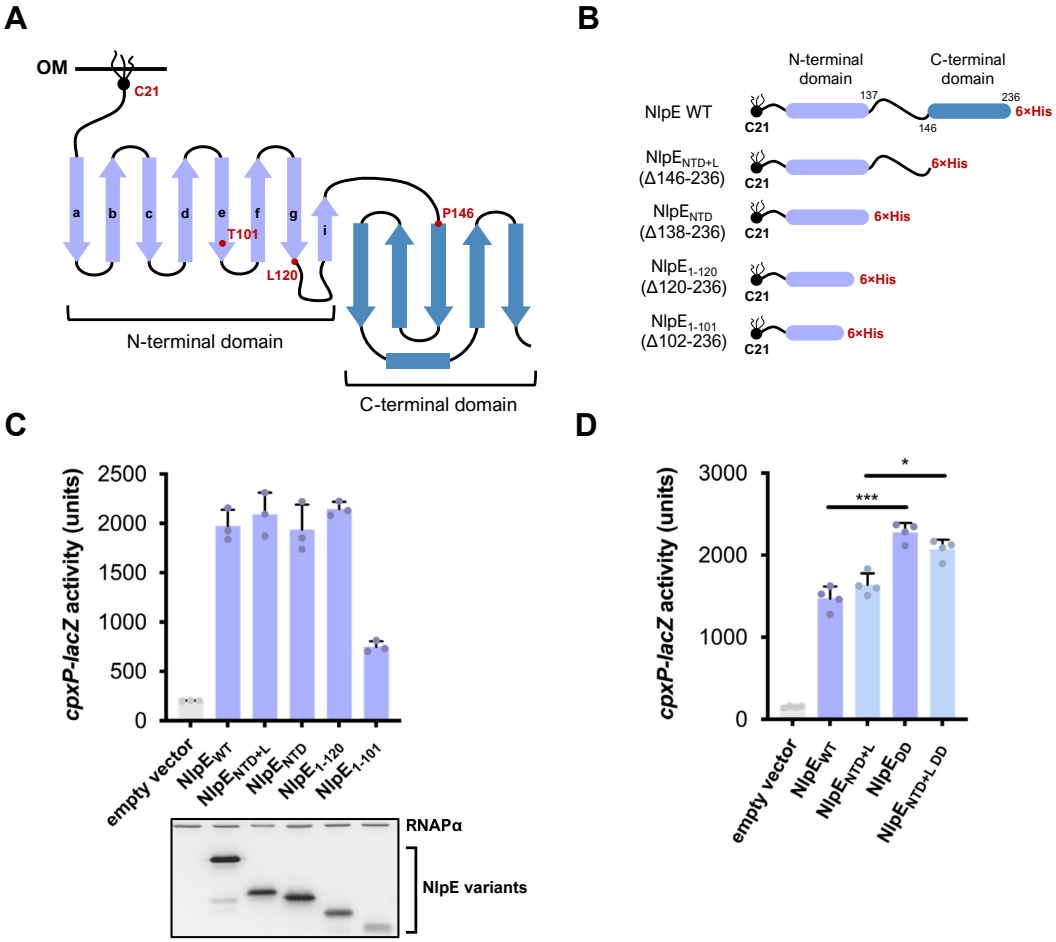

Figure 3-1. Overexpression of the N-terminal domain of NlpE is sufficient for CpxA activation.

(A) Cartoon representation of the hypothetical monomer model proposed by Hirano and colleagues (2007). The β-strands of the N-terminal domain are shown as arrows and labelled with letters. Key residues used as points of truncation are shown in red. **(B)** NlpE truncation constructs cloned into pTrc99A with C-terminal 6×His tags. The amino acid number includes the signal peptide (i.e. the lipid-modified N-terminal cysteine is labelled Cys21 not Cys1). **(C)** Overexpression of NlpE truncation mutants. Strains were grown until midlog phase (OD 0.4-0.6) and induced with IPTG for 30 minutes before *cpxP-lacZ* activity was measured. Expression levels of each NlpE variant is shown underneath the graph with an RNAP α subunit loading control also shown. **(D)** Forced mislocalization of NlpE to the inner membrane leads to higher levels of CpxA

activation than overexpression of WT NlpE. Strains were grown until mid-log phase and induced with 0.2% L-arabinose for 1 hour. For **(C)** and **(D)**, shown are means of 3-4 biological replicates with standard deviation. Data were analyzed with a Tukey HSD multiple comparisons test (*p<0.05, ***p<0.001).

NlpE in *E. coli* possesses globular N- and C-terminal domains (Figure 3-1A) (Hirano et al., 2007). To investigate the contribution of NlpE's domains to activating CpxA at the inner membrane, we generated vectors in the pTrc99A background expressing C-terminal truncations of His-tagged NlpE (Figure 3-1B). We confirmed that the C-terminal domain of NlpE is not required for activating CpxA during overexpression, as reported by others (Figure 3-1C) (Delhaye et al., 2019; May et al., 2019). A reduction of activation of CpxA is only seen when a significant truncation is made to the N-terminal domain of NlpE (in the $NlpE_{1\text{-}101}$ variant) (Figure 3-1C). However, while all other variants of NlpE are stably expressed, $NlpE_{1\text{-}101}$ is significantly less stable. Despite the lower levels of expression, $NlpE_{1\text{-}101}$ still activates the Cpx response suggesting that CpxA activation is proportional to the protein levels of NlpE and that the region responsible for activating CpxA is still contained on $NlpE_{1\text{-}101}$. We also confirmed previous results that overexpression of a permanently inner membrane bound NlpE leads to enhanced activation of CpxA (Figure 3-1D) (Miyadai et al., 2004). We used site-directed mutagenesis to generate vectors expressing full length and truncated NlpE where the +2 and +3 residues are changed to aspartates ($NlpE_{DD}$). Interestingly, we were only able to create this variant when NlpE was expressed from a much more stringently controlled P*ara* promoter in pBAD18, as opposed to from the leakier P*trc* promoter of pTrc99A, suggesting that inner membrane-localized NlpE is toxic and strongly selected against. The C-terminal domain is again dispensable for activation, suggesting that the N-terminal domain is both necessary and sufficient for CpxA activation in this context.

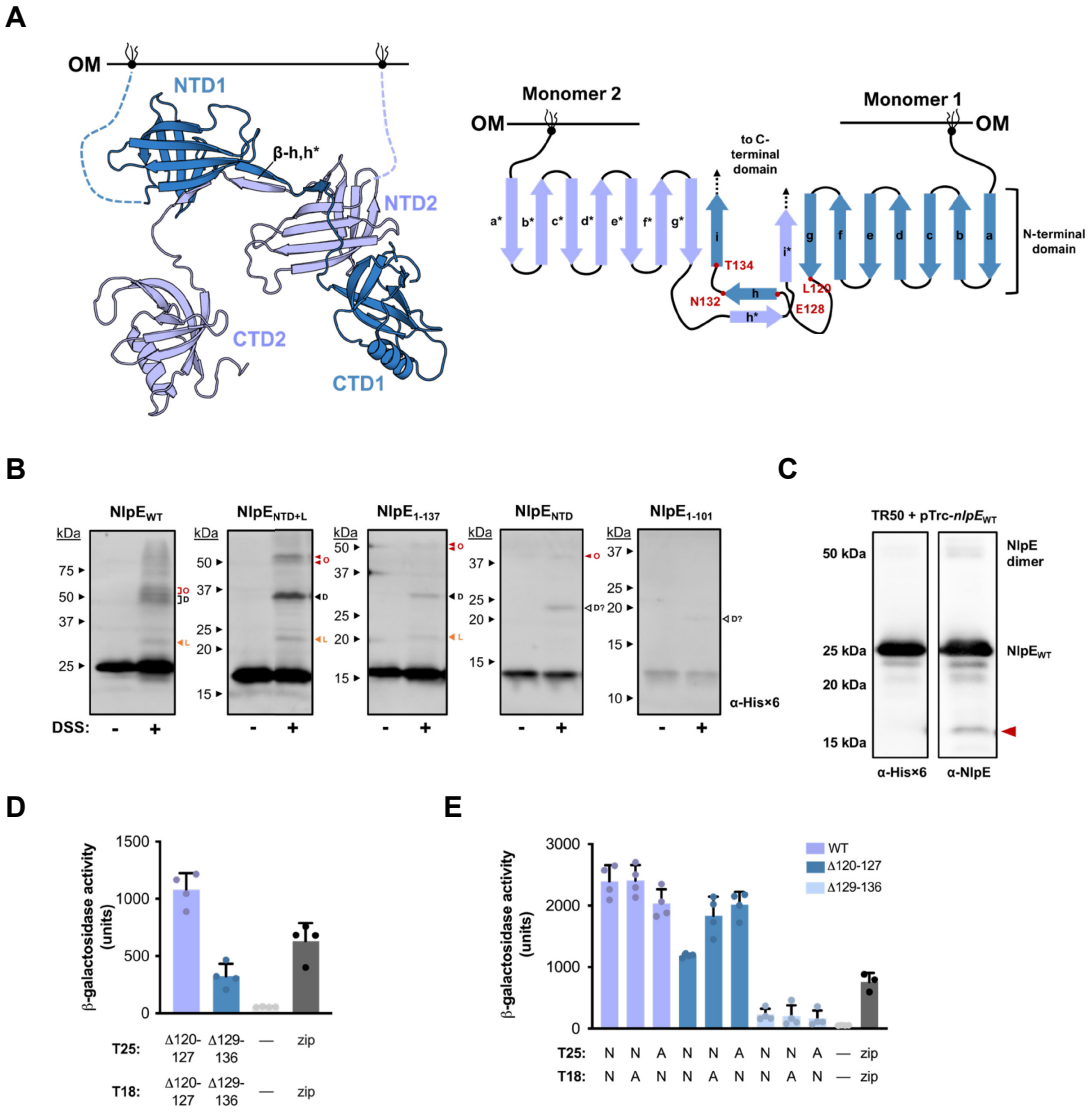

Figure 3-2. NlpE dimerizes via its N-terminal domain.

(A) The crystal dimer structure from (Hirano et al., 2007) as well as a cartoon diagram of the secondary structure elements of the dimer excluding the C-terminal domains. **(B)** *in vivo* crosslinking of NlpE truncation mutants with 0.5 mM DSS for 30 minutes. D indicates the putative NlpE dimer, O indicates NlpE-OmpA complexes and L indicates NlpE-Lpp complexes. These complexes are confirmed and explored in Chapter 4. **(C)** NlpE dimers are resistant to SDS and heat denaturation. Cells were grown to mid-log stage and induced with 0.1 mM IPTG for 30 minutes before being processed for SDS-PAGE. Blots were conducted with both anti-NlpE and -6×His antibody. Red arrow indicates a potential C-terminal cleavage product of NlpE. **(D)**

Two-hybrid assays of different NlpE deletion mutants. "—" indicates a negative control strain with no fusion to T25 or T18 subunits, and "zip" indicates a positive control strain with a leucine zipper fusion to the enzymatic subunits. **(E)** shows two-hybrid assays testing variants of NlpE (N) against itself or the sensor domain of CpxA (A, aa31-163). The variants of NlpE used are shown in the legend. For **(D)** and **(E)**, the means of 3-4 biological replicates are shown with standard deviation.

A structural study of NlpE found that it crystallizes as an asymmetric domain-swapped dimer where the β-barrel of each protomer's N-terminal domain is completed by a terminal β-strand from the other protomer (Figure 3-2A) (Hirano et al., 2007). The C-terminal domain does not appear to be significantly involved in dimerization in this model. To validate this structure, we conducted *in vivo* crosslinking with disuccinimidyl suberate (DSS) in strains overexpressing truncations of NlpE (Figure 3-2B). We found species corresponding to NlpE dimers whenever an intact N-terminal domain is expressed, as expected, with only weak dimerization observed when significant truncations are made into the N-terminal domain (as is the case in $NlpE_{1-101}$). We also observed crosslinking to several other proteins, such as OmpA and Lpp, which will be explored in the next chapter. Further, we found that NlpE dimers may be resistant to denaturation by SDS and heating; a roughly 50 kDa species is seen when overexpressing NlpE even in the absence of crosslinker in denaturing and reducing conditions (Figure 3-2C).

To further investigate NlpE dimerization, we conducted a modified bacterial two-hybrid assay where proteins of interest are fused to both an OppB transmembrane domain and the T25/T18 subunits of the adenylate cyclase enzyme (Ouellette et al., 2014). This system allows for the periplasmic localization of fusion proteins and cytoplasmic localization of the enzymatic subunits, which require ATP. Upon interaction of fusion proteins, cAMP is produced by the reconstituted adenylate cyclase enzyme, which is read out as β-galactosidase activity in our

reporter strain. We cloned full-length NlpE to T25 and T18 subunits as well as specific deletions of regions responsible for the domain-swapped crystal structure (Figure 3-2D,E). These assays revealed that full-length is able to interact with the sensor domain of CpxA. Furthermore, we found that, like the experimentally reported structure, the full-length NlpE construct can self interact. When we deleted a region between the β-g and β-h strands of NlpE (Δ120-127), we observed that NlpE is still able to dimerize. However, a reduction in NlpE-NlpE interactions were observed when a region corresponding to the entirety of β-h and β-i (Δ129-136) was deleted, supporting the dimer structure proposed by Hirano and colleague's (2007) study. Interestingly, we found that the ability of NlpE to dimerize corresponds with its ability to interact with CpxA's sensor domain in two-hybrid assays (Figure 3-2E); full-length NlpE is able to both self-interact and interact with CpxA's sensor domain strongly. $NlpE_{\Delta 120\text{-}127}$ appears to self-interact more weakly than WT NlpE but interacts equally strongly with CpxA. However, $NlpE_{\Delta 129\text{-}136}$ neither self-interacts nor interacts strongly with CpxA's sensor domain. The decreased ability of the dimerization-deficient $NlpE_{\Delta 129\text{-}136}$ to interact with CpxA or itself may be due decreased stability of these constructs or because dimerization is directly required for NlpE-CpxA interactions.

Overexpression of NlpE leads to inner membrane mislocalization

Overexpression of NlpE is one of the earliest characterized inducing cues of the Cpx response (Snyder et al., 1995). While recent and older works suggest that mislocalized NlpE activates the Cpx response (Delhaye et al., 2019; May et al., 2019; Miyadai et al., 2004), direct connection between overproduction and mislocalization of NlpE has not yet been established. To experimentally verify that NlpE overexpression leads to its mislocalization to the inner membrane, we conducted sucrose density gradient ultracentrifugation to separate inner and outer membrane protein containing fractions from crude membrane extracts (Dunstan et al., 2017). We found that at native levels of expression, NlpE is exclusively found in outer membrane

protein containing fractions (Figure 3-3A). However, even with modest overexpression without IPTG from the ASKA library vector pCA-*nlpE*, NlpE becomes present in inner membrane fractions (Figure 3-3B), confirming that overexpression leads to NlpE mislocalization.

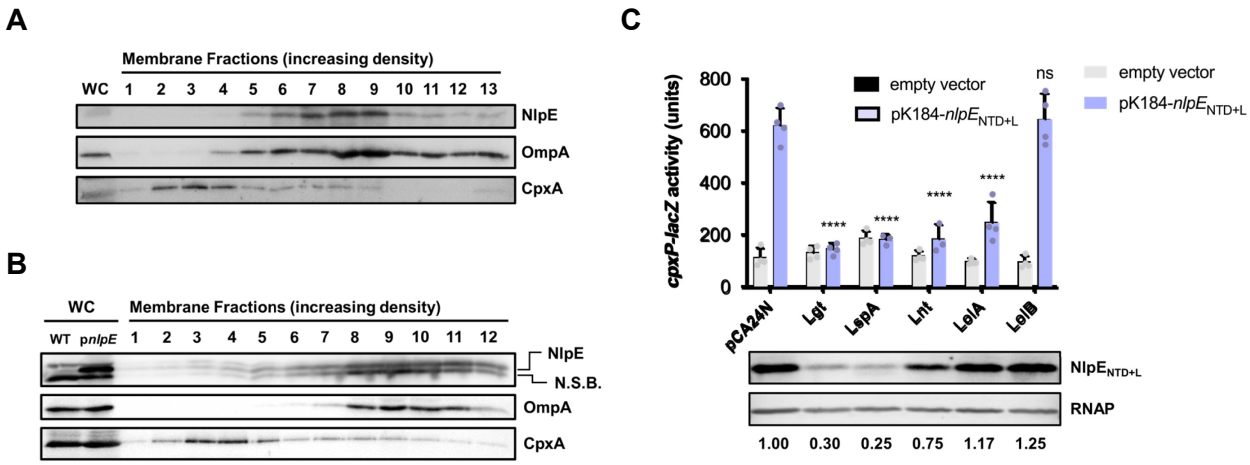

Figure 3-3. NlpE mislocalizes during overexpression due to overloaded biogenesis machinery.

Sucrose density gradient-separated membrane fractions of WT **(A)** and NlpE overexpressing **(B)** cells. NlpE was expressed from pCA-*nlpE* without IPTG induction. Membrane fractions and whole cell lysates (WC) were analyzed by Western blotting. Anti-OmpA was used to detect OM fractions, whereas anti-CpxA-MBP was used for inner membrane fractions. A band of unknown identity detected by the anti-NlpE antibody in **(B)** is indicated with N.S.B. **(C)** TR50 containing pK184 (empty vector) or pK184-*nlpE*$_{NTD+L}$ and pCA24N (empty vector) or pCA-*lgt, -lspA, -lnt, -lolA,* or *-lolB* were grown to OD ~0.4 and induced with 0.1 mM IPTG for 30 minutes. Shown are mean *cpxP-lacZ* activities of 4 biological replicates with standard deviation and analyzed by Tukey HSD post-hoc test (ns=non-significant, ****p<0.0001). The mean *cpxP-lacZ* activity of each NlpE overexpression strain was compared to NlpE overexpression in the pCA24N strain. Expression level of NlpE$_{NTD+L}$ in whole cell lysates from these strains is shown below the graph with the quantification of NlpE standardized to the loading control (RNAP).

We hypothesized that NlpE mislocalization is due to overloaded lipoprotein biogenesis machinery. Based on this, we reasoned that simultaneously overexpressing different

enzymes/proteins involved in lipoprotein maturation or trafficking during NlpE overexpression may relieve potential bottlenecks and reduce activation of CpxA. To test this, we co-expressed the lipoprotein maturation enzymes Lgt, LspA, and Lnt or trafficking proteins LolA and LolB with $NlpE_{NTD+L}$ from a compatible vector and then measured the activity of a *cpxP-lacZ* reporter (Figure 3-3C). We observed that overexpression of any one of Lgt, LspA, or Lnt is sufficient to abolish or very strongly reduce activation of the Cpx response during NlpE overexpression (Figure 3-3C). A much more modest two-fold induction of *cpxP-lacZ* reporter activity is seen in LolA overexpression strains while overexpressing LolB had no impact on Cpx activation compared to the pCA24N vector control strain. This result makes sense as LolB is itself an outer membrane lipoprotein and thus its trafficking would be similarly impacted by overexpression.

While we initially thought that overexpressing almost any component of the lipoprotein biogenesis pathway is sufficient to relieve the backlog of overexpressed NlpE, examining the protein levels of NlpE in these backgrounds reveals a more complicated situation. We observed that NlpE expression levels are strongly reduced in Lgt and LspA overexpression strains, suggesting that NlpE is degraded in these strains, potentially along with Lgt/LspA. NlpE levels are only slightly reduced in the *N*-acyl transferase Lnt overexpression strain compared to the pCA24N vector control strain but a significant reduction in *cpxP-lacZ* activity is seen. NlpE expression levels in the LolA overexpression strain were similar, if not slightly higher compared to vector control, but a significant decrease in CpxA activity is seen, suggesting that LolA overexpression may increase the trafficking of NlpE to the outer membrane, reducing activation of CpxA. NlpE protein levels in the LolB are similar to vector control despite having essentially the same level of CpxA activation, which suggests there is likely increased NlpE at the inner membrane in this background. Overall, these results suggest that mislocalized NlpE during overexpression is due to insufficient amounts of maturation or trafficking proteins available for

processing increased levels of NlpE. Increasing the maturation or trafficking of NlpE by overexpressing Lnt or LolA is sufficient to significantly reduce this backlog and as well as Cpx activation.

Basic residues on the N-terminal domain of NlpE mediate interaction with CpxA

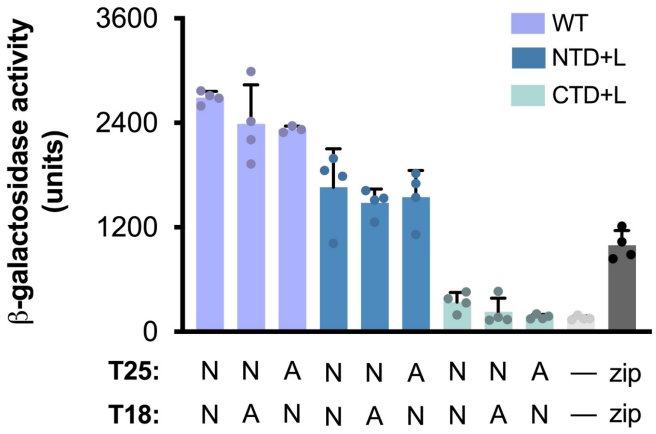

Figure 3-4. The N- but not C-terminal domain of NlpE is sufficient for interaction with CpxA.

Modified two-hybrid assays with periplasm-localized full length NlpE (WT), $NlpE_{1-146}$ (NTD+L), $NlpE_{\Delta 24-120}$ (CTD+L), CpxA sensing domain aa31-163 (A), no fusion protein (—, negative control), and leucine zipper (zip, positive control). "N" indicates that the indicated variant of NlpE was fused to either the T25 or T18 subunit. Shown are means of 4 biological replicates with standard deviation.

To further characterize NlpE-CpxA interactions, we used the modified two-hybrid assay to determine which domains of NlpE contribute to its ability to interact with CpxA at the inner membrane (Figure 3-4). We found that deletion of the C-terminal domain did not impact NlpE's ability to directly interact with CpxA, which is in line with our finding and others that the N-terminal domain is sufficient for activation (Figure 3-1C) ((Delhaye et al., 2019; May et al., 2019). Consistent with our crosslinking results and the crystal structure (Hirano et al., 2007), these

assays also support N-terminal domain-dependent NlpE dimerization, at least when NlpE is expressed at high levels, as no self-interaction is seen in two-hybrid assays in the absence of the N-terminal domain.

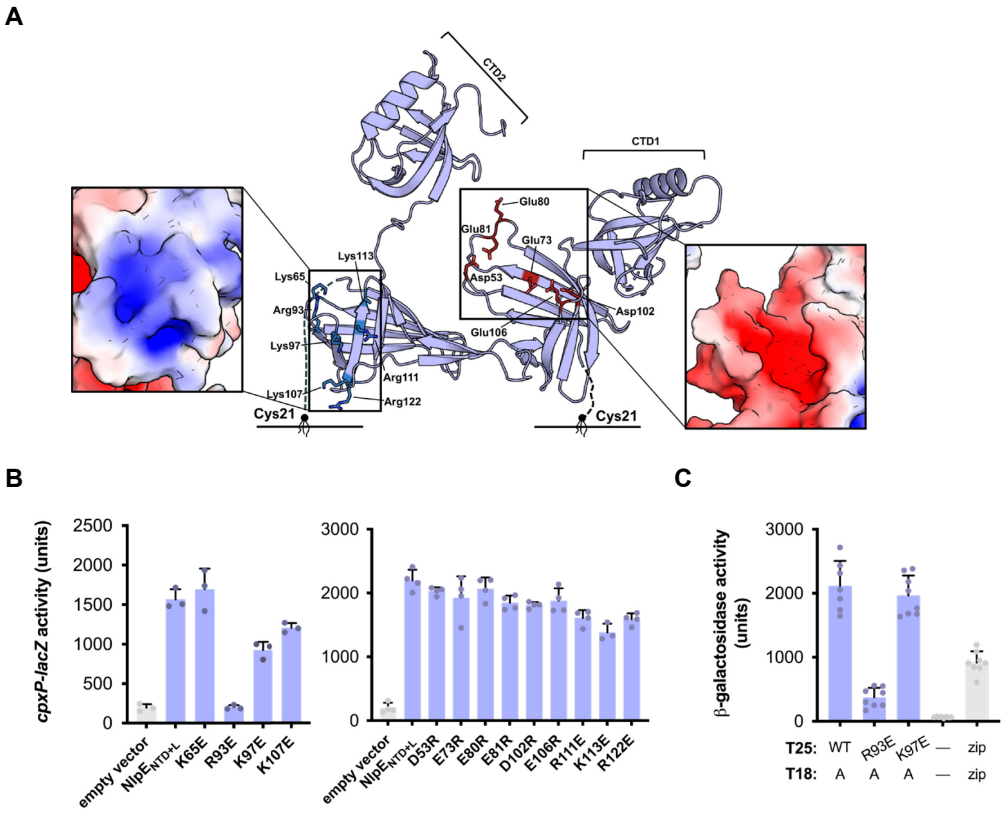

Figure 3-5. Basic residues on the N-terminal domain of NlpE mediate CpxA activation.

(A) Charged patches (blue = positive, red = negative) on the N-terminal domain of NlpE (RCSB PDB no. 2Z4H) as seen on the NlpE N-terminal domain dimer (aa41-137). Insets show basic and acidic patches on the surface of the N-terminal domain of NlpE. Surface charged patches on NlpE were visualized using the APBS Electrostatics Plugin on PyMOL. **(B)** The ability of $NlpE_{NTD+L}$ charge swap mutants expressed from pK184 (leaky expression) to activate the Cpx response as measured by quantifying *cpxP-lacZ* activity in mid-log phase cells. Shown are the mean of 3 biological replicates' *cpxP-lacZ* activity with standard deviations. **(C)** Two-hybrid assay testing the ability of charge swap mutants R93E and K97E (fused to the T25 subunit) to physically interact with the periplasmic sensing domain of CpxA (T18-A; amino acids 31-163). — indicates no fusion protein (negative control) and zip, leucine zipper (positive control). Shown are means of 8 biological replicates with standard deviation.

We then wanted to further focus in on the structural features of the N-terminal domain responsible for Cpx activation. We observed that NlpE possesses several charged patches on the surface of the N-terminal domain (Figure 3-5A) and wondered if NlpE-CpxA interactions at the IM are mediated through these amino acids. To investigate this, we created vectors expressing charge-swap mutants of these amino acids of $NlpE_{NTD+L}$ and measured the ability of these variants to activate the Cpx response when overexpressed. We found that the positive-to-negative swap R93E completely abrogated activation of the Cpx response when overexpressed (Figure 3-5B). Charge swaps of other basic residues such as K97, K107, and K113 lead to slight reductions in CpxA activation. None of the negative-to-positive swap mutants displayed significantly altered activation of the Cpx response upon overexpression.

To investigate if these mutations impact NlpE-CpxA interactions, we conducted two-hybrid assays with vectors expressing R93E and K97E NlpE variants (Figure 3-5C). These assays show that the R93E charge swap mutation disrupts NlpE-CpxA sensor domain interactions, suggesting that the lack of Cpx activation during overexpression of this variant is due its inability to interact with CpxA. In contrast, K97E, which showed a weaker reduction of Cpx activation upon overexpression, did not significantly impact the strength of CpxA-NlpE interactions as measured in this assay; this mutation may instead affect other aspects of the NlpE-CpxA interaction that influence activation such as the ability of CpxA to undergo the conformational changes required to activate kinase activity. Overall, these results suggest that NlpE activation of CpxA at the IM occurs by direct protein-protein interactions mediated by charged residues present on the surface of the N-terminal domain of NlpE. Furthermore, these effects on Cpx activation are likely due to the charge-swaps themselves and not due to any differences in expression as compared to the WT $NlpE_{NTD+L}$ (Figure 3-6).

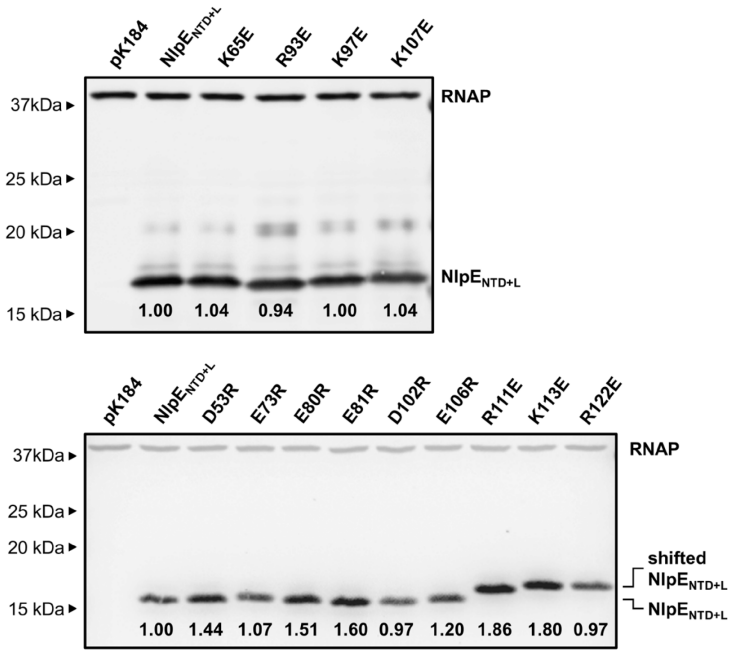

Figure 3-6. ***Expression levels of NlpE charge-swap mutants*****.**

Cells containing pK184-based NlpE$_{NTD+L}$ expression vectors were grown to mid-log phase (OD ~0.5-0.6) and processed for SDS-PAGE and Western blotting with anti-NlpE and anti-RNAP (loading control) antibody. Levels of NlpE were standardized to RNAP loading controls and then standardized to level of WT NlpE$_{NTD+L}$.

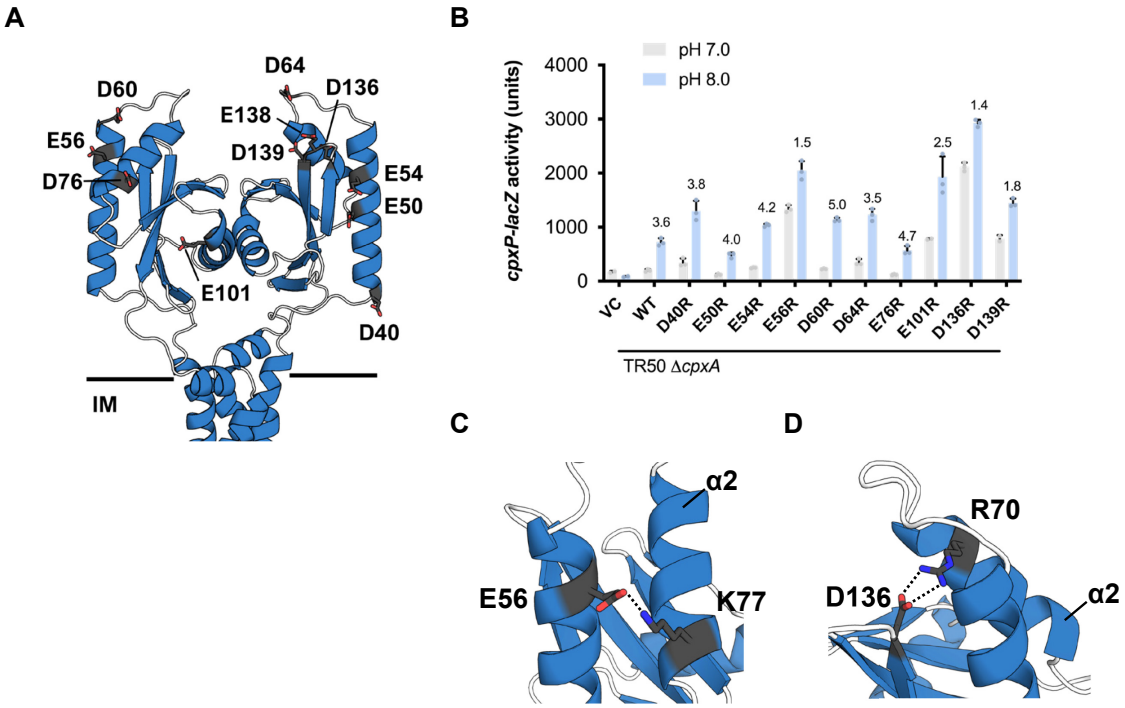

Figure 3-7. Acidic residues on the sensor domain of CpxA impact activation.

(A) Acidic residues on the surface of the sensor domain of CpxA. **(B)** Ability of charge swaps of acidic residues to sensor alkaline pH. Charge swaps were introduced on a vector expressing CpxA (pK184-*cpxA*) and then expressed in a Δ*cpxA* strain. Strains were grown to midlog in pH 7.0 LB and then introduced to LB media buffered to the indicated pH and grown for 2 hours more before β-galactosidase activity was measured. The fold induction in alkaline pH is shown above each bar. Shown are means of 3 biological replicates with standard deviation. **(C)** and **(D)** show interactions between E56 and D136 and residues on the α2 helix of the CpxA sensor domain according to the AlphaFold model.

Because the basic R93 residue on NlpE is important for CpxA activation, we wondered if negatively charged residues on the sensor domain of CpxA are important for sensing NlpE overexpression. We previously used AlphaFold2 to investigate the structure of the dimeric CpxA (see Chapter 2). Using the same plasmid based CpxA expression system, we generated charge

swap variants of several negatively charged residues on the surface of CpxA's sensor domain (Figure 3-7A). Plasmids expressing these variants were transformed into a ΔcpxA strain with a cpxP-lacZ reporter (RM53). We first tested the ability of these variants to sense a well known Cpx inducing cue, alkaline pH (Figure 3-7B) (Danese and Silhavy, 1998; DiGiuseppe and Silhavy, 2003). These mutations possessed varying phenotypes. Some of these charge swaps possessed activity similar to WT CpxA. This includes D40R, E50R, E54R, D60R, D64R, and E76R, which all possess similar basal activation at pH 7.0 to WT CpxA and are induced about 3-5 fold at pH 8.0. E101R and D139R possess slightly higher basal activation and reduced sensitivity to alkaline pH (about 2-fold). Significantly, we found two mutations, E56R and D136R, which are hyper-activated basally (i.e. at pH 7.0) and insensitive to alkaline pH. This phenotype is reminiscent of early *cpxA** mutations (Cosma et al., 1995b; Raivio and Silhavy, 1997). Interestingly, both of these negatively charged residues form salt bridges to positively charged residues on the α2 helix of the sensor domain (Figure 3-7 C and D show interactions between K77-E56 and K70-D136), suggesting that this helix is highly stabilized and disrupting the interactions that hold this helix in place strongly activates CpxA.

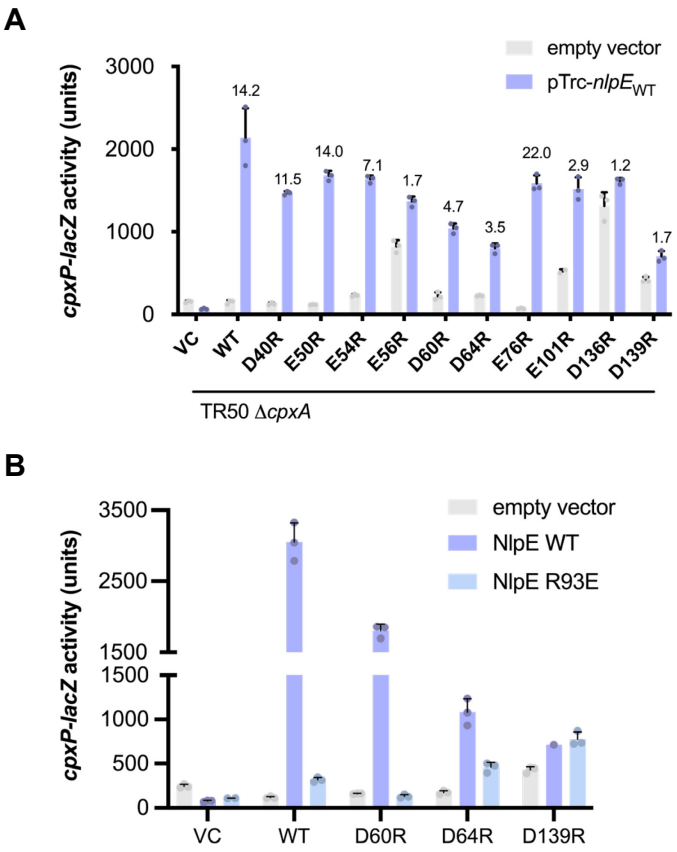

Figure 3-8. Acidic residues on the sensor domain of CpxA impact activation during NlpE overexpression.

(A) Ability of CpxA charge swap mutants to sense NlpE overexpression. Strains were grown to midlog in pH 7.0 LB and then introduced to LB media buffered to the indicated pH and grown for 2 hours more before β-galactosidase activity was measured. The fold induction in alkaline pH is shown above each bar. Shown are means of 3 biological replicates with standard deviation. **(B)** shows a similar experiment, except the indicated CpxA variants (bottom axis) were coexpresssed with the indicated NlpE variants (legend).

We used this system to then test the ability of these *cpxA* mutants to sense NlpE overexpression (Figure 3-8A). Again, E56R and D136R showed *cpxA**-like phenotypes, being hyper-activated in the vector control strain and relatively insensitive to NlpE overexpression. The hyper-activation of these mutations makes it difficult to judge whether the lack of activation seen

is because these variants are not interacting with NlpE. While no single residue here appears to be responsible for sensing NlpE overexpression, the D60R and D64R mutations significantly reduced the sensitivity of CpxA to NlpE overexpression. Interestingly, both of these residues are located on the linker that connects the α1 and α2 helices of CpxA's sensor domain, suggesting that the position of these helices is important for activating CpxA. We wondered if any of these mutations would restore the ability of CpxA to sense NlpE R93E, which we had previously shown to not activate CpxA (Figure 3-8B). Our results here were largely inconclusive. While D60R and D64R are less sensitive to NlpE overexpression and a slight increase in CpxA activation was observed in a strain expressing CpxA D64R while overexpressing NlpE R93E, neither mutation on its own is able to restore CpxA sensing of NlpE R93E. Similarly, the NlpE-insenstitive CpxA D139R variant is activated similarly by WT and R93E NlpE. Overall, while acidic residues on CpxA's sensor domain may regulate activation of CpxA, none of the residues tested here can conclusively be said to interact with NlpE based on this analysis.

The length of NlpE's linker does not impact signaling

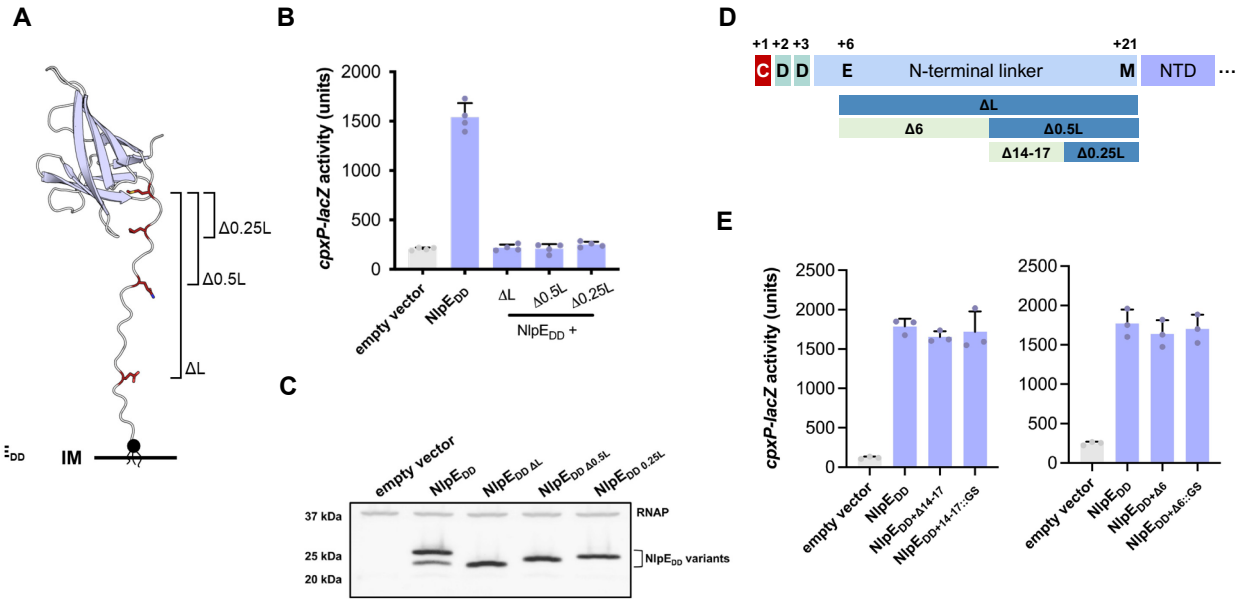

Figure 3-9. The length of NlpE's N-terminal linker does not impact CpxA activation.

(A) NlpE possesses a linker between its acylated cysteine and its globular N-terminal domain. Deletions in this linker region of varying lengths are shown (full length linker deletion, ΔL=Δ26-41; half-length linker deletion, Δ0.5L=Δ34-41; quarter-length linker deletion, Δ0.25L=Δ38-41). **(B)** Ability of linker deletion mutants in permanently inner membrane NlpE ($NlpE_{DD}$) to activate CpxA. Cells were grown to mid-log phase and induced with 0.2% L-arabinose for 1 hour. Shown are the mean *cpxP-lacZ* activity of 3 biological replicates with standard deviation shown. **(C)** shows the protein expression levels of the NlpE variants shown in **(B)** with RNAP α subunit protein levels shown as a loading control. **(D)** is a representation of the location of each different linker deletion tested. The highlighted region indicates the region that was deleted or replaced in experiments **(E)** shows the ability of additional linker deletions in $NlpE_{DD}$ to activate CpxA.

Like many other outer membrane lipoproteins, NlpE's acylated cysteine is connected to its N-terminal globular domain by a long unstructured linker region (El Rayes et al., 2021). This linker is approximately 20 amino acids in length, spanning from Cys21 to Met41 (Figure 3-9A). We wondered if the length of this linker is critical for activating CpxA at the inner membrane. We

introduced deletions of different lengths into this region in $NlpE_{DD}$, the largest being a 16 amino acid Δ26-41 (ΔL) deletion and successive smaller deletions comprising Δ0.5L (Δ34-41) and Δ0.25L (Δ38-41) of eight and four amino acids, respectively. Strikingly, even the smallest 4 amino acid deletion in this region was sufficient to abolish activation by inner membrane NlpE (Figure 3-9B). This was not because of any decreased stability of these variants as all linker deletions are stably expressed (Figure 3-9C).

However, we observed that the terminal residue deleted in all these deletions, Met41, is folded in towards the barrel of NlpE's N-terminal domain in both the crystal structure and AlphaFold models (Hirano et al., 2007). To test if this region may be affecting activation of CpxA, we generated a different set of deletions avoiding this region (Figure 3-9D). In contrast to what we found before, other four or eight amino acid deletions which left Met41 intact did not impact the ability of CpxA to sense NlpE overexpression (Figure 3-9E). Replacing these alternative deletions with glycine-serine repeat sequences similarly did not impact activation of CpxA. Taken together, these results suggest that CpxA is able to sense NlpE that is anchored to the inner membrane at various lengths. This may suggest that CpxA's sensor domain as a whole possesses a degree of flexibility that allows it to "bend" down towards the inner membrane when it senses inner membrane NlpE, a model which is consistent with the dimer-disruption model of CpxA activation proposed in Chapter 2. Furthermore, these results suggest that this region of the N-terminal linker may contain residues that are important for NlpE-CpxA interactions.

NlpE is stabilized by CpxP and DegP

At various points in this study, we observed that NlpE is subject to possible degradation or cleavage. During overexpression, we observe that a NlpE species around the size of the N-terminal domain alone can be detected using a polyclonal anti-NlpE antibody but not anti-His antibody, suggesting that the C-terminal domain of NlpE can get cleaved to leave behind just the N-terminal domain (see Figures 3-1C, 3-2C). NlpE appears to get degraded when simultaneously overexpressed with the lipoprotein maturation enzymes Lgt and LspA, directly reducing activation of CpxA (Figure 3-3C). We thus wanted to explore proteolysis of NlpE as a novel axis of signaling.

Previous studies identified a potential protease inhibitor signal on the N-terminal domain of NlpE (Hirano et al., 2007; Snyder et al., 1995), although no experimental evidence that this sequence modifies NlpE stability has been presented. Snyder and colleagues (1995) suggested that NlpE may interact with DegP directly to inhibit its serine protease activity. This putative protease inhibitor motif comprises the loop between the β-g and β-i strands in the monomer of NlpE (Figure 3-10AB, (Hirano et al., 2007)). We generated two different deletions of this sequence in pTrc-*nlpE* (ΔPIS1 corresponding to Δ122-131 and ΔPIS2 to Δ120-133) as well as a vector expressing NlpE where this sequence is replaced with an equivalent length glycine-serine repeat sequence (PIS::GS). Activation of CpxA is not significantly impacted by the absence of this putative protease inhibitor signal, with CpxA activation occurring at similar to even slightly higher levels compared to WT NlpE overexpression, suggesting that the stability of NlpE is not significantly altered (Figure 3-10C). While we cannot rule out that this sequence may regulate the activity of serine proteases such as DegP, these results suggest that this sequence does not significantly impact the stability of NlpE or that NlpE itself is not the target of degradation by serine proteases.

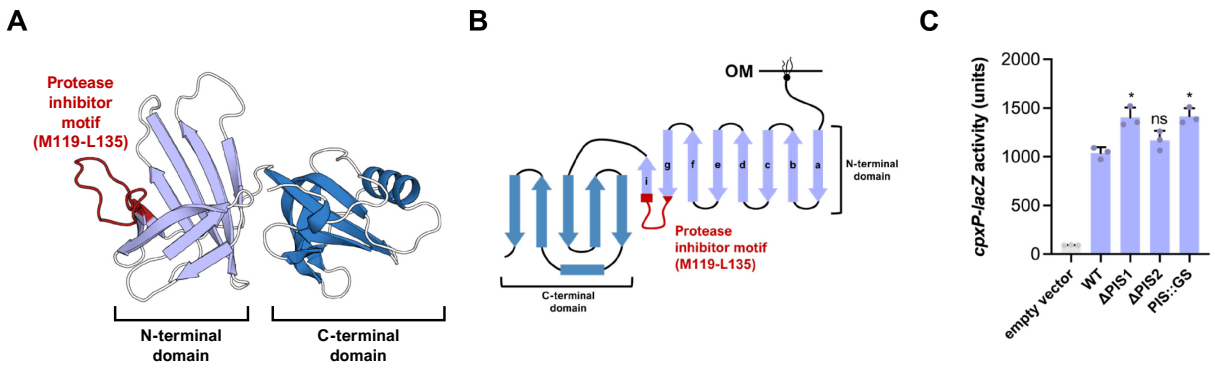

Figure 3-10. NlpE's putative protease inhibitor sequence does not impact activation of CpxA.

The location of the putative protease inhibitor sequence (M119-L135) is shown in both **(A)** the monomer model of NlpE according to AlphaFold database (https://alphafold.ebi.ac.uk/) and **(B)** a cartoon representation of the NlpE monomer. **(C)** Ability of protease inhibitor sequence deletion or substitution variants of NlpE to activate CpxA when overexpressed. Cells were grown to mid-log phase and induced with IPTG for 30 minutes. Shown are the mean of 3 biological replicates with standard deviation, analyzed with a Tukey HSD post-hoc test (ns=non-significant, *p<0.05). Comparisons are to reporter activity when WT NlpE is overexpressed.

Previously, we observed that activation of CpxA by NlpE can be relieved by increased degradation of NlpE (Figure 3-3C). We first wondered if degradation of NlpE is dependent on activation of CpxA by NlpE. In this model, activation of CpxA by inner membrane NlpE stimulates the expression of Cpx regulated proteolytic factors that may degrade aberrantly localized NlpE, preventing toxic levels of Cpx activation. To test this, we repeated the experiments shown in Figure 3-3C (where we simultaneously overexpressed NlpE and lipoprotein biogenesis genes) except this time overexpressing the CpxA-blind variant NlpE R93E variant (Figure 3-11A). As expected, NlpE R93E is unable to activate CpxA in any context. However, NlpE R93E is degraded in almost the exact same way as WT NlpE is; NlpE R93E is strongly degraded in the Lgt and LspA backgrounds, more weakly so in the Lnt overexpression background, and almost

not at all in the LolA and LolB backgrounds. Thus, it's not likely CpxA activation itself stimulates proteolytic degradation of NlpE.

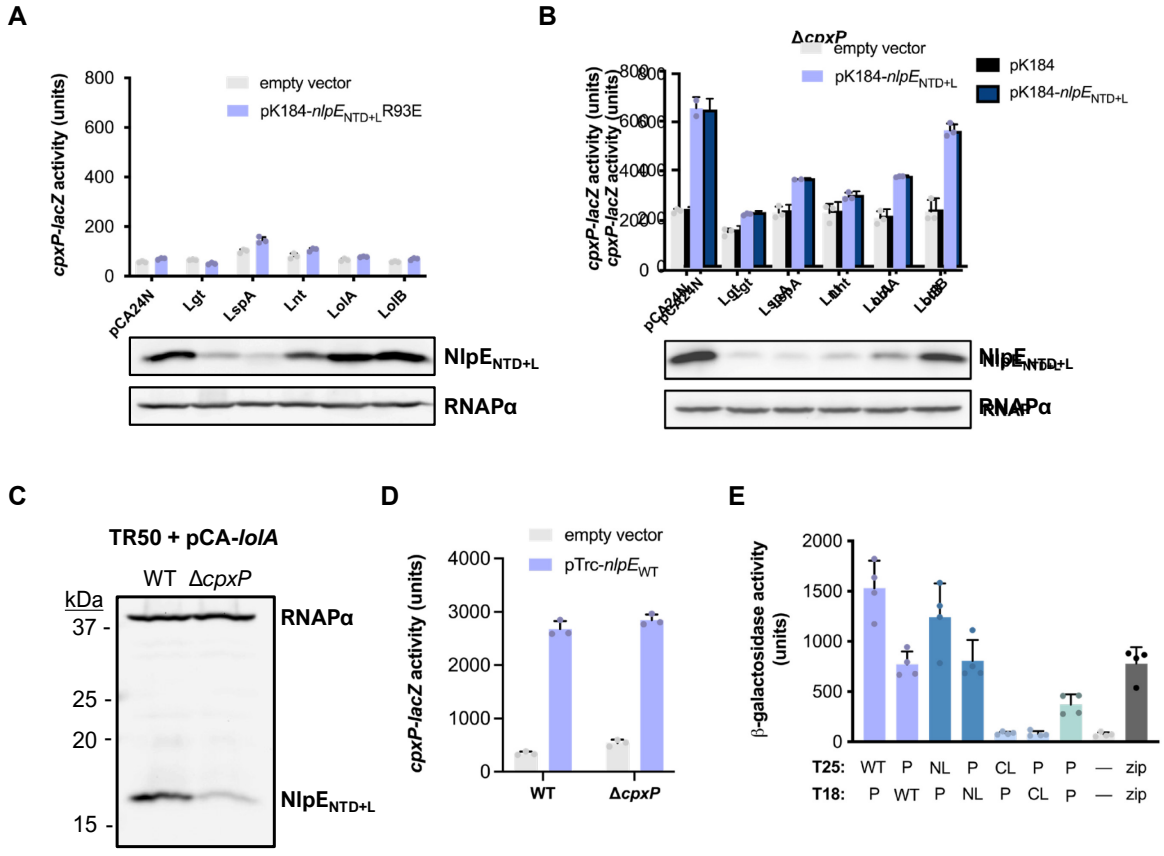

Figure 3-11. CpxP is involved in the stabilization of NlpE at the outer membrane.

Activation of *cpxP-lacZ* during simultaneous overexpression NlpE and lipoprotein biogenesis genes when **(A)** the CpxA-blind NlpE R93E variant is expressed or when **(B)** *cpxP* is deleted. Shown are means of three biological replicates with standard deviation shown. Protein levels as determined by Western blot with anti-NlpE and anti-RNAPα (loading control) antibodies are shown below each graph. **(C)** shows a comparison between the protein levels of NlpENTD+L in WT and Δ*cpxP* strains overexpressing LolA. **(D)** CpxP is not required for CpxA to sense NlpE overexpression in the absence of LolA overexpression. Strains were grown to mid-log and induced with 0.1 mM IPTG before β-galactosidase activity was measured. **(E)** Modified two-hybrid assays of WT, NTD+L (NL), and CTD+L (CL) NlpE tested against CpxP (P). "—" indicates negative control fusions and "zip" indicates positive controls. Shown are means of four replicates with standard deviation.

Previous studies showed that CpxP stimulates proteolysis of overexpressed Pap pilus subunits (Isaac et al., 2005). We wondered if CpxP may be similarly involved in the degradation of NlpE (Figure 3-11B). Contrary to our hypothesis, NlpE expression levels remain low during Lgt and LspA overexpression in the *cpxP* deletion strain, suggesting that CpxP is not responsible for the degradation of NlpE in these backgrounds. Surprisingly, protein levels of NlpE were reduced even during Lnt and LolA expression in the *cpxP* deletion strain, strains where we previously hypothesized that more NlpE is reaching the outer membrane. We directly compared the protein levels of $NlpE_{NTD+L}$ in WT and *cpxP* deletion strains during LolA overexpression and again found that NlpE levels are reduced in the absence of CpxP (Figure 3-11C). These results suggest that CpxP may directly stabilize NlpE, and that this stabilization may occur when NlpE is outer membrane localized. CpxP is not required for activation of CpxA during NlpE overexpression in the absence of LolA overexpression as this background was where we saw the most degradation in the Δ*cpxP* strain (Figure 3-11D), suggesting that CpxP may stabilize NlpE specifically in the outer membrane and not when it is activating CpxA at the inner membrane. We wondered if CpxP might directly interact with NlpE to stabilize it. We used the modified two-hybrid assay to test for direct NlpE-CpxP interactions (Figure 3-11E). As expected from the published structures, CpxP self-interacts in two-hybrid assays (Thede et al., 2011; Zhou et al., 2011). Two-hybrid assays suggest that NlpE directly interacts with CpxP via its N-terminal domain, as NlpE constructs lacking this domain no longer show interaction in this assay. Taken together, these results show a surprising role for CpxP in stabilizing NlpE, potentially by directly interacting with its N-terminal domain.

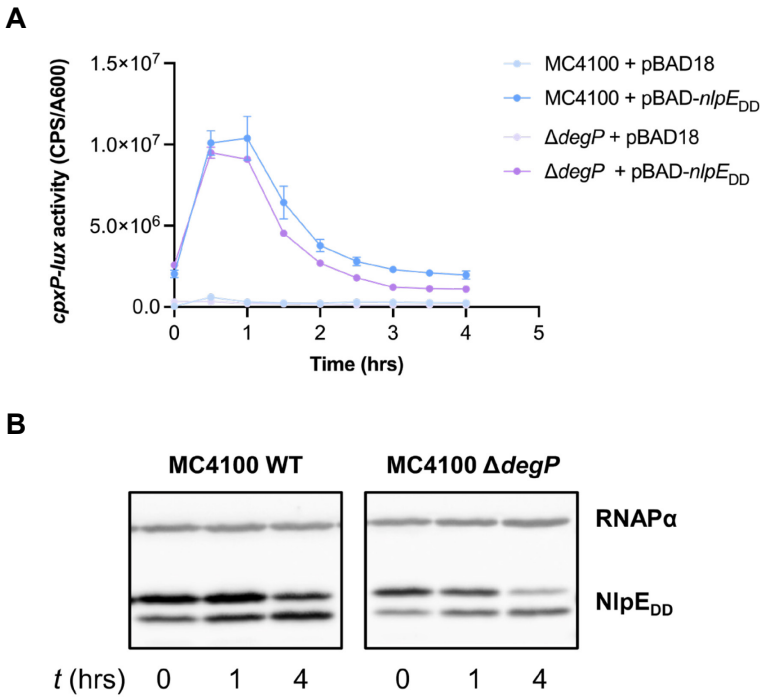

Figure 3-12. DegP stabilizes inner membrane NlpE.

(A) Time course reporter assay monitoring activation of the Cpx response after induction of $NlpE_{DD}$ expression. Cells grown to mid-log phase were induced with 0.2% L-arabinose for one hour. After induction, cells were spun down and media was replaced with LB without inducer. *cpxP-lux* reporter activity was measured at 30 minute intervals after inducer removal. Each of the indicated strains were grown and measured in triplicate. Shown are means with standard deviation. **(B)** follows a similar protocol except samples were collected at the indicated times post inducer removal and then processed for SDS-PAGE and Western blotting with anti-His×6 and anti-RNAPα (loading control) antibody.

Finally, we wondered if the Cpx-regulated protease DegP is involved in the proteolytic regulation of NlpE. We ran a time-course experiment where, after growing up cells expressing permanently inner membrane localized $NlpE_{DD}$, L-arabinose inducer was removed by pelleting cells and the media was replaced with fresh LB. *cpxP-lux* activity was measured at 30-minute intervals after NlpE induction was removed (Figure 3-12A). We observed that activation of the

Cpx response after NlpE induction is stopped reduces over time, suggesting that inner membrane NlpE may be subject to some kind of turnover. Because we used permanently inner membrane localized NlpE for this experiment, we know that this turnover is not due to trafficking of NlpE to the outer membrane. Interestingly, we observed that activation of the *cpxP-lux* reporter at almost all points was lower in a Δ*degP* strain, suggesting that turnover of $NlpE_{DD}$ may occur faster in this strain. Puzzlingly, this suggests that DegP acts to stabilize NlpE. We wondered if this could be verified at the protein level and repeated the inducer-removal experiment, collected samples at the indicated times post inducer removal, and conducted Western blots for NlpE (Figure 3-12B). These results matched our reporter assays almost exactly; NlpE expression levels at almost all points were lower in the Δ*degP* than in WT strains. While by four hours post inducer removal, levels of $NlpE_{DD}$ are reduced in both backgrounds, $NlpE_{DD}$ expression levels were much lower at the end of the experiment in the Δ*degP* strain, and more degradation is seen by one hour post inducer removal. Interestingly, a second, faster running band is observed whenever $NlpE_{DD}$ is expressed (also seen in Figure 3-9C). The intensity of this band appears to be reciprocal to the main NlpE band. It is tempting to speculate that this band may be NlpE that is processed differently. At the very least, this band is unlikely to be due to simple C-terminal cleavage of NlpE as it can still be detected using the anti-His×6 antibody. Taken together, these results suggest that DegP, in a somewhat paradoxical manner, may stabilize NlpE at the inner membrane.

Discussion

In this chapter, we systematically examine the structural features of NlpE and their contribution to activating CpxA at the inner membrane, particularly based on the crystal structure published by Hirano and colleagues (2007) and the monomer model available via the AlphaFold database, which is essentially identical to the hypothetical monomer model proposed in the structural study.

NlpE's N-terminal domain directly interacts with CpxA

Our studies indicate that the N-terminal domain of NlpE is sufficient for activation of CpxA when NlpE is overexpressed (Figure 3-1C). Furthermore, two-hybrid assays indicate that NlpE directly interacts with CpxA in the periplasm and that the N-terminal domain is sufficient for interaction (Figure 3-4). This is in line with findings that were published independently during the completion of the work on this thesis (Delhaye et al., 2019; Marotta et al., 2023a; May et al., 2019). Furthermore, analysis of the surface exposed charges on the N-terminal domain revealed a key role for arginine 93 in mediating activation of CpxA; CpxA is completely blind to NlpE with a charge swap mutation of this residue (R93E). $NlpE_{R93E}$ interacts weakly with CpxA in two-hybrid assays, but this interaction is not as weak as that seen in the negative control group, indicating that $NlpE_{R93E}$ may still interact weakly with CpxA's sensor domain. In contrast, a nearby positive-to-negative swap of lysine 97 ($NlpE_{K97E}$) does not significantly impact NlpE-CpxA interactions while slightly reducing activation of CpxA suggesting that other positively charged residues on the N-terminal domain of NlpE may stabilize or otherwise facilitate NlpE-CpxA interactions without being absolutely essential for them.

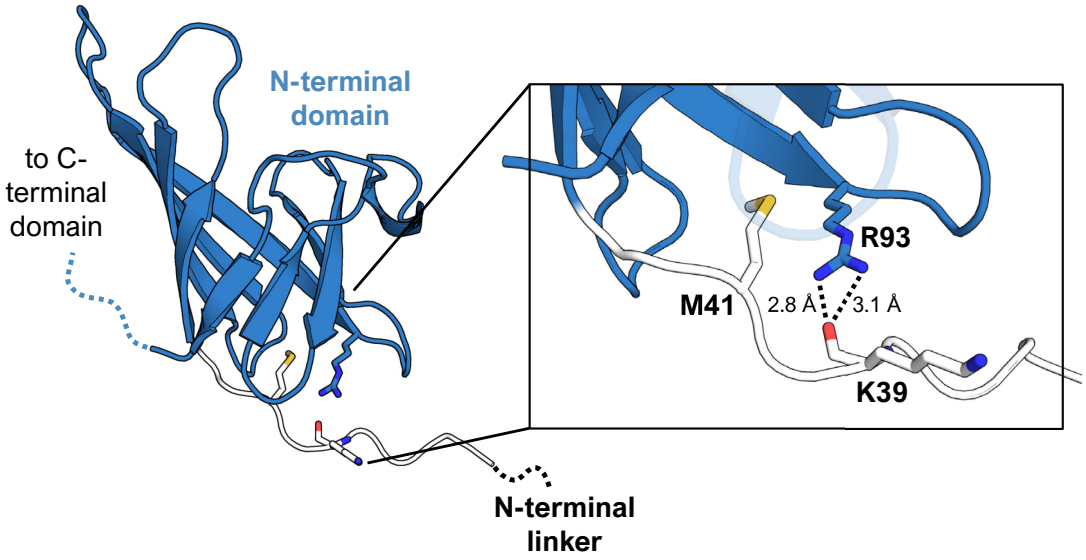

Figure 3-13. Arginine 93 may interact with key linker residues.

The AlphaFold2 model of the N-terminal domain of NlpE monomer (https://alphafold.ebi.ac.uk/). A portion of the N-terminal linker is shown in white. M41 is the first residue present on the crystal structure of NlpE (Hirano et al., 2007). Inset shows the interactions predicted between the C-terminal portion of the linker and key residue R93.

Interestingly, R93 is not completely exposed on the surface of the N-terminal domain; instead, this residue is oriented in towards the lumen of the β-barrel of the N-terminal domain (Figure 3-13). The AlphaFold2 model of the NlpE monomer predicts that R93 makes two hydrogen bonds with the main chain carboxyl group of K39 present on the N-terminal linker of NlpE. While the crystal structure of NlpE begins with residue M41 (and thus no experimental structure with K39 exists), the confidence metrics of these residues allow for a reasonable prediction that this interaction is physiologically relevant (Jumper et al., 2021). The position of R93 is predicted with a very high local confidence score (pLDDT=92.33) which generally corresponds to accurate predictions of both main and side chain positions. The confidence of K39 is still high, albeit lower than for R93 (pLDDT=78.37), allowing for prediction of main chain

position. Because AlphaFold2 predicts R93's side chain to interact with the main chain of K39, we are quite confident that this interaction exists.

This region of the linker is especially interesting as our deletion studies implicated this region in activating CpxA (Figure 3-9). A modest deletion of the last four residues before the N-terminal β-barrel of NlpE (L38-M41) is sufficient to render CpxA unable to sense inner membrane NlpE. This region includes K39 and is overall modelled with high confidence (pLDDT values between 71-83). In contrast, residues preceding this region are modelled with low confidence (pLDDT below 70), suggesting that this region may be significantly more flexible. Likewise, we find that deletions of this region do not impact activation of CpxA (see $NlpE_{DD\Delta 14\text{-}17}$). Taken together, these results can be interpreted to mean the region encoding L38-M41 may form a "cap" like structure that covers the bottom of the NlpE N-terminal β-barrel and this structure is held in place by R93. This finding has several implications. First, the fact that R93 is not immediately exposed to the solvent suggests that conformational changes/misfolding may allow it to become available for interaction with CpxA. However, the L38-M41 region also appears to play an active role in facilitating activation of CpxA, perhaps by helping position R93, as deletion of the region encoding L38-M41 completely abrogates CpxA activation. Recent work from the Grabowicz lab bears out many of these predictions. Marotta and colleagues used a mutagenesis screen to independently find that R93 (numbered as R73 in their study) is critical for activation of CpxA (Marotta et al., 2023a). Their AlphaFold2 model of NlpE-CpxA interactions appears to show that interactions between R93 and K39 are broken in order to allow for NlpE-CpxA interactions.

In contrast to the deletion of L38-M41, deletions of other portions of the linker do not impact the ability of NlpE to signal to CpxA. The largest deletion in this region we tested spanned eight amino acids, which corresponds to roughly 20 Å. This is a significant change in length.

Furthermore, these mutations were all created in inner membrane localized NlpE and thus it is unlikely that these variants become associated with LolA. Thus, a model where LolA carrying NlpE interacts with CpxA during transit is unlikely. The fact that CpxA is able to sense this truncated NlpE at the membrane suggests that the sensor domains of CpxA may possess significant flexibility and be able to "bend" down towards the membrane during activation. In Chapter 2, we proposed a model where the non-canonical dimer structure of CpxA's sensor domains is disrupted during activation. A "bending" type of movement of the sensor domains, perhaps stimulated by binding of a ligand like NlpE or during the presence of inner membrane defects, may facilitate disrupt the CpxA sensor domain dimer, leading to activation of CpxA.

We also find that basic residues on the N-terminal domain of NlpE are important for activating CpxA. Marotta and colleagues (2023) also reported interactions between R93 and negatively charged residues on CpxA' sensor domain, namely D136, E138, and D139 according to an AlphaFold2 model. These are residues we also tested in our study (Figure 3-8). In our experiments, we found that mutation of many of these residues lead to activation of CpxA basally (Figure 3-7B). In particular, D136R possessed a *cpxA** like phenotype, making it difficult to determine whether it is insensitive to NlpE overexpression because it no longer interacts with NlpE. Marotta and colleagues (2023) report that alanine substitutions of these residues do not lead to hyperactivation basally and are still sensitive to Pap pilus overexpression, while no longer being as sensitive to NlpE overexpression. Thus, there is strong evidence that these acidic residues mediate CpxA sensing of NlpE.

While we found that the D60R and D64R mutations reduce the sensitivity of CpxA to NlpE overexpression while not significantly impacting its ability to sense alkaline pH (Figure 3-7A), neither of these residues restore the ability of CpxA to sense signaling-incompetent $NlpE_{R93E}$ making it unlikely that these residues directly interact with NlpE R93. However, the location of

these residues on the loop between the α1 and α2 helices of CpxA may give us clues as to how CpxA becomes activated during NlpE overexpression. D136 on the sensor domain of CpxA interacts via salt bridge with R70 on the α2 of CpxA's sensor domain and disruption of this interaction by introducing the D136R charge swap hyper-activates CpxA. CpxA D136R is also insensitive to NlpE overexpression. The fact that an alanine substitution at this residue does not possess as dramatic of a phenotype (Marotta et al., 2023a) suggests that a larger disturbance to α2 helix positioning may be required to hyper-activate CpxA. Based on these results, we propose the following model: in the presence of inner membrane NlpE, NlpE R93 may disrupt the position of the α2 helix of the CpxA sensor domain by interacting with D136. This conformational change leads to activation of CpxA. Supporting this hypothesis, the CpxA E56R mutation similarly causes hyper-activation of CpxA, potentially by disrupting a separate interaction with the α2 helix. However, neither our study or Marotta and colleague's (2023) conclusively prove interactions between R93 and acidic residues on CpxA's sensor domain. Thus, more work, for example by determining the structure of NlpE-CpxA complexes and via site-specific crosslinking, will be required to determine the precise molecular nature of NlpE-CpxA interactions.

NlpE stability may be controlled by Cpx-regulated factors

Hirano and colleague's (2007) structure of NlpE possessed several interesting but unexplored structural features. One of the most striking is that the NlpE dimer is asymmetric and that dimerization occurs through exchange of the β-i strands between each protomer to complete their N-terminal β-barrel domains. Consistent with the published domain-swapped dimer structure of NlpE, we report the formation of NlpE dimers *in vivo* when NlpE is overexpressed. The precise relevance of this dimer for NlpE signaling, however, is unclear. Domain-swapping has both positive and negative functional consequences for many different

proteins, sometimes leading to aggregation and loss of function, and in other proteins promoting function (Mascarenhas and Gosavi, 2017). NlpE dimerization may be important for protein stability as dimers are stable in the presence of heat and SDS. Significantly, we do not know if NlpE dimers form at native levels of NlpE expression and in our studies, dimers are only observed during exogenous expression of NlpE. Nevertheless, dimerization-deficient variants of NlpE do not appear to interact with CpxA and previous work in the Raivio lab reported that these same deletion strains are unable to activate a Cpx regulated *yjiN-lacZ* reporter (Junshu Wang, PhD thesis). While studies of NlpE at native levels are difficult because of its relatively low level of expression, further studies should aim to determine if NlpE dimers can be observed without overexpression. Biochemical studies should test if NlpE dimers are more stable than monomers.

Throughout our studies, we noticed that overexpressed NlpE appears to be the target of proteolytic processing. Furthermore, this degradation appears to remove the C-terminal portions of NlpE as the C-terminal His-tag is not present in this product (Figure 3-2C). We observed that overexpression of the lipoprotein processing enzymes Lgt and LspA (and to a lesser extent Lnt) actually decreases the protein expression levels of NlpE when overexpressed (Figure 2E). Potentially, "jammed" complexes between NlpE and these proteins when NlpE is overexpressed may be the targets of proteolysis in the envelope. Alternatively, because these experiments were conducted with NlpE constructs that lack the C-terminal domain, it's possible that this domain is required for stability once NlpE reaches the outer membrane. NlpE possesses a putative protease inhibitor sequence at the C-terminal end of the N-terminal domain (Hirano et al., 2007). This region was originally identified as a potential serine protease inhibitor signal by Snyder and colleagues (1995) via computational analysis. However, no experimental evidence thus far has examined the contribution of this region to NlpE stability or its ability to directly inhibit serine protease activity. NlpE variants that lack this region (e.g. $NlpE_{1\text{-}120}$ and especially $NlpE_{1\text{-}101}$) show

decreased stability. However, deletion of this region in the full-length protein does not significantly impact activation of CpxA (Figure 3-10), making it more likely that misfolding caused by truncations of the N-terminal domain is more likely leading to increased NlpE degradation. Further studies will be required to determine if this sequence truly functions to inhibit NlpE proteolysis.

Surprisingly, we found that both CpxP and DegP appear to stabilize NlpE, albeit in different contexts. We found that Cpx activation is significantly lowered when LolA and NlpE are co-expressed, suggesting that more NlpE is being removed from the inner membrane in this strain. In this context, CpxP is required for NlpE stability, as a significant decrease in NlpE protein levels is seen in a Δ*cpxP* background. A similar stabilization is seen in the Lnt overexpression background, although to a lesser degree. This suggests that CpxP may have a role in stabilizing NlpE at the outer membrane. Alternatively, it's possible that during LolA overexpression, more NlpE is found associated with LolA and released from the inner membrane but not necessarily inserted into the outer membrane. In this case, CpxP may stabilize periplasmic complexes of NlpE and LolA. In any case, a role for CpxP in stabilizing NlpE is highly unusual as CpxP is thought of as a factor that promotes the degradation of harmful envelope proteins (Buelow and Raivio, 2005; Isaac et al., 2005; Thede et al., 2011; Tschauner et al., 2014; Zhou et al., 2011).

The mechanisms by which CpxP functions as a chaperone are largely mysterious. Some clues may be gleaned from other proteins that are structurally related to CpxP. CpxP belongs to a family of chaperones including Spy and ZraP (Kwon et al., 2010). Both CpxP and Spy fold into dimers that consist of α-helices that form into a concave oval shape (Kwon et al., 2010; Quan et al., 2011; Thede et al., 2011; Zhou et al., 2011). Spy has been shown to prevent periplasmic protein aggregation, promote refolding, and increase the stability of several envelope proteins,

including outer membrane β-barrel proteins such as OmpX and OmpA (He et al., 2021; Mitra et al., 2021; Quan et al., 2011). It is tempting to speculate CpxP may have a similar role in stabilizing NlpE. Two-hybrid assays suggest CpxP and NlpE's N-terminal β-barrel directly interact further supporting a model where CpxP directly stabilizes NlpE in manner analogous to how Spy stabilizes β-barrel proteins. However, the context in which CpxP accomplishes this is not clear as CpxP is not required for activation of the Cpx response during NlpE overexpression (Raivio et al., 1999) (Figure 3-11D). However, it's possible that high levels of NlpE expression are sufficient to saturate CpxA and therefore any stabilizing effects of CpxP are negligible in this context. CpxP itself is subject to proteolytic degradation by DegP (Isaac et al., 2005), so it's possible that NlpE may play a role in stabilizing CpxP (although this is highly speculative).

We also present (emerging) evidence that DegP may be involved in stabilizing NlpE (Figure 3-12). DegP is a key envelope protein quality control factor. Expression of DegP is controlled by both the σ^E and Cpx envelope stress responses (Danese and Silhavy, 1997; Pogliano et al., 1997). Like CpxP, DegP is associated with the degradation of misfolded envelope proteins (Danese et al., 1995; Isaac et al., 2005; Snyder et al., 1995). The mechanism by which inner membrane NlpE protein levels are increased in the presence of DegP are mysterious. The simplest explanation is that DegP directly binds and protects NlpE from degradation. While DegP is reported to have chaperone activity (Braselmann et al., 2016; Krojer et al., 2008; Spiess et al., 1999), this is somewhat controversial, with some studies arguing that DegP functions exclusively as a protease (Chang, 2016; Ge et al., 2014; Kim et al., 1999). Interestingly, while unfolded OMPs are thought to be the main substrate of DegP, studies have shown that OmpA is the exception and that DegP can bind to the folded, periplasmic globular domain of OmpA and that this domain is resistant to degradation by DegP (Ge et al., 2014; Zhang et al., 2019). However, given these results, it's not clear if DegP directly promotes NlpE stability given OmpA's cell wall

binding domain does not share any significant similarities to NlpE. The other possibility is that DegP degrades an unknown factor that promotes the proteolysis of NlpE.

At this point, we lack the evidence to make strong claims either way but this finding, along with the finding that CpxP stabilizes NlpE, nonetheless suggests a novel regulatory loop in the Cpx response; after activating CpxA, NlpE may be stabilized by several Cpx-regulated factors. Increasing the stability of NlpE may be a mechanism of extending or amplifying the signal from NlpE. There's probably little benefit to this in a context where there is already overexpression of much more NlpE than would ever normally be found in the envelope. However, in the presence of a physiologically relevant stressor such as copper or compounds that inhibit lipoprotein biogenesis, which activate the Cpx response through NlpE (May et al., 2019), stabilization may function as a much more important mechanism of signal amplification. Indeed, throughout our studies we have noticed that NlpE is difficult to detect at native levels of expression and ribosome profiling puts NlpE expression levels at about 300-500 copies per cell in rich media, significantly less than the 1000-3000 copies estimated for RcsF, another envelope stress sensing outer membrane lipoprotein (Li et al., 2014). Thus, stabilization of NlpE may be an economical way for cells to ensure sufficient activation of the Cpx response during stress. In line with this, May and colleagues (2019) report only relatively modest induction of the Cpx response through NlpE in the presence of copper. Future studies should investigate the roles of DegP and CpxP during the cellular response to a physiological stressor such as copper and the protein levels of NlpE in order expand on this potentially novel axis of NlpE signaling.

Conclusions

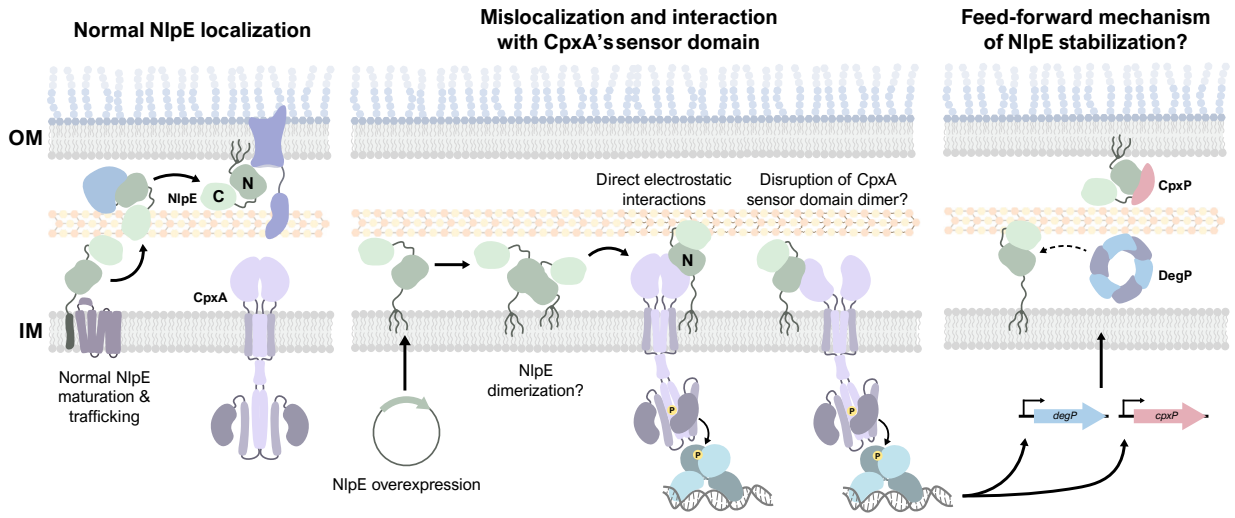

Figure 3-14. NlpE signals to CpxA at the inner membrane.

In the absence of stressors to lipoprotein biogenesis, NlpE is secreted, processed, and trafficked to the outer membrane (right-most panel). Overexpression of NlpE leads to inner membrane accumulation, dimerization, and, most importantly, direct interaction with the sensor domain of CpxA. Activation of CpxA in this contact may involve significant movement of the sensor domain away from its basal dimer configuration. Once induced, several Cpx-regulated factors, including CpxP and DegP may promote the stability of NlpE.

The outer membrane lipoprotein NlpE is a key activator of the CpxRA system. Recent literature suggests that NlpE monitors lipoprotein biogenesis by virtue of its localization; while normally trafficked to the outer membrane by the Lol pathway, NlpE can mislocalize to the inner membrane when lipoprotein maturation or trafficking is disrupted and directly activate CpxA (Delhaye et al., 2019; Grabowicz and Silhavy, 2017a; Marotta et al., 2023a; May et al., 2019). In this chapter, we expand our understanding of how NlpE signals to CpxA at the inner membrane and how CpxA may get activated in this context (Figure 3-14). Furthermore, we report a novel axis of regulation whereby Cpx regulated factors promote the stability of NlpE, which may be a

mechanism of signal amplification. Understanding the role of the Cpx response and NlpE specifically as a system that senses and mitigates threats to lipoprotein biogenesis will be an important area of study as these pathways increasingly become the targets of novel therapeutic development (Lehman and Grabowicz, 2019; McLeod et al., 2015; Nickerson et al., 2018).

Materials and Methods

Bacterial strains, growth, and strain construction

The strains used in this study are listed in Table 3-1. All strains were grown in lysogeny broth (LB) at 37°C with shaking at 225 RPM that was supplemented with the following concentrations of antibiotics as appropriate: ampicillin (100 µg/ml), kanamycin (50 µg/ml), chloramphenicol (25 µg/ml), and spectinomycin (25 µg/ml). To induce expression from inducible promoters, 0.1 mM isopropyl β-d-1-thiogalactopyranoside (IPTG) or 0.2% L-arabinose was added to cultures that were grown to an optical density of 0.4-0.6 (A_{600}) for 0.5-2 hours depending on the experiment. All whole gene deletion mutants were constructed by P1 transduction using lysates derived from the corresponding mutants from the Keio library (Baba et al., 2006). Kan^R cassettes were removed using FLP-mediated recombination as previously described (Datsenko and Wanner, 2000). Strains containing plasmids were transformed via chemically-induced competence.

Expression vector construction and site-directed mutagenesis

The plasmids used in this study are listed in Table S2. Overexpression plasmids were created by restriction digest cloning utilizing standard procedures and the primers listed in Table 3-2. Site-directed mutagenesis was used to introduce deletions and substitutions into expression vectors using the Q5 site directed mutagenesis kit (New England Biolabs) and according to manufacturer's instructions. The primers used for site-directed mutagenesis are listed in Table S3. For consistency, the numbering of amino acids in envelope proteins throughout this study includes the amino acids of the signal peptide. The sequence of inserts/mutants were confirmed by sequencing (Molecular Biology Facility, University of Alberta).

Vectors used in two-hybrid assays were created using Gateway cloning (Invitrogen) according to manufacturer's instructions and the corresponding primers in Table 3-3. Briefly, primers were designed to amplify *nlpE* and *nlpE* variants as well as the region encoding the periplasmic CpxA sensing domain (aa31-163) flanked by *attB1* and *attB2* sites. PCR products were recombined into pDONR-DEST in BP reactions. Sequence-confirmed entry clones were used in LR recombination reactions to recombine our genes of interest into pSTM25-DEST and pUTM18C-DEST, which encode for the adenylate cyclase T25 and T18 subunits, respectively, with an OppB transmembrane domain between the subunits and the recombination site (Ouellette et al., 2014). The reaction mixture was transformed into OneShot OmniMAX 2 $T1^R$ chemically competent cells (Invitrogen), and plasmids were sequenced to confirm that no abnormalities were introduced throughout the cloning process.

β-galactosidase assays

cpxP-lacZ activity and cAMP production during two-hybrid assays were measured by quantifying β-galactosidase activity as previously describe (Buelow and Raivio, 2005; Slauch and Silhavy, 1991). Briefly, *E. coli* TR50 (MC4100 *cpxP-lacZ*) were grown overnight in LB and then subcultured in 2 ml LB. Cultures were spun down and cell pellets were resuspended in Z-buffer (Miller, 1972). The optical density (OD at A_{600}) was measured and then each culture was treated with chloroform and sodium dodecyl sulfate (SDS) and vortexed to release β-galactosidase. β-galactosidase activity was quantified by measuring the A_{420} of each culture 25 times at 30s intervals after the addition of 10 mg/ml ortho-nitrophenyl β-galactoside (ONPG). *cpxP-lacZ* activity was calculated as the maximum slope of the linear region of A_{420} measurements standardized to that culture's OD. The statistical significance was calculated using two-way ANOVA tests with a Tukey post-hoc test for multiple comparisons (Prism, Graphpad).

Gateway-compatible modified bacterial two-hybrid assays

Vectors containing genes encoding proteins of interest fused to the adenylate cyclase T25 or T18 subunits were co-transformed into *E. coli* BTH101 and plated on media with antibiotics, 0.1 mM IPTG, and 20 µg/ml 5-bromo-4-chloro-3-indolyl-β-D-galactopyranoside (X-gal). Transformants were incubated for two nights at 30°C. From transformants, 2 ml overnight cultures were created in LB with antibiotics and 0.1 mM IPTG and grown at 30°C with shaking for 20-22 hours. β-galactosidase activity was then measured as detailed above to quantify cAMP production.

Sucrose density membrane fractionation

To determine NlpE localization, sucrose-density membrane fractionation was conducted as described in (Dunstan et al., 2017). 500 ml LB subcultures were created from overnight cultures and grown to an OD of ~0.8. Cells were then pelleted at 4°C washed once with 10 mM Tris-HCl (pH 7.5) and resuspended in Tris-sucrose (TS) buffer (10 mM Tris-HCl pH7.5, 0.75 M sucrose) with 50 µg/ml lysozyme and 2 mM phenylmethylsufonyl fluoride (PMSF). 1.65 mM ethylenediaminetetraacetic acid (EDTA) was slowly added, and this mixture was incubated on ice for 10-15 minutes before being lysed with two passes through a French press. An aliquot this whole cell lysate was processed for SDS-PAGE, and the rest of the lysate was centrifuged at 15,000×g for 20 minutes at 4°C to pellet debris/unlysed cells. 25 ml of this cleared whole cell lysate was centrifuged in a Beckman Optima LE-80K ultracentrifuge at 38,000 RPM for 45 minutes at 4°C in a Type 50.2 Ti fixed angle rotor (Beckman-Coulter) to pellet the total membrane fraction. The supernatant was kept and processed as the cytoplasmic fraction. The total membrane fraction was washed once with 25 ml Tris-EDTA-sucrose (TES) buffer (1 part TS buffer to 2 parts 1.65 mM EDTA) and centrifuged again. The resulting total membrane fraction was resuspended in 500 µl of 25% (w/w) sucrose in 5 mM EDTA pH 7.5.

The remaining total membrane fraction resuspended in 25% sucrose was then subject to sucrose density gradient fractionation. The sucrose gradients were prepared immediately before use by carefully pouring equal volume layers of 35-60% (w/w) sucrose-5 mM EDTA in 26.5 ml polycarbonate tubes with caps (Beckman-Coulter), starting with the 60% (i.e. 60%, then 55%, etc.). Once prepared, 400 µl of the total membrane fraction in 25% sucrose was carefully layered on top of the 35% sucrose top layer and then centrifuged in the Type 50.2 Ti rotor at 40,000 RPM for 18 hours at 4°C. After centrifugation, equal-volume fractions were collected from the top of each tube, and fractions were processed for SDS-PAGE.

In vivo crosslinking

in vivo crosslinking with the membrane permeable crosslinker disuccinimidyl suberate (DSS; Thermo Scientific) was conducted as previously described with minor modifications (Lu et al., 2012). The optical density (A_{600}) of cultures was used to collect a standardized amount of cells corresponding to an OD 2.0 in 200 µl. Cells were washed four times with phosphate buffered saline (PBS) and then subjected to crosslinking with 0.5 or 1 mM DSS for 30 minutes at room temperature. 5 µl of 1 M Tris-HCl was added to quench any excess crosslinking reagent for 5-10 minutes. Cells were then washed one more time with PBS. Cell lysates were prepared by resuspending pellets in MilliQ H_2O and 2×Laemmli sample buffer (Sigma) and heating at 95°C for 5 minutes. SDS-PAGE and Western blotting was used to visualize crosslinked complex formation.

SDS-polyacrylamide gel electrophoresis and Western blotting

SDS-PAGE and Western blotting was conducted according to standard protocols. Where indicated, protein concentrations of solutions were determined by BCA protein assay (Pierce) following manufacturer's instructions. Briefly, samples were separated on 8-12% SDS-PAGE gels

and transferred to nitrocellulose membranes using semi-dry transfer (BioRad Trans-Blot Semi-Dry Transfer Cell). Membranes were blocked in 5% non-fat milk in Tris-buffered saline with 0.1% Tween-20 (TBST) and probed with primary antibody overnight at 4°C in 2% BSA in TBST at the following concentrations: anti-NlpE (rabbit polyclonal, this study, 1:8,000-40,000), anti-His×6 (mouse monoclonal, Invitrogen, 1:10,000-20,000), anti-OmpA (rabbit polyclonal, Antibody Research Corporation, 1:5,000-10,000), anti-CpxA-MBP (rabbit polyclonal, (Raivio and Silhavy, 1997), 1:10,000) and anti-RNAP (mouse monoclonal, BioLegend, 1:5,000). Chemiluminescent alkaline phosphatase (AP)-conjugated (BioRad) or fluorescent IRDye 800CW (goat anti-rabbit) and 680RD (goat anti-mouse) antibodies were used to detect proteins. Chemiluminescent signal was generated using the Immun-Star AP chemiluminescence kit according to manufacturer's instructions (BioRad). All blots were imaged using the BioRad ChemiDoc imaging system. Where applicable, relative levels of protein bands were quantified using ImageJ.

Luminescent reporter assay

Strains derived from MC4100 (WT or Δ*degP*) were transformed with the plasmid pJW1 encoding a transcriptional fusion of the promoter region of *cpxP* to the genes of the *lux* operon (Price and Raivio, 2009). Overnight cultures were grown in triplicate at 37°C with shaking in LB with antibiotics. The next day, overnight cultures were subcultured with a 1/50 dilution into fresh media and were grown until cells reached mid-log phase (OD 0.4-0.6). L-arabinose was then added to a final concentration of 0.2% in each culture and $NlpE_{DD}$ expression was induced for 1 hour at 37°C with shaking. After induction, cultures were centrifuged at 5000 RPM for 10 minutes, supernatants were aspirated, and replaced with fresh LB with antibiotics. An initial measurement of the luminescence (measured in counts per second, CPS) and optical density of each culture (absorbance at 600 nm) was measured (t=0 hrs). Luminescence and OD readings were taken at 30-minute intervals for 4 hours. For each replicate and time point, the

luminescence reading was standardized to that culture's optical density (giving the final readout of CPS/A600). Results were graphed in Prism (GraphPad). To quantify corresponding protein levels, the experimental procedure was repeated with samples collected for SDS-PAGE analysis at 0, 1, and 4 hours post inducer removal.

Acknowledgements

We would like to thank Dr. Jun Lu (Glover Lab, University of Alberta) for generating and providing the NlpE charge swap expression vectors in pK184; Vincent Man for strain VM40; Valeria Tsviklist for strain VT97; Dr. Scot Oullette (University of Nebraska Medical Center) for providing the modified vectors used for the modified two-hybrid assays; and Dr. R. Glen Uhrig (University of Alberta) for the use of his ultracentrifuge for fractionations.

Tables

Table 3-1. Strains used in this study.

Strain	Description	Source
MC4100	F_ *araD139* (*argF-lac*)*U169 rpsL150* (Strr) *relA1 flbB5301 decC1 ptsF25 rbsR*	(Casadaban, 1976)
TR50	MC4100 λRS88[*cpxP'-lacZ*$^{+}$]	(Raivio and Silhavy, 1997)
TC209	TR50 + pTrc-*nlpE*$_{WT}$	This study
TC210	TR50 + pTrc-*nlpE*$_{NTD+L}$	This study
TC211	TR50 + pTrc-*nlpE*$_{1-137}$	This study
TC212	TR50 + pTrc-*nlpE*$_{NTD}$	This study
TC213	TR50 + pTrc-*nlpE*$_{1-101}$	This study
TC214	TR50 + pTrc99A	This study
TC453	TR50 + pBAD18	This study
TC454	TR50 + pBAD18-*nlpE*$_{WT}$	This study
TC455	TR50 + pBAD18-*nlpE*$_{NTD+L}$	This study
TC468	TR50 + pBAD18-*nlpE*$_{DD}$	This study
TC469	TR50 + pBAD18-*nlpE*$_{NTDL+DD}$	This study
TC70	TR50 + pCA-*nlpE*	This study
TC71	TR50 + pCA24N	This study
TC363	TR50 + pK184 + pCA24n	This study
TC364	TR50 + pK184 + pCA-*lgt*	This study
TC365	TR50 + pK184 + pCA-*lspA*	This study
TC366	TR50 + pK184 + pCA-*lnt*	This study
TC367	TR50 + pK184 + pCA-*lolA*	This study
TC368	TR50 + pK184 + pCA-*lolB*	This study
TC369	TR50 + pK184-*nlpE*$_{NTD+L}$ + pCA24n	This study
TC370	TR50 + pK184-*nlpE*$_{NTD+L}$ + pCA-*lgt*	This study
TC371	TR50 + pK184-*nlpE*$_{NTD+L}$ + pCA-*lspA*	This study
TC372	TR50 + pK184-*nlpE*$_{NTD+L}$ + pCA-*lnt*	This study
TC373	TR50 + pK184-*nlpE*$_{NTD+L}$ + pCA-*lolA*	This study
TC374	TR50 + pK184-*nlpE*$_{NTD+L}$ + pCA-*lolB*	This study
TC327	TR50 + pK184-*nlpE*$_{NTD+L}$	This study
TC328	TR50 + pK184-*nlpE*$_{K65E}$	This study
TC329	TR50 + pK184-*nlpE*$_{R93E}$	This study
TC330	TR50 + pK184-*nlpE*$_{K97E}$	This study
TC331	TR50 + pK184-*nlpE*$_{K107E}$	This study
TC354	TR50 + pK184-*nlpE*$_{D53R}$	This study
TC355	TR50 + pK184-*nlpE*$_{D73R}$	This study
TC356	TR50 + pK184-*nlpE*$_{D80R}$	This study
TC357	TR50 + pK184-*nlpE*$_{D81R}$	This study
TC358	TR50 + pK184-*nlpE*$_{D102R}$	This study
TC359	TR50 + pK184-*nlpE*$_{E106R}$	This study
TC360	TR50 + pK184-*nlpE*$_{R111E}$	This study

TC361	TR50 + pK184-*nlpE*$_{K113E}$	This study
TC362	TR50 + pK184-*nlpE*$_{R123E}$	This study
RM53	TR50 Δ*cpxA*	Roxana Malpica
TC666	RM53 + pK184-*cpxA*$_{E50R}$	This study
TC667	RM53 + pK184-*cpxA*$_{E54R}$	This study
TC668	RM53 + pK184-*cpxA*$_{D60R}$	This study
TC669	RM53 + pK184-*cpxA*$_{D76R}$	This study
TC670	RM53 + pK184-*cpxA*$_{E101R}$	This study
TC671	RM53 + pK184-*cpxA*$_{D136R}$	This study
TC672	RM53 + pK184-*cpxA*$_{D139R}$	This study
TC673	RM53 + pK184-*cpxA*$_{D40R}$	This study
TC676	RM53 + pK184-*cpxA*$_{E56R}$	This study
TC677	RM53 + pK184-*cpxA*$_{D64R}$	This study
TC678	RM53 + pK184-*cpxA*$_{D40R}$ + pTrc99A	This study
TC679	RM53 + pK184-*cpxA*$_{E50R}$ + pTrc99A	This study
TC680	RM53 + pK184-*cpxA*$_{E54R}$ + pTrc99A	This study
TC681	RM53 + pK184-*cpxA*$_{E56R}$ + pTrc99A	This study
TC682	RM53 + pK184-*cpxA*$_{D60R}$ + pTrc99A	This study
TC683	RM53 + pK184-*cpxA*$_{D64R}$ + pTrc99A	This study
TC684	RM53 + pK184-*cpxA*$_{D76R}$ + pTrc99A	This study
TC685	RM53 + pK184-*cpxA*$_{E101R}$ + pTrc99A	This study
TC686	RM53 + pK184-*cpxA*$_{D136R}$ + pTrc99A	This study
TC687	RM53 + pK184-*cpxA*$_{D139R}$ + pTrc99A	This study
TC688	RM53 + pK184-*cpxA*$_{D40R}$ + pTrc-*nlpE*$_{WT}$	This study
TC689	RM53 + pK184-*cpxA*$_{E50R}$ + pTrc-*nlpE*$_{WT}$	This study
TC690	RM53 + pK184-*cpxA*$_{E54R}$ + pTrc-*nlpE*$_{WT}$	This study
TC691	RM53 + pK184-*cpxA*$_{E56R}$ + pTrc-*nlpE*$_{WT}$	This study
TC692	RM53 + pK184-*cpxA*$_{D60R}$ + pTrc-*nlpE*$_{WT}$	This study
TC693	RM53 + pK184-*cpxA*$_{D64R}$ + pTrc-*nlpE*$_{WT}$	This study
TC694	RM53 + pK184-*cpxA*$_{D76R}$ + pTrc-*nlpE*$_{WT}$	This study
TC695	RM53 + pK184-*cpxA*$_{E101R}$ + pTrc-*nlpE*$_{WT}$	This study
TC696	RM53 + pK184-*cpxA*$_{D136R}$ + pTrc-*nlpE*$_{WT}$	This study
TC697	RM53 + pK184-*cpxA*$_{D139R}$ + pTrc-*nlpE*$_{WT}$	This study
TC854	RM53 + pK184-*cpxA*$_{D60R}$ + pTrc-*nlpE*$_{R93E}$	This study
TC855	RM53 + pK184-*cpxA*$_{D64R}$ + pTrc-*nlpE*$_{R93E}$	This study
TC856	RM53 + pK184-*cpxA*$_{D139R}$ + pTrc-*nlpE*$_{R93E}$	This study
TC630	TR50 + pBAD18-*nlpE*$_{DD+\Delta L}$	This study
TC631	TR50 + pBAD18-*nlpE*$_{DD+\Delta 0.5L}$	This study
TC632	TR50 + pBAD18-*nlpE*$_{DD+\Delta 0.25L}$	This study
TC779	TR50 + pBAD18-*nlpE*$_{DD+\Delta 14-17}$	This study
TC780	TR50 + pBAD18-*nlpE*$_{DD+14-17::GS}$	This study
TC809	TR50 + pBAD18-*nlpE*$_{DD+\Delta 6}$	This study
TC810	TR50 + pBAD18-*nlpE*$_{DD+\Delta 6::GS}$	This study
TC864	TR50 + pTrc-*nlpE*$_{\Delta PIS1}$	This study
TC865	TR50 + pTrc-*nlpE*$_{\Delta PIS2}$	This study
TC866	TR50 + pTrc-*nlpE*$_{PIS::GS}$	This study

TC766	TR50 Δ*cpxP* + pK184 + pCA24N	This study
TC767	TR50 Δ*cpxP* + pK184 + pCA-*lgt*	This study
TC768	TR50 Δ*cpxP* + pK184 + pCA-*lspA*	This study
TC769	TR50 Δ*cpxP* + pK184 + pCA-*lnt*	This study
TC770	TR50 Δ*cpxP* + pK184 + pCA-*lolA*	This study
TC771	TR50 Δ*cpxP* + pK184 + pCA-*lolB*	This study
TC772	TR50 Δ*cpxP* + pK184-*nlpE*$_{NTD+L}$ + pCA24N	This study
TC773	TR50 Δ*cpxP* + pK184-*nlpE*$_{NTD+L}$ + pCA-*lgt*	This study
TC774	TR50 Δ*cpxP* + pK184-*nlpE*$_{NTD+L}$ + pCA-*lspA*	This study
TC775	TR50 Δ*cpxP* + pK184-*nlpE*$_{NTD+L}$ + pCA-*lnt*	This study
TC776	TR50 Δ*cpxP* + pK184-*nlpE*$_{NTD+L}$ + pCA-*lolA*	This study
TC777	TR50 Δ*cpxP* + pK184-*nlpE*$_{NTD+L}$ + pCA-*lolB*	This study
TC778	TR50 Δ*cpxP* + pK184-*nlpE*$_{R93E}$ + pCA24N	This study
TC779	TR50 Δ*cpxP* + pK184-*nlpE*$_{R93E\ L}$ + pCA-*lgt*	This study
TC780	TR50 Δ*cpxP* + pK184-*nlpE*$_{R93E}$ + pCA-*lspA*	This study
TC781	TR50 Δ*cpxP* + pK184-*nlpE*$_{R93E}$ + pCA-*lnt*	This study
TC782	TR50 Δ*cpxP* + pK184-*nlpE*$_{R93E}$ + pCA-*lolA*	This study
TC783	TR50 Δ*cpxP* + pK184-*nlpE*$_{R93E}$ + pCA-*lolB*	This study
TC188	VM40 (TR50 Δ*cpxP*) + pCA24N	This study
TC189	VM40 (TR50 Δ*cpxP*) + pCA-*nlpE*	This study
TC857	MC4100 + pBAD18	This study
TC858	MC4100 + pBAD-*nlpE*$_{DD}$	This study
VT97	MC4100 Δ*degP*	(Tsviklist et al., 2022)
TC859	VT97 + pBAD18	This study
TC860	VT97 + pBAD-*nlpE*$_{DD}$	This study

Table 3-2. Plasmids used in this study.

Plasmid	Description	Source
pCA24N	Empty ASKA library vector	(Kitagawa et al., 2006)
pCA-*nlpE*	NlpE expression, IPTG-inducible, ASKA library (GFP-)	(Kitagawa et al., 2006)
pCA-*lgt*	Lgt expression, IPTG-inducible, ASKA library (GFP-)	(Kitagawa et al., 2006)
pCA-*lspA*	LspA expression, IPTG-inducible, ASKA library (GFP-)	(Kitagawa et al., 2006)
pCA-*lnt*	Lnt expression, IPTG-inducible, ASKA library (GFP-)	(Kitagawa et al., 2006)
pCA-*lolA*	LolA expression, IPTG-inducible, ASKA library (GFP-)	(Kitagawa et al., 2006)
pCA-*lolB*	LolB expression, IPTG-inducible, ASKA library (GFP-)	(Kitagawa et al., 2006)
pTrc99A	Empty expression vector, IPTG-inducible expression from *trc* promoter	(Amann et al., 1988)
pTrc-*nlpE*$_{WT}$	NlpE$_{WT}$ expression vector; C-terminal 6×His tag	This study
pTrc-*nlpE*$_{NTD+L}$	NlpE$_{NTD+L}$ expression vector; C-terminal 6×His tag	This study
pTrc-*nlpE*$_{NTD}$	NlpE$_{NTD}$expression vector; C-terminal 6×His tag	This study
pTrc-*nlpE*$_{1-120}$	NlpE$_{1-120}$ expression vector; C-terminal 6×His tag	This study
pTrc-*nlpE*$_{1-101}$	NlpE$_{1-101}$ expression vector; C-terminal 6×His tag	This study
pTrc-*nlpE*$_{R93E}$	NlpE$_{R93E}$ expression vector; C-terminal 6×His tag	This study
pK184	P15A ori-based empty expression vector	(Jobling and Holmes, 1990)
pK184-*nlpE*$_{NTD+L}$	P15A ori-based NlpE$_{NTD+L}$ expression vector; IPTG-inducible	Jun Lu
pK184-*nlpE*$_{K65E}$	K65E charge swap expression vector	Jun Lu
pK184-*nlpE*$_{R93E}$	R93E charge swap expression vector	Jun Lu
pK184-*nlpE*$_{K97E}$	K97E charge swap expression vector	Jun Lu
pK184-*nlpE*$_{K107E}$	K107E charge swap expression vector	Jun Lu
pK184-*nlpE*$_{D53R}$	D53R charge swap expression vector	Jun Lu
pK184-*nlpE*$_{D73R}$	D73R charge swap expression vector	Jun Lu
pK184-*nlpE*$_{D80R}$	D80R charge swap expression vector	Jun Lu
pK184-*nlpE*$_{D81R}$	D81R charge swap expression vector	Jun Lu
pK184-*nlpE*$_{D102R}$	D102R charge swap expression vector	Jun Lu
pK184-*nlpE*$_{E106R}$	E106R charge swap expression vector	Jun Lu
pK184-*nlpE*$_{R111E}$	R111E charge swap expression vector	Jun Lu
pK184-*nlpE*$_{K113E}$	K113E charge swap expression vector	Jun Lu
pK184-*nlpE*$_{R123E}$	R123E charge swap expression vector	Jun Lu
pK184-*cpxA*	P15A ori-based CpxA expression vector; IPTG-inducible	Rodrigo Margain-Quevedo
pK184-*cpxA*$_{D40R}$	CpxA D40R expression vector	This study

pK184-*cpxA*$_{E50R}$	CpxA E50R expression vector	This study
pK184-*cpxA*$_{E54R}$	CpxA E54R expression vector	This study
pK184-*cpxA*$_{E56R}$	CpxA E56R expression vector	This study
pK184-*cpxA*$_{D60R}$	CpxA D60R expression vector	This study
pK184-*cpxA*$_{D64R}$	CpxA D64R expression vector	This study
pK184-*cpxA*$_{D76R}$	CpxA D76R expression vector	This study
pK184-*cpxA*$_{E101R}$	CpxA E101R expression vector	This study
pK184-*cpxA*$_{D136R}$	CpxA D136R expression vector	This study
pK184-*cpxA*$_{D139R}$	CpxA D139R expression vector	This study
pBAD18	Empty expression vector, arabinose-inducible	(Guzman et al., 1995)
pBAD18-*nlpE*$_{WT}$	NlpE$_{WT}$ expression vector; C-terminal 6×His tag	This study
pBAD18-*nlpE*$_{NTD+L}$	NlpE$_{NTD+L}$ expression vector; C-terminal 6×His tag	This study
pBAD18-*nlpE*$_{DD}$	Full length NlpE with +2/3 DD Lol avoidance sequence expression vector; C-terminal 6×His tag	This study
pBAD18-*nlpE*$_{NTDL+DD}$	NlpE$_{NTD+L}$ with +2/3 DD Lol avoidance sequence expression vector; C-terminal 6×His tag	This study
pBAD18-*nlpE*$_{DD+\Delta L}$	NlpE$_{DD}$ expression with full length linker deletion	This study
pBAD18-*nlpE*$_{DD+\Delta 0.5L}$	NlpE$_{DD}$ expression with half length linker deletion	This study
pBAD18-*nlpE*$_{DD+\Delta 0.25L}$	NlpE$_{DD}$ expression with quarter length linker deletion	This study
pBAD18-*nlpE*$_{DD+\Delta 14-17}$	NlpE$_{DD}$ expression with deletion of aa14-17	This study
pBAD18-*nlpE*$_{DD+14-17::GS}$	NlpE$_{DD}$ expression with substitution of aa14-17	This study
pBAD18-*nlpE*$_{DD+\Delta 6}$	NlpE$_{DD}$ expression with alternate half linker deletion	This study
pBAD18-*nlpE*$_{DD+\Delta 6::GS}$	NlpE$_{DD}$ expression with alternate half linker substitution	This study
pTrc-*nlpE*$_{\Delta PIS1}$	NlpE expression with protease inhibitor sequence deletion 1	This study
pTrc-*nlpE*$_{\Delta PIS2}$	NlpE expression with protease inhibitor sequence deletion 2	This study
pTrc-*nlpE*$_{\Delta PIS::GS}$	NlpE expression with protease inhibitor sequence substitution with GS repeat	This study
pJW1	Vector encoding *cpxP-lux* transcriptional reporter	(Price and Raivio, 2009)
pUTM18C-DEST	Modified two-hybrid assay Gateway-compatible vector; encodes *cyaA* T18 subunit and OppB transmembrane 1 domain	(Ouellette et al., 2014)
pSTM25-DEST	Modified two-hybrid assay Gateway-compatible vector; encodes *cyaA* T25 subunit and OppB transmembrane 1 domain	(Ouellette et al., 2014)
pUTM18C-zip	Modified two-hybrid assay Gateway-compatible vector; encodes leucine zipper sequence (positive control), *cyaA* T18 subunit, and OppB transmembrane 1 domain	(Ouellette et al., 2014)
pKTM25-zip	Modified two-hybrid assay Gateway-compatible vector; encodes leucine zipper sequence (positive	(Ouellette et al., 2014)

	control), *cyaA* T25 subunit, and OppB transmembrane 1 domain	
pUTM18C	Empty vector for two-hybrid assays (negative control)	(Ouellette et al., 2014)
pSTM25	Empty vector for two-hybrid assays (negative control)	(Ouellette et al., 2014)
pSTM25-*nlpE*$_{WT}$	Vector encoding NlpE$_{WT}$ fused to T25 subunit	This study
pUTM18C-*nlpE*$_{WT}$	Vector encoding NlpE$_{WT}$ fused to T18 subunit	This study
pSTM25-*nlpE*$_{NL}$	Vector encoding NlpE$_{NTD+L}$ fused to T25 subunit	This study
pUTM18C-*nlpE*$_{NL}$	Vector encoding NlpE$_{NTD+L}$ fused to T18 subunit	This study
pSTM25-*nlpE*$_{N}$	Vector encoding NlpE$_{NTD}$ fused to T25 subunit	This study
pUTM18C-*nlpE*$_{N}$	Vector encoding NlpE$_{NTD}$ fused to T18 subunit	This study
pSTM25-*nlpE*$_{CL}$	Vector encoding NlpE$_{CTD+L}$ fused to T25 subunit	This study
pUTM18C-*nlpE*$_{CL}$	Vector encoding NlpE$_{CTD+L}$ fused to T18 subunit	This study
pSTM25-*nlpE*$_{C}$	Vector encoding NlpE$_{CTD}$ fused to T25 subunit	This study
pUTM18C-*nlpE*$_{C}$	Vector encoding NlpE$_{CTD}$ fused to T18 subunit	This study
pSTM25-*cpxA*$_{PP}$	Vector encoding CpxA periplasmic domain fused to T25 subunit	This study
pUTM18C-*cpxA*$_{PP}$	Vector encoding CpxA periplasmic domain fused to T18 subunit	This study
pSTM25-*cpxP*	Vector encoding CpxP fused to T25 subunit	This study
pUTM18C-*cpxP*	Vector encoding CpxP fused to T18 subunit	This study
pSTM25-*nlpE*$_{\Delta 120\text{-}127}$	Vector encoding NlpE Δ120-127 fused to T25 subunit	This study
pUTM18C-*nlpE*$_{\Delta 120\text{-}127}$	Vector encoding NlpE Δ120-127 fused to T18 subunit	This study
pSTM25-*nlpE*$_{\Delta 129\text{-}136}$	Vector encoding NlpE Δ129-136 fused to T25 subunit	This study
pUTM18C-*nlpE*$_{\Delta 129\text{-}136}$	Vector encoding NlpE Δ129-136 fused to T18 subunit	This study
pSTM25-*nlpE*$_{R93E}$	Vector encoding NlpE R93E fused to T25 subunit	This study
pSTM25-*nlpE*$_{K97E}$	Vector encoding NlpE K97E fused to T25 subunit	This study
pDONR22-DEST	Cloning vector used to create entry clones during Gateway cloning	Invitrogen

Table 3-3. Primers used in this study.

Primer Name	Sequence	Notes
GW_cpxApp_fw	GGGG ACA AGT TTG TAC AAA AAA GCA GGC TTC CTC GAT TCA CGC CAG ATG ACC	For Gateway cloning CpxA periplasmic domain into two-hybrid vectors
GW_cpxApp_rv	GGGG AC CAC TTT GTA CAA GAA AGC TGG GTC CTA GCG GTC AAA CAG TAA GTT AAT	For Gateway cloning CpxA periplasmic domain into two-hybrid vectors
GW_nlpE_fw	GGGG ACA AGT TTG TAC AAA AAA GCA GGC TTC ACC GAC AGC AAA GGT GAA AAG TCA	For Gateway cloning NlpE into two-hybrid vectors
GW_nlpE_rv	GGGG AC CAC TTT GTA CAA GAA AGC TGG GTC TTA CTG CCC CAA ACT ACT GCA ATC	For Gateway cloning NlpE into two-hybrid vectors
GW_nlpE_NTD_cor_rv	GGGG AC CAC TTT GTA CAA GAA AGC TGG GTC TTA CAT CTC CAG CGC ATC GCC TTT	For Gateway cloning NlpE NTD into two-hybrid vectors
GW_nlpE_linker_cor_rv	GGGG AC CAC TTT GTA CAA GAA AGC TGG GTC TTA CGG CGT CAT AGG TAA ACT GGA	For Gateway cloning NlpE NTD into two-hybrid vectors
GW_nlpE_CTD_cor_fw	GGGG ACA AGT TTG TAC AAA AAA GCA GGC TTC ATG ACC CTG CGG GGC ATG TAT	For Gateway cloning NlpE CTD into two-hybrid vectors
GW_nlpE_linker_cor_fw	GGGG ACA AGT TTG TAC AAA AAA GCA GGC TTC CTC GAT CGT GAA GGC AAT CCG	For Gateway cloning NlpE CTD into two-hybrid vectors
nlpE_NcoI_F	CGCA CCATGG TG AAA AAA GCG ATA GTG ACA G	For cloning *nlpE* into pTrc99A
nlpE_EcoRI_F	GCA GAATTC ATG GTG AAA AAA GCG ATA GTG	For cloning *nlpE* into pBAD18
nlpE_WT_His_HindIII_R	TGCC AAGCTT TTA GTG GTG GTG GTG GTG GTG CT CGA GCT GCC CCA AAC TAC TGC AAT C	For cloning *nlpE* into pBAD18/pTrc99A
nlpE_NTDL_His_HindIII_R	TGCC AAGCTT TTA GTG GTG GTG GTG GTG GTG CT CGA GCG GCG TCA TAG GTA AAC TGG A	For cloning *nlpE* into pBAD18/pTrc99A
nlpE_NTD_His_HindIII_R	TGCC AAGCTT TTA GTG GTG GTG GTG GTG GTG CT CGA GCA TCT CCA GCG CAT CGC CTT T	For cloning *nlpE* into pBAD18/pTrc99A
nlpE137_His_HindIII_R	TGCC AAGCTT TTA GTG GTG GTG GTG GTG GTG CT CGA GCG CTT CCA GCG TAT AGT TGA A	For cloning *nlpE* into pBAD18/pTrc99A
nlpE101_His_HindIII_R	TGCC AAGCTT TTA GTG GTG GTG GTG GTG GTG CT CGA GGG TTA ATA CCA GCT TGT CAG C	For cloning *nlpE* into pBAD18/pTrc99A
Q5SDM_NlpEDD_F	GAT GGG ATG TGA TGA TCG GGC CGA AG	For SDM to create $NlpE_{DD}$
Q5SDM_NlpEDD_R	AGA GTA AAG AGG CTG ATT ACA G	For SDM to create $NlpE_{DD}$
Q5SDM_PISdel1_F	AAC TAT ACG CTG GAA GC	For SDM to delete PIS1
Q5SDM_PISdel1_R	ATC GAG CAT CTC CAG	For SDM to delete PIS1
Q5SDM_PICdel2_F	ACG CTG GAA GCG GCA C	For SDM to delete PIS2
Q5SDM_PICdel2_R	CAT CTC CAG CGC ATC GC	For SDM to delete PIS2
Q5SDM_PICGS_F	GCA GCG GCA GCG GCA GCG GCA CGC TGG AAG CGG CAC	For SDM to substitute PIS with GS repeats

Q5SDM_PICGS_R	CGC TGC CGC TGC CGC TGC CCA TCT CCA GCG CAT CGC	For SDM to substitute PIS with GS repeats
Q5SDM_del0.5n_F	CAG GCT GCC GAA CTG	For SDM to delete portion of NlpE N-terminal linker
Q5SDM_del0.5n_R	GGC CCG ATC ATC ACA TC	For SDM to delete portion of NlpE N-terminal linker
Q5SDM_0.5GS_F	GGC AGC GGC AGC CAG GCT GCC GAA CTG	For SDM to substitute portion of NlpE N-terminal linker
Q5SDM_0.5GS_R	GCT GCC GCT GCC GGC CCG ATC ATC ACA TC	For SDM to substitute portion of NlpE N-terminal linker
Q5SDM_14-17del_F	CTG AAA CCG ATG CCG	For SDM to delete portion of NlpE N-terminal linker
Q5SDM_14-17del_R	CGC CGG AGA AAG CGT	For SDM to delete portion of NlpE N-terminal linker
Q5SDM_GS sub_F	GGC AGT CTG AAA CCG ATG CCG	For SDM to substitute aa14-17 portion of NlpE N-terminal linker
Q5SDM_GS sub_R	ACT GCC CGC CGG AGA AAG CG	For SDM to substitute aa14-17 portion of NlpE N-terminal linker
Q5SDM_nlpER93E_F	TAC ATG GGC GGA AAC CGC TGA CA	For SDM to create R93E mutation in *nlpE*
Q5SDM_nlpER93E_R	CCG TAG GAA GCG AAG GAG	For SDM to create R93E mutation in *nlpE*
Q5SDM_cpxA_D40E_F	CGA GCT TCT GCG TAG CGA ACA GCG	For SDM to create the indicated charge swap in *cpxA*
Q5SDM_cpxA_D40R_R	GTC ATC TGG CGT GAA TCG	For SDM to create the indicated charge swap in *cpxA*
Q5SDM_cpxA_E50R_F	GCT GAT GAT TCG TCA GCA TGT CGA AGC G	For SDM to create the indicated charge swap in *cpxA*
Q5SDM_cpxA_E50R_R	CCC TGA CGC TGT TCG CTA	For SDM to create the indicated charge swap in *cpxA*
Q5SDM_cpxA_E54R_F	GCA GCA TGT CCG TGC GGA GCT GG	For SDM to create the indicated charge swap in *cpxA*
Q5SDM_cpxA_E54R_R	TCA ATC ATC AGC CCC TGA C	For SDM to create the indicated charge swap in *cpxA*
Q5SDM_cpxA_E56R_F	TGT CGA AGC GCG TCT GGC GAA CG	For SDM to create the indicated charge swap in *cpxA*
Q5SDM_cpxA_E56R_R	TGC TGC TCA ATC ATC AGC	For SDM to create the indicated charge swap in *cpxA*
Q5SDM_cpxA_D60R_F	GCT GGC GAA CCG TCC GCC CAA CG	For SDM to create the indicated charge swap in *cpxA*
Q5SDM_cpxA_D60R_R	TCC GCT TCG ACA TGC TGC	For SDM to create the indicated charge swap in *cpxA*
Q5SDM_cpxA_D64R_F	TCC GCC CAA CCG TTT AAT GTG GTG GCG GC	For SDM to create the indicated charge swap in *cpxA*
Q5SDM_cpxA_D64R_R	TCG TTC GCC AGC TCC GCT	For SDM to create the indicated charge swap in *cpxA*
Q5SDM_cpxA_D76R_F	CCG GGC GAT TCG TAA GTG GGC ACC G	For SDM to create the indicated charge swap in *cpxA*
Q5SDM_cpxA_D76R_R	AAC AGA CGC CGC CAC CAC	For SDM to create the indicated charge swap in *cpxA*
Q5SDM_cpxA_E101R_F	TGA ACG CAG CCG TAT GCA GAT CAT TCG TAA CTT TAT TGG TCA GGC C	For SDM to create the indicated charge swap in *cpxA*
Q5SDM_cpxA_E101R_R	GCG CCG ATC ACG CGG CCT	For SDM to create the indicated charge swap in *cpxA*
Q5SDM_cpxA_D136R_F	CTC CGT GCG TCG TGG CGA AGA TAA TTA C	For SDM to create the indicated charge swap in *cpxA*
Q5SDM_cpxA_D136R_R	AAC GGA CCG ACC AGT TCC	For SDM to create the indicated charge swap in *cpxA*
Q5SDM_cpxA_D139R_F	TGA TGG CGA ACG TAA TTA CCA ACT TTA TCT GAT TCG TCC GGC C	For SDM to create the indicated charge swap in *cpxA*
Q5SDM_cpxA_D139R_R	CGC ACG GAG AAC GGA CCG	For SDM to create the indicated charge swap in *cpxA*

Chapter 4 – NlpE is an OmpA-associated outer membrane sensor of the Cpx envelope stress response[‡]

[‡] Modified from Cho, T.H.S., Wang, J., Raivio, T.L., 2023. NlpE Is an OmpA-Associated Outer Membrane Sensor of the Cpx Envelope Stress Response. J Bacteriol 205, e00407-22. https://doi.org/10.1128/jb.00407-22

Abstract

Gram-negative bacteria utilize several envelope stress responses (ESRs) to sense and respond to diverse signals within a multi-layered cell envelope. The CpxRA ESR responds to multiple stresses that perturb envelope protein homeostasis. Signaling in the Cpx response is regulated by auxiliary factors such as the outer membrane (OM) lipoprotein NlpE, an activator of the response. NlpE communicates surface adhesion to the Cpx response; however, the mechanism by which NlpE accomplishes this remains unknown. In this study, we report a novel interaction between NlpE and the major OMP OmpA. Both NlpE and OmpA are required to activate the Cpx response in surface-adhered cells. Furthermore, NlpE senses OmpA overexpression and the NlpE C-terminal domain transduces this signal to the Cpx response, revealing a novel signaling function for this domain. Mutation of OmpA peptidoglycan binding residues abrogates signaling during OmpA overexpression suggesting that NlpE signaling from the outer membrane through the cell wall is coordinated via OmpA. AlphaFold3 modelling and whole cell dot blot assays suggest that NlpE may become surface exposed, providing a potential mechanism for how NlpE senses surface-related signals. Overall, these findings reveal NlpE to be a versatile envelope sensor that takes advantage of its structure, localization, and cooperation with other envelope proteins to initiate adaptation to OM-based signals.

Introduction

Gram-negative bacteria such as *Escherichia coli* possess dozens of two-component signal transduction pathways which regulate diverse and key cellular processes (Yamamoto et al., 2005). Most sensor kinases are inner membrane (IM)-bound; thus, signals originating outside of the cell or in the envelope itself must be transduced through the envelope to activate these systems. However, signaling in and across the Gram-negative envelope is complicated by several unique challenges. Namely, the periplasmic space between the IM and outer membrane (OM) lacks ATP, often used for phosphotransfer reactions in common signaling relays and as an energy source for many different processes. The envelope is also a spatially complex compartment where the IM and OM are physically separated by a peptidoglycan cell wall, and signals in distinct compartments of the envelope must also navigate through this layer to activate IM sensors.

The Cpx envelope stress response is a major adaptive system of Gram-negative bacteria that responds to stresses that disrupt envelope protein folding and homeostasis, particularly at the IM (Vogt and Raivio, 2012). As a canonical two-component system, the Cpx response utilizes an IM sensor kinase, CpxA, to phosphorylate and modulate the activity of a DNA-binding transcriptional regulator, CpxR. Signaling by the Cpx response is also regulated by at least two other factors: CpxP and NlpE. The periplasmic chaperone-like protein CpxP inhibits activation of the system in the absence of specific cues (Buelow and Raivio, 2005; Isaac et al., 2005). In contrast, the OM lipoprotein NlpE is an activator of the response. Early studies of the Cpx response identified NlpE as an activator of the Cpx pathway when overproduced (Snyder et al., 1995), and subsequent studies suggest that NlpE also senses cell-surface events, namely, adhesion to hydrophobic surfaces and certain epithelial cell lines (Otto and Silhavy, 2002; Shimizu et al., 2016). The most recent studies of NlpE suggest that NlpE functions as a sensor

for defects in OM lipoprotein biogenesis (Delhaye et al., 2019; Grabowicz and Silhavy, 2017a; Marotta et al., 2023a; May et al., 2019); chemical agents or mutations that disrupt lipoprotein processing or trafficking also disrupt NlpE biogenesis, allowing NlpE to signal the presence of these stresses to the Cpx response due to its mislocalization to the IM. New NlpE synthesis is required to sense impaired lipoprotein biogenesis, suggesting that NlpE continuously functions as a cellular indicator of OM lipoprotein health (May et al., 2019).

NlpE's structure was solved as a domain-swapped dimer with each monomer consisting of independently-folding N- and C-terminal domains connected by a linker region (Hirano et al., 2007). This structure lends itself to a model for signaling from the OM where OM-anchored NlpE uses the C-terminal domain to reach across the periplasm to activate CpxA under certain inducing cues (e.g. surface adhesion). In the hypothetical monomer structure proposed in this study, secondary structure elements largely limit the length of the region between the N- and C-terminal domains when NlpE is fully folded, leading Hirano and colleagues to speculate that selective unfolding of the N-terminal domain may extend the C-terminal domain into the periplasm to facilitate activation of CpxA. Current studies have established that the N-terminal domain is sufficient for activation of the response when NlpE is overexpressed or mislocalized to the IM, suggesting that NlpE-CpxA interactions at the IM occur independently of the C-terminal domain (Delhaye et al., 2019; May et al., 2019). Delhaye and colleagues have shown the disulfide bond in the C-terminal domain of NlpE may be involved in sensing periplasmic redox state, although it is unclear how this is communicated to CpxA (Delhaye et al., 2019). Thus, no studies have yet precisely elucidated how NlpE signals from the OM where the NTD is presumably localized in close proximity to the OM by virtue of its acylated N-terminus (May et al., 2019).

In this study, we investigate the mechanisms of NlpE signaling from its OM context. We report a novel interaction between NlpE and the major OM protein OmpA. Both NlpE and OmpA

are required to activate the Cpx response in surface adhered cells. Further, NlpE activates the Cpx response during OmpA overexpression, and this signal is transduced via the NlpE C-terminal domain. Mutating residues involved in OmpA dimerization or cell wall binding, however, abolishes signaling during OmpA overexpression, suggesting that NlpE and OmpA cooperate to signal across the cell wall. Taken together, these results demonstrate that NlpE is a bona fide OM sensor that uses its localization, multidomain structure, and interactions with other envelope proteins to sense and transduce diverse signals to the Cpx response.

Results

NlpE interacts with OmpA

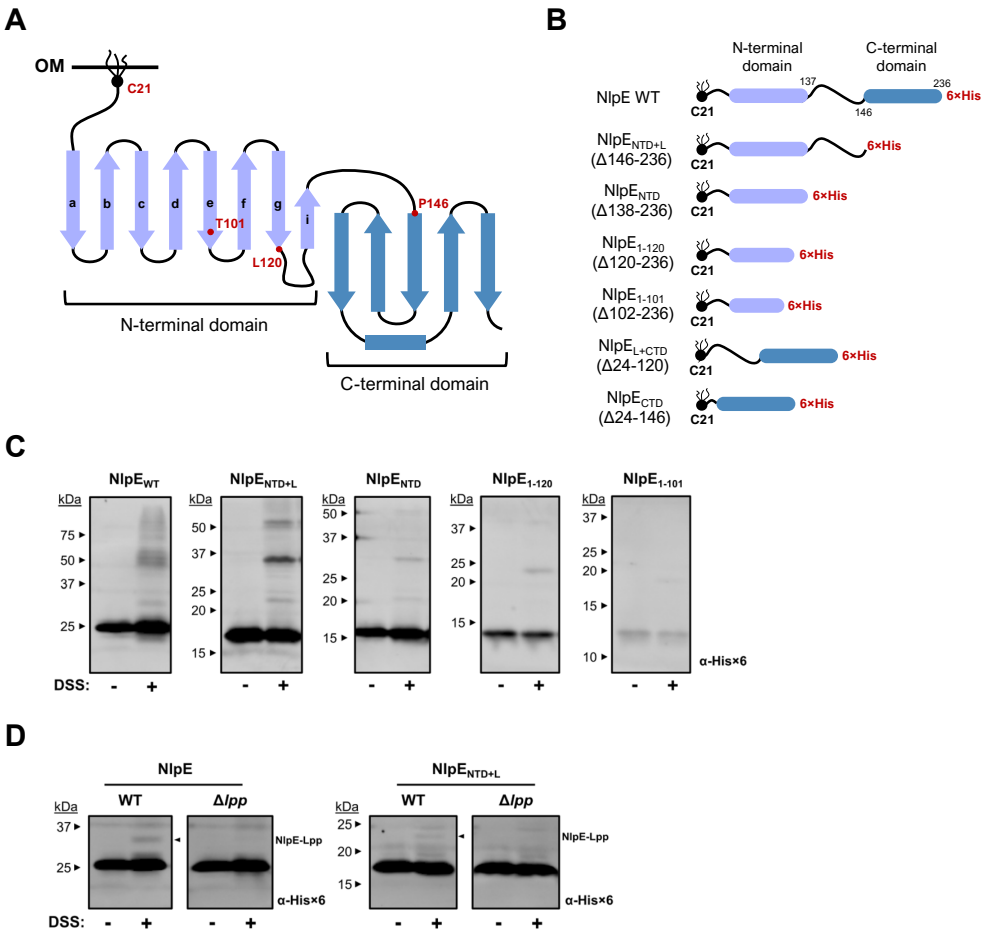

Figure 4-1. NlpE cross-links to many proteins in the cell envelope.

(A) The structure of NlpE based on the hypothetical monomer model proposed by Hirano and colleagues (Hirano et al., 2007). β-strands (with directionality) are represented as arrows whereas α-helices are represented without arrowheads. The β-strands making up the N-terminal domain are lettered a-i. **(B)** Representations of the NlpE variants expressed from various plasmids used in this study. The amino acid number includes the signal peptide (i.e. the lipid-modified N-terminal cysteine is labelled Cys21 not Cys1). **(C)** *In vivo* DSS crosslinking of cells expressing His-tagged NlpE variants containing the N-terminal domain. **(D)** shows crosslinking experiments with the indicated NlpE variants in WT and Δ*lpp* backgrounds. NlpE variants were expressed via leaky expression from pTrc99A and then subjected to crosslinking. Samples were analyzed by Western blotting with anti-His×6 antibody.

As detailed in the previous chapter, we generated a set of expression vectors expressing C-terminally His-tagged NlpE. These vectors expressed a series of NlpE truncations from both the C- and N-terminus while preserving the native signal sequence, lipobox, and localization signals (Figure 4-1AB). To study NlpE protein-protein interactions *in vivo,* we conducted disuccinimidyl suberate (DSS) crosslinking on strains expressing these variants (Figure 4-1C). These assays revealed the presence of several NlpE-containing protein complexes. One of these complexes appears to be with the abundant Braun's lipoprotein (Lpp), as a small band corresponding to the size of NlpE plus an additional ~5 kDa disappears in an *lpp::kan* mutant (Figure 4-1D). Western blots showed that variants containing an intact N-terminal domain are stably expressed, while those lacking a complete N-terminal domain showed decreased stability (Figure 4-2).

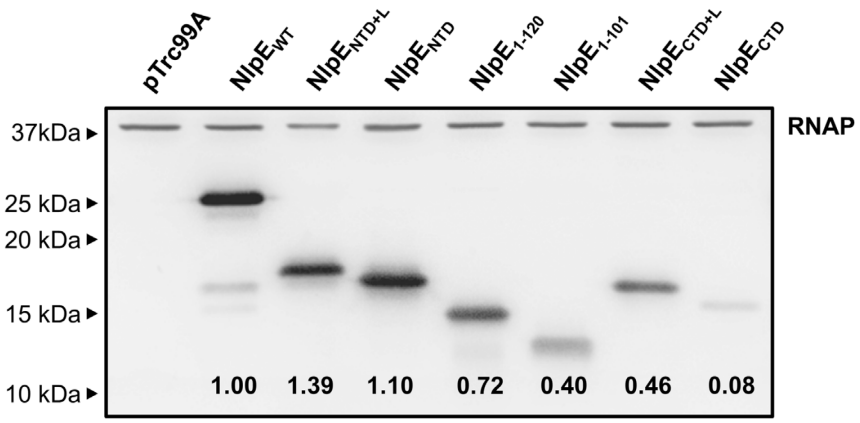

Figure 4-2. Expression levels of NlpE variants.

Western blots with anti-His×6 and anti-RNAPα subunit (RNAP; loading control) antibody. Strains containing pTrc99A-based NlpE overexpression vectors were grown to mid-log phase at 37°C with shaking, and NlpE expression was induced with 0.1 mM IPTG for 30 minutes. Cultures were standardized to the same OD, lysed with sample buffer with heating, and subjected to SDS-PAGE and Western blotting analysis. Levels of NlpE were standardized to RNAP loading controls and then standardized to level of WT NlpE. The numbers below each lane indicates the relative level of expression level of NlpE compared to WT NlpE (set to 1.00).

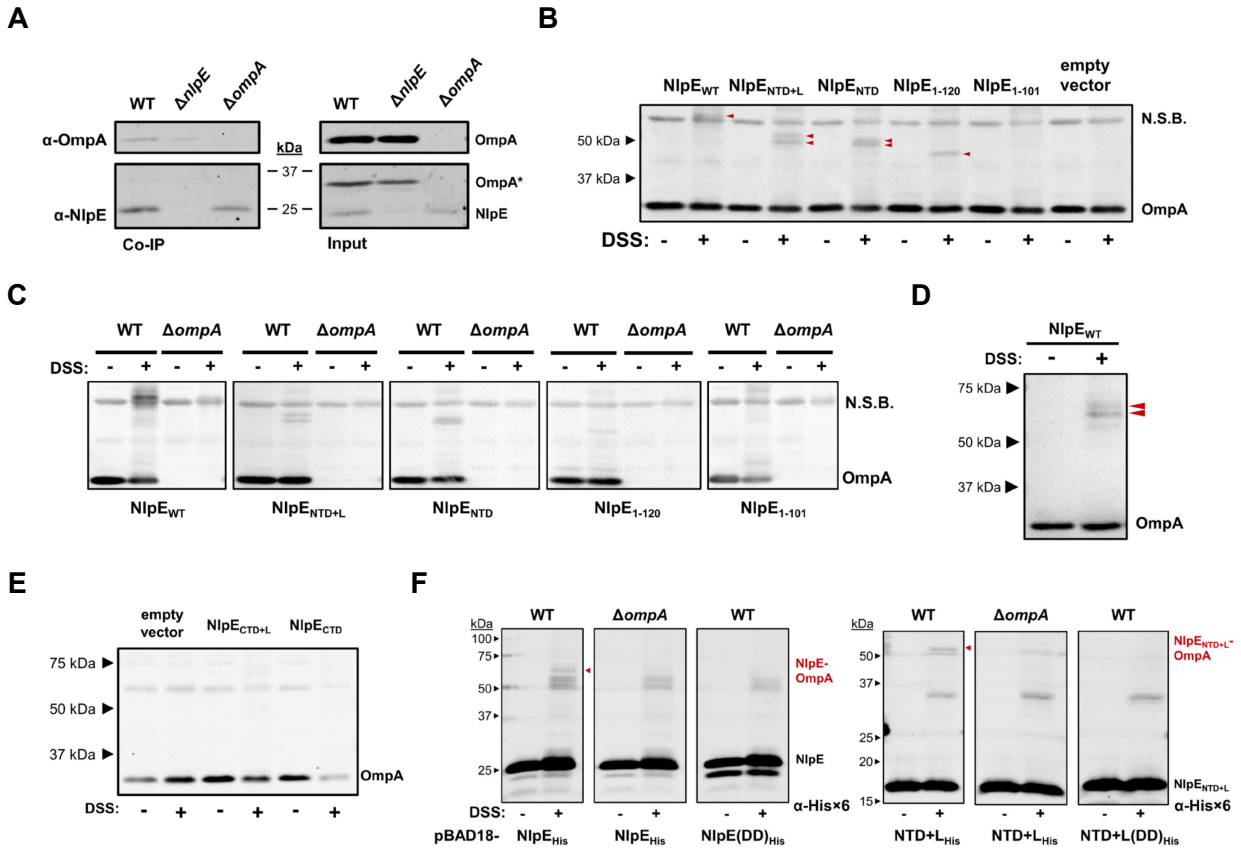

Figure 4-3. The N-terminal domain of NlpE interacts with OmpA at the OM.

(A) *in vivo* co-immunoprecipitation assays confirm NlpE-OmpA interactions at native expression levels of NlpE. "Input" comprises solubilized membrane preparations from the indicated strains. Complexes were precipitated with anti-NlpE antibodies immobilized on agarose beads, and eluted proteins were analyzed by SDS-PAGE and Western blotting with anti-NlpE (bottom panels) and OmpA (top panels) antibodies. **(B**) and **(C)** show that NlpE-OmpA complexes are observed by in vivo DSS crosslinking. Cells expressing His-tagged NlpE and variants (induced with 0.1 mM IPTG for 30 minutes) from pTrc99A were subjected to crosslinking with 0.5 mM DSS for 30 minutes. Samples were analyzed by Western blotting with anti-OmpA antibody. Resulting OmpA-NlpE complexes are indicated with red arrowheads. N.S.B. indicates a non-specific band detected by the anti-OmpA antibody. **(D)** The presence of a double band between NlpE WT and OmpA is visible in the absence of non-specific banding, which was eliminated by multiple uses of the solution containing the anti-OmpA antibody. **(E)** NlpE CTD containing constructs do not crosslink to OmpA under the tested conditions. **(F)** *in vivo* crosslinking with His-tagged WT and IM NlpE (DD) variants. NlpE expression was induced from a P*ara* promoter

on pBAD18 with 0.2% L-arabinose for 1 hour and cells were subjected to crosslinking with 1 mM DSS for 30 minutes. The strain background in which NlpE was expressed is shown above each panel. Samples were analyzed by Western blotting with anti-His×6 antibody.

Previous work in the Raivio lab reported that NlpE interacts with the OM protein OmpA. To confirm NlpE-OmpA interactions *in vivo*, we conducted co-immunoprecipitation experiments on cells expressing NlpE at native levels (Figure 4-3A). Throughout our studies, we have observed that NlpE is expressed at low levels natively. To overcome this challenge, we enriched for NlpE-containing fractions by isolating crude membrane fractions. NlpE-specific antisera was immobilized on protein A agarose beads and treated with membrane extracts from wildtype, Δ*nlpE*, and Δ*ompA* cells. We found that OmpA co-immunoprecipitated with NlpE in WT cells, despite low levels of natively expressed NlpE (Figure 4-3A). However, we also detected a fainter OmpA band in the co-IP fraction of Δ*nlpE* cultures. This appears to be due to cross-reaction of our anti-NlpE antisera with OmpA as confirmed by the presence of bands corresponding to OmpA in WT and Δ*nlpE* but not Δ*ompA* membrane preparations (Figure 4-3A, input lanes). Despite this, less OmpA was pulled down in Δ*nlpE* vs WT lysates, suggesting that NlpE can interact with OmpA at native levels of expression. The cross-reactivity of the anti-NlpE antisera with OmpA may originate from pre-exposure of rabbits to OmpA, which is highly immunogenic (Confer and Ayalew, 2013). Alternatively, it may also result from OmpA which co-purified with NlpE that was used for antisera generation, which could provide further evidence for an interaction between these two proteins.

We then performed the *in vivo* crosslinking experiments with WT NlpE and N-terminal domain containing NlpE truncation variants while immunoblotting for OmpA to confirm NlpE-OmpA interactions and determine which NlpE domains contribute to this interaction (Figure 4-3B). Because of the challenges of working with NlpE at its native levels of expression, we utilized

NlpE expressed from plasmids. We confirmed that WT NlpE crosslinks to OmpA and observed that the N-terminal domain of NlpE is sufficient to mediate NlpE-OmpA interactions (Figure 4-3B). Complexes were not observed when the N-terminal domain was disrupted by the deletion of its C-terminal portion ($NlpE_{1\text{-}101}$). However, this may be due to lower levels of expression of $NlpE_{1\text{-}101}$ as this construct is significantly less stable than variants containing an intact N-terminal domain (Figure 4-2). To confirm the identity of these bands, we repeated the experiment in an *ompA* knock-out strain, where no complexes were detected (Figure 4-3C). Cross-linking experiments using cells expressing $NlpE_{WT}$, $NlpE_{NTD+L}$, and $NlpE_{NTD}$ yielded two distinct NlpE-OmpA bands (Figure 4-3B). These dual bands are somewhat obscured by a non-specific band when $NlpE_{WT}$ is expressed but are clearly observable in when repeating the blots with an anti-OmpA primary antibody solution which was used for several previous experiments, which removed non-specific binding (Figure 4-3D).

We wondered if the NlpE C-terminal domain can interact with OmpA independently from the N-terminal domain; DSS crosslinking on strains expressing His-tagged NlpE C-terminal domain with linker ($NlpE_{L+CTD}$) and NlpE C-terminal domain only ($NlpE_{CTD}$) with the native NlpE signal sequence and lipobox sequence failed to produce clear evidence for $NlpE_{CTD}$-OmpA complexes (Figure 4-3E). While we did observe a very faint crosslinked band when the $NlpE_{L+CTD}$ construct was expressed, no bands were seen when expressing the C-terminal domain on its own. Thus, it's likely that the N-terminal domain of NlpE, not the C-terminal domain, is mostly responsible for the interaction between NlpE and OmpA. Furthermore, we found that bands corresponding to NlpE-OmpA complexes are absent when expressing a permanently IM-localized variant of NlpE ($NlpE_{DD}$) where the +2 and +3 amino acids after the acylated cysteine are mutated to aspartic acid to create a Lol avoidance signal (Miyadai et al., 2004) (Figure 4-3F), ruling out the possibility that IM localized NlpE interacts with OmpA. The identity of NlpE-OmpA

complexes were confirmed by conducting crosslinking experiments with normally trafficked NlpE in a Δ*ompA* background. Taken together, these results place NlpE-OmpA complexes in the OM where the NlpE N-terminal domain is proximal to OmpA, rather than in a configuration where IM-localized NlpE spans across the periplasm to interact with OmpA via the C-terminal domain.

NlpE senses OmpA overexpression

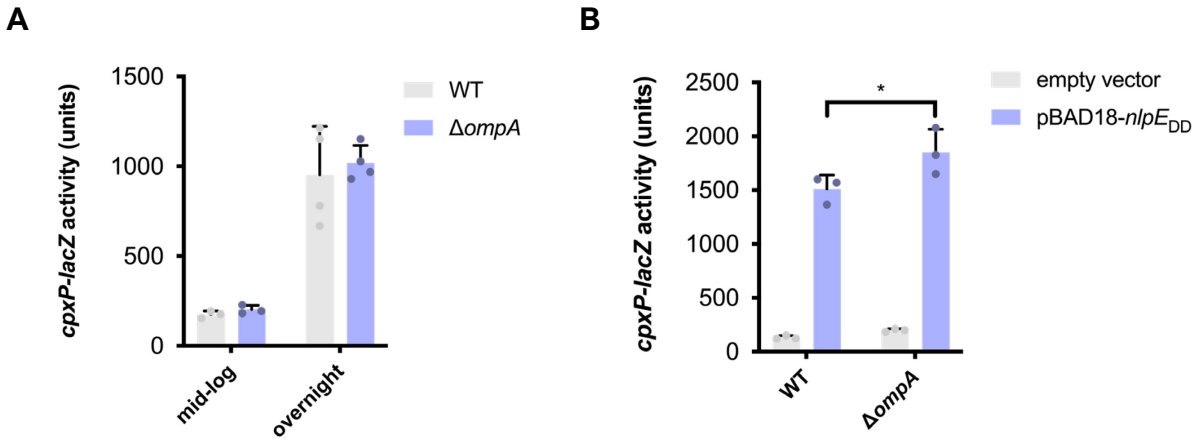

Figure 4-4. OmpA does not impact CpxA's basal activation or ability to sense IM NlpE expression.

(A) β-galactosidase assays of mid-log (OD 0.6) and overnight cultures of WT and Δ*ompA* MC4100. No statistically significant differences were seen between strains within each culture type. **(B)** β-galactosidase assays of WT and Δ*ompA* MC4100 expressing permanently IM bound NlpE (NlpE$_{DD}$) from plasmid. Cultures were grown to mid-log phase (OD 0.4-0.6), and NlpE expression was induced from a P*ara* promoter on pBAD18 with 0.2% L-arabinose for 1 hour. Shown are means with standard deviation of 3-4 biological replicates, analyzed by Tukey HSD test (* $p<0.05$).

We sought to further examine the signaling relationship between OmpA and signaling in the Cpx response. Deletion of *ompA* did not lead to significant changes in the activation of the Cpx response in both mid-log phase and stationary phase cells (Figure 4-4A). Furthermore, the absence of *ompA* did not impact the ability of IM-bound NlpE to activate the Cpx response

(Figure 4-4B), suggesting that the NlpE-OmpA interaction is relevant for NlpE signaling from the OM and not when NlpE is in the IM as might be the case during lipoprotein trafficking defects (Delhaye et al., 2019; May et al., 2019). A previous study reported that OmpA protein levels are increased in both pathogenic and lab strains of *E. coli* grown in surface-adhered biofilms (Orme et al., 2006). Previous work in the Raivio lab also reported that the Cpx response is activated by OmpA overexpression in an NlpE-dependent manner (Junshu Wang, PhD thesis). We found that overexpression of OmpA from a plasmid activates the Cpx response in WT cells, but this activation is strongly reduced in the absence of NlpE (Figure 4-5). We wondered if NlpE senses OMP overexpression in general or if the signal sensed is specific to NlpE-OmpA interactions. To test this, we overexpressed two sets of OMPs: larger OMPs that fold into 16-stranded β-barrels (OmpC, OmpF, and LamB; Figure 4-5A) and smaller OMPs that fold into 8-10 stranded β-barrels (OmpX, OmpW, and OmpT; Figure 4-5B). While overexpression of these OMPs lead to activation of the Cpx response to differing extents, Cpx activation in all cases, except for overexpression of OmpA (and to a small extent OmpX) occurred independently of NlpE. Therefore, the signal sensed by NlpE during OmpA overexpression is unlikely to be a general signal or stress associated with OMP overexpression.

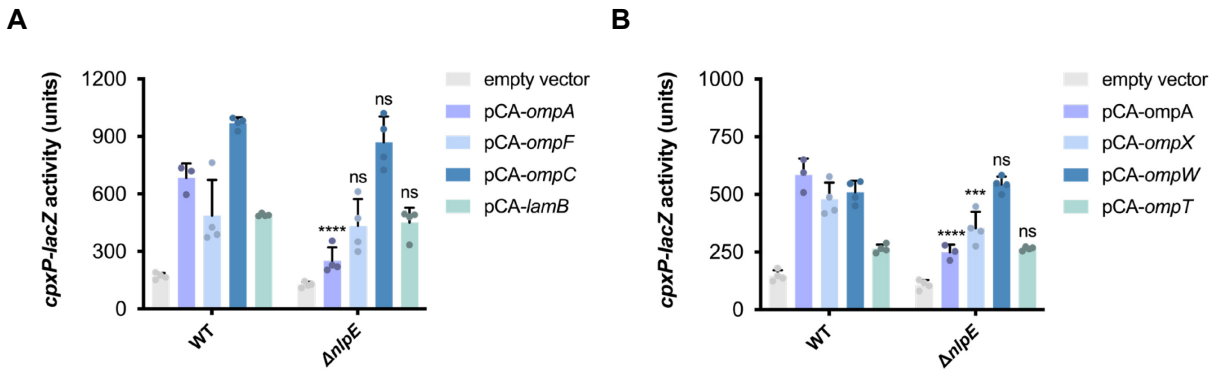

Figure 4-5. NlpE senses overexpression of OmpA but not other OMPs.

OMP expression was induced with 0.1 mM IPTG for 1 hour in WT and Δ*nlpE* cells when cultures reached mid-log phase. Cpx activation was determined by measuring *cpxP-lacZ* activity in β-galactosidase assays. The OMPs expressed were **(A)** larger, 16-stranded and **(B)** smaller, 8-10 stranded OMPs. Shown are means with standard deviation of 3-4 biological replicates, analyzed by Tukey HSD test (ns=non-significant, *p<0.05, **p<0.001, ****p<0.0001). Shown comparisons are between WT and Δ*nlpE* strains expressing the same OMPs.

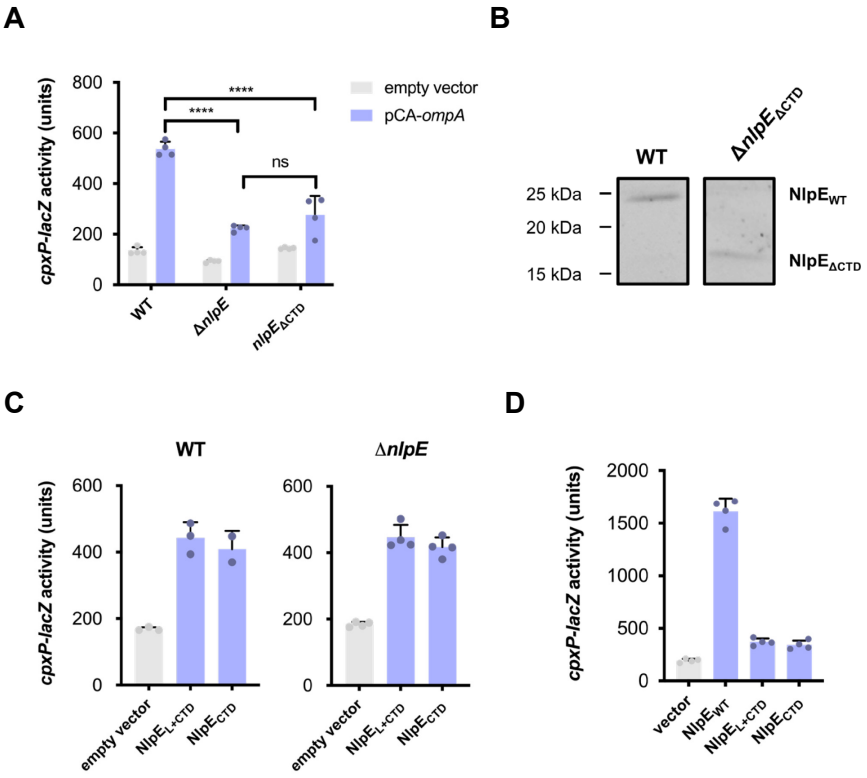

Figure 4-6. The C-terminal domain mediates NlpE signaling from the OM.

(A) The ability of OmpA overexpression to activate the Cpx response in WT, Δ*nlpE,* or nlpE$_{\Delta CTD}$ (NlpE with the C-terminal domain deleted) cells. **(B)** Expression levels of WT NlpE and NlpE$_{\Delta CTD}$ expressed from their native chromosomal loci. The immunoblots were conducted on crude membrane fractions isolated by ultracentrifugation. **(C)** The ability of NlpE lacking the N-terminal domain (NlpE$_{L+CTD}$) or lacking the N-terminal domain and linker (NlpE$_{CTD}$) to activate the Cpx response when overexpressed in WT and Δ*nlpE* cells. For (A) and (B), mean *cpxP-lacZ* activities with standard deviations are shown (Tukey HSD test **p<0.01, ****p<0.0001). **(D)** Comparison of the activation of a *cpxP-lacZ* reporter during overexpression of WT NlpE compared to NlpE lacking the N-terminal domain (L+CTD and CTD).

Previous studies have reported that NlpE lacking the C-terminal domain can still signal to the CpxA when NlpE is in the IM (Delhaye et al., 2019; May et al., 2019). Because we found that the N-terminal domain of NlpE interacts with OmpA, we hypothesized that the C-terminal domain

of NlpE mediates activation of the Cpx response from the OM. To test this, we deleted the C-terminal domain of the chromosomal *nlpE* locus by allelic exchange and tested if this chromosomally expressed $NlpE_{\Delta CTD}$ variant (equivalent to $NlpE_{NTD+L}$) can sense OmpA overexpression. We found that $NlpE_{\Delta CTD}$ is no longer able to sense OmpA overexpression; Δ*nlpE* and $nlpE_{\Delta CTD}$ strains showed significantly reduced Cpx activation during OmpA overexpression, and overexpressing OmpA leads to similar levels of fold-activation in Δ*nlpE* (2.4 fold) and $nlpE_{\Delta CTD}$ (1.9 fold) strains as opposed to WT (4.0 fold) (Figure 4-6A). Thus, while the N-terminal domain interacts with OmpA, the C-terminal domain appears to be responsible for transmitting this signal to CpxA. Our data from overexpressed NlpE variants suggests that NlpE lacking the C-terminal domain is stably expressed (Figure 4-2); natively expressed $NlpE_{\Delta CTD}$ is also expressed comparably to WT (Figure 4-6B), confirming that our results are likely not due to changes in NlpE expression level.

We also found that overexpressing variants of NlpE that lack the N-terminal domain leads to activation of the Cpx response (Figure 4-6C), albeit to a much weaker extent than overexpressing the N-terminal domain (Figure 4-6D). This weaker activation, however, may be due to comparatively lower levels of expression of these constructs (Figure 4-2). To rule out the possibility that overexpressing these constructs decreases the efficiency of lipoprotein biogenesis/trafficking, causing WT NlpE to activate CpxA at the IM, we repeated these experiments in an Δ*nlpE* mutant and found the same results (Figure 4-6C). Overall, these results suggest that the C-terminal domain can activate the Cpx response independently of the N-terminal domain.

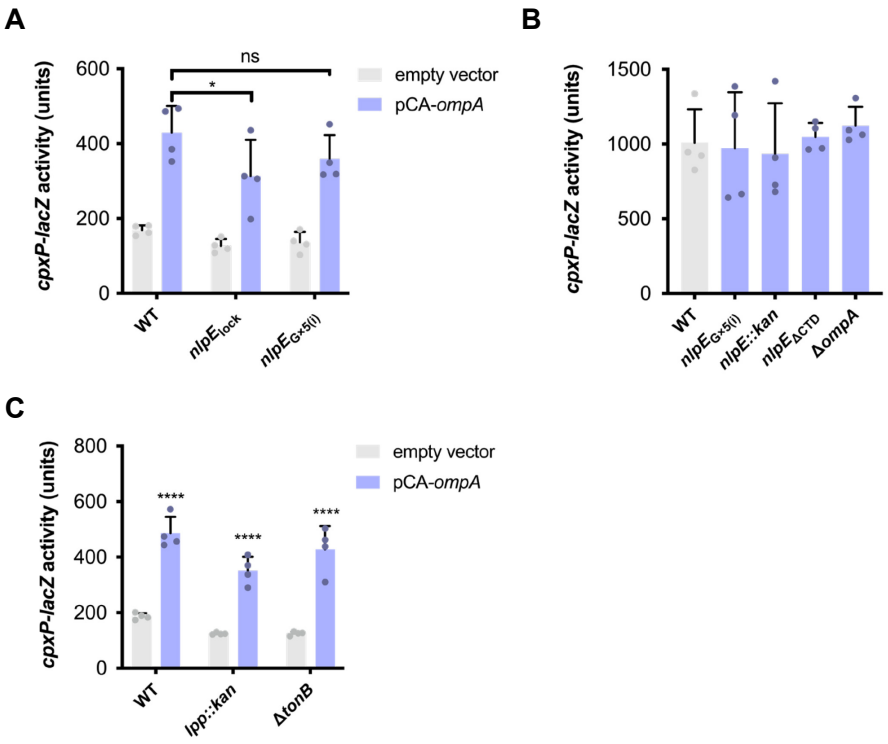

Figure 4-7. NlpE signaling from the OM does not appear to involve NlpE unfolding, Lpp, or TonB.

(A) shows *cpxP-lacZ* activity in strains expressing chromosomal variants of NlpE with cysteine substitutions (E118C and T124C) that should lock together the β-g and β-i strands ($NlpE_{lock}$) or a variant that prevents the formation of the these interactions ($NlpE_{G\times5(i)}$). **(B)** shows basal CpxA activity via *cpxP-lacZ* reporter activity of MC4100 with different chromosomal mutants of NlpE or an *ompA* deletion. **(C)** shows the ability of NlpE to sense OmpA overexpression in *lpp::kan* or Δ*tonB* backgrounds. Shown are means with standard deviations of 3-4 biological replicates analyzed by Tukey HSD test (ns=non-significant, *p<0.05, ****p<0.0001).

The original structural characterization study of NlpE posited that limited unfolding of the region between the N- and C-terminal domains of NlpE could allow the C-terminal domain to extend through the periplasmic space and activate CpxA (Hirano et al., 2007). Hirano and colleagues predicted that an partially unfolded NlpE, including a 20 amino acid linker region from the acylated cysteine to the beginning of the N-terminal domain, would extend to a length of

about 160 Å, which would be sufficient for OM-anchored NlpE to span the periplasm. To test this hypothesis, we generated two different mutations of the chromosomal copy of NlpE. *nlpE*$_{lock}$ contains two cysteine insertions (E118C and T124C) on adjacent β-strands (β-g and β-i) of the N-terminal domain of NlpE, which is an approach that has been used in the context of BamA studies to restrict it to certain conformations (Noinaj et al., 2014; Rodríguez-Alonso et al., 2020; Warner et al., 2017; Wu et al., 2021). Formation of a disulfide bond between these two strands in NlpE could prevent the unfolding of this region and thus prevent the formation of the hypothetical unfolded NlpE intermediate proposed by Hirano and colleagues. The second mutation was the *nlpE*$_{G\times5(i)}$ construct where 5 residues in the β-i strand were replaced with glycines, which is known to disrupt secondary structure elements due to its high flexibility (Imai and Mitaku, 2005). This variant should have the opposite effect as *nlpE*$_{lock}$ and should permanently unfold to Hirano et al.'s unfolded NlpE.

Neither of these two variants of NlpE abrogated its ability to sense OmpA overexpression (Figure 4-7A), suggesting that NlpE unfolding is not a significant contributor to signaling from the OM, at least in the context of OmpA overexpression. The "unfolded" *nlpE*$_{G\times5(i)}$ mutation on its own does not lead to activation of the Cpx response in the absence of OmpA overexpression (Figure 4-7B), as might be expected if unfolding leads to activation via NlpE, casting further doubt on the hypothesis that NlpE unfolding is critical to signaling. To further probe the signaling pathway for NlpE, we tested the hypothesis that other proteins may be involved in transducing the OmpA overexpression signal to CpxA. We previously found that NlpE crosslinks to Lpp (Figure 4-1D). Previous work by Raivio lab PhD student Junshu Wang also reported that the TonB transport energization protein may be involved in regulating signaling in the Cpx response (Junshu Wang, PhD thesis). However, deletion of these proteins did not impact the ability of NlpE to sense OmpA overexpression (Figure 4-7C), suggesting that these proteins are not involved in

this signaling pathway. Thus, while the C-terminal domain of NlpE is involved in signal transduction, the path it takes to activate CpxA does not appear to involve its extension into the periplasm to interact with CpxA by misfolding, nor does it directly involve Lpp or TonB (although the possibility that other proteins may be involved in signal transduction cannot be ruled out).

NlpE may be a surface exposed lipoprotein

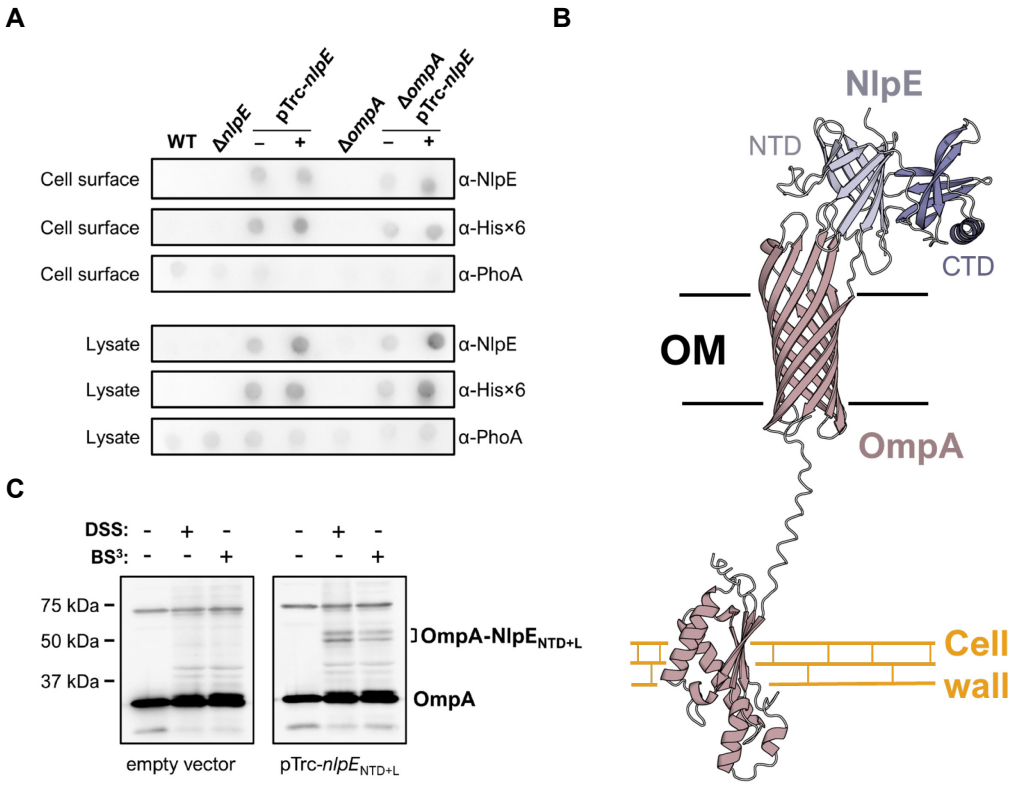

Figure 4-8. NlpE may be a surface-exposed lipoprotein.

(A) Dot blots of MC4100 strains of the indicated backgrounds. Treatments with the pTrc-*nlpE* plasmids were expressing WT NlpE with a C-terminal 6×His tag. – and + indicate the absence of presence of inducer (0.1 mM IPTG for 30 min). Cell surface blots were conducted on whole cells spotted onto nitrocellulose membranes. Membranes were blotted with anti-NlpE, anti-His×6, and anti-PhoA (periplasmic control) antibodies. **(B)** AlphaFold3 model of NlpE-OmpA complexes in *E. coli* (ipTM = 0.29 and pTM = 0.41). **(C)** *in vivo* crosslinking with both DSS (membrane permeable) and BS^3 (membrane impermeable) crosslinkers. Samples were crosslinked with 0.5 mM DSS or BS^3 for 30 minutes. Samples were analyzed by Western blotting with anti-OmpA antibody.

While the canonical pathway for OM lipoproteins ends with their insertion into the inner leaflet of the OM, accumulating evidence makes it clear that this is not an ironclad rule and that many lipoproteins become surface exposed (reviewed in (Konovalova and Silhavy, 2015)). The fact that NlpE is an OM lipoprotein implicated in sensing surface adhesion ((Otto and Silhavy, 2002; Shimizu et al., 2016) led us to hypothesize that NlpE may be surface exposed, allowing it to sense surface signals. To investigate this, we conducted a whole cell dot blot (Konovalova et al., 2014). While we did not observe NlpE on cell surfaces at native levels of NlpE expression (possibly due to its relatively low levels of expression), we did observe that NlpE could become surface exposed when expressing it from plasmid (Figure 4-8A). Slightly more NlpE is observed on cell surfaces in the presence of inducer (IPTG), as expected. NlpE surface exposure appears to be independent of OmpA as NlpE is detected in whole cells in its absence. Because of the cross reactivity of the anti-NlpE antisera with OmpA (leading to potential detection of surface exposed loops of OmpA), we also conducted dot blots with an anti-His×6 antibody to detect a C-terminal His-tag on NlpE expressed from plasmid; these blots indicated that NlpE's C-terminus becomes surface exposed. Dot blots conducted on whole cells with anti-PhoA (periplasmic alkaline phosphatase) antibody showed that there was minimal leakage of periplasmic contents in the cell surface dot blots; thus, it is unlikely that the NlpE detected is due to membrane lysis.

While NlpE does not depend on OmpA for surface exposure, we wanted to further investigate NlpE-OmpA complexes for insights into what NlpE might be doing at the cell surface. We modelled NlpE-OmpA complexes using AlphaFold3 (Abramson et al., 2024),. To our surprise, AlphaFold3 predicted that NlpE interacts with OmpA in *E. coli* K12 at the cell surface (i.e. the outer leaflet of the OM), specifically, with the extracellular loops of OmpA. The overall confidence for the model, however, was relatively low (ipTM = 0.29 and pTM = 0.41), indicating that this model may not be physiological relevant. However, the AlphaFold3 model of NlpE and

OmpA is consistent with several points of data from work presented previously in this chapter. The model predicts NlpE's N-terminal domain interacts with OmpA, which is consistent with our crosslinking results (Figure 4-3B). Furthermore, the model appears to localize the entirety of NlpE to the cell surface, which is consistent with our observation of the NlpE C-terminal domain on the cell surface (Figure 4-8A).

To further investigate the AlphaFold3 model, we repeated *in vivo* crosslinking assays but modified the assay to include a crosslinking treatment with a hydrophilic, non-membrane permeable crosslinker bis(sulfosuccinimidyl)suberate (BS^3) in addition to the membrane permeable DSS crosslinker used previously. Like DSS, BS^3 possesses an 8 carbon spacer between N-homoserine lactone moieties which react with primary amines; thus, the crosslinkers possess identical chemistries, but BS^3 only labels interactions on the cell surface (Boudreau et al., 2012). Equimolar concentrations of DSS and BS^3 were used. Because of the non-specific band that obscures full length NlpE-OmpA complexes (Figure 4-3B), we used a plasmid expressing the N-terminal domain of NlpE for crosslinking. Crosslinking of NlpE-OmpA complexes was observed with both membrane permeable (DSS) and impermeable (BS^3) crosslinkers (Figure 4-8C), providing further evidence that NlpE is surface exposed and that the AlphaFold3 model may represent true NlpE-OmpA complexes. Crosslinking was slightly weaker with BS^3, which is consistent with its inability to cross the OM and crosslink sites inside the periplasm or within the membrane. Taken together, these results suggest that NlpE, at least when overexpressed, may become surface exposed and interact with OmpA at the cell surface.

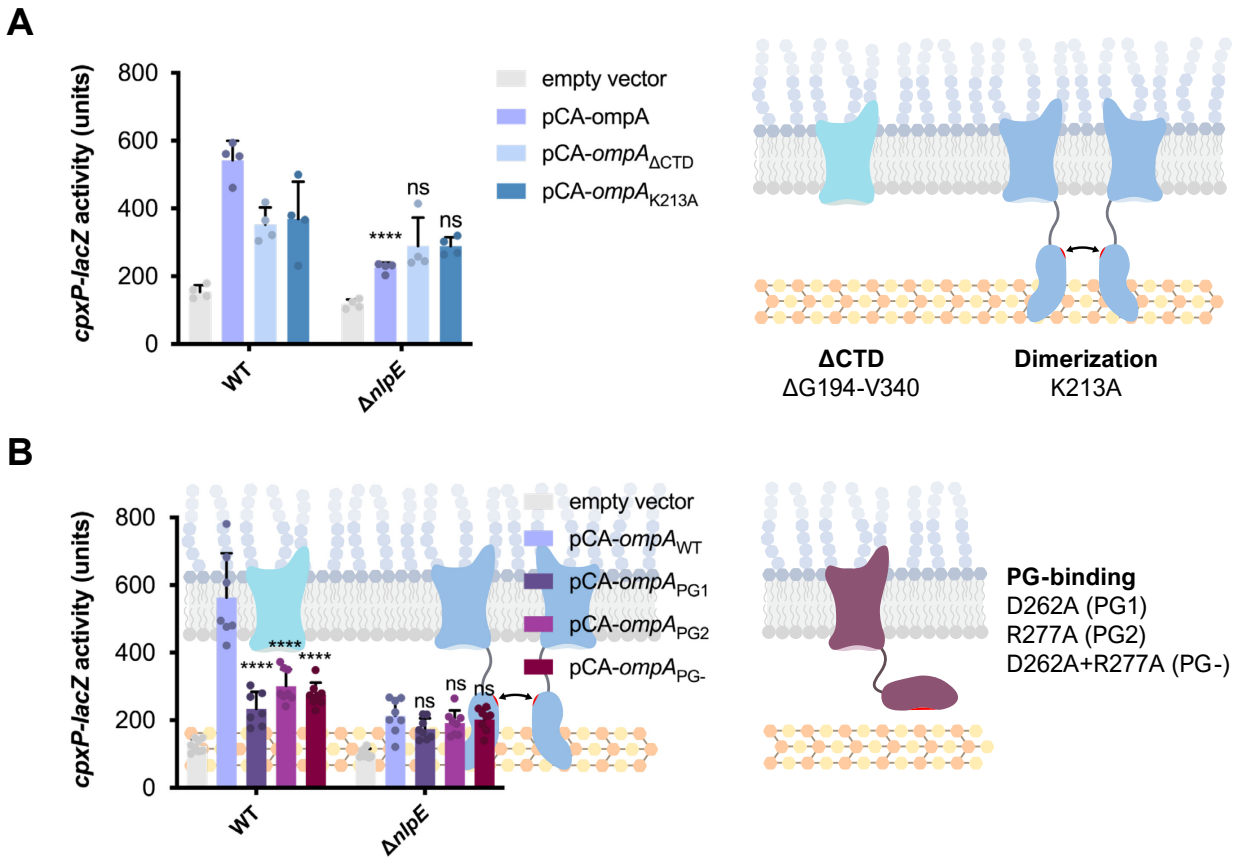

Figure 4-9. The OmpA C-terminal domain influences signaling through NlpE.

The ability of WT OmpA and variants that **(A)** lack the periplasmic C-terminal domain or are mutated in the residue involved in dimerization (K213A) or **(B)** are mutated in residues involved in peptidoglycan binding to activate the Cpx response in WT and Δ*nlpE* cells. OmpA expression was induced with 0.1 mM IPTG for 1 hour after cultures reached mid-log phase of growth. Shown are mean *cpxP-lacZ* activities with standard deviations (Tukey HSD test, **p<0.01, ***p<0.005, ****p<0.0001). Significance markers shown directly above bars indicate tests comparing reporter activity in that strain to that of same strain background overexpressing WT OmpA.

OmpA is a unique OM protein in both its structure and function. Structurally, OmpA consists of two distinct domains: an N-terminal, OM-integral β-barrel domain and a C-terminal

globular periplasmic domain with a proline-rich unstructured linker connecting these two elements (Ortiz-Suarez et al., 2016; Smith et al., 2007). OmpA is also thought to adopt a larger pore conformation, although the physiological circumstances under which this form occurs remain unclear (Zakharian and Reusch, 2005, 2003). OmpA also appears to dimerize via C-terminal domain to C-terminal domain interactions (Marcoux et al., 2014; Zheng et al., 2011). To further investigate how NlpE senses OmpA overexpression, we created vectors expressing variants of OmpA by site-directed mutagenesis and expressed these variants in WT or Δ*nlpE* cells. These variants lack the C-terminal domain all together ($OmpA_{\Delta CTD}$) or contain an alanine substitution for the K213 residue essential for dimerization (Marcoux et al., 2014; Zheng et al., 2011). Despite this, we observed that the Cpx response is activated to similar levels during overexpression of both variants, albeit at lower overall levels compared to when the wildtype OmpA is overexpressed (Figure 4-9A). However, unlike when overexpressing WT OmpA, a significant decrease in Cpx activity was not seen in the absence of NlpE suggesting that both the OmpA C-terminal domain and OmpA dimerization are necessary for NlpE signaling from the OM.

The OmpA C-terminal domain non-covalently binds the peptidoglycan (PG) cell wall, thus regulating the spatial characteristics of the envelope by providing structural support (Park et al., 2012; Wang, 2002). Two charged residues located in the C-terminal domain are important for PG binding: D262 and R277. While these residues were determined in the OmpA of *Acinetobacteri baumanii* (Park et al., 2012), these residues are conserved across Gram-negative bacteria, including *E. coli*. We mutated these two residues individually (named PG1 and PG2) and in combination (PG-) and determined the ability of these variants to activate the Cpx response through NlpE when overexpressed. We observed that mutating any of the OmpA PG-binding residues to alanine significantly reduces activation of the Cpx response upon

overexpression in WT cells to a similar extent as deleting *nlpE* (Figure 4-9B), despite these mutants being expressed at similar levels to WT (Figure S4B). Expressing these variants in a Δ-*nlpE* strain resulted in comparable levels of activation to WT (1.9-2.4 fold in WT vs. 1.7-2.0 fold in Δ*nlpE*) suggesting that these mutations impact ability of NlpE to sense the OmpA variant being expressed. Furthermore, we did not observe significantly different levels of Cpx induction when expressing WT OmpA or the PG binding mutants in the Δ*nlpE* background.

Importantly, the level of OmpA present in membrane fractions were similar across all these variants, making it unlikely that periplasmic accumulation of OmpA leads to NlpE signaling (Figure 4-10A). Co-immunoprecipitation assays also suggest that the variants of OmpA tested here are able to pull down with NlpE, although the extent to which these variants co-immunoprecipitate differ between variants (Figure 4-10A). While the OmpA K213A variant is expressed comparably to WT OmpA, levels of the $OmpA_{\Delta CTD}$ construct were lower than wildtype, suggesting this variant is unstable (Figure 4-10B). However, the lack of detection of $OmpA_{\Delta CTD}$ may also be due to OmpA C-terminal domain being the antigen used during commercial antibody development due to its solubility (therefore relative ease of purification). The specific antigen used to generate this particular antibody used in this blot was not specified by the company producing the antibody. The fact that slight activation is seen in the C-terminal domain deletion strain suggests that some protein is still being expressed in these strains. Taken together, our results suggest that the OmpA C-terminal domain, and in particular its ability to bind the cell wall and mediate dimerization, plays a key role in activating the Cpx response through NlpE when OmpA is overexpressed.

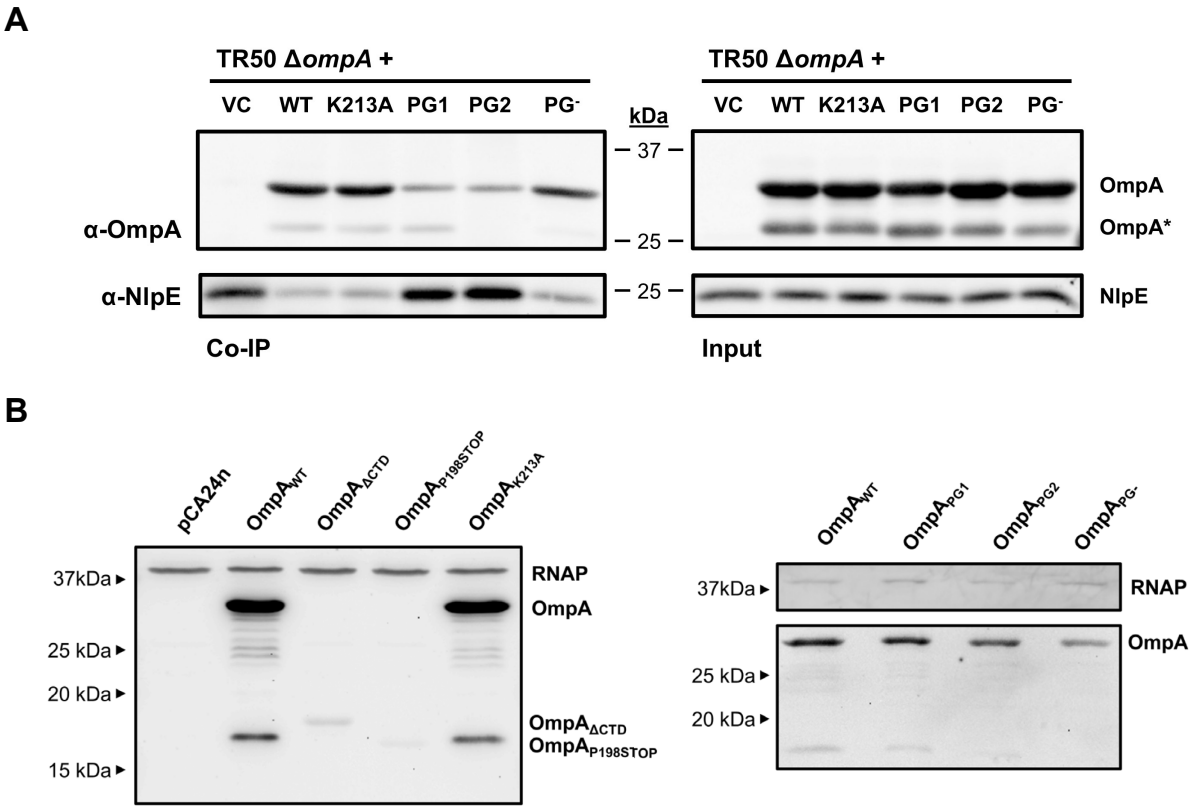

Figure 4-10. OmpA mutants still interact with NlpE.

(A) *in vivo* co-immunoprecipitation assays of strains expressing OmpA PG binding mutants. Expression of OmpA was induced with 0.1 mM IPTG for 1 hour after cultures reached mid-log phase of growth. “Input” comprises solubilized membrane preparations from the indicated strains. Complexes were precipitated with anti-NlpE antibodies immobilized on agarose beads, and eluted proteins were analyzed by SDS-PAGE and Western blotting with anti-NlpE (bottom panels) and OmpA (top panels) antibodies. **(B)** Expression levels of OmpA variants expressed from plasmid with 0.1 mM IPTG for 1 hour after cultures reached mid-log phase. Lysates were separated by SDS-PAGE and probed with anti-OmpA and anti-RNAPα (loading control) antibody. Plasmids were expressed in a Δ*ompA* expression strain (i.e. in the absence of native OmpA expression).

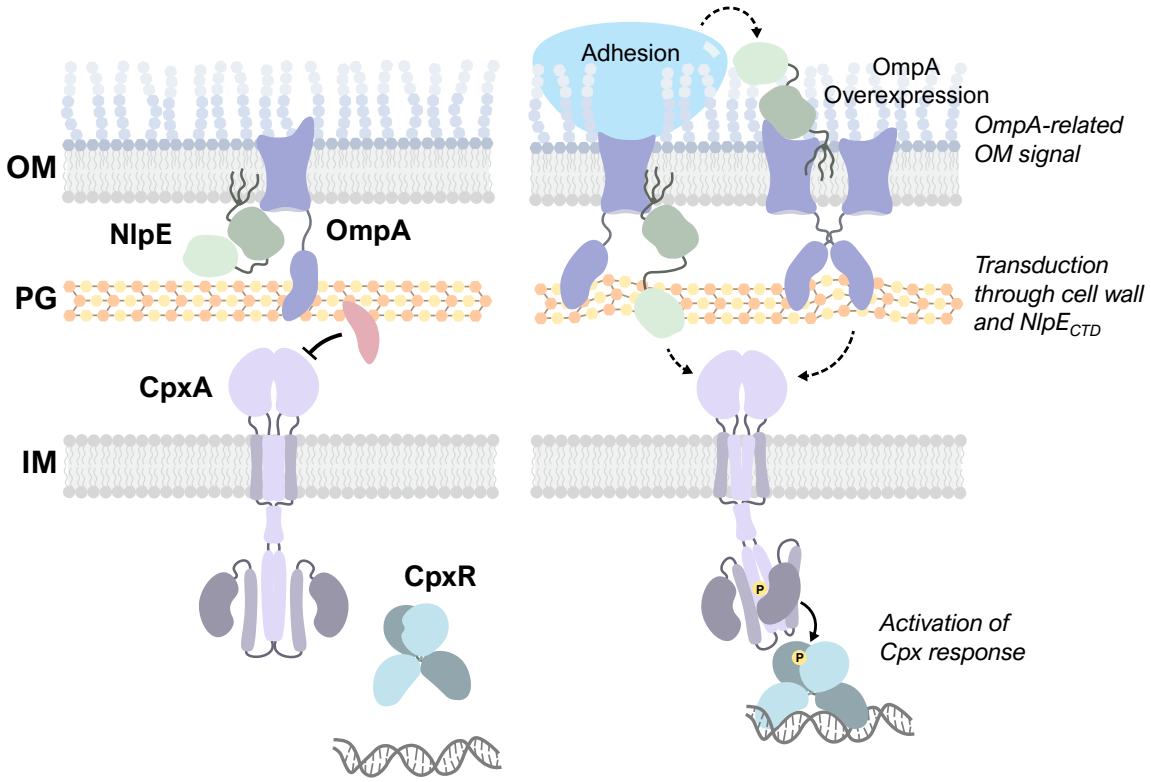

Figure 4-11. NlpE is an OmpA-associated OM sensor.

In the absence of inducing cues, NlpE is efficiently trafficked to the OM where it forms complexes with OmpA via its N-terminal domain. In the presence of a surface-related cue, such as surface adhesion, or OmpA overexpression, NlpE and OmpA cooperate to transduce a signal through the cell wall to CpxA through the C-terminal domains of both NlpE and OmpA.

While emerging work has focused on how NlpE senses OM lipoprotein trafficking defects (Delhaye et al., 2019; Grabowicz and Silhavy, 2017a; Marotta et al., 2023a; May et al., 2019), its role as an OM lipoprotein and how it activates the Cpx system in response to surface adhesion remains unclear (Otto and Silhavy, 2002; Shimizu et al., 2016). In this study, we reveal that NlpE does not function alone in this latter signaling role but cooperates with the major OMP OmpA and utilizes its distinct two-domain structure to mediate activation of the Cpx ESR in the presence of OM-associated signals (Figure 4-11).

NlpE and OmpA mediate adaptation to surfaces

Bacterial surface adhesion and biofilm growth are complex processes influenced by many factors including nutrient availability, mechanical stimuli, stress responses, and small molecule signaling (reviewed in (Berne et al., 2018; O'Toole and Wong, 2016)). Some evidence has implicated the Cpx response in sensing surfaces (Ma and Wood, 2009; Otto and Silhavy, 2002; Shimizu et al., 2016) and regulating processes related to surface adhesion and growth (Dorel et al., 2006, 1999; Hung, 2001; Jones, 1997; Jubelin et al., 2005; Lacanna et al., 2016; Ma and Wood, 2009; Prigent-Combaret et al., 2001; Raivio et al., 2013). However, the precise role of the Cpx response in mediating adhesion and surface growth appears to be quite complex. The Cpx response regulates the expression and assembly of adhesion-related appendages such as curli (Dorel et al., 1999), and chaperone-usher and type IV pili (Hernday et al., 2004; Humphries et al., 2010; Nevesinjac and Raivio, 2005; Vogt et al., 2010) while also downregulating motility (De Wulf et al., 1999; Price and Raivio, 2009; Shimizu et al., 2016). Overexpression of NlpE increases biofilm production through the Cpx-regulated diguanylate cyclase DgcZ (Lacanna et al., 2016), and deletion of *cpxR* and *nlpE* diminishes attachment to hydrophobic surfaces (Otto and Silhavy, 2002).

Our study suggests that NlpE-OmpA complexes are a part of the mechanism by which the Cpx response responds to signals related to surface growth. OmpA and its homologues are prominent Gram-negative adhesins and invasins involved in the pathogenesis of several Gram-negative species (reviewed in (Confer and Ayalew, 2013)). In agreement with emerging literature, our results expand our understanding of OmpA not only as a virulence factor with direct implications for host cell adhesion and invasion, but also as a signaling factor mediating the transduction of surface-related signals to regulatory systems such as the Cpx and Rcs envelope stress responses. Deleting *ompA* is sufficient to abolish activation during surface

adhesion (T. H. S. Cho et al., 2023b), suggesting that NlpE interacts primarily with OmpA to mediate signaling unlike RcsF, which appears to interact with several OMPs in a similar capacity (Konovalova et al., 2014).

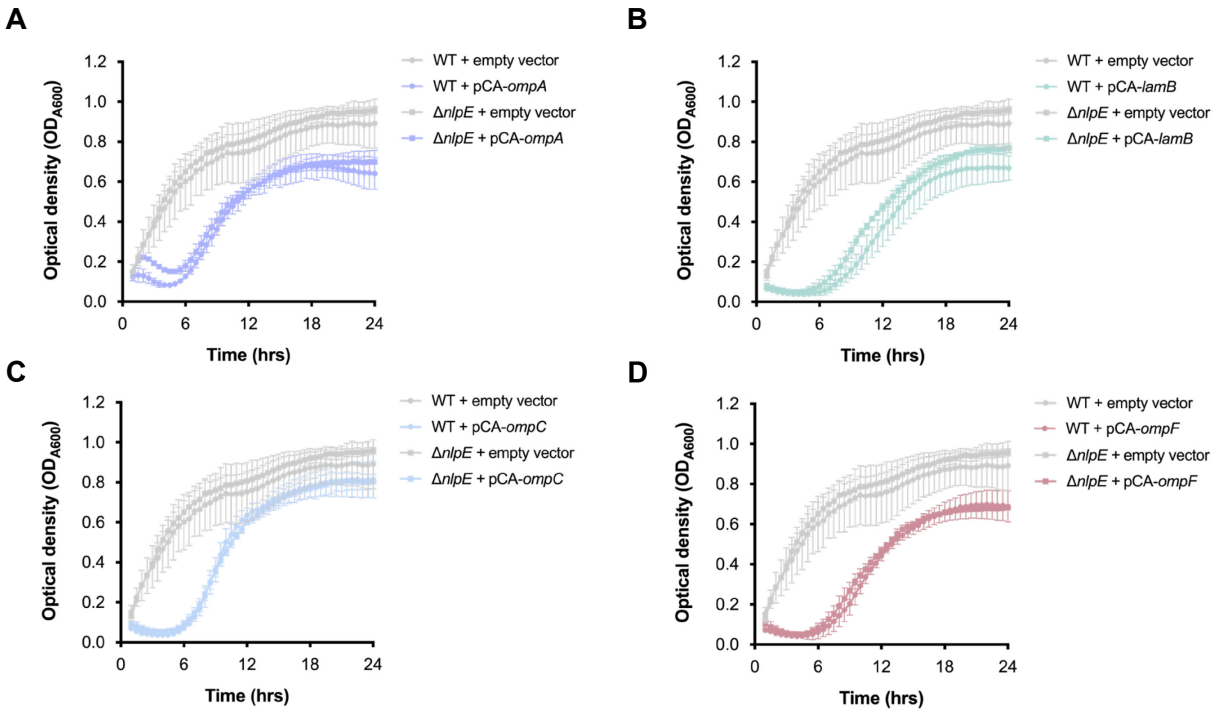

Figure 4-12. Outer membrane protein overexpression leads to a general growth defect. Growth curves of strains overexpressing **(A)** OmpA, **(B)** LamB, **(C)** OmpC, or **(D)** OmpF. Indicated strains were grown in the presence of 0.1 mM IPTG (inducer) for 24 hours at 37°C with shaking. Optical density was read every 30 minutes and plotted as the mean of 3 replicates with standard deviation.

While defects in OMP biogenesis are a classical inducing cue of the σ^E response, we find that overexpression of several OMPs induces the Cpx response. This is observed even with OmpA in the absence of NlpE (Figures 2-5, 2-6, 2-9). This is in line with studies reporting that the Cpx response may respond to defective OMP biogenesis as a means to protect the IM; the small regulatory RNA (sRNA) CpxQ downregulates the expression of the chaperone Skp,

preventing BAM-independent incorporation of OMPs into the IM (Chao and Vogel, 2016; Grabowicz et al., 2016). Similarly, it's possible that induction of the Cpx response by OMP overexpression observed in this study (Figure 4-5), may increase Skp-dependent IM incorporation of OMPs, thereby activating the Cpx response. In support of this, we noticed that overexpression of OMPs such as OmpA, OmpC, OmpF, and LamB lead to similar growth defects (Figure 4-12), suggesting aberrant expression of these proteins generates significant stress for cells. Overall, this conclusion aligns with the finding that Cpx activation by most OMPs is not NlpE dependent, and that OmpA overexpression residually induces the Cpx pathway in absence of NlpE (Figures 4-5, 4-6, 4-9).

The NlpE-OmpA interaction appears to be unique. NlpE does not sense the overexpression of other OMPs in a similar manner to OmpA (Figure 4-5). Furthermore, if OMP overexpression does lead to a general increase IM stress, this stress is sensed independently of NlpE, further reinforcing its role as an OM-specific sensor. While a previous study suggested that OmpA production leads to increased envelope stress, activating the Cpx response and inducing biofilm formation via regulation of cellulose production (Ma and Wood, 2009), our results suggest that NlpE cooperates with OmpA to activate the Cpx response in surface-adhered cells. OMP overexpression does appear to lead to envelope stress as indicated by an extended lag phase in growth curves (Figure 4-12); however, it's unlikely that NlpE senses or mitigates the stress generated by OmpA overexpression as deleting *nlpE* does not significantly alter growth and overexpressing other OMPs leads to similar growth phenotypes as overexpressing OmpA. Thus, rather than functioning as an OMP stress sensor in this role, we hypothesize that NlpE operates together with OmpA in a signal transduction pathway to mediate Cpx activation in the presence of a surface-adhesion related inducing signal.

Interestingly, recent work suggests that NlpE may cooperate with several stress responses to mediate a response to surface adhesion. Feng and colleagues report that Enterohemorrhagic *E. coli* (EHEC) O157:H7 utilizes NlpE to sense adhesion to HeLa cells (Feng et al., 2022). However, the authors report that NlpE is required for activating the BaeS sensor kinase of the BaeRS envelope stress response. Activation of BaeS leads to upregulation of locus of enterocyte effacement (LEE) pathogenesis genes, similar to the pathway reported by Shimizu and colleagues (Shimizu et al., 2016), except instead of activating LEE through the regulator LrhA, BaeS activation induces the expression of the regulator AirA. Thus, distinct from the pathway reported by (Shimizu et al., 2016), NlpE may serve as a sensor of surface adhesion to promote adhesion-dependent virulence processes.

The precise nature of this surface signal remains mysterious as it is unclear whether NlpE senses surfaces themselves or some cue present in surface-adhered/biofilm cells. Both studies on the role of NlpE in surface sensing in *E. coli* (Otto and Silhavy, 2002; Shimizu et al., 2016), as well as the study upon which this chapter is based (T. H. S. Cho et al., 2023b), underscore the importance of hydrophobic surfaces. Furthermore, Shimizu and colleague's studies as well as a more recent study find that NlpE may sense adhesion to biotic surfaces, presumably key for mediating stable colonization of intestinal epithelia in the case of both commensal and pathogenic *E. coli* (Feng et al., 2022; Shimizu et al., 2016). Surface sensing may be mediated by OmpA's surface exposed loops (Confer and Ayalew, 2013) or, at least as suggested by the emerging work presented here, directly by surface exposed NlpE.

A recent study questions the role of the Cpx response in direct surface sensing based on the finding that Cpx-regulated fluorescent reporters are not activated in cells grown in flow chamber surfaces (Kimkes and Heinemann, 2018). Thus, it is possible that the Cpx response does not directly sense surfaces themselves but is activated in response to some other signal

present in surface-adhered cells. To explain the contradictory findings, the authors reason that cell lysis due to harsh treatment may lead to increased measurement error (and thus Cpx activation). Kimkes and Heinemann further speculate that the induction of the Cpx response in the original Otto and Silhavy (2002) study may be due to residual copper present on the beads used in that study.

We find this study's conclusions and reasoning unsatisfying for several reasons. Historical speculation about the possibility of copper present in the reagents used in the Otto and Silhavy study (2002) activating the Cpx response is roundly refuted by the fact that supernatants from solutions containing the hydrophobic beads themselves do not activate the Cpx response, as reported in the original study. Furthermore, while cell lysis during β-galactosidase reporter assays may lead to measurement error, it is unclear how this leads to Cpx activation in a specific subset of treatments, particularly considering that the errors present in the original 2002 study are relatively small, indicating consistent and reliable measurements. The Kimkes and Heinemann (2018) study also does not faithfully attempt to recreate the β-galactosidase reporter assay protocol used in the Otto and Silhavy study, further calling into question the validity of any methodological critiques. Finally, the burden of evidence lies heavily against the Kimkes and Heinemann study as several studies using techniques not involving harsh treatment of cells report a role for NlpE in surface sensing (T. H. S. Cho et al., 2023b; Feng et al., 2022; Otto and Silhavy, 2002; Shimizu et al., 2016). The authors suggestions also do not explain how the Cpx response is differentially induced by the type of abiotic surface adhered to (e.g. hydrophobic vs. hydrophilic) (Otto and Silhavy, 2002; Shimizu et al., 2016) or the activation of the response in cells adhered directly to living cells in tissue culture (Feng et al., 2022; Shimizu et al., 2016).

We argue that the most parsimonious explanation for the work presented in the field is that CpxRA is indeed sensing some sort of surface signal. OmpA itself is a major surface-

exposed antigen of Gram-negative bacteria with roles in adhesion and biofilm formation (Confer and Ayalew, 2013). Furthermore, we show that NlpE may itself become surface exposed (Figure 4-8), suggesting that the Cpx response may directly sense surfaces through complexes of NlpE and OmpA. It has previously been reported that OmpA levels are increased, both in clinical and nonclinical strains of *E. coli*, when cells are grown in surface-adhered biofilms (Orme et al., 2006). We report that NlpE senses OmpA overexpression, suggesting that the level of OmpA in the OM may be part of the mechanism by which OmpA and NlpE mediate activation of the Cpx response in adhered cells.

Signal transduction by NlpE-OmpA complexes

Several studies have implicated OmpA in activating the Cpx response under different conditions, but no clear mechanisms have been proposed (Ma and Wood, 2009; Vogt and Raivio, 2014). Our study reports that NlpE interacts with OmpA to signal certain OM signals to the Cpx response. While caution is required in interpreting our crosslinking data as OmpA is an incredibly abundant OM protein (Koebnik, 1995), we were able to find evidence for this interaction using several methods, including co-immunoprecipitations and pull down assays in our published study (T. H. S. Cho et al., 2023b). That NlpE signals from the OM and not the IM is made clear by the observations that the N-terminal domain not the C-terminal domain of NlpE likely interacts with OmpA (Figures 2-3B,E) and that permanently IM-bound NlpE does not crosslink to OmpA (Figure 4-3F). These findings imply that direct N-terminal domain-CpxA interactions do not mediate activation of the response in this context. The fact that deleting the C-terminal domain greatly diminishes induction of the Cpx response during OmpA overexpression provides support for this interpretation and strong evidence for a model where signals sensed by NlpE in the OM in conjunction with OmpA are transduced through the C-terminal domain to induce the Cpx response.

Our findings naturally draw comparisons to RcsF, another lipoprotein activator of an envelope stress response (the Rcs phosphorelay) that interacts with OmpA (Cho et al., 2014; Dekoninck et al., 2020; Hart et al., 2019; Konovalova et al., 2016, 2014; Rodríguez-Alonso et al., 2020; Tata et al., 2021; Tata and Konovalova, 2019). While RcsF can be folded into the OmpA β-barrel, as evidenced by the requirement for unfolded OmpA for complex formation *in vitro* (Konovalova et al., 2014), pull-down assays suggest that NlpE can interact with already folded OmpA (T. H. S. Cho et al., 2023b), suggesting that NlpE-OmpA complexes do not necessarily form during OMP biogenesis. Dekoninck and colleagues report that the globular OmpA C-terminal domain interacts directly with RcsF's C-terminal domain and propose a buffer mechanism where OmpA competes with IgaA for RcsF binding (Dekoninck et al., 2020), although evidence contrary to this model indicates that more work is required to elucidate the precise mechanisms of OmpA-RcsF signaling (Konovalova et al., 2014; Tata et al., 2021).

In contrast, the NlpE-OmpA signaling interaction appears to be more cooperative than competitive in nature. While both CpxA and OmpA bind the NlpE N-terminal domain, the spatial and structural characteristics of this domain make it unlikely that CpxA and OmpA compete for binding. Furthermore, deleting OmpA does not lead to constitutive activation of the response (Figure 4-4A) as would be expected if release of NlpE from OmpA is responsible for Cpx activation. However, it is possible that this is because NlpE may interact with other OMPs. Our experiments with IM-bound NlpE indicate that NlpE may interact with several OM proteins (Figure 4-1C); more work is required to determine if NlpE, like RcsF, associates with multiple OMPs. Regardless, it appears that the relationship between NlpE and OmpA is unique, given that overexpression of other OMPs does not lead to Cpx activation in an NlpE-dependent fashion.

Signal transduction by the C-terminal domain of NlpE

Our work supports a model where signals are transduced through the NlpE C-terminal domain to activate the Cpx response, akin to the models of signaling proposed in the original structural study (Hirano et al., 2007). However, the precise mechanisms by which the C-terminal domain accomplishes this remain unclear. Hirano and colleagues propose that partial unfolding of the N-terminal domain allows for the linker region to extend into the periplasm enough for the C-terminal domain to directly interact with CpxA (Hirano et al., 2007). However, experiments with putatively unfolded and permanently folded NlpE do not provide evidence for such a mechanism. Furthermore, we and previous studies find that the NlpE C-terminal domain is not needed for direct interaction with the CpxA sensor domain (Delhaye et al., 2019, see Chapter 3 of this this thesis.

This suggests that another mechanism besides direct physical interaction between NlpE and CpxA may mediate CpxA activation by the NlpE C-terminal domain. One possibility is that other envelope proteins may mediate NlpE signaling from the OM; we observed that several crosslinked products are only present when overexpressing OM-localized NlpE compared to permanently IM-bound NlpE (Figure 4-3F). A recent study in *Pseudomonas aeruginosa*, reports that a novel OM complex of MipA and MipB, where MipA folds into an OM-integral β-barrel and MipB comprises an OM lipoprotein with an N-terminal β-lactamase fold with additional C-terminal domains (Janet-Maitre et al., 2024). This MipAB complex senses polymyxins and activates the ParS-ParR two-component system, mounting a protective response by upregulating efflux. The authors note that one of the C-terminal domains of MipA possesses high structural similarity to the N-terminal domain of *E. coli*'s NlpE, providing an OMP-lipoprotein pairing with functional similarity to the NlpE-OmpA complex reported here. The presence of additional domains on both MipB suggests that other domains may be involved in signal

transduction for this complex. Thus, a far more expansive network of envelope proteins than what is currently known may be involved in mediating signal transduction through NlpE across the envelope.

Another (not mutually exclusive) possibility is that the redox state of the disulfide bond present on the C-terminal domain may mediate signaling through the C-terminal domain of NlpE (Andrieu et al., 2023; Delhaye et al., 2019). Delhaye and colleagues (2019) found that the absence of the envelope oxidoreductase DsbA leads to Cpx induction through NlpE. NlpE may be a substrate for DsbA, specifically its C-terminal disulfide bond (forming between C165 and C221). Substituting these cysteines for alanines leads to Cpx induction to a similar extent as deletion of *dsbA*, suggesting that the reduction status of the disulfide bond on NlpE's C-terminal domain is important for sensing periplasmic redox. This mechanism utilizing the redox state of cysteine residues is a well-characterized of oxidative stress sensing (Vázquez-Torres, 2012). Further evidence for the involvement of NlpE's C-terminal domain in sensing periplasmic redox comes from a recent study in *Salmonella* Typhimurium showing that *N*-chlorotaurine, a reactive chlorine species, activates the Cpx response through NlpE to mount a protective response against oxidative folding stress (Andrieu et al., 2023).

How exactly redox state contributes to surface sensing is unclear. However, a recent study from the Burrows lab suggests that such a connection is plausible (Yaeger et al., 2024). In their study of biofilm formation in *P. aeruginosa,* Yaeger and colleagues identified the OmpA homologue in this species, OprF, as a key factor in promoting biofilm formation. The authors note that OprF contains 4 cysteine residues that are capable of forming disulfide bonds and the status of these bonds control the folding of OprF (Sugawara et al., 2010). Furthermore, *Salmonella* sp. utilize their OmpA homologue to respond to oxidative stress (van der Heijden et al., 2016). Yaeger and colleagues identified other proteins involved in oxidative folding of periplasmic

proteins, such as DsbA, in their screen. Treatment of cells with a dithiothreitol (DTT), a reducing agent which should reduce disulfide bonds, abolishes biofilm formation, suggesting that proper regulation of redox is important for promoting growth on surfaces.

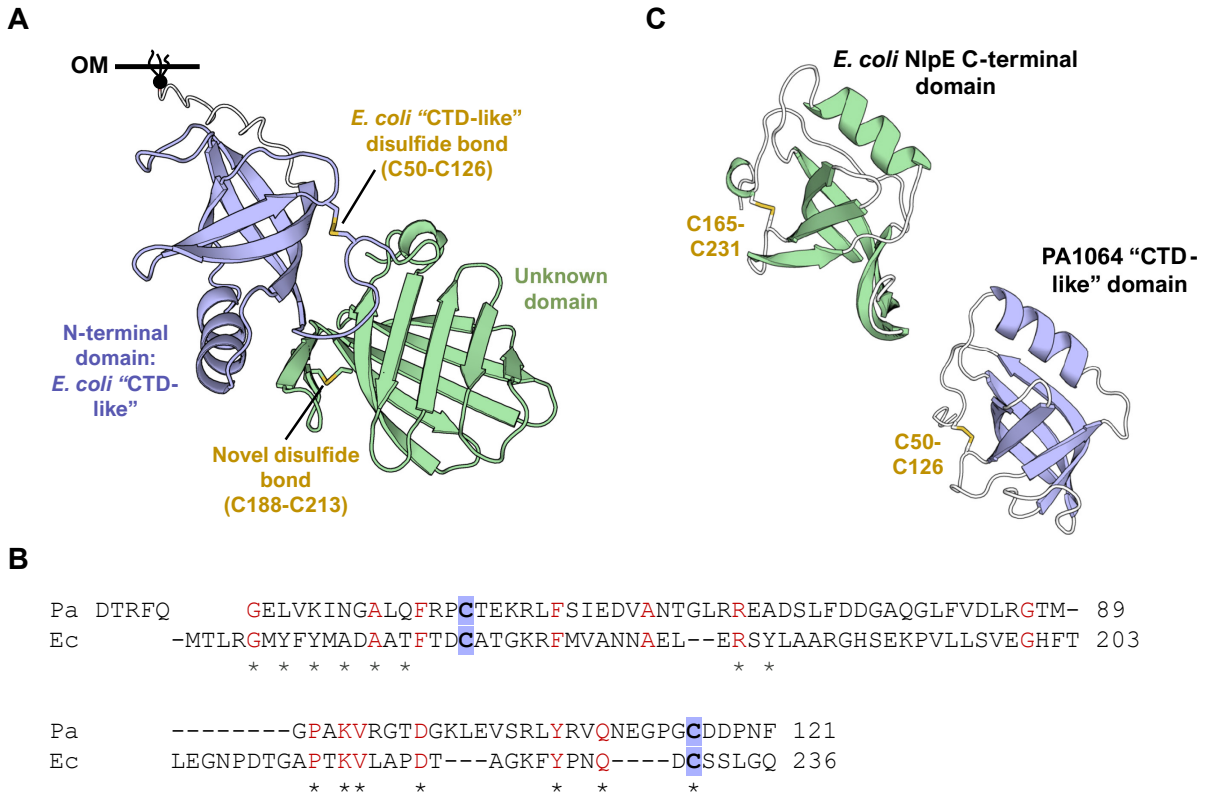

Figure 4-13. NlpE C-terminal domain disulfide bonds are conserved across species.

(A) AlphaFold2 structure of PA1064, an uncharacterized lipoprotein of *Pseudomonas aeruginosa* with a domain resembling the C-terminal domain of *E. coli* NlpE from the AlphaFold database (https://alphafold.ebi.ac.uk/). Key structural features are indicated in the panel. **(B)** Clustal Omega alignment of the sequence of the *E. coli* CTD-like domain of PA1064 (aa31-121) with the C-terminal domain of *E. coli* NlpE (aa147-236). All conserved residues are indicated with an asterisk. Conserved disulfide bond residues are indicated with the blue highlighting and other conserved residues are coloured red. **(C)** Side by side comparison of the PA1064 N-terminal domain with the C-terminal of *E. coli* NlpE.

While the authors note our findings in (T. H. S. Cho et al., 2023b) that NlpE and OmpA form a surface sensing unit in *E. coli*, the authors were also unable to find an NlpE homologue in *P. aeruginosa*. However (as will be described more extensively in the Appendix), combination

searches of domains of *E. coli* NlpE's N- and C-terminal domains using the UniProt database protein basic local alignment search tool (Protein BLAST) with the structures available on the AlphaFold protein structure database (https://alphafold.ebi.ac.uk/) reveals an uncharacterized lipoprotein in *P. aeruginosa*, PA1064, which possesses a domain resembling the C-terminal domain of *E. coli* NlpE (Figure 4-13A). These two domains share a low percent identity of approximately 18% (Figure 4-13B). PA1064 lacks a domain resembling the *E. coli* N-terminal domain. Instead, the C-terminal domain-like fold is present at its N-terminus with a second unknown domain present at its C-terminus. Important, the shared *E. coli* C-terminal domain-like fold possesses an identical disulfide bond to the one present in *E. coli* NlpE (Figure 4-13C), which was previously reported to be important for sensing redox state (Delhaye et al., 2019). Although it is currently unknown if PA1064 forms a complex with OprF (AlphaFold3 predicts a low confidence model between these two proteins not shown here), future studies of OmpA homologues across bacteria will provide interesting and novel hypotheses about the function of the NlpE-OmpA complex discussed here. Future studies in *E. coli* will also investigate the contribution of the disulfide bonds of NlpE to signaling from the surface in conjunction with OmpA.

The OmpA C-terminal domain is involved in signal transduction

We observed that overexpression of OmpA lacking the C-terminal domain results in low level activation (less than two-fold) of the Cpx response independently of NlpE (Figure 4-9A). The C-terminal globular domain of OmpA is involved in a number of different functions including homodimerization (Marcoux et al., 2014) and cell wall binding (Park et al., 2012). Interestingly, we found that, similar to deleting the C-terminal domain, mutating amino acids associated with these functions leads to lower levels of Cpx activation and abolishes the dependence of the remaining activation on NlpE (Figure 4-9). There is controversy around the exact conformation of

OmpA *in vivo;* some studies suggest that switching between small pore (presumably with a globular C-terminal domain) and large pore conformations is possible (Arora et al., 2000; Zakharian and Reusch, 2005, 2003). Furthermore, portions of the OmpA C-terminal domain can become surface exposed in *Salmonella enterica* (Singh et al., 2003). However, the fact that altering functions associated with the globular C-terminal domain impacts signaling through NlpE suggests that NlpE interacts with the small-pore, periplasmic domain-containing conformation of OmpA rather than the larger pore form.

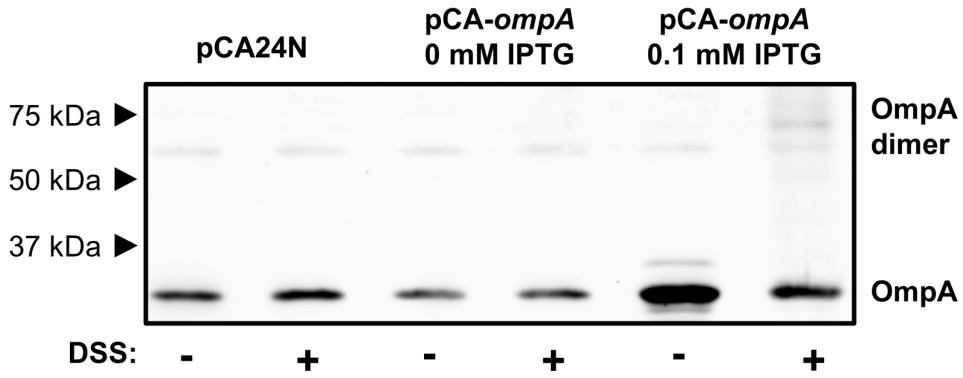

Figure 4-14. OmpA dimers are observed during OmpA overexpression.

Cultures of WT MC4100 containing the specified plasmids were subjected to *in vivo* crosslinking with 0.5 mM DSS for 30 minutes. Samples were subjected to SDS-PAGE and Western blotting with anti-OmpA antibody.

The molecular basis for how NlpE senses OmpA overexpression also requires further study. It is possible that increased levels of OmpA may lead to higher levels of OmpA dimers and/or OmpA bound to the cell wall, which may exclude interaction with NlpE. However, deletion of *ompA* does not lead to significant changes in Cpx activation (Figure 4-4), suggesting that "free" NlpE is not sufficient for NlpE signaling from the OM. Thus, it's likely that OmpA overexpression leads to a conformational change in OmpA which allows NlpE to signal through the envelope in association with OmpA. This conformational change may involve OmpA dimerization and PG binding, as OmpA dimerization and PG binding mutants show reduced

ability to activate the Cpx response through NlpE when overexpressed (Figure 4-9). Furthermore, we have observed putative crosslinked OmpA dimers only during OmpA overexpression and not at native levels of expression (Figure 4-14), suggesting that OmpA dimers are more significantly more abundant during overexpression. Molecular dynamics simulation studies of OmpA suggest that OmpA dimerization alters how OmpA binds to the cell wall, allowing the C-terminal domain to bind peptidoglycan at a distance from the OM (Samsudin et al., 2016). Thus, overexpressing OmpA may increase the number of OmpA dimers bound to the cell wall, altering the properties of the cell wall to allow signaling through it. Alternatively, NlpE may bind to the same sites in the OmpA CTD as the cell wall such that mutating these sites also impacts its interaction with NlpE, preventing signaling. The spatial characteristics of the periplasm, namely the distance between the OM and IM, was previously shown to be a crucial factor in allowing RcsF to signal across the envelope (Asmar et al., 2017). The association between signaling proteins such as NlpE and PG-binding proteins such as OmpA may therefore function to overcome the challenge of signaling across the cell wall by allowing OmpA to "guide" OM-localized signaling proteins across the cell wall where they can access the IM. Further investigation of PG-binding envelope proteins and their role in signal transduction may shed light on how signals are communicated across physically segregated spaces in the envelope.

NlpE surface exposure and its implications

All of the above discussion on the signaling by NlpE from the OM is complicated by the possibility that NlpE may become exposed on the surface of cells (Figure 4-8). Our results indicate that both the N- and C-terminal domains of NlpE can become exposed on the surface of cells. Surface crosslinking further supports the AlphaFold3 model that NlpE interacts with the extracellular loops of OmpA. This conformation raises questions about NlpE's role in sensing redox. For example, if NlpE is exclusively periplasmic, its disulfide bond formation will be more

tightly regulated by the Dsb system (Ito and Inaba, 2008). However, a surface exposed NlpE would be subject to environmental factors impacting redox state. Surface exposed NlpE may also suggest a signaling model where NlpE itself is the main molecular sensor of adhesion to surfaces and OmpA serves as a signal transduction factor, perhaps through its C-terminal PG binding domain. Surface exposed NlpE may also be directly involved in adhesion; indeed, Otto and Silhavy (2002) report that *nlpE* deletion strains are unable to attach to hydrophobic glass beads. However, our results should be considered with several important caveats. Physical evidence for surface exposed NlpE is also only present in experiments where NlpE was expressed from a plasmid at higher than native levels. While exogenous expression of NlpE is necessary because of its low level of expression natively, this approach does raise concerns about whether the NlpE seen on the surface is a physiologically relevant phenomenon.

The AlphaFold3 model of *E. coli* NlpE-OmpA is also low confidence, with ipTM values below the 0.6 threshold for possible false predictions. However, the model does align with other findings, namely that the N-terminal domain of NlpE interacts with OmpA at the OM. Interestingly, AlphaFold3 predicts that NlpE-OmpA pairs from other species, including those with NlpE that resembles *E. coli*'s closely such as from *Yersinia pseudotuberculosis* and *Salmonella* Typhimurium, form interactions at OmpA's periplasmic C-terminal domain, not on its extracellular loops (Figure 4-15). These alternative complexes suggest three possibilities. First, the *E. coli* complex is a true structure but is an anomaly. Second, the AlphaFold3 model of *E. coli* NlpE-OmpA is incorrect. Finally, it could suggest that NlpE-OmpA complexes may exist in multiple conformations, with NlpE present both inside and outside of the cell. Unfortunately, the above models are low confidence, either matching the confidence of *E. coli* NlpE-OmpA or being substantially lower, making it difficult to draw confident conclusions.

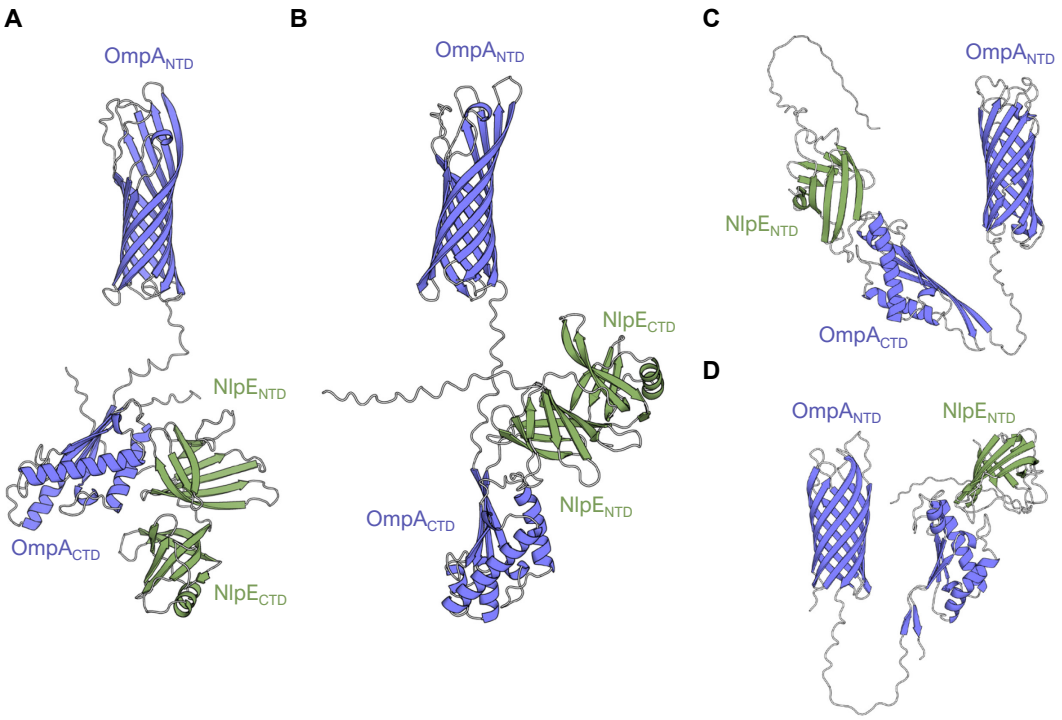

Figure 4-15. AlphaFold3 predicts that NlpE interacts with the C-terminal domain of OmpA in other organisms.

AlphaFold3 predictions of NlpE-OmpA complexes from four Gram-negative species possessing either type I (NTD and CTD containing) or type II NlpE (NTD only). Type I examples include *E. coli* (as shown in elsewhere in this chapter), **(A)** *Yersinia pseudotuberculosis* (ipTM = 0.32, pTM = 0.42) **(B)** *Salmonella enterica* sv. Typhimurium (ipTM = 0.16, pTM = 0.36). Type II examples included here are from **(C)** *Acinetobacter baumanii* (ipTM = 0.13, pTM = 0.37) and **(D)** *Vibrio cholerae* (ipTM = 0.18, pTM = 0.35).

With these caveats in mind, our results still raise a number of interesting considerations about NlpE OM signaling. First, surface exposed lipoproteins in *E. coli* is not without precedent. RcsF is thought to be a surface exposed lipoprotein (Konovalova et al., 2014), and its surface exposure allows it to sense defects in lipopolysaccharide (Konovalova et al., 2016). RcsF, however, appears to become exposed *through* OM β-barrel proteins such as OmpF, OmpC, and OmpA, and thus biogenesis of these complexes is intrinsically tied to their insertion in the OM

through BamA (Cho et al., 2014; Rodríguez-Alonso et al., 2020; Tata et al., 2021; Tata and Konovalova, 2019). NlpE, however, can be surface exposed in the absence of OmpA. NlpE is also structurally distinct from RcsF; the former is a dual-domain lipoprotein (Hirano et al., 2007) whereas the latter consists of a simpler, single small globular domain attached to an N-terminal unstructured region (Leverrier et al., 2011). Thus, while the small globular domain of RcsF can insert itself into the barrel of BamA (Rodríguez-Alonso et al., 2020), it is unclear if NlpE would be able to do the same.

Instead, the structure of NlpE bears stronger resemblance to a different class of surface exposed lipoproteins: those brought to the surface by Slam. Slam (surface lipoprotein assembly modulator) was identified in *Neisseria* spp. as an OM protein necessary for the display of bacterial surface lipoproteins (SLPs) on the surface of the OM (Hooda et al., 2016). SLPs are encoded by several Gram-negative organisms, functioning in nutrient acquisition and immune evasion (Hooda et al., 2017b, 2017a). Many characterized SLPs possess small β-barrel domains, much like NlpE's N-terminal domain and often contain multiple domains. However, surface display of Neisserial SLPs in *E. coli* is only possible with concurrent Slam expression (Hooda et al., 2016), and K12 strains of *E. coli* (used in this chapter and throughout this thesis) lack a Slam homologue (personal communication, Trevor Moraes, University of Toronto). Interestingly, the C-terminal domain was noted to have an oligonucleotide/oligosaccharide (OB) fold (Hirano et al., 2007); surface exposed NlpE would have access, then, to a wide array of potential binding partners outside the cell, possibly in parallel to the nutrient acquisition functions of SLPs in *Neisseria* spp. Thus, while the mechanism of surface exposed lipoproteins in *E. coli* remains unclear, it is possible that an undiscovered machinery may be responsible for the display of lipoproteins such as NlpE in a manner analogous to Slam. Future work should solidify the existence of surface exposed NlpE, especially at native levels of expression using assays such as

proteinase K “shaving” assays or surface protein labelling (e.g. with ^{3}H-palmitoyl labelling) (Hooda et al., 2017b) and seek to identify if other *E. coli* lipoproteins which become surface exposed.

Conclusions

Recent studies of RcsF clearly establish close links between outer membrane lipoprotein and OMP biogenesis with significant consequences for bacterial envelope homeostasis (Cho et al., 2014; Dekoninck et al., 2020; Hart et al., 2019; Konovalova et al., 2016, 2014; Rodríguez-Alonso et al., 2020; Tata et al., 2021; Tata and Konovalova, 2019). Our findings show that RcsF is not exceptional in this regard. The implication of OmpA in Cpx response signaling through NlpE further expands our understanding of OmpA as a novel signal transduction factor that regulates key adaptive systems and the complex interdependence of envelope biogenesis pathways that facilitate stress adaptation. Further study of these envelope signaling complexes will be key to understanding how bacteria respond to stress as well as sense and adapt to the environmental cues essential for *in vivo* success.

Materials and Methods

Bacterial strains, growth, and strain construction

The strains used in this study are listed in Table 2-1. All strains were grown in lysogeny broth (LB) at 37°C with shaking at 225 RPM that was supplemented with the following concentrations of antibiotics as appropriate: ampicillin (100 µg/ml), kanamycin (50 µg/ml), chloramphenicol (25 µg/ml), tetracycline (12 µg/ml), and spectinomycin (25 µg/ml). To induce expression from inducible promoters, 0.1 mM isopropyl β-d-1-thiogalactopyranoside (IPTG) or 0.2% L-arabinose was added to cultures that were grown to an optical density of 0.4-0.6 (A_{600}) for 0.5-2 hours depending on the experiment.

All whole gene deletion mutants were constructed by P1 transduction using lysates derived from the corresponding mutants from the Keio library (Baba et al., 2006). Kan^R cassettes were removed using FLP-mediated recombination as previously described (Datsenko and Wanner, 2000). *nlpE* chromosomal mutants were created by allelic exchange. To create TR50 $nlpE_{\Delta CTD}$, 1 kb up and downstream of *nlpE* was amplified by PCR, and Gibson assembly (New England Biolabs) was used to recombine these fragments into pRE112 digested with XbaI and PaeI. Gibson reaction products were transformed into OneShot PIR1 competent cells (Thermo Fisher). Allelic exchange vectors were sequenced prior to conjugation (Molecular Biology Facility, University of Alberta). Suicide vectors were then transformed into the donor strain MFDλpir and mated with the recipient TR50 strains on LB plates with 0.3 mM diaminopimelic acid (DAP). Transconjugants were selected by plating on LB with chloramphenicol and incubating overnight. To select for double crossovers, a chloramphenicol-resistant colony was grown in LB with no antibiotics for 6 hours and plated onto LB without NaCl with 5% sucrose and incubated at room temperature for two nights. Sucrose-resistant colonies were screened by PCR to identify colonies with the correct mutation.

Expression vector construction and site-directed mutagenesis

The plasmids used in this study are listed in Table 2-2. Overexpression plasmids were created by restriction digest cloning utilizing standard procedures and the primers listed in Table 2-3. Site-directed mutagenesis was used to introduce deletions and substitutions into expression vectors using the Q5 site-directed mutagenesis kit (New England Biolabs) and according to manufacturer's instructions. The primers used for site-directed mutagenesis are listed in Table 2-3. For consistency, the numbering of amino acids in envelope proteins throughout this study includes the amino acids of the signal peptide. The sequence of inserts/mutants were confirmed by sequencing (Molecular Biology Facility, University of Alberta).

β-galactosidase assays

cpxP-lacZ activity was measured by quantifying β-galactosidase activity as previously describe (Buelow and Raivio, 2005; Slauch and Silhavy, 1991). Briefly, *E. coli* TR50 (MC4100 *cpxP-lacZ*) were grown overnight in LB and then subcultured in 2 ml LB. Cultures were spun down and cell pellets were resuspended in Z-buffer (Miller, 1972). The optical density (OD at A_{600}) was measured and then each culture was treated with chloroform and sodium dodecyl sulfate (SDS) and vortexed to release β-galactosidase. β-galactosidase activity was quantified by measuring the A_{420} of each culture 25 times at 30s intervals after the addition of 10 mg/ml ortho-nitrophenyl β-galactoside (ONPG). *cpxP-lacZ* activity was calculated as the maximum slope of the linear region of A_{420} measurements standardized to that culture's OD. The statistical significance was calculated using unpaired *t*-tests (Prism, Graphpad).

In vivo DSS crosslinking

In vivo crosslinking with the membrane permeable crosslinker disuccinimidyl suberate (DSS; Thermo Scientific) was conducted as previously described with minor modifications (Lu et

al., 2012). The optical density (A_{600}) of cultures was used to collect a standardized amount of cells corresponding to an OD 2.0 in 200 µl. Cells were washed four times with phosphate buffered saline (PBS) and then subjected to crosslinking with 0.5 or 1 mM DSS for 30 minutes at room temperature. 5 µl of 1 M Tris-HCl was added to quench any excess crosslinking reagent for 5-10 minutes. Cells were then washed one more time with PBS. Cell lysates were prepared by resuspending pellets in MilliQ H_2O and 2×Laemmli sample buffer (Sigma) and heating at 95°C for 5 minutes. SDS-PAGE and Western blotting was used to visualize crosslinked complex formation.

Co-immunoprecipitation assays

Large volume cultures were growth to OD 1.0 at 37°C with shaking at 225 RPM. Cells were harvested and washed once with PBS. The optical density was standardized across all cultures at this stage (~OD 12 in 20 ml of PBS). Cells were gently lysed using the BugBuster Master Mix reagent (EMD Millipore) with 1 tablet per sample of cOmplete Protease Inhibitor Cocktail (Roche) for approximately 2 hours. Debris and unlysed cells were pelleted by centrifugation at 15,000×g for 20 minutes. Lysates were then centrifuged at 43,000 RPM at 4°C for 45 minutes to pellet membranes. Membrane pellets were solubilized in membrane solubilization buffer (25 mM Tris-HCl pH 7.4, 150 mM NaCl, 0.5% Triton X-100) overnight with gentle rotation. Co-immunoprecipitations were conducted with the Pierce Crosslink IP Kit essentially according to manufacturer's instructions. BCA assays (Pierce) were used to calculate sample protein concentrations; 1 µg of membrane preparations was used in assays. Co-immunoprecipitations were conducted overnight at 4°C with gentle rotation. Eluates from co-immunoprecipitations were analyzed by SDS-PAGE and Western blotting.

SDS-polyacrylamide gel electrophoresis and Western blotting

SDS-PAGE and Western blotting was conducted according to standard protocols. Where indicated, protein concentrations of solutions were determined by BCA protein assay (Pierce) following manufacturer's instructions. Briefly, samples were separated on 8-12% SDS-PAGE gels and transferred to nitrocellulose membranes using semi-dry transfer (BioRad Trans-Blot Semi-Dry Transfer Cell). Membranes were blocked in 5% non-fat milk in Tris-buffered saline with 0.1% Tween-20 (TBST) and probed with primary antibody overnight at 4°C in 2% BSA in TBST at the following concentrations: anti-NlpE (rabbit polyclonal, this study, 1:8,000-40,000), anti-His×6 (mouse monoclonal, Invitrogen, 1:10,000-20,000), anti-OmpA (rabbit polyclonal, Antibody Research Corporation, 1:5,000-10,000), anti-CpxA-MBP (rabbit polyclonal, (Raivio and Silhavy, 1997), 1:10,000) and anti-RNAP alpha subunit (mouse monoclonal, BioLegend, 1:5,000). Chemiluminescent alkaline phosphatase (AP)-conjugated (BioRad) or fluorescent IRDye 800CW (goat anti-rabbit) and 680RD (goat anti-mouse) antibodies were used to detect proteins. Chemiluminescent signal was generated using the Immun-Star AP chemiluminescence kit according to manufacturer's instructions (BioRad). All blots were imaged using a BioRad ChemiDoc imaging system. Where applicable, relative levels of protein bands were quantified using ImageJ.

Whole cell dot blotting

Dot blot assays were conducted as previously reported (Konovalova et al., 2014). Briefly, cell cultures grown to mid-log phase were concentrated to an OD of 1.0 in phosphate buffered saline (PBS). Each standardized sample was split in half; one half was lysed using a sonicator (cell lysate control) and spotted onto nitrocellulose membranes and the other half was spotted directly onto nitrocellulose membranes. After spots were allowed to air dry, membranes were blocked and probed as described above. Alkaline phosphatase conjucated secondary antibodies

were used and images were developed using the Immun-Star AP chemiluminescence kit according to manufacturer's instructions (BioRad) and imaged using a BioRad ChemiDoc imaging system.

Growth curves

Growth curves were conducted with cultures grown in 96-well plates. Briefly, 2 ml subcultures of all strains were grown for 1 hour at 37°C with shaking at 225 RPM. At 1 hour, 0.1 mM IPTG was added to each culture and 200 µl was aliquoted into 96-well plates. This plate was then grown in a Cytation5 plate reader (BioTek) at 37°C with continuous shaking. OD600 was read every 30 minutes for 24 hours and curves were plotted in Prism (Graphpad).

Acknowledgements

We would like to thank Dr. Ratmir Derda for the use of the Cytation 5 plate reader for growth curves; Vincent Man for providing strain VM36 (TR50 Δ*nlpE*) used in this study; the reviewers of this manuscript for their construct comments and feedback; and the members of the Tracy Raivio and Jon Dennis labs for many fruitful discussions during the formation of this manuscript.

Tables

Table 4-1. Strains used in this study.

Strain	Description	Source
MC4100	F_ *araD139* (*argF-lac*)*U169 rpsL150* (Strr) *relA1 flbB5301 decC1 ptsF25 rbsR*	(Casadaban, 1976)
TR50	MC4100 λRS88[*cpxP'-lacZ*$^{+}$]	(Raivio and Silhavy, 1997)
VM36	TR50 Δ*nlpE*	Vincent Man
TC451	TR50 Δ*nlpE ompA::kan*	This study
TC70	TR50 + pCA-*nlpE*	This study
TC209	TR50 + pTrc-$nlpE_{WT}$	This study
TC210	TR50 + pTrc-$nlpE_{NTD+L}$	This study
TC211	TR50 + pTrc-$nlpE_{1-137}$	This study
TC212	TR50 + pTrc-$nlpE_{NTD}$	This study
TC213	TR50 + pTrc-$nlpE_{1-101}$	This study
TC214	TR50 + pTrc99A	This study
TC322	TR50 + pTrc-$nlpE_{CTD+L}$	This study
TC322	TR50 + pTrc-$nlpE_{CTD}$	This study
TC453	TR50 + pBAD18	This study
TC454	TR50 + pBAD18-$nlpE_{WT}$	This study
TC455	TR50 + pBAD18-$nlpE_{NTD+L}$	This study
TC468	TR50 + pBAD18-$nlpE_{DD}$	This study
TC469	TR50 + pBAD18-$nlpE_{NTDL+DD}$	This study
TC272	TR50 + pCA24N	This study
TC273	TR50 + pCA-*ompA*	This study
TC274	TR50 + pCA-*ompF*	This study
TC275	TR50 + pCA-*ompC*	This study
TC276	TR50 + pCA-*lamB*	This study
TC277	VM36 (TR50 Δ*nlpE*) + pCA24N	This study
TC278	VM36 + pCA-*ompA*	This study
TC279	VM36 + pCA-*ompF*	This study
TC280	VM36 + pCA-*ompC*	This study
TC281	VM36 + pCA-*lamB*	This study
TC375	TR50 + pCA-*ompX*	This study
TC376	TR50 + pCA-*ompW*	This study
TC377	TR50 + pCA-*ompT*	This study
TC378	VM36 + pCA-*ompX*	This study
TC379	VM36 + pCA-*ompW*	This study
TC380	VM36 + pCA-*ompT*	This study
TC408	TR50 + pCA-$ompA_{\Delta CTD}$	This study
TC414	TR50 + pCA-$ompA_{P198STOP}$	This study
TC415	TR50 + pCA-$ompA_{K213A}$	This study
TC416	VM36 + pCA-$ompA_{P198STOP}$	This study

TC417	VM36 + pCA-*ompA*$_{K213A}$	This study
TC462	TR50 + pCA-*ompA*$_{PG1}$	This study
TC463	TR50 + pCA-*ompA*$_{PG2}$	This study
TC464	TR50 + pCA-*ompA*$_{PG^-}$	This study
TC465	VM36 + pCA-*ompA*$_{PG1}$	This study
TC466	VM36 + pCA-*ompA*$_{PG2}$	This study
TC467	VM36 + pCA-*ompA*$_{PG^-}$	This study
TC352	TR50 Δ*ompA*	This study
TC427	TC352 + pCA24N	This study
TC428	TC352 + pCA-*ompA*	This study
TC429	TC352 + pCA-*ompA*$_{\Delta CTD}$	This study
TC430	TC352 + pCA-*ompA*$_{P198STOP}$	This study
TC431	TC352 + pCA-*ompA*$_{K213A}$	This study
TC478	TC352 + pCA-*ompA*$_{PG1}$	This study
TC479	TC352 + pCA-*ompA*$_{PG2}$	This study
TC480	TC352 + pCA-*ompA*$_{PG^-}$	This study
TC494	TC492 + pBAD18-*nlpE*$_{WT}$	This study
TC495	TC492 + pBAD18-*nlpE*$_{NTD+L}$	This study
TC472	OneShot PIR1 + pRE112-*nlpE*$_{NTD+L}$	This study
TC493	MFDpir + pRE112-*nlpE*$_{NTD+L}$	This study
TC496	TR50 *nlpE*$_{\Delta CTD}$	This study
TC498	TC496 + pCA24N	This study
TC499	TC496 + pCA-*ompA*	This study
TC564	TC561 + pCA24N	This study
TC565	TC561 + pCA-*ompA*	This study
TC561	TR50 *nlpE*$_{lock\ (E118C+T134C)}$	This study
TC556	TR50 *nlpE*$_{G\times5(i)}$	This study
TC492	TR50 *lpp::kan*	This study
TC494	TC492 + pBAD18-*nlpE*$_{WT}$	This study
TC495	TC492 + pBAD18-*nlpE*$_{NTD+L}$	This study
VM34	TR50 Δ*tonB*	Vincent Man
TC531	VM34 pCA24N	This study
TC532	VM34 pCA-*ompA*	This study

Table 4-2. Plasmids used in this study.

Plasmid	Description	Source
pCA24N	Empty ASKA library vector	(Kitagawa et al., 2006)
pCA-*nlpE*	NlpE expression, IPTG-inducible, ASKA library (GFP-)	(Kitagawa et al., 2006)
pCA-*ompA*	OmpA expression, IPTG-inducible, ASKA library (GFP-)	(Kitagawa et al., 2006)
pCA-*ompF*	OmpF expression, IPTG-inducible, ASKA library (GFP-)	(Kitagawa et al., 2006)
pCA-*ompC*	OmpC expression, IPTG-inducible, ASKA library (GFP-)	(Kitagawa et al., 2006)
pCA-*lamB*	LamB expression, IPTG-inducible, ASKA library (GFP-)	(Kitagawa et al., 2006)
pCA-*ompX*	OmpX expression, IPTG-inducible, ASKA library (GFP-)	((Kitagawa et al., 2006)
pCA-*ompW*	OmpW expression, IPTG-inducible, ASKA library (GFP-)	((Kitagawa et al., 2006)
pCA-*ompT*	OmpT expression, IPTG-inducible, ASKA library (GFP-)	(Kitagawa et al., 2006)
pCA-*ompA*$_{\Delta CTD}$	Expresses OmpA$_{\Delta 194\text{-}340}$; based on pCA-*ompA*	This study
pCA-*ompA*$_{P198STOP}$	Expresses OmpA$_{1\text{-}197}$; based on pCA-*ompA*	This study
pCA-*ompA*$_{K213A}$	Expresses OmpA$_{K213A}$; based on pCA-*ompA*	This study
pCA-*ompA*$_{PG1}$	Expresses OmpA$_{D262A}$; based on pCA-*ompA*	This study
pCA-*ompA*$_{PG2}$	Expresses OmpA$_{R277A}$; based on pCA-*ompA*	This study
pCA-*ompA*$_{PG^-}$	Expresses OmpA$_{D262A+R277A}$; based on pCA-*ompA*	This study
pTrc99A	Empty expression vector, IPTG-inducible expression from *trc* promoter	(Amann et al., 1988)
pTrc-*nlpE*$_{WT}$	NlpE$_{WT}$ expression vector; C-terminal 6×His tag	This study
pTrc-*nlpE*$_{NTD+L}$	NlpE$_{NTD+L}$ expression vector; C-terminal 6×His tag	This study
pTrc-*nlpE*$_{1\text{-}137}$	NlpE$_{1\text{-}137}$ expression vector; C-terminal 6×His tag	This study
pTrc-*nlpE*$_{NTD}$	NlpE$_{NTD}$ expression vector; C-terminal 6×His tag	This study
pTrc-*nlpE*$_{1\text{-}101}$	NlpE$_{1\text{-}101}$ expression vector; C-terminal 6×His tag	This study
pTrc-*nlpE*$_{L+CTD}$	NlpE$_{CTD+L}$ expression vector; C-terminal 6×His tag	This study
pTrc-*nlpE*$_{CTD}$	NlpE$_{CTD}$ expression vector; C-terminal 6×His tag	This study
pBAD18	Empty expression vector, arabinose-inducible	(Guzman et al., 1995)
pBAD18-*nlpE*$_{WT}$	NlpE$_{WT}$ expression vector; C-terminal 6×His tag	This study
pBAD18-*nlpE*$_{NTD+L}$	NlpE$_{NTD+L}$ expression vector; C-terminal 6×His tag	This study
pBAD18-*nlpE*$_{DD}$	Full length NlpE with +2/3 DD Lol avoidance sequence expression vector; C-terminal 6×His tag	This study
pBAD18-*nlpE*$_{NTDL+DD}$	NlpE$_{NTD+L}$ with +2/3 DD Lol avoidance sequence expression vector; C-terminal 6×His tag	This study
pJW1	Vector encoding *cpxP-lux* transcriptional reporter	(Price and Raivio, 2009)

Table 4-3. Primers used in this study.

Primer Name	Sequence	Notes
nlpE_NcoI_F	CGCA CCATGG TG AAA AAA GCG ATA GTG ACA G	Forward primer for cloning *nlpE* into pTrc99A
nlpE_EcoRI_F	GCA GAATTC ATG GTG AAA AAA GCG ATA GTG	Forward primer for cloning *nlpE* into pBAD18
nlpE_WT_His_HindIII_R	TGCC AAGCTT TTA GTG GTG GTG GTG GTG GTG CT CGA GCT GCC CCA AAC TAC TGC AAT C	Reverse primer for cloning full length *nlpE* with C-term His tag into pTrc99A and pBAD18
nlpE_NTDL_His_HindIII_R	TGCC AAGCTT TTA GTG GTG GTG GTG GTG GTG CT CGA GCG GCG TCA TAG GTA AAC TGG A	Same as above but for *nlpE* Δ146-236 (NTD+L)
nlpE_NTD_His_HindIII_R	TGCC AAGCTT TTA GTG GTG GTG GTG GTG GTG CT CGA GCA TCT CCA GCG CAT CGC CTT T	Same as above but for *nlpE* Δ138-236 (NTD)
nlpE120_His_HindIII_R	TGCC AAGCTT TTA GTG GTG GTG GTG GTG GTG CT CGA GCG CTT CCA GCG TAT AGT TGA A	Same as above but for *nlpE* Δ120-236 (1-120)
nlpE101_His_HindIII_R	TGCC AAGCTT TTA GTG GTG GTG GTG GTG GTG CT CGA GGG TTA ATA CCA GCT TGT CAG C	Same as above but for *nlpE* Δ102-236 (1-101)
Q5SDM_CTD_F	ATG ACC CTG CGG GGC ATG	For generating pTrc-*nlpE*$_{CTD}$
Q5SDM_CTD_R	CCG ATT ATT ACA TCC CAT CAG AGT AAA GAG	For generating pTrc-*nlpE*$_{CTD}$
Q5SDM_CTDL_F	CTC GAT CGT GAA GGC AAT C	For generating pTrc-*nlpE*$_{L+CTD}$
Q5SDM_CTDL_R	CCG ATT ATT ACA TCC CAT CAG	For generating pTrc-*nlpE*$_{L+CTD}$
Q5SDM_K213A_F	AGT ACA GAC CGC GCA CTT CAC TCT GAA GTC TGA CGT TCT G	For generating pCA-*ompA*$_{K213A}$
Q5SDM_K13A_R	TCC GGT GCC GGA GCT GGA	For generating pCA-*ompA*$_{K213A}$
Q5SDM_delCTD_F	GTA ACT CAG CCG CAG GCT	For generating pCA-*ompA*$_{\Delta CTD}$
Q5SDM_delCTD_R	CTG ACC GAA ACG GTA GGA AAC	For generating pCA-*ompA*$_{\Delta CTD}$
Q5SDM_OmpAPG1_F	GGG TTA CAC CGC CCG CAT CGG TT	For generating pCA-*ompA*$_{PG1}$
Q5SDM_OmpAPG1_R	AGA ACA ACT ACG GAA CCG TCT TTC	For generating pCA-*ompA*$_{PG1}$
Q5SDM_OmpAPG2_F	GTC CGA GCG CGC CGC TCA GTC TG	For generating pCA-*ompA*$_{PG2}$
Q5SDM_OmpAPG2_R	AGA CCC TGG TTG TAA GCG	For generating pCA-*ompA*$_{PG2}$
Q5SDM_NlpEDD_F	GAT GGG ATG TGA TGA TCG GGC CGA AG	For generating pBAD18-*nlpE*$_{DD}$, *nlpE*$_{NTDL+DD}$
Q5SDM_NlpEDD_R	AGA GTA AAG AGG CTG ATT ACA G	For generating pBAD18-*nlpE*$_{DD}$, *nlpE*$_{NTDL+DD}$
GIB_NTDL_UP_F	GAG CTC GAT ATC GCA TGC GGC GAA AGT AAG CGC CTT TG	For generation of suicide vector to delete NlpE$_{CTD}$ (upstream fragment)
GIB_NTDL_UP_R	ACG GGT TAC GGC GTC ATA GGT AAA CTG GA	See above
GIB_NTDL_DWN_F	GAC GCC GTA ACC CGT CTT GAG ACA GAA ACA AAC G	For generation of suicide vector to delete NlpE$_{CTD}$ (downstream fragment)
GIB_NTDL_DWN_R	CGA TCC CAA GCT TCT TCT AGA CTG TTT CTC CCC AGC TTT CTT TTA CT	See above
pTrc99A_F	GTT CTG GCA AAT ATT CTG AAA	For checking inserts in pTrc99A
pTrc99A_R	ATT TAA TCT GTA TCA GGC TGA	For checking inserts in pTrc99A
ompA_F	TCT CTT CTG TAA ATT GTC GCT	For checking *ompA* chromosomal locus
ompA_R	GCA AAA AAT CGA TCG ATC TGG	For checking *ompA* chromosomal locus

Overall Conclusions

The envelope is an essential and complicated structure that is carefully constructed, monitored, and protected. As the global antimicrobial resistance crisis deepens (Murray et al., 2022), efforts to understand how bacteria combat stress to this layer are critical. Envelope stress responses such as the CpxRA system play an essential role in the cell's overall strategy to preserve the integrity of the envelope. This protection, however, extends beyond model organisms such as laboratory strains of *E. coli*. The Cpx response has long been noted for its role in the pathogenesis and colonization of several key Gram-negative bacteria (Flores-Kim and Darwin, 2014; Hews et al., 2019; Raivio, 2005). Deleting the CpxRA system in organisms such as *Citrobacter rodentium* and mouse commensals strains of *E. coli* is sufficient to completely prevent colonization *in vivo* (Lasaro et al., 2014; Thomassin et al., 2017, 2015).

In Chapter 2 of this thesis, we (with our long-time collaborators in Dr. Mark Glover's lab) investigate the periplasmic domain of CpxA and how it regulates signaling in this system. This domain, while adopting a rather common sensory PAS fold, is unique in that it arranges them in a dimer not seen in other sensor kinases. The study initially characterizing several hyper-active *cpxA** mutations in the periplasmic domain of CpxA was published over 20 years ago (Raivio and Silhavy, 1997). Our model of CpxA provides a compelling molecular basis for these historical alleles, answering decades old questions about why so many mutations in this region of CpxA hyper activate it and render it blind to inducing signals. Furthermore, this model contributes to our understanding that sensor kinases utilize diverse sensor domains (Bhate et al., 2015; Cheung and Hendrickson, 2010; Gao and Stock, 2009). While sensor kinases possess use many different folds as sensor domains, our study reports that CpxA uses a common fold in a unique and creative way. Given the breadth of signals that sensor kinases recognize, it is

unsurprising that even common domains, such as PAS domains, can be evolved to be used in "unorthodox" ways, perhaps allowing sensor kinases to sense an even more set of stimuli.

From a more practical angle, the results of this study may facilitate efforts to target CpxA via novel therapeutics. Recent studies have isolated compounds that lead to aberrant CpxA activation and attenuate the virulence of uropathogenic *E. coli* in a mouse model (Dbeibo et al., 2018; Fortney et al., 2022; Li et al., 2019; van Rensburg et al., 2015). Several other studies note that aberrant activation of the CpxA response strongly represses the virulence of organisms such as *Haemophilus ducreyi* and *Salmonella* Typhimurium (Humphreys et al., 2004; Spinola et al., 2010); thus, hyper-activation of CpxA may be a viable strategy for anti-virulence drugs (T. H. S. Cho et al., 2023a). Because our structure focuses on the activation of CpxA, this structure and our model of CpxA activation will be a useful tool for targeted studies of CpxA as a drug target going forward.

In Chapters 3 and 4, we explore the outer membrane lipoprotein NlpE in detail, especially focusing on how it signals in the Cpx response. The emerging picture over about 20 years of study is that NlpE is a versatile lipoprotein sensor that plays roles in sensing lipoprotein biogenesis defects, surface sensing, metals, and periplasmic redox state (Delhaye et al., 2019; Grabowicz and Silhavy, 2017a; Gupta et al., 1995; May et al., 2019; Otto and Silhavy, 2002; Shimizu et al., 2016; Snyder et al., 1995). We expand on the molecular mechanisms of NlpE signaling at the inner membrane via interacting with CpxA and suggest that cells may regulate NlpE signaling by controlling its stability. Furthermore, we report a novel role for it's C-terminal domain in activating CpxA from the outer membrane and report the molecular details of how NlpE interacts with the major OMP OmpA. In particular, OmpA's ability to bind the cell wall is critical for signaling from the outer membrane, suggesting that NlpE signaling in the envelope is coordinated with OMP (via OmpA) and cell wall biogenesis/structure.

Like with CpxA, understanding the mechanisms of NlpE signaling has several practical applications. Biofilms are a key contributor to antimicrobial resistance (Singh et al., 2017). The NlpE homolog of *Acinetobacter baumanii* is highly induced in a multi-drug resistant strain that is a strong producer of biofilms (Siroy et al., 2006). Thus, study of NlpE and OmpA signaling in the Cpx response is highly relevant for understanding how bacteria sense surfaces and form biofilms. NlpE's inner membrane signaling role is also significant in light of emerging and established antimicrobials that target lipoprotein biogenesis (Nickerson et al., 2018; Olatunji et al., 2020). Work implicating NlpE in sensing and resisting stress caused by metals such as copper (Gupta et al., 1995; May et al., 2019) is especially relevant given the importance of copper in human innate immune strategies against bacterial pathogens (Besold et al., 2016; Chaturvedi and Henderson, 2014; Dupont et al., 2011; Festa and Thiele, 2012).

Understanding the mechanisms of sensing and transducing signals in the Cpx response is essential to our overall understanding of this system; to effectively counter damage to the envelope, the CpxRA system must first detect relevant signals and transduce them before activating a global transcriptional response. This thesis significantly contributes to our understanding of how the sensor kinase CpxA becomes activated and how the outer membrane lipoprotein NlpE functions as an activator of CpxA in several contexts. Continued studies of these proteins will expand our understanding of how bacteria sense signals in their envelopes and how we can leverage this knowledge to face future challenges surrounding antimicrobial resistance and bacterial disease.

References

Abellón-Ruiz, J., Kaptan, S.S., Baslé, A., Claudi, B., Bumann, D., Kleinekathöfer, U., van den Berg, B., 2017. Structural basis for maintenance of bacterial outer membrane lipid asymmetry. Nat Microbiol 2, 1616–1623. https://doi.org/10.1038/s41564-017-0046-x

Abramson, J., Adler, J., Dunger, J., Evans, R., Green, T., Pritzel, A., Ronneberger, O., Willmore, L., Ballard, A.J., Bambrick, J., Bodenstein, S.W., Evans, D.A., Hung, C.-C., O'Neill, M., Reiman, D., Tunyasuvunakool, K., Wu, Z., Žemgulytė, A., Arvaniti, E., Beattie, C., Bertolli, O., Bridgland, A., Cherepanov, A., Congreve, M., Cowen-Rivers, A.I., Cowie, A., Figurnov, M., Fuchs, F.B., Gladman, H., Jain, R., Khan, Y.A., Low, C.M.R., Perlin, K., Potapenko, A., Savy, P., Singh, S., Stecula, A., Thillaisundaram, A., Tong, C., Yakneen, S., Zhong, E.D., Zielinski, M., Žídek, A., Bapst, V., Kohli, P., Jaderberg, M., Hassabis, D., Jumper, J.M., 2024. Accurate structure prediction of biomolecular interactions with AlphaFold 3. Nature 630, 493–500. https://doi.org/10.1038/s41586-024-07487-w

Acosta, N., Pukatzki, S., Raivio, T.L., 2015. The Vibrio cholerae Cpx Envelope Stress Response Senses and Mediates Adaptation to Low Iron. J. Bacteriol. 197, 262–276. https://doi.org/10.1128/JB.01957-14

Ades, S.E., 2008. Regulation by destruction: design of the σE envelope stress response. Current Opinion in Microbiology, Growth and Development: Eukaryotes/Prokaryotes 11, 535–540. https://doi.org/10.1016/j.mib.2008.10.004

Ades, S.E., Connolly, L.E., Alba, B.M., Gross, C.A., 1999. The Escherichia coli sigma(E)-dependent extracytoplasmic stress response is controlled by the regulated proteolysis of an anti-sigma factor. Genes Dev 13, 2449–2461. https://doi.org/10.1101/gad.13.18.2449

Affandi, T., Issaian, A.V., McEvoy, M.M., 2016. The Structure of the Periplasmic Sensor Domain of the Histidine Kinase CusS Shows Unusual Metal Ion Coordination at the Dimeric Interface. Biochemistry 55, 5296–5306. https://doi.org/10.1021/acs.biochem.6b00707

Afonine, P.V., Grosse-Kunstleve, R.W., Echols, N., Headd, J.J., Moriarty, N.W., Mustyakimov, M., Terwilliger, T.C., Urzhumtsev, A., Zwart, P.H., Adams, P.D., 2012. Towards automated crystallographic structure refinement with ıt phenix.refine. Acta Crystallographica Section D 68, 352–367. https://doi.org/10.1107/S0907444912001308

Alba, B.M., Gross, C.A., 2004. Regulation of the Escherichia coli sigma-dependent envelope stress response. Mol Microbiol 52, 613–619. https://doi.org/10.1111/j.1365-2958.2003.03982.x

Alberts, B., Johnson, A., Lewis, J., Raff, M., Roberts, K., Walter, P., 2002. The Lipid Bilayer, in: Molecular Biology of the Cell. 4th Edition. Garland Science.

Albin, R., Silverman, P.M., 1984a. Identification of the Escherichia coli K-12 cpxA locus as a single gene: construction and analysis of biologically-active cpxA gene fusions. Mol Gen Genet 197, 272–279. https://doi.org/10.1007/BF00330973

Albin, R., Silverman, P.M., 1984b. Physical and genetic structure of the glpK-cpxA interval of the Escherichia coli K-12 chromosome. Mol Gen Genet 197, 261–271. https://doi.org/10.1007/BF00330972

Albin, R., Weber, R., Silverman, P.M., 1986. The Cpx proteins of Escherichia coli K12. Immunologic detection of the chromosomal cpxA gene product. Journal of Biological Chemistry 261, 4698–4705. https://doi.org/10.1016/S0021-9258(17)38558-7

Albrecht, R., Schütz, M., Oberhettinger, P., Faulstich, M., Bermejo, I., Rudel, T., Diederichs, K., Zeth, K., 2014. Structure of BamA, an essential factor in outer membrane protein biogenesis. Acta Crystallogr D Biol Crystallogr 70, 1779–1789. https://doi.org/10.1107/S1399004714007482

Alvira, S., Watkins, D.W., Troman, L.A., Allen, W.J., Lorriman, J.S., Degliesposti, G., Cohen, E.J., Beeby, M., Daum, B., Gold, V.A., Skehel, J.M., Collinson, I., 2020. Inter-membrane

association of the Sec and BAM translocons for bacterial outer-membrane biogenesis. eLife 9, e60669. https://doi.org/10.7554/eLife.60669
Amann, E., Ochs, B., Abel, K.-J., 1988. Tightly regulated tac promoter vectors useful for the expression of unfused and fused proteins in Escherichia coli. Gene 69, 301–315. https://doi.org/10.1016/0378-1119(88)90440-4
Andrieu, C., Loiseau, L., Vergnes, A., Gagnot, S., Barré, R., Aussel, L., Collet, J.-F., Ezraty, B., 2023. Salmonella Typhimurium uses the Cpx stress response to detect N-chlorotaurine and promote the repair of oxidized proteins. Proceedings of the National Academy of Sciences 120, e2215997120. https://doi.org/10.1073/pnas.2215997120
Anfinsen, C.B., Scheraga, H.A., 1975. Experimental and Theoretical Aspects of Protein Folding, in: Anfinsen, C.B., Edsall, J.T., Richards, F.M. (Eds.), Advances in Protein Chemistry. Academic Press, pp. 205–300. https://doi.org/10.1016/S0065-3233(08)60413-1
Appia-Ayme, C., Hall, A., Patrick, E., Rajadurai, S., Clarke, T.A., Rowley, G., 2012. ZraP is a periplasmic molecular chaperone and a repressor of the zinc-responsive two-component regulator ZraSR. Biochemical Journal 442, 85–93. https://doi.org/10.1042/BJ20111639
Appleby, J.L., Parkinson, J.S., Bourret, R.B., 1996. Signal Transduction via the Multi-Step Phosphorelay: Not Necessarily a Road Less Traveled. Cell 86, 845–848. https://doi.org/10.1016/S0092-8674(00)80158-0
Arora, A., Rinehart, D., Szabo, G., Tamm, L.K., 2000. Refolded Outer Membrane Protein A of *Escherichia coli*Forms Ion Channels with Two Conductance States in Planar Lipid Bilayers*. Journal of Biological Chemistry 275, 1594–1600. https://doi.org/10.1074/jbc.275.3.1594
Asmar, A.T., Ferreira, J.L., Cohen, E.J., Cho, S.-H., Beeby, M., Hughes, K.T., Collet, J.-F., 2017. Communication across the bacterial cell envelope depends on the size of the periplasm. PLoS Biol 15, e2004303. https://doi.org/10.1371/journal.pbio.2004303
Auclair, S.M., Bhanu, M.K., Kendall, D.A., 2012. Signal peptidase I: Cleaving the way to mature proteins. Protein Sci 21, 13–25. https://doi.org/10.1002/pro.757
Audrain, B., Ferrières, L., Zairi, A., Soubigou, G., Dobson, C., Coppée, J.-Y., Beloin, C., Ghigo, J.-M., 2013. Induction of the Cpx Envelope Stress Pathway Contributes to Escherichia coli Tolerance to Antimicrobial Peptides. Appl Environ Microbiol 79, 7770–7779. https://doi.org/10.1128/AEM.02593-13
Baba, T., Ara, T., Hasegawa, M., Takai, Y., Okumura, Y., Baba, M., Datsenko, K.A., Tomita, M., Wanner, B.L., Mori, H., 2006. Construction of *Escherichia coli* K-12 in-frame, single-gene knockout mutants: the Keio collection. Mol Syst Biol 2. https://doi.org/10.1038/msb4100050
Bahadur, R., Chodisetti, P.K., Reddy, M., 2021. Cleavage of Braun's lipoprotein Lpp from the bacterial peptidoglycan by a paralog of l,d-transpeptidases, LdtF. Proc Natl Acad Sci U S A 118, e2101989118. https://doi.org/10.1073/pnas.2101989118
Baikalov, I., Schröder, I., Kaczor-Grzeskowiak, M., Grzeskowiak, K., Gunsalus, R.P., Dickerson, R.E., 1996. Structure of the Escherichia coli Response Regulator NarL,. Biochemistry 35, 11053–11061. https://doi.org/10.1021/bi960919o
Balbás, P., Soberón, X., Merino, E., Zurita, M., Lomeli, H., Valle, F., Flores, N., Bolivar, F., 1986. Plasmid vector pBR322 and its special-purpose derivatives — a review. Gene 50, 3–40. https://doi.org/10.1016/0378-1119(86)90307-0
Banzhaf, M., Yau, H.C., Verheul, J., Lodge, A., Kritikos, G., Mateus, A., Cordier, B., Hov, A.K., Stein, F., Wartel, M., Pazos, M., Solovyova, A.S., Breukink, E., van Teeffelen, S., Savitski, M.M., den Blaauwen, T., Typas, A., Vollmer, W., 2020. Outer membrane lipoprotein NlpI scaffolds peptidoglycan hydrolases within multi-enzyme complexes in Escherichia coli. EMBO J 39, e102246. https://doi.org/10.15252/embj.2019102246
Belas, R., 2014. Biofilms, flagella, and mechanosensing of surfaces by bacteria. Trends in Microbiology 22, 517–527. https://doi.org/10.1016/j.tim.2014.05.002

Benn, G., Mikheyeva, I.V., Inns, P.G., Forster, J.C., Ojkic, N., Bortolini, C., Ryadnov, M.G., Kleanthous, C., Silhavy, T.J., Hoogenboom, B.W., 2021. Phase separation in the outer membrane of Escherichia coli. Proceedings of the National Academy of Sciences 118, e2112237118. https://doi.org/10.1073/pnas.2112237118

Bernal-Cabas, M., Ayala, J.A., Raivio, T.L., 2015. The Cpx Envelope Stress Response Modifies Peptidoglycan Cross-Linking via the l,d-Transpeptidase LdtD and the Novel Protein YgaU. J. Bacteriol. 197, 603–614. https://doi.org/10.1128/JB.02449-14

Berne, C., Ellison, C.K., Ducret, A., Brun, Y.V., 2018. Bacterial adhesion at the single-cell level. Nat Rev Microbiol 16, 616–627. https://doi.org/10.1038/s41579-018-0057-5

Bertani, B., Ruiz, N., 2018. Function and biogenesis of lipopolysaccharides. EcoSal Plus 8, 10.1128/ecosalplus.ESP-0001–2018. https://doi.org/10.1128/ecosalplus.ESP-0001-2018

Besold, A.N., Culbertson, E.M., Culotta, V.C., 2016. The Yin and Yang of copper during infection. J Biol Inorg Chem 21, 137–144. https://doi.org/10.1007/s00775-016-1335-1

Bhate, M.P., Molnar, K.S., Goulian, M., DeGrado, W.F., 2015. Signal Transduction in Histidine Kinases: Insights from New Structures. Structure 23, 981–994. https://doi.org/10.1016/j.str.2015.04.002

Bi, S., Lai, L., 2015. Bacterial chemoreceptors and chemoeffectors. Cell. Mol. Life Sci. 72, 691–708. https://doi.org/10.1007/s00018-014-1770-5

Biasini, M., Bienert, S., Waterhouse, A., Arnold, K., Studer, G., Schmidt, T., Kiefer, F., Cassarino, T.G., Bertoni, M., Bordoli, L., Schwede, T., 2014. SWISS-MODEL: modelling protein tertiary and quaternary structure using evolutionary information. Nucleic Acids Research 42, W252–W258. https://doi.org/10.1093/nar/gku340

Bishop, R.E., 2008. Structural biology of membrane-intrinsic β-barrel enzymes: Sentinels of the bacterial outer membrane. Biochimica et Biophysica Acta (BBA) - Biomembranes, Structural proteomics of the cell envelope of Gram-negative bacteria 1778, 1881–1896. https://doi.org/10.1016/j.bbamem.2007.07.021

Bishop, R.E., 2005. The lipid A palmitoyltransferase PagP: molecular mechanisms and role in bacterial pathogenesis. Molecular Microbiology 57, 900–912. https://doi.org/10.1111/j.1365-2958.2005.04711.x

Blount, Z.D., 2015. The unexhausted potential of E. coli. eLife 4, e05826. https://doi.org/10.7554/eLife.05826

Bogdanov, M., Pyrshev, K., Yesylevskyy, S., Ryabichko, S., Boiko, V., Ivanchenko, P., Kiyamova, R., Guan, Z., Ramseyer, C., Dowhan, W., 2020. Phospholipid distribution in the cytoplasmic membrane of Gram-negative bacteria is highly asymmetric, dynamic, and cell shape-dependent. Sci Adv 6, eaaz6333. https://doi.org/10.1126/sciadv.aaz6333

Boudreau, A.C., Milovanovic, M., Conrad, K.L., Nelson, C., Ferrario, C.R., Wolf, M.E., 2012. A protein crosslinking assay for measuring cell surface expression of glutamate receptor subunits in the rodent brain after in vivo treatments. Curr Protoc Neurosci CHAPTER, Unit-5.3019. https://doi.org/10.1002/0471142301.ns0530s59

Bouveret, E., Bénédetti, H., Rigal, A., Loret, E., Lazdunski, C., 1999. In Vitro Characterization of Peptidoglycan-Associated Lipoprotein (PAL)–Peptidoglycan and PAL–TolB Interactions. J Bacteriol 181, 6306–6311.

Braselmann, E., Chaney, J.L., Champion, M.M., Clark, P.L., 2016. DegP Chaperone Suppresses Toxic Inner Membrane Translocation Intermediates. PLoS One 11, e0162922. https://doi.org/10.1371/journal.pone.0162922

Braun, V., Hantke, K., 2019. Lipoproteins: Structure, Function, Biosynthesis. Subcell Biochem 92, 39–77. https://doi.org/10.1007/978-3-030-18768-2_3

Braun, V., Rehn, K., 1969. Chemical characterization, spatial distribution and function of a lipoprotein (murein-lipoprotein) of the E. coli cell wall. The specific effect of trypsin on the membrane structure. Eur J Biochem 10, 426–438. https://doi.org/10.1111/j.1432-1033.1969.tb00707.x

Brewer, S., Tolley, M., Trayer, I.P., Barr, G.C., Dorman, C.J., Hannavy, K., Higgins, C.F., Evans, J.S., Levine, B.A., Wormald, M.R., 1990. Structure and function of X-Pro dipeptide repeats in the TonB proteins of Salmonella typhimurium and Escherichia coli. J Mol Biol 216, 883–895. https://doi.org/10.1016/S0022-2836(99)80008-4

Brooks, B.E., Buchanan, S.K., 2008. Signaling mechanisms for activation of extracytoplasmic function (ECF) sigma factors. Biochimica et Biophysica Acta (BBA) - Biomembranes, Structural proteomics of the cell envelope of Gram-negative bacteria 1778, 1930–1945. https://doi.org/10.1016/j.bbamem.2007.06.005

Brülle, J.K., Grau, T., Tschumi, A., Auchli, Y., Burri, R., Polsfuss, S., Keller, P.M., Hunziker, P., Sander, P., 2010. Cloning, expression and characterization of *Mycobacterium tuberculosis* lipoprotein LprF. Biochemical and Biophysical Research Communications 391, 679–684. https://doi.org/10.1016/j.bbrc.2009.11.120

Brüser, T., Sanders, C., 2003. An alternative model of the twin arginine translocation system. Microbiol Res 158, 7–17. https://doi.org/10.1078/0944-5013-00176

Buchanan, S.K., Smith, B.S., Venkatramani, L., Xia, D., Esser, L., Palnitkar, M., Chakraborty, R., van der Helm, D., Deisenhofer, J., 1999. Crystal structure of the outer membrane active transporter FepA from Escherichia coli. Nat Struct Mol Biol 6, 56–63. https://doi.org/10.1038/4931

Buelow, D.R., Raivio, T.L., 2005. Cpx Signal Transduction Is Influenced by a Conserved N-Terminal Domain in the Novel Inhibitor CpxP and the Periplasmic Protease DegP. J Bacteriol 187, 6622–6630. https://doi.org/10.1128/JB.187.19.6622-6630.2005

Buist, G., Steen, A., Kok, J., Kuipers, O.P., 2008. LysM, a widely distributed protein motif for binding to (peptido)glycans. Mol Microbiol 68, 838–847. https://doi.org/10.1111/j.1365-2958.2008.06211.x

Bunkóczi, G., Read, R.J., 2011. Improvement of molecular-replacement models with ıt Sculptor. Acta Crystallographica Section D 67, 303–312. https://doi.org/10.1107/S0907444910051218

Bury-Moné, S., Nomane, Y., Reymond, N., Barbet, R., Jacquet, E., Imbeaud, S., Jacq, A., Bouloc, P., 2009. Global Analysis of Extracytoplasmic Stress Signaling in Escherichia coli. PLoS Genet 5, e1000651. https://doi.org/10.1371/journal.pgen.1000651

Cabeen, M.T., Jacobs-Wagner, C., 2005. Bacterial cell shape. Nat Rev Microbiol 3, 601–610. https://doi.org/10.1038/nrmicro1205

Callewaert, L., Vanoirbeek, K.G.A., Lurquin, I., Michiels, C.W., Aertsen, A., 2009. The Rcs Two-Component System Regulates Expression of Lysozyme Inhibitors and Is Induced by Exposure to Lysozyme. Journal of Bacteriology 191, 1979–1981. https://doi.org/10.1128/jb.01549-08

Cameron, T.A., Margolin, W., 2024. Insights into the assembly and regulation of the bacterial divisome. Nat Rev Microbiol 22, 33–45. https://doi.org/10.1038/s41579-023-00942-x

Campbell, E.A., Tupy, J.L., Gruber, T.M., Wang, S., Sharp, M.M., Gross, C.A., Darst, S.A., 2003. Crystal structure of Escherichia coli sigmaE with the cytoplasmic domain of its anti-sigma RseA. Mol Cell 11, 1067–1078. https://doi.org/10.1016/s1097-2765(03)00148-5

Casadaban, M.J., 1976. Transposition and fusion of the lac genes to selected promoters in Escherichia coli using bacteriophage lambda and Mu. Journal of Molecular Biology 104, 541–555. https://doi.org/10.1016/0022-2836(76)90119-4

Cascales, E., Bernadac, A., Gavioli, M., Lazzaroni, J.-C., Lloubes, R., 2002. Pal Lipoprotein of Escherichia coli Plays a Major Role in Outer Membrane Integrity. Journal of Bacteriology 184, 754–759. https://doi.org/10.1128/jb.184.3.754-759.2002

Casino, P., Rubio, V., Marina, A., 2010. The mechanism of signal transduction by two-component systems. Current Opinion in Structural Biology 20, 763–771. https://doi.org/10.1016/j.sbi.2010.09.010

Castanié-Cornet, M.-P., Cam, K., Jacq, A., 2006. RcsF Is an Outer Membrane Lipoprotein Involved in the RcsCDB Phosphorelay Signaling Pathway in *Escherichia coli*. J Bacteriol 188, 4264–4270. https://doi.org/10.1128/JB.00004-06
Celia, H., Botos, I., Ni, X., Fox, T., De Val, N., Lloubes, R., Jiang, J., Buchanan, S.K., 2019. Cryo-EM structure of the bacterial Ton motor subcomplex ExbB–ExbD provides information on structure and stoichiometry. Commun Biol 2, 1–6. https://doi.org/10.1038/s42003-019-0604-2
Cezairliyan, B.O., Sauer, R.T., 2007. Inhibition of regulated proteolysis by RseB. Proceedings of the National Academy of Sciences 104, 3771–3776. https://doi.org/10.1073/pnas.0611567104
Chan, J.M., Hackett, K.T., Woodhams, K.L., Schaub, R.E., Dillard, J.P., 2022. The AmiC/NlpD Pathway Dominates Peptidoglycan Breakdown in Neisseria meningitidis and Affects Cell Separation, NOD1 Agonist Production, and Infection. Infect Immun 90, e0048521. https://doi.org/10.1128/IAI.00485-21
Chang, C., Tesar, C., Gu, M., Babnigg, G., Joachimiak, A., Pokkuluri, P.R., Szurmant, H., Schiffer, M., 2010. Extracytoplasmic PAS-Like Domains Are Common in Signal Transduction Proteins. J Bacteriol 192, 1156–1159. https://doi.org/10.1128/JB.01508-09
Chang, Z., 2016. The function of the DegP (HtrA) protein: Protease versus chaperone. IUBMB Life 68, 904–907. https://doi.org/10.1002/iub.1561
Chao, Y., Vogel, J., 2016. A 3′ UTR-Derived Small RNA Provides the Regulatory Noncoding Arm of the Inner Membrane Stress Response. Molecular Cell 61, 352–363. https://doi.org/10.1016/j.molcel.2015.12.023
Chaturvedi, K.S., Henderson, J.P., 2014. Pathogenic adaptations to host-derived antibacterial copper. Front. Cell. Infect. Microbiol. 4. https://doi.org/10.3389/fcimb.2014.00003
Chen, H.D., Groisman, E.A., 2013. The Biology of the PmrA/PmrB Two-Component System: The Major Regulator of Lipopolysaccharide Modifications. Annual Review of Microbiology 67, 83–112. https://doi.org/10.1146/annurev-micro-092412-155751
Cheung, J., Bingman, C.A., Reyngold, M., Hendrickson, W.A., Waldburger, C.D., 2008. Crystal Structure of a Functional Dimer of the PhoQ Sensor Domain. Journal of Biological Chemistry 283, 13762–13770. https://doi.org/10.1074/jbc.M710592200
Cheung, J., Hendrickson, W.A., 2010. Sensor domains of two-component regulatory systems. Current Opinion in Microbiology 13, 116–123. https://doi.org/10.1016/j.mib.2010.01.016
Cheung, J., Hendrickson, W.A., 2009. Structural Analysis of Ligand Stimulation of the Histidine Kinase NarX. Structure 17, 190–201. https://doi.org/10.1016/j.str.2008.12.013
Cheung, J., Hendrickson, W.A., 2008. Crystal Structures of C4-Dicarboxylate Ligand Complexes with Sensor Domains of Histidine Kinases DcuS and DctB. Journal of Biological Chemistry 283, 30256–30265. https://doi.org/10.1074/jbc.M805253200
Chi, X., Fan, Q., Zhang, Y., Liang, K., Wan, L., Zhou, Q., Li, Y., 2020. Structural mechanism of phospholipids translocation by MlaFEDB complex. Cell Res 30, 1127–1135. https://doi.org/10.1038/s41422-020-00404-6
Chiaradia, L., Lefebvre, C., Parra, J., Marcoux, J., Burlet-Schiltz, O., Etienne, G., Tropis, M., Daffé, M., 2017. Dissecting the mycobacterial cell envelope and defining the composition of the native mycomembrane. Sci Rep 7, 12807. https://doi.org/10.1038/s41598-017-12718-4
Chimalakonda, G., Ruiz, N., Chng, S.-S., Garner, R.A., Kahne, D., Silhavy, T.J., 2011. Lipoprotein LptE is required for the assembly of LptD by the β-barrel assembly machine in the outer membrane of Escherichia coli. Proceedings of the National Academy of Sciences 108, 2492–2497. https://doi.org/10.1073/pnas.1019089108
Chimento, D.P., Mohanty, A.K., Kadner, R.J., Wiener, M.C., 2003. Substrate-induced transmembrane signaling in the cobalamin transporter BtuB. Nat Struct Mol Biol 10, 394–401. https://doi.org/10.1038/nsb914

Chng, S.-S., Gronenberg, L.S., Kahne, D., 2010. Proteins Required for Lipopolysaccharide Assembly in Escherichia coli Form a Transenvelope Complex. Biochemistry 49, 4565–4567. https://doi.org/10.1021/bi100493e
Cho, S.-H., Dekoninck, K., Collet, J.-F., 2023. Envelope-Stress Sensing Mechanism of Rcs and Cpx Signaling Pathways in Gram-Negative Bacteria. J Microbiol. 61, 317–329. https://doi.org/10.1007/s12275-023-00030-y
Cho, S.-H., Szewczyk, J., Pesavento, C., Zietek, M., Banzhaf, M., Roszczenko, P., Asmar, A., Laloux, G., Hov, A.-K., Leverrier, P., Van der Henst, C., Vertommen, D., Typas, A., Collet, J.-F., 2014. Detecting Envelope Stress by Monitoring β-Barrel Assembly. Cell 159, 1652–1664. https://doi.org/10.1016/j.cell.2014.11.045
Cho, T.H.S., Pick, K., Raivio, T.L., 2023a. Bacterial envelope stress responses: Essential adaptors and attractive targets. Biochimica et Biophysica Acta (BBA) - Molecular Cell Research 1870, 119387. https://doi.org/10.1016/j.bbamcr.2022.119387
Cho, T.H.S., Wang, J., Raivio, T.L., 2023b. NlpE Is an OmpA-Associated Outer Membrane Sensor of the Cpx Envelope Stress Response. J Bacteriol 205, e00407-22. https://doi.org/10.1128/jb.00407-22
Cho, U.S., Bader, M.W., Amaya, M.F., Daley, M.E., Klevit, R.E., Miller, S.I., Xu, W., 2006. Metal Bridges between the PhoQ Sensor Domain and the Membrane Regulate Transmembrane Signaling. Journal of Molecular Biology 356, 1193–1206. https://doi.org/10.1016/j.jmb.2005.12.032
Confer, A.W., Ayalew, S., 2013. The OmpA family of proteins: Roles in bacterial pathogenesis and immunity. Veterinary Microbiology 163, 207–222. https://doi.org/10.1016/j.vetmic.2012.08.019
Connolly, L., Peñas, A.D.L., Alba, B.M., Gross, C.A., 1997. The response to extracytoplasmic stress in *Escherichia coli* is controlled by partially overlapping pathways. Genes Dev. 11, 2012–2021. https://doi.org/10.1101/gad.11.15.2012
Cosma, C.L., Danese, P.N., Carlson, J.H., Silhavy, T.J., Snyder, W.B., 1995a. Mutational activation of the Cpx signal transduction pathway of Escherichia coli suppresses the toxicity conferred by certain envelope-associated stresses. Mol Microbiol 18, 491–505. https://doi.org/10.1111/j.1365-2958.1995.mmi_18030491.x
Cosma, C.L., Danese, P.N., Carlson, J.H., Silhavy, T.J., Snyder, W.B., 1995b. Mutational activation of the Cpx signal transduction pathway of Escherichia coli suppresses the toxicity conferred by certain envelope-associated stresses. Mol Microbiol 18, 491–505. https://doi.org/10.1111/j.1365-2958.1995.mmi_18030491.x
Costa, T.R.D., Felisberto-Rodrigues, C., Meir, A., Prevost, M.S., Redzej, A., Trokter, M., Waksman, G., 2015. Secretion systems in Gram-negative bacteria: structural and mechanistic insights. Nat Rev Microbiol 13, 343–359. https://doi.org/10.1038/nrmicro3456
Coudray, N., Isom, G.L., MacRae, M.R., Saiduddin, M.N., Bhabha, G., Ekiert, D.C., 2020. Structure of bacterial phospholipid transporter MlaFEDB with substrate bound. eLife 9, e62518. https://doi.org/10.7554/eLife.62518
Danese, P.N., Oliver, G.R., Barr, K., Bowman, G.D., Rick, P.D., Silhavy, T.J., 1998. Accumulation of the Enterobacterial Common Antigen Lipid II Biosynthetic Intermediate Stimulates *degP* Transcription in *Escherichia coli*. J Bacteriol 180, 5875–5884. https://doi.org/10.1128/JB.180.22.5875-5884.1998
Danese, P.N., Silhavy, T.J., 1998. CpxP, a Stress-Combative Member of the Cpx Regulon. J Bacteriol 180, 831–839. https://doi.org/10.1128/JB.180.4.831-839.1998
Danese, P.N., Silhavy, T.J., 1997. The sigma(E) and the Cpx signal transduction systems control the synthesis of periplasmic protein-folding enzymes in Escherichia coli. Genes Dev. 11, 1183–1193. https://doi.org/10.1101/gad.11.9.1183

Danese, P.N., Snyder, W.B., Cosma, C.L., Davis, L.J., Silhavy, T.J., 1995. The Cpx two-component signal transduction pathway of Escherichia coli regulates transcription of the gene specifying the stress-inducible periplasmic protease, DegP. Genes Dev. 9, 387–398. https://doi.org/10.1101/gad.9.4.387
Dartois, V., Djavakhishvili, T., Hoch, J.A., 1997. KapB is a lipoprotein required for KinB signal transduction and activation of the phosphorelay to sporulation in Bacillus subtilis. Mol Microbiol 26, 1097–1108. https://doi.org/10.1046/j.1365-2958.1997.6542024.x
Datsenko, K.A., Wanner, B.L., 2000. One-step inactivation of chromosomal genes in Escherichia coli K-12 using PCR products. Proceedings of the National Academy of Sciences 97, 6640–6645. https://doi.org/10.1073/pnas.120163297
Davidson, A.L., Dassa, E., Orelle, C., Chen, J., 2008. Structure, Function, and Evolution of Bacterial ATP-Binding Cassette Systems. Microbiol Mol Biol Rev 72, 317–364. https://doi.org/10.1128/MMBR.00031-07
Davis, B.D., Chen, L.L., Tai, P.C., 1986. Misread protein creates membrane channels: an essential step in the bactericidal action of aminoglycosides. Proc Natl Acad Sci U S A 83, 6164–6168.
Dbeibo, L., van Rensburg, J.J., Smith, S.N., Fortney, K.R., Gangaiah, D., Gao, H., Marzoa, J., Liu, Y., Mobley, H.L.T., Spinola, S.M., 2018. Evaluation of CpxRA as a Therapeutic Target for Uropathogenic Escherichia coli Infections. Infect Immun 86, e00798-17. https://doi.org/10.1128/IAI.00798-17
De Geyter, J., Tsirigotaki, A., Orfanoudaki, G., Zorzini, V., Economou, A., Karamanou, S., 2016. Protein folding in the cell envelope of Escherichia coli. Nat Microbiol 1, 1–13. https://doi.org/10.1038/nmicrobiol.2016.107
De Wulf, P., Kwon, O., Lin, E.C.C., 1999. The CpxRA Signal Transduction System of *Escherichia coli* : Growth-Related Autoactivation and Control of Unanticipated Target Operons. J Bacteriol 181, 6772–6778. https://doi.org/10.1128/JB.181.21.6772-6778.1999
Dean, C.R., Neshat, S., Poole, K., 1996. PfeR, an enterobactin-responsive activator of ferric enterobactin receptor gene expression in Pseudomonas aeruginosa. J Bacteriol 178, 5361–5369.
Dean, C.R., Poole, K., 1993. Expression of the ferric enterobactin receptor (PfeA) of Pseudomonas aeruginosa: involvement of a two-component regulatory system. Molecular Microbiology 8, 1095–1103. https://doi.org/10.1111/j.1365-2958.1993.tb01654.x
Dekoninck, K., Létoquart, J., Laguri, C., Demange, P., Bevernaegie, R., Simorre, J.-P., Dehu, O., Iorga, B.I., Elias, B., Cho, S.-H., Collet, J.-F., 2020. Defining the function of OmpA in the Rcs stress response. eLife 9, e60861. https://doi.org/10.7554/eLife.60861
Delhaye, A., Collet, J.-F., Laloux, G., 2016. Fine-Tuning of the Cpx Envelope Stress Response Is Required for Cell Wall Homeostasis in Escherichia coli. mBio 7, e00047-00016. https://doi.org/10.1128/mBio.00047-16
Delhaye, A., Laloux, G., Collet, J.-F., 2019. The Lipoprotein NlpE Is a Cpx Sensor That Serves as a Sentinel for Protein Sorting and Folding Defects in the *Escherichia coli* Envelope. J Bacteriol 201. https://doi.org/10.1128/JB.00611-18
Den Blaauwen, T., de Pedro, M.A., Nguyen-Distèche, M., Ayala, J.A., 2008. Morphogenesis of rod-shaped sacculi. FEMS Microbiology Reviews 32, 321–344. https://doi.org/10.1111/j.1574-6976.2007.00090.x
Deng, M., Misra, R., 1996. Examination of AsmA and its effect on the assembly of Escherichia coli outer membrane proteins. Molecular Microbiology 21, 605–612. https://doi.org/10.1111/j.1365-2958.1996.tb02568.x
Depuydt, M., Leonard, S.E., Vertommen, D., Denoncin, K., Morsomme, P., Wahni, K., Messens, J., Carroll, K.S., Collet, J.-F., 2009. A periplasmic reducing system protects single

cysteine residues from oxidation. Science 326, 1109–1111. https://doi.org/10.1126/science.1179557
DiGiuseppe, P.A., Silhavy, T.J., 2003. Signal Detection and Target Gene Induction by the CpxRA Two-Component System. J Bacteriol 185, 2432–2440. https://doi.org/10.1128/JB.185.8.2432-2440.2003
Dikiy, I., Edupuganti, U.R., Abzalimov, R.R., Borbat, P.P., Srivastava, M., Freed, J.H., Gardner, K.H., 2019. Insights into histidine kinase activation mechanisms from the monomeric blue light sensor EL346. Proceedings of the National Academy of Sciences 116, 4963–4972. https://doi.org/10.1073/pnas.1813586116
Doerner, P.A., Sousa, M.C., 2017. Extreme Dynamics in the BamA β-Barrel Seam. Biochemistry 56, 3142–3149. https://doi.org/10.1021/acs.biochem.7b00281
Domínguez-Bernal, G., Pucciarelli, M.G., Ramos-Morales, F., García-Quintanilla, M., Cano, D.A., Casadesús, J., García-del Portillo, F., 2004. Repression of the RcsC-YojN-RcsB phosphorelay by the IgaA protein is a requisite for Salmonella virulence: Role of IgaA in Salmonella virulence. Molecular Microbiology 53, 1437–1449. https://doi.org/10.1111/j.1365-2958.2004.04213.x
Dong, C., Beis, K., Nesper, J., Brunkan, A.L., Clarke, B.R., Whitfield, C., Naismith, J.H., 2006. The structure of Wza, the translocon for group 1 capsular polysaccharides in Escherichia coli, identifies a new class of outer membrane protein. Nature 444, 226–229. https://doi.org/10.1038/nature05267
Dong, H., Xiang, Q., Gu, Y., Wang, Z., Paterson, N.G., Stansfeld, P.J., He, C., Zhang, Y., Wang, W., Dong, C., 2014. Structural basis for outer membrane lipopolysaccharide insertion. Nature 511, 52–56. https://doi.org/10.1038/nature13464
Dong, H., Zhang, Z., Tang, X., Paterson, N.G., Dong, C., 2017. Structural and functional insights into the lipopolysaccharide ABC transporter LptB2FG. Nat Commun 8, 222. https://doi.org/10.1038/s41467-017-00273-5
Dong, J., Shiro, luchi, Hoi-Shan, K., Zhe, L., Lin, E.C.C., 1993. The deduced amino-acid sequence of the cloned cpxR gene suggests the protein is the cognate regulator for the membrane sensor, CpxA, in a two-component signal transduction system of Escherichia coli. Gene 136, 227–230. https://doi.org/10.1016/0378-1119(93)90469-J
Dorel, C., Lejeune, P., Rodrigue, A., 2006. The Cpx system of Escherichia coli, a strategic signaling pathway for confronting adverse conditions and for settling biofilm communities? Research in Microbiology 157, 306–314. https://doi.org/10.1016/j.resmic.2005.12.003
Dorel, C., Vidal, O., Prigent-Combaret, C., Vallet, I., Lejeune, P., 1999. Involvement of the Cpx signal transduction pathway of *E. coli* in biofilm formation. FEMS Microbiology Letters 178, 169–175. https://doi.org/10.1111/j.1574-6968.1999.tb13774.x
Douglass, M.V., McLean, A.B., Trent, M.S., 2022. Absence of YhdP, TamB, and YdbH leads to defects in glycerophospholipid transport and cell morphology in Gram-negative bacteria. PLOS Genetics 18, e1010096. https://doi.org/10.1371/journal.pgen.1010096
Dowhan, W., 2011. The Raetz Pathway for Lipid A Biosynthesis: Christian Rudolf Hubert Raetz, MD PhD, 1946–2011. Journal of Lipid Research 52, 1857–1860. https://doi.org/10.1194/jlr.E020701
Doyle, M.T., Bernstein, H.D., 2019. Bacterial outer membrane proteins assemble via asymmetric interactions with the BamA β-barrel. Nat Commun 10, 3358. https://doi.org/10.1038/s41467-019-11230-9
Doyle, M.T., Jimah, J.R., Dowdy, T., Ohlemacher, S.I., Larion, M., Hinshaw, J.E., Bernstein, H.D., 2022. Cryo-EM structures reveal multiple stages of bacterial outer membrane protein folding. Cell 185, 1143-1156.e13. https://doi.org/10.1016/j.cell.2022.02.016
Du, S., Lutkenhaus, J., 2017. Assembly and activation of the Escherichia coli divisome. Molecular Microbiology 105, 177–187. https://doi.org/10.1111/mmi.13696

Duerr, C.U., Zenk, S.F., Chassin, C., Pott, J., Gütle, D., Hensel, M., Hornef, M.W., 2009. O-Antigen Delays Lipopolysaccharide Recognition and Impairs Antibacterial Host Defense in Murine Intestinal Epithelial Cells. PLOS Pathogens 5, e1000567. https://doi.org/10.1371/journal.ppat.1000567
Dunstan, R.A., Hay, I.D., Lithgow, T., 2017. Defining Membrane Protein Localization by Isopycnic Density Gradients. Methods Mol Biol 1615, 81–86. https://doi.org/10.1007/978-1-4939-7033-9_6
Dupont, C.L., Grass, G., Rensing, C., 2011. Copper toxicity and the origin of bacterial resistance—new insights and applications. Metallomics 3, 1109. https://doi.org/10.1039/c1mt00107h
Egan, A.J.F., Jean, N.L., Koumoutsi, A., Bougault, C.M., Biboy, J., Sassine, J., Solovyova, A.S., Breukink, E., Typas, A., Vollmer, W., Simorre, J.-P., 2014. Outer-membrane lipoprotein LpoB spans the periplasm to stimulate the peptidoglycan synthase PBP1B. Proc Natl Acad Sci U S A 111, 8197–8202. https://doi.org/10.1073/pnas.1400376111
El Rayes, J., Szewczyk, J., Deghelt, M., Csoma, N., Matagne, A., Iorga, B.I., Cho, S.-H., Collet, J.-F., 2021. Disorder is a critical component of lipoprotein sorting in Gram-negative bacteria. Nat Chem Biol 17, 1093–1100. https://doi.org/10.1038/s41589-021-00845-z
Emami, K., Topakas, E., Nagy, T., Henshaw, J., Jackson, K.A., Nelson, K.E., Mongodin, E.F., Murray, J.W., Lewis, R.J., Gilbert, H.J., 2009. Regulation of the Xylan-degrading Apparatus of Cellvibrio japonicus by a Novel Two-component System*. Journal of Biological Chemistry 284, 1086–1096. https://doi.org/10.1074/jbc.M805100200
Emsley, P., Cowtan, K., 2004. *Coot*: model-building tools for molecular graphics. Acta Crystallographica Section D 60, 2126–2132. https://doi.org/10.1107/S0907444904019158
Epstein, E.A., Reizian, M.A., Chapman, M.R., 2009. Spatial clustering of the curlin secretion lipoprotein requires curli fiber assembly. J Bacteriol 191, 608–615. https://doi.org/10.1128/JB.01244-08
Evans, K., Grossmann, J.G., Fordham-Skelton, A.P., Papiz, M.Z., 2006. Small-Angle X-ray Scattering Reveals the Solution Structure of a Bacteriophytochrome in the Catalytically Active Pr State. Journal of Molecular Biology 364, 655–666. https://doi.org/10.1016/j.jmb.2006.09.045
Evans, K.L., Kannan, S., Li, G., de Pedro, M.A., Young, K.D., 2013. Eliminating a Set of Four Penicillin Binding Proteins Triggers the Rcs Phosphorelay and Cpx Stress Responses in Escherichia coli. J Bacteriol 195, 4415–4424. https://doi.org/10.1128/JB.00596-13
Fairman, J.W., Noinaj, N., Buchanan, S.K., 2011. The structural biology of β-barrel membrane proteins: a summary of recent reports. Current Opinion in Structural Biology, Engineering and design / Membranes 21, 523–531. https://doi.org/10.1016/j.sbi.2011.05.005
Farris, C., Sanowar, S., Bader, M.W., Pfuetzner, R., Miller, S.I., 2010. Antimicrobial Peptides Activate the Rcs Regulon through the Outer Membrane Lipoprotein RcsF. Journal of Bacteriology 192, 4894–4903. https://doi.org/10.1128/jb.00505-10
Fei, K., Chao, H.-J., Hu, Y., Francis, M.S., Chen, S., 2021. CpxR regulates the Rcs phosphorelay system in controlling the Ysc-Yop type III secretion system in Yersinia pseudotuberculosis. Microbiology 167, 000998. https://doi.org/10.1099/mic.0.000998
Feng, L., Yang, B., Xu, Y., Xiong, Y., Wang, F., Liu, B., Yang, W., Yao, T., Wang, L., 2022. Elucidation of a complete mechanical signaling and virulence activation pathway in enterohemorrhagic Escherichia coli. Cell Reports 39, 110614. https://doi.org/10.1016/j.celrep.2022.110614
Festa, R.A., Thiele, D.J., 2012. Copper at the Front Line of the Host-Pathogen Battle. PLoS Pathog 8, e1002887. https://doi.org/10.1371/journal.ppat.1002887

Flores-Kim, J., Darwin, A.J., 2016. The Phage Shock Protein Response. Annual Review of Microbiology 70, 83–101. https://doi.org/10.1146/annurev-micro-102215-095359
Flores-Kim, J., Darwin, A.J., 2014. Regulation of bacterial virulence gene expression by cell envelope stress responses. Virulence 5, 835–851. https://doi.org/10.4161/21505594.2014.965580
Flynn, J.M., Neher, S.B., Kim, Y.-I., Sauer, R.T., Baker, T.A., 2003. Proteomic Discovery of Cellular Substrates of the ClpXP Protease Reveals Five Classes of ClpX-Recognition Signals. Molecular Cell 11, 671–683. https://doi.org/10.1016/S1097-2765(03)00060-1
Fortney, K.R., Smith, S.N., van Rensburg, J.J., Brothwell, J.A., Gardner, J.J., Katz, B.P., Ahsan, N., Duerfeldt, A.S., Mobley, H.L.T., Spinola, S.M., 2022. CpxA Phosphatase Inhibitor Activates CpxRA and Is a Potential Treatment for Uropathogenic Escherichia coli in a Murine Model of Infection. Microbiol Spectr 10, e02430-21. https://doi.org/10.1128/spectrum.02430-21
Frain, K.M., van Dijl, J.M., Robinson, C., 2019. The Twin-Arginine Pathway for Protein Secretion. EcoSal Plus 8. https://doi.org/10.1128/ecosalplus.ESP-0040-2018
Francez-Charlot, A., Laugel, B., Van Gemert, A., Dubarry, N., Wiorowski, F., Castanié-Cornet, M.-P., Gutierrez, C., Cam, K., 2003. RcsCDB His-Asp phosphorelay system negatively regulates the flhDC operon in Escherichia coli. Mol Microbiol 49, 823–832. https://doi.org/10.1046/j.1365-2958.2003.03601.x
Freinkman, E., Chng, S.-S., Kahne, D., 2011. The complex that inserts lipopolysaccharide into the bacterial outer membrane forms a two-protein plug-and-barrel. Proc. Natl. Acad. Sci. U.S.A. 108, 2486–2491. https://doi.org/10.1073/pnas.1015617108
Freinkman, E., Okuda, S., Ruiz, N., Kahne, D., 2012. Regulated assembly of the transenvelope protein complex required for lipopolysaccharide export. Biochemistry 51, 4800–4806. https://doi.org/10.1021/bi300592c
Galperin, M.Y., 2006. Structural Classification of Bacterial Response Regulators: Diversity of Output Domains and Domain Combinations. J Bacteriol 188, 4169–4182. https://doi.org/10.1128/JB.01887-05
Galperin, M.Y., 2004. Bacterial signal transduction network in a genomic perspective. Environ Microbiol 6, 552–567. https://doi.org/10.1111/j.1462-2920.2004.00633.x
Gao, R., Bouillet, S., Stock, A.M., 2019. Structural Basis of Response Regulator Function. Annual Review of Microbiology 73, 175–197. https://doi.org/10.1146/annurev-micro-020518-115931
Gao, R., Mack, T.R., Stock, A.M., 2007. Bacterial Response Regulators: Versatile Regulatory Strategies from Common Domains. Trends Biochem Sci 32, 225–234. https://doi.org/10.1016/j.tibs.2007.03.002
Gao, R., Stock, A.M., 2009. Biological insights from structures of two-component proteins. Annu Rev Microbiol 63, 133–154. https://doi.org/10.1146/annurev.micro.091208.073214
Garde, S., Chodisetti, P.K., Reddy, M., 2021. Peptidoglycan: Structure, Synthesis, and Regulation. EcoSal Plus 9. https://doi.org/10.1128/ecosalplus.ESP-0010-2020
Gasteiger, E., Hoogland, C., Gattiker, A., Duvaud, S., Wilkins, M.R., Appel, R.D., Bairoch, A., 2005. Protein Identification and Analysis Tools on the ExPASy Server, in: Walker, J.M. (Ed.), The Proteomics Protocols Handbook, Springer Protocols Handbooks. Humana Press, Totowa, NJ, pp. 571–607. https://doi.org/10.1385/1-59259-890-0:571
Ge, X., Wang, R., Ma, J., Liu, Y., Ezemaduka, A.N., Chen, P.R., Fu, X., Chang, Z., 2014. DegP primarily functions as a protease for the biogenesis of β-barrel outer membrane proteins in the Gram-negative bacterium Escherichia coli. FEBS J 281, 1226–1240. https://doi.org/10.1111/febs.12701
Gerken, H., Charlson, E.S., Cicirelli, E.M., Kenney, L.J., Misra, R., 2009. MzrA: a novel modulator of the EnvZ/OmpR two-component regulon. Molecular Microbiology 72, 1408–1422. https://doi.org/10.1111/j.1365-2958.2009.06728.x

Gerken, H., Misra, R., 2010. MzrA-EnvZ Interactions in the Periplasm Influence the EnvZ/OmpR Two-Component Regulon. J Bacteriol 192, 6271–6278. https://doi.org/10.1128/JB.00855-10
Giacometti, S.I., MacRae, M.R., Dancel-Manning, K., Bhabha, G., Ekiert, D.C., 2022. Lipid Transport Across Bacterial Membranes. Annual Review of Cell and Developmental Biology 38, 125–153. https://doi.org/10.1146/annurev-cellbio-120420-022914
Gogol, E.B., Rhodius, V.A., Papenfort, K., Vogel, J., Gross, C.A., 2011. Small RNAs endow a transcriptional activator with essential repressor functions for single-tier control of a global stress regulon. Proc. Natl. Acad. Sci. U.S.A. 108, 12875–12880. https://doi.org/10.1073/pnas.1109379108
Gohlke, U., Pullan, L., McDevitt, C.A., Porcelli, I., de Leeuw, E., Palmer, T., Saibil, H.R., Berks, B.C., 2005. The TatA component of the twin-arginine protein transport system forms channel complexes of variable diameter. Proceedings of the National Academy of Sciences 102, 10482–10486. https://doi.org/10.1073/pnas.0503558102
Goldberg, S.D., Soto, C.S., Waldburger, C.D., DeGrado, W.F., 2008. Determination of the Physiological Dimer Interface of the PhoQ Sensor Domain. Journal of Molecular Biology 379, 656–665. https://doi.org/10.1016/j.jmb.2008.04.023
Gooderham, W.J., Hancock, R.E.W., 2009. Regulation of virulence and antibiotic resistance by two-component regulatory systems in Pseudomonas aeruginosa. FEMS Microbiol Rev 33, 279–294. https://doi.org/10.1111/j.1574-6976.2008.00135.x
Gordeliy, V.I., Labahn, J., Moukhametzianov, R., Efremov, R., Granzin, J., Schlesinger, R., Büldt, G., Savopol, T., Scheidig, A.J., Klare, J.P., Engelhard, M., 2002. Molecular basis of transmembrane signalling by sensory rhodopsin II–transducer complex. Nature 419, 484–487. https://doi.org/10.1038/nature01109
Grabowicz, M., 2019. Lipoproteins and Their Trafficking to the Outer Membrane. EcoSal Plus 8. https://doi.org/10.1128/ecosalplus.ESP-0038-2018
Grabowicz, M., Koren, D., Silhavy, T.J., 2016. The CpxQ sRNA Negatively Regulates Skp To Prevent Mistargeting of β-Barrel Outer Membrane Proteins into the Cytoplasmic Membrane. mBio 7, e00312-16. https://doi.org/10.1128/mBio.00312-16
Grabowicz, M., Silhavy, T.J., 2017a. Redefining the essential trafficking pathway for outer membrane lipoproteins. Proc. Natl. Acad. Sci. U.S.A. 114, 4769–4774. https://doi.org/10.1073/pnas.1702248114
Grabowicz, M., Silhavy, T.J., 2017b. Envelope Stress Responses: An Interconnected Safety Net. Trends in Biochemical Sciences 42, 232–242. https://doi.org/10.1016/j.tibs.2016.10.002
Green, E.R., Mecsas, J., 2016. Bacterial Secretion Systems – An overview. Microbiol Spectr 4, 10.1128/microbiolspec.VMBF-0012–2015. https://doi.org/10.1128/microbiolspec.VMBF-0012-2015
Grimm, J., Shi, H., Wang, W., Mitchell, A.M., Wingreen, N.S., Huang, K.C., Silhavy, T.J., 2020. The inner membrane protein YhdP modulates the rate of anterograde phospholipid flow in Escherichia coli. Proc Natl Acad Sci U S A 117, 26907–26914. https://doi.org/10.1073/pnas.2015556117
Groisman, E.A., Duprey, A., Choi, J., 2021. How the PhoP/PhoQ System Controls Virulence and Mg2+ Homeostasis: Lessons in Signal Transduction, Pathogenesis, Physiology, and Evolution. Microbiology and Molecular Biology Reviews 85, 10.1128/mmbr.00176-20. https://doi.org/10.1128/mmbr.00176-20
Guest, R.L., Court, E.A., Waldon, J.L., Schock, K.A., Raivio, T.L., 2019. Impaired Efflux of the Siderophore Enterobactin Induces Envelope Stress in Escherichia coli. Front. Microbiol. 10, 2776. https://doi.org/10.3389/fmicb.2019.02776

Guest, R.L., Wang, J., Wong, J.L., Raivio, T.L., 2017. A Bacterial Stress Response Regulates Respiratory Protein Complexes To Control Envelope Stress Adaptation. J Bacteriol 199. https://doi.org/10.1128/JB.00153-17
Gunn, J.S., 2008. The *Salmonella* PmrAB regulon: lipopolysaccharide modifications, antimicrobial peptide resistance and more. Trends in Microbiology 16, 284–290. https://doi.org/10.1016/j.tim.2008.03.007
Guo, H., Suzuki, T., Rubinstein, J.L., 2018. Structure of a bacterial ATP synthase. eLife 8, e43128. https://doi.org/10.7554/eLife.43128
Guo, L., Lim, K.B., Gunn, J.S., Bainbridge, B., Darveau, R.P., Hackett, M., Miller, S.I., 1997. Regulation of lipid A modifications by Salmonella typhimurium virulence genes phoP-phoQ. Science 276, 250–253. https://doi.org/10.1126/science.276.5310.250
Guo, M.S., Updegrove, T.B., Gogol, E.B., Shabalina, S.A., Gross, C.A., Storz, G., 2014. MicL, a new σE-dependent sRNA, combats envelope stress by repressing synthesis of Lpp, the major outer membrane lipoprotein. Genes Dev 28, 1620–1634. https://doi.org/10.1101/gad.243485.114
Gupta, R.S., 2011. Origin of diderm (Gram-negative) bacteria: antibiotic selection pressure rather than endosymbiosis likely led to the evolution of bacterial cells with two membranes. Antonie van Leeuwenhoek 100, 171–182. https://doi.org/10.1007/s10482-011-9616-8
Gupta, S.D., Lee, B.T., Camakaris, J., Wu, H.C., 1995. Identification of cutC and cutF (nlpE) genes involved in copper tolerance in Escherichia coli. J Bacteriol 177, 4207–4215. https://doi.org/10.1128/jb.177.15.4207-4215.1995
Gupta, S.D., Wu, H.C., 1991. Identification and subcellular localization of apolipoprotein N-acyltransferase in Escherichia coli. FEMS Microbiology Letters 78, 37–41. https://doi.org/10.1111/j.1574-6968.1991.tb04413.x
Guzman, L.M., Belin, D., Carson, M.J., Beckwith, J., 1995. Tight regulation, modulation, and high-level expression by vectors containing the arabinose PBAD promoter. J Bacteriol 177, 4121–4130. https://doi.org/10.1128/jb.177.14.4121-4130.1995
Hagan, C.L., Wzorek, J.S., Kahne, D., 2015. Inhibition of the β-barrel assembly machine by a peptide that binds BamD. Proceedings of the National Academy of Sciences 112, 2011–2016. https://doi.org/10.1073/pnas.1415955112
Hara, T., Matsuyama, S., Tokuda, H., 2003. Mechanism underlying the inner membrane retention of Escherichia coli lipoproteins caused by Lol avoidance signals. J Biol Chem 278, 40408–40414. https://doi.org/10.1074/jbc.M307836200
Harper, C.E., Zhang, W., Lee, J., Shin, J.-H., Keller, M.R., van Wijngaarden, E., Chou, E., Wang, Z., Dörr, T., Chen, P., Hernandez, C.J., 2023. Mechanical stimuli activate gene expression via a cell envelope stress sensing pathway. Sci Rep 13, 13979. https://doi.org/10.1038/s41598-023-40897-w
Hart, E.M., Gupta, M., Wühr, M., Silhavy, T.J., 2019. The Synthetic Phenotype of Δ *bamB* Δ *bamE* Double Mutants Results from a Lethal Jamming of the Bam Complex by the Lipoprotein RcsF. mBio 10, e00662-19. https://doi.org/10.1128/mBio.00662-19
Hartl, F.U., Lecker, S., Schiebel, E., Hendrick, J.P., Wickner, W., 1990. The binding cascade of SecB to SecA to SecY/E mediates preprotein targeting to the E. coli plasma membrane. Cell 63, 269–279. https://doi.org/10.1016/0092-8674(90)90160-g
Hayden, J.D., Ades, S.E., 2008. The Extracytoplasmic Stress Factor, σE, Is Required to Maintain Cell Envelope Integrity in Escherichia coli. PLOS ONE 3, e1573. https://doi.org/10.1371/journal.pone.0001573
He, H., Pramanik, A.S., Swanson, S.K., Johnson, D.K., Florens, L., Zückert, W.R., 2022. A Borrelia burgdorferi LptD Homolog Facilitates Flipping of Surface Lipoproteins Through the Spirochetal Outer Membrane. https://doi.org/10.1101/2022.12.21.521298

He, W., Yu, G., Li, T., Bai, L., Yang, Y., Xue, Z., Pang, Y., Reichmann, D., Hiller, S., He, L., Liu, M., Quan, S., 2021. Chaperone Spy Protects Outer Membrane Proteins from Folding Stress via Dynamic Complex Formation. mBio 12, e0213021. https://doi.org/10.1128/mBio.02130-21
Hefti, M.H., Françoijs, K.-J., de Vries, S.C., Dixon, R., Vervoort, J., 2004. The PAS fold: A redefinition of the PAS domain based upon structural prediction. European Journal of Biochemistry 271, 1198–1208. https://doi.org/10.1111/j.1432-1033.2004.04023.x
Heinrich, J., Wiegert, T., 2009. Regulated intramembrane proteolysis in the control of extracytoplasmic function sigma factors. Res Microbiol 160, 696–703. https://doi.org/10.1016/j.resmic.2009.08.019
Heinz, E., Selkrig, J., Belousoff, M.J., Lithgow, T., 2015. Evolution of the Translocation and Assembly Module (TAM). Genome Biol Evol 7, 1628–1643. https://doi.org/10.1093/gbe/evv097
Henry, J.T., Crosson, S., 2011. Ligand-Binding PAS Domains in a Genomic, Cellular, and Structural Context. Annual Review of Microbiology 65, 261–286. https://doi.org/10.1146/annurev-micro-121809-151631
Hermansen, S., Linke, D., Leo, J.C., 2022. Transmembrane β-barrel proteins of bacteria: From structure to function, in: Donev, R. (Ed.), Advances in Protein Chemistry and Structural Biology, Membrane Proteins. Academic Press, pp. 113–161. https://doi.org/10.1016/bs.apcsb.2021.07.002
Hernday, A., Braaten, B., Broitmanmaduro, G., Engelberts, P., Low, D., 2004. Regulation of the Pap Epigenetic Switch by CpxARPhosphorylated CpxR Inhibits Transition to the Phase ON State by Competition with Lrp. Molecular Cell 16, 537–547. https://doi.org/10.1016/S1097-2765(04)00646-X
Hersch, S.J., Watanabe, N., Stietz, M.S., Manera, K., Kamal, F., Burkinshaw, B., Lam, L., Pun, A., Li, M., Savchenko, A., Dong, T.G., 2020. Envelope stress responses defend against type six secretion system attacks independently of immunity proteins. Nat Microbiol 5, 706–714. https://doi.org/10.1038/s41564-020-0672-6
Hews, C.L., Cho, T., Rowley, G., Raivio, T.L., 2019. Maintaining Integrity Under Stress: Envelope Stress Response Regulation of Pathogenesis in Gram-Negative Bacteria. Front. Cell. Infect. Microbiol. 9, 313. https://doi.org/10.3389/fcimb.2019.00313
Hirakawa, H., Inazumi, Y., Masaki, T., Hirata, T., Yamaguchi, A., 2004. Indole induces the expression of multidrug exporter genes in Escherichia coli: Indole signal induces some drug exporters. Molecular Microbiology 55, 1113–1126. https://doi.org/10.1111/j.1365-2958.2004.04449.x
Hirano, Y., Hossain, Md.M., Takeda, K., Tokuda, H., Miki, K., 2007. Structural Studies of the Cpx Pathway Activator NlpE on the Outer Membrane of Escherichia coli. Structure 15, 963–976. https://doi.org/10.1016/j.str.2007.06.014
Hirano, Y., Hossain, Md.M., Takeda, K., Tokuda, H., Miki, K., 2006. Purification, crystallization and preliminary X-ray crystallographic analysis of the outer membrane lipoprotein NlpE from *Escherichia coli*. Acta Crystallogr F Struct Biol Cryst Commun 62, 1227–1230. https://doi.org/10.1107/S1744309106045313
Ho, Y.-S.J., Burden, L.M., Hurley, J.H., 2000. Structure of the GAF domain, a ubiquitous signaling motif and a new class of cyclic GMP receptor. EMBO J 19, 5288–5299. https://doi.org/10.1093/emboj/19.20.5288
Hoang, T.T., Karkhoff-Schweizer, R.R., Kutchma, A.J., Schweizer, H.P., 1998. A broad-host-range Flp-FRT recombination system for site-specific excision of chromosomally-located DNA sequences: application for isolation of unmarked Pseudomonas aeruginosa mutants. Gene 212, 77–86. https://doi.org/10.1016/s0378-1119(98)00130-9
Hoch, J.A., 2000. Two-component and phosphorelay signal transduction. Current Opinion in Microbiology 3, 165–170. https://doi.org/10.1016/S1369-5274(00)00070-9

Holm, L., Sander, C., 1995. Dali: a network tool for protein structure comparison. Trends in Biochemical Sciences 20, 478–480. https://doi.org/10.1016/S0968-0004(00)89105-7
Höltje, J.-V., 1998. Growth of the Stress-Bearing and Shape-Maintaining Murein Sacculus of Escherichia coli. Microbiol Mol Biol Rev 62, 181–203.
Hooda, Y., Lai, C.C.-L., Judd, A., Buckwalter, C.M., Shin, H.E., Gray-Owen, S.D., Moraes, T.F., 2016. Slam is an outer membrane protein that is required for the surface display of lipidated virulence factors in Neisseria. Nat Microbiol 1, 1–9. https://doi.org/10.1038/nmicrobiol.2016.9
Hooda, Y., Lai, C.C.L., Moraes, T.F., 2017a. Identification of a Large Family of Slam-Dependent Surface Lipoproteins in Gram-Negative Bacteria. Front. Cell. Infect. Microbiol. 7. https://doi.org/10.3389/fcimb.2017.00207
Hooda, Y., Shin, H.E., Bateman, T.J., Moraes, T.F., 2017b. Neisserial surface lipoproteins: structure, function and biogenesis. Pathogens and Disease 75. https://doi.org/10.1093/femspd/ftx010
Huang, J., Li, C., Song, J., Velkov, T., Wang, L., Zhu, Y., Li, J., 2020. Regulating Polymyxin Resistance in Gram-Negative Bacteria: Roles of Two-Component Systems PhoPQ and PmrAB. Future Microbiology 15, 445–459. https://doi.org/10.2217/fmb-2019-0322
Huang, K.C., Mukhopadhyay, R., Wen, B., Gitai, Z., Wingreen, N.S., 2008. Cell shape and cell-wall organization in Gram-negative bacteria. Proceedings of the National Academy of Sciences 105, 19282–19287. https://doi.org/10.1073/pnas.0805309105
Hughes, G.W., Hall, S.C.L., Laxton, C.S., Sridhar, P., Mahadi, A.H., Hatton, C., Piggot, T.J., Wotherspoon, P.J., Leney, A.C., Ward, D.G., Jamshad, M., Spana, V., Cadby, I.T., Harding, C., Isom, G.L., Bryant, J.A., Parr, R.J., Yakub, Y., Jeeves, M., Huber, D., Henderson, I.R., Clifton, L.A., Lovering, A.L., Knowles, T.J., 2019. Evidence for phospholipid export from the bacterial inner membrane by the Mla ABC transport system. Nat Microbiol 4, 1692–1705. https://doi.org/10.1038/s41564-019-0481-y
Hummels, K.R., Berry, S.P., Li, Z., Taguchi, A., Min, J.K., Walker, S., Marks, D.S., Bernhardt, T.G., 2023. Coordination of bacterial cell wall and outer membrane biosynthesis. Nature 615, 300–304. https://doi.org/10.1038/s41586-023-05750-0
Humphreys, S., Rowley, G., Stevenson, A., Anjum, M.F., Woodward, M.J., Gilbert, S., Kormanec, J., Roberts, M., 2004. Role of the Two-Component Regulator CpxAR in the Virulence of *Salmonella enterica* Serotype Typhimurium. Infect Immun 72, 4654–4661. https://doi.org/10.1128/IAI.72.8.4654-4661.2004
Humphries, R.M., Griener, T.P., Vogt, S.L., Mulvey, G.L., Raivio, T., Donnenberg, M.S., Kitov, P.I., Surette, M., Armstrong, G.D., 2010. N-acetyllactosamine-induced retraction of bundle-forming pili regulates virulence-associated gene expression in enteropathogenic Escherichia coli: BFP retraction alters EPEC gene expression. Molecular Microbiology 76, 1111–1126. https://doi.org/10.1111/j.1365-2958.2010.07192.x
Hung, D.L., 2001. Cpx signaling pathway monitors biogenesis and affects assembly and expression of P pili. The EMBO Journal 20, 1508–1518. https://doi.org/10.1093/emboj/20.7.1508
Hunke, S., Betton, J.-M., 2003. Temperature effect on inclusion body formation and stress response in the periplasm of Escherichia coli: Temperature effect on inclusion body formation. Molecular Microbiology 50, 1579–1589. https://doi.org/10.1046/j.1365-2958.2003.03785.x
Hussein, N.A., Cho, S.-H., Laloux, G., Siam, R., Collet, J.-F., 2018. Distinct domains of Escherichia coli IgaA connect envelope stress sensing and down-regulation of the Rcs phosphorelay across subcellular compartments. PLoS Genet 14, e1007398. https://doi.org/10.1371/journal.pgen.1007398

Huynh, M.S., Hooda, Y., Li, Y.R., Jagielnicki, M., Lai, C.C.-L., Moraes, T.F., 2022. Reconstitution of surface lipoprotein translocation through the Slam translocon. eLife 11, e72822. https://doi.org/10.7554/eLife.72822
Hwang Fu, Y.-H., Huang, W.Y.C., Shen, K., Groves, J.T., Miller, T., Shan, S., 2017. Two-step membrane binding by the bacterial SRP receptor enable efficient and accurate Co-translational protein targeting. eLife 6, e25885. https://doi.org/10.7554/eLife.25885
Hwang, P.M., Choy, W.-Y., Lo, E.I., Chen, L., Forman-Kay, J.D., Raetz, C.R.H., Privé, G.G., Bishop, R.E., Kay, L.E., 2002. Solution structure and dynamics of the outer membrane enzyme PagP by NMR. Proceedings of the National Academy of Sciences 99, 13560–13565. https://doi.org/10.1073/pnas.212344499
Imai, K., Mitaku, S., 2005. Mechanisms of secondary structure breakers in soluble proteins. Biophysics (Nagoya-shi) 1, 55–65. https://doi.org/10.2142/biophysics.1.55
Isaac, D.D., Pinkner, J.S., Hultgren, S.J., Silhavy, T.J., 2005. The extracytoplasmic adaptor protein CpxP is degraded with substrate by DegP. Proc. Natl. Acad. Sci. U.S.A. 102, 17775–17779. https://doi.org/10.1073/pnas.0508936102
Islam, S.T., Lam, J.S., 2014. Synthesis of bacterial polysaccharides via the Wzx/Wzy-dependent pathway. Can. J. Microbiol. 60, 697–716. https://doi.org/10.1139/cjm-2014-0595
Isom, G.L., Davies, N.J., Chong, Z.-S., Bryant, J.A., Jamshad, M., Sharif, M., Cunningham, A.F., Knowles, T.J., Chng, S.-S., Cole, J.A., Henderson, I.R., 2017. MCE domain proteins: conserved inner membrane lipid-binding proteins required for outer membrane homeostasis. Sci Rep 7, 8608. https://doi.org/10.1038/s41598-017-09111-6
Ito, K., Inaba, K., 2008. The disulfide bond formation (Dsb) system. Current Opinion in Structural Biology 18, 450–458. https://doi.org/10.1016/j.sbi.2008.02.002
Itou, H., Tanaka, I., 2001. The OmpR-family of proteins: insight into the tertiary structure and functions of two-component regulator proteins. J Biochem 129, 343–350. https://doi.org/10.1093/oxfordjournals.jbchem.a002863
Jackowski, S., Rock, C.O., 1986. Transfer of fatty acids from the 1-position of phosphatidylethanolamine to the major outer membrane lipoprotein of Escherichia coli. J Biol Chem 261, 11328–11333.
Jacob-Dubuisson, F., Mechaly, A., Betton, J.-M., Antoine, R., 2018. Structural insights into the signalling mechanisms of two-component systems. Nat Rev Microbiol 16, 585–593. https://doi.org/10.1038/s41579-018-0055-7
Janausch, I.G., Garcia-Moreno, I., Unden, G., 2002. Function of DcuS from Escherichia coli as a fumarate-stimulated histidine protein kinase in vitro. J Biol Chem 277, 39809–39814. https://doi.org/10.1074/jbc.M204482200
Janet-Maitre, M., Job, V., Bour, M., Robert-Genthon, M., Brugière, S., Triponney, P., Cobessi, D., Couté, Y., Jeannot, K., Attrée, I., 2024. Pseudomonas aeruginosa MipA-MipB envelope proteins act as new sensors of polymyxins. mBio 15, e02211-23. https://doi.org/10.1128/mbio.02211-23
Janssens, A., Nguyen, V.S., Cecil, A.J., Van der Verren, S.E., Timmerman, E., Deghelt, M., Pak, A.J., Collet, J.-F., Impens, F., Remaut, H., 2024. SlyB encapsulates outer membrane proteins in stress-induced lipid nanodomains. Nature 626, 617–625. https://doi.org/10.1038/s41586-023-06925-5
Jobling, M.G., Holmes, R.K., 1990. Construction of vectors with the p15a replicon, kanamycin resistance, inducible lacZ alpha and pUC18 or pUC19 multiple cloning sites. Nucleic Acids Res 18, 5315–5316. https://doi.org/10.1093/nar/18.17.5315
Johnson, L., Horsman, S.R., Charron-Mazenod, L., Turnbull, A.L., Mulcahy, H., Surette, M.G., Lewenza, S., 2013. Extracellular DNA-induced antimicrobial peptide resistance in Salmonella enterica serovar Typhimurium. BMC Microbiol 13, 115. https://doi.org/10.1186/1471-2180-13-115

Joly, N., Engl, C., Jovanovic, G., Huvet, M., Toni, T., Sheng, X., Stumpf, M.P.H., Buck, M., 2010. Managing membrane stress: the phage shock protein (Psp) response, from molecular mechanisms to physiology. FEMS Microbiology Reviews 34, 797–827. https://doi.org/10.1111/j.1574-6976.2010.00240.x

Jones, C.H., 1997. The chaperone-assisted membrane release and folding pathway is sensed by two signal transduction systems. The EMBO Journal 16, 6394–6406. https://doi.org/10.1093/emboj/16.21.6394

Jovanovic, G., Engl, C., Mayhew, A.J., Burrows, P.C., Buck, M., 2010. Properties of the phage-shock-protein (Psp) regulatory complex that govern signal transduction and induction of the Psp response in Escherichia coli. Microbiology (Reading) 156, 2920–2932. https://doi.org/10.1099/mic.0.040055-0

Jubelin, G., Vianney, A., Beloin, C., Ghigo, J.-M., Lazzaroni, J.-C., Lejeune, P., Dorel, C., 2005. CpxR/OmpR Interplay Regulates Curli Gene Expression in Response to Osmolarity in *Escherichia coli*. J Bacteriol 187, 2038–2049. https://doi.org/10.1128/JB.187.6.2038-2049.2005

Jumper, J., Evans, R., Pritzel, A., Green, T., Figurnov, M., Ronneberger, O., Tunyasuvunakool, K., Bates, R., Žídek, A., Potapenko, A., Bridgland, A., Meyer, C., Kohl, S.A.A., Ballard, A.J., Cowie, A., Romera-Paredes, B., Nikolov, S., Jain, R., Adler, J., Back, T., Petersen, S., Reiman, D., Clancy, E., Zielinski, M., Steinegger, M., Pacholska, M., Berghammer, T., Bodenstein, S., Silver, D., Vinyals, O., Senior, A.W., Kavukcuoglu, K., Kohli, P., Hassabis, D., 2021. Highly accurate protein structure prediction with AlphaFold. Nature 596, 583–589. https://doi.org/10.1038/s41586-021-03819-2

Kalmokoff, M.L., Austin, J.W., Cyr, T.D., Hefford, M.A., Teather, R.M., Selinger, L.B., 2009. Physical and genetic characterization of an outer-membrane protein (OmpM1) containing an N-terminal S-layer-like homology domain from the phylogenetically Gram-positive gut anaerobe Mitsuokella multacida. Anaerobe 15, 74–81. https://doi.org/10.1016/j.anaerobe.2009.01.001

Kandler, J.L., Holley, C.L., Reimche, J.L., Dhulipala, V., Balthazar, J.T., Muszyński, A., Carlson, R.W., Shafer, W.M., 2016. The MisR Response Regulator Is Necessary for Intrinsic Cationic Antimicrobial Peptide and Aminoglycoside Resistance in Neisseria gonorrhoeae. Antimicrob Agents Chemother 60, 4690–4700. https://doi.org/10.1128/AAC.00823-16

Kaplan, E., Greene, N.P., Crow, A., Koronakis, V., 2018. Insights into bacterial lipoprotein trafficking from a structure of LolA bound to the LolC periplasmic domain. Proceedings of the National Academy of Sciences 115, E7389–E7397. https://doi.org/10.1073/pnas.1806822115

Kashyap, D.R., Wang, M., Liu, L.-H., Boons, G.-J., Gupta, D., Dziarski, R., 2011. Peptidoglycan recognition proteins kill bacteria by activating protein-sensing two-component systems. Nat Med 17, 676–683. https://doi.org/10.1038/nm.2357

Kato, M., Mizuno, T., Shimizu, T., Hakoshima, T., 1997. Insights into Multistep Phosphorelay from the Crystal Structure of the C-Terminal HPt Domain of ArcB. Cell 88, 717–723. https://doi.org/10.1016/S0092-8674(00)81914-5

Kehry, M.R., Dahlquist, F.W., 1982. Adaptation in bacterial chemotaxis: CheB-dependent modification permits additional methylations of sensory transducer proteins. Cell 29, 761–772. https://doi.org/10.1016/0092-8674(82)90438-X

Keller, R., Havemann, J., Hunke, S., 2011. Different regulatory regions are located on the sensor domain of CpxA to fine-tune signal transduction. Research in Microbiology 162, 405–409. https://doi.org/10.1016/j.resmic.2011.02.008

Kiehler, B., Haggett, L., Fujita, M., 2017. The PAS domains of the major sporulation kinase in Bacillus subtilis play a role in tetramer formation that is essential for the autokinase activity. MicrobiologyOpen 6, e00481. https://doi.org/10.1002/mbo3.481

Kihara, A., Akiyama, Y., Ito, K., 1995. FtsH is required for proteolytic elimination of uncomplexed forms of SecY, an essential protein translocase subunit. Proceedings of the National Academy of Sciences 92, 4532–4536. https://doi.org/10.1073/pnas.92.10.4532
Kim, K.I., Park, S.C., Kang, S.H., Cheong, G.W., Chung, C.H., 1999. Selective degradation of unfolded proteins by the self-compartmentalizing HtrA protease, a periplasmic heat shock protein in Escherichia coli. J Mol Biol 294, 1363–1374. https://doi.org/10.1006/jmbi.1999.3320
Kimkes, T.E.P., Heinemann, M., 2019. How bacteria recognise and respond to surface contact. FEMS Microbiol Rev 44, 106–122. https://doi.org/10.1093/femsre/fuz029
Kimkes, T.E.P., Heinemann, M., 2018. Reassessing the role of the Escherichia coli CpxAR system in sensing surface contact. PLoS ONE 13, e0207181. https://doi.org/10.1371/journal.pone.0207181
Kitagawa, M., Ara, T., Arifuzzaman, M., Ioka-Nakamichi, T., Inamoto, E., Toyonaga, H., Mori, H., 2006. Complete set of ORF clones of Escherichia coli ASKA library (A Complete Set of E. coli K-12 ORF Archive): Unique Resources for Biological Research. DNA Research 12, 291–299. https://doi.org/10.1093/dnares/dsi012
Knowles, T.J., Scott-Tucker, A., Overduin, M., Henderson, I.R., 2009. Membrane protein architects: the role of the BAM complex in outer membrane protein assembly. Nat Rev Microbiol 7, 206–214. https://doi.org/10.1038/nrmicro2069
Ko, J.-K., Ma, J., 2005. A rapid and efficient PCR-based mutagenesis method applicable to cell physiology study. American Journal of Physiology-Cell Physiology 288, C1273–C1278. https://doi.org/10.1152/ajpcell.00517.2004
Kobayashi, R., Suzuki, T., Yoshida, M., 2007. Escherichia coli phage-shock protein A (PspA) binds to membrane phospholipids and repairs proton leakage of the damaged membranes. Molecular Microbiology 66, 100–109. https://doi.org/10.1111/j.1365-2958.2007.05893.x
Koebnik, R., 1995. Proposal for a peptidoglycan-associating alpha-helical motif in the C-terminal regions of some bacterial cell-surface proteins. Molecular Microbiology 16, 1269–1270. https://doi.org/10.1111/j.1365-2958.1995.tb02348.x
Kojima, S., Ko, K.-C., Takatsuka, Y., Abe, N., Kaneko, J., Itoh, Y., Kamio, Y., 2010. Cadaverine Covalently Linked to Peptidoglycan Is Required for Interaction between the Peptidoglycan and the Periplasm-Exposed S-Layer-Homologous Domain of Major Outer Membrane Protein Mep45 in Selenomonas ruminantium. J Bacteriol 192, 5953–5961. https://doi.org/10.1128/JB.00417-10
Konovalova, A., Kahne, D.E., Silhavy, T.J., 2017. Outer Membrane Biogenesis. Annu. Rev. Microbiol. 71, 539–556. https://doi.org/10.1146/annurev-micro-090816-093754
Konovalova, A., Mitchell, A.M., Silhavy, T.J., 2016. A lipoprotein/β-barrel complex monitors lipopolysaccharide integrity transducing information across the outer membrane. eLife 5, e15276. https://doi.org/10.7554/eLife.15276
Konovalova, A., Perlman, D.H., Cowles, C.E., Silhavy, T.J., 2014. Transmembrane domain of surface-exposed outer membrane lipoprotein RcsF is threaded through the lumen of β-barrel proteins. Proc. Natl. Acad. Sci. U.S.A. 111. https://doi.org/10.1073/pnas.1417138111
Konovalova, A., Silhavy, T.J., 2015. Outer membrane lipoprotein biogenesis: Lol is not the end. Phil. Trans. R. Soc. B 370, 20150030. https://doi.org/10.1098/rstb.2015.0030
Krell, T., Lacal, J., Busch, A., Silva-Jiménez, H., Guazzaroni, M.-E., Ramos, J.L., 2010. Bacterial Sensor Kinases: Diversity in the Recognition of Environmental Signals. Annu. Rev. Microbiol. 64, 539–559. https://doi.org/10.1146/annurev.micro.112408.134054
Krin, E., Danchin, A., Soutourina, O., 2010. RcsB plays a central role in H-NS-dependent regulation of motility and acid stress resistance in *Escherichia coli*. Research in Microbiology 161, 363–371. https://doi.org/10.1016/j.resmic.2010.04.002

Krojer, T., Sawa, J., Schäfer, E., Saibil, H.R., Ehrmann, M., Clausen, T., 2008. Structural basis for the regulated protease and chaperone function of DegP. Nature 453, 885–890. https://doi.org/10.1038/nature07004
Kumar, S., Ruiz, N., 2023. Bacterial AsmA-Like Proteins: Bridging the Gap in Intermembrane Phospholipid Transport. Contact (Thousand Oaks) 6, 25152564231185931. https://doi.org/10.1177/25152564231185931
Kumazaki, K., Kishimoto, T., Furukawa, A., Mori, H., Tanaka, Y., Dohmae, N., Ishitani, R., Tsukazaki, T., Nureki, O., 2014. Crystal structure of Escherichia coli YidC, a membrane protein chaperone and insertase. Sci Rep 4, 7299. https://doi.org/10.1038/srep07299
Kunkle, D.E., Bina, X.R., Bina, J.E., 2017. The *Vibrio cholerae* VexGH RND Efflux System Maintains Cellular Homeostasis by Effluxing Vibriobactin. mBio 8, e00126-17. https://doi.org/10.1128/mBio.00126-17
Kwon, E., Kim, D.Y., Gross, C.A., Gross, J.D., Kim, K.K., 2010. The crystal structure *Escherichia coli* Spy: The Crystal Structure of EcSpy. Protein Science 19, 2252–2259. https://doi.org/10.1002/pro.489
Kwon, E., Kim, D.Y., Ngo, T.D., Gross, C.A., Gross, J.D., Kim, K.K., 2012a. The crystal structure of the periplasmic domain of *Vibrio parahaemolyticus* CpxA: Periplasmic Domain of Vibrio parahaemolyticus CpxA. Protein Science 21, 1334–1343. https://doi.org/10.1002/pro.2120
Kwon, E., Kim, D.Y., Ngo, T.D., Gross, C.A., Gross, J.D., Kim, K.K., 2012b. The crystal structure of the periplasmic domain of *Vibrio parahaemolyticus* CpxA: Periplasmic Domain of Vibrio parahaemolyticus CpxA. Protein Science 21, 1334–1343. https://doi.org/10.1002/pro.2120
Lacanna, E., Bigosch, C., Kaever, V., Boehm, A., Becker, A., 2016. Evidence for Escherichia coli Diguanylate Cyclase DgcZ Interlinking Surface Sensing and Adhesion via Multiple Regulatory Routes. J Bacteriol 198, 2524–2535. https://doi.org/10.1128/JB.00320-16
Lach, S.R., Kumar, S., Kim, S., Im, W., Konovalova, A., 2023. Conformational rearrangements in the sensory RcsF/OMP complex mediate signal transduction across the bacterial cell envelope. PLOS Genetics 19, e1010601. https://doi.org/10.1371/journal.pgen.1010601
Lasaro, M., Liu, Z., Bishar, R., Kelly, K., Chattopadhyay, S., Paul, S., Sokurenko, E., Zhu, J., Goulian, M., 2014. Escherichia coli Isolate for Studying Colonization of the Mouse Intestine and Its Application to Two-Component Signaling Knockouts. J Bacteriol 196, 1723–1732. https://doi.org/10.1128/JB.01296-13
Lau, C.H.-F., Fraud, S., Jones, M., Peterson, S.N., Poole, K., 2013. Mutational Activation of the AmgRS Two-Component System in Aminoglycoside-Resistant Pseudomonas aeruginosa. Antimicrob Agents Chemother 57, 2243–2251. https://doi.org/10.1128/AAC.00170-13
Laubacher, M.E., Ades, S.E., 2008. The Rcs Phosphorelay Is a Cell Envelope Stress Response Activated by Peptidoglycan Stress and Contributes to Intrinsic Antibiotic Resistance. J Bacteriol 190, 2065–2074. https://doi.org/10.1128/JB.01740-07
Laventie, B.-J., Jenal, U., 2020. Surface Sensing and Adaptation in Bacteria. Annual Review of Microbiology 74, 735–760. https://doi.org/10.1146/annurev-micro-012120-063427
Laventie, B.-J., Sangermani, M., Estermann, F., Manfredi, P., Planes, R., Hug, I., Jaeger, T., Meunier, E., Broz, P., Jenal, U., 2019. A Surface-Induced Asymmetric Program Promotes Tissue Colonization by *Pseudomonas aeruginosa*. Cell Host & Microbe 25, 140-152.e6. https://doi.org/10.1016/j.chom.2018.11.008
Lee, J., Tomchick, D.R., Brautigam, C.A., Machius, M., Kort, R., Hellingwerf, K.J., Gardner, K.H., 2008. Changes at the KinA PAS-A Dimerization Interface Influence Histidine Kinase Function,. Biochemistry 47, 4051–4064. https://doi.org/10.1021/bi7021156

Lee, L.J., Barrett, J.A., Poole, R.K., 2005. Genome-Wide Transcriptional Response of Chemostat-Cultured *Escherichia coli* to Zinc. J Bacteriol 187, 1124–1134. https://doi.org/10.1128/JB.187.3.1124-1134.2005
Lee, Y.M., DiGiuseppe, P.A., Silhavy, T.J., Hultgren, S.J., 2004. P Pilus Assembly Motif Necessary for Activation of the CpxRA Pathway by PapE in *Escherichia coli*. J Bacteriol 186, 4326–4337. https://doi.org/10.1128/JB.186.13.4326-4337.2004
Lehman, K.M., Grabowicz, M., 2019. Countering Gram-Negative Antibiotic Resistance: Recent Progress in Disrupting the Outer Membrane with Novel Therapeutics. Antibiotics 8, 163. https://doi.org/10.3390/antibiotics8040163
Lehman, K.M., May, K.L., Marotta, J., Grabowicz, M., 2024. Genetic analysis reveals a robust and hierarchical recruitment of the LolA chaperone to the LolCDE lipoprotein transporter. mBio 15, e03039-23. https://doi.org/10.1128/mbio.03039-23
Léonard, R.R., Sauvage, E., Lupo, V., Perrin, A., Sirjacobs, D., Charlier, P., Kerff, F., Baurain, D., 2022. Was the Last Bacterial Common Ancestor a Monoderm after All? Genes 13, 376. https://doi.org/10.3390/genes13020376
Leonhartsberger, S., Huber, A., Lottspeich, F., Böck, A., 2001. The hydH/G genes from Escherichia coli code for a zinc and lead responsive two-component regulatory system. Journal of Molecular Biology 307, 93–105. https://doi.org/10.1006/jmbi.2000.4451
Leverrier, P., Declercq, J.-P., Denoncin, K., Vertommen, D., Hiniker, A., Cho, S.-H., Collet, J.-F., 2011. Crystal Structure of the Outer Membrane Protein RcsF, a New Substrate for the Periplasmic Protein-disulfide Isomerase DsbC. J Biol Chem 286, 16734–16742. https://doi.org/10.1074/jbc.M111.224865
Leyton, D.L., Belousoff, M.J., Lithgow, T., 2015. The β-Barrel Assembly Machinery Complex. Methods Mol Biol 1329, 1–16. https://doi.org/10.1007/978-1-4939-2871-2_1
Leyton, D.L., Rossiter, A.E., Henderson, I.R., 2012. From self sufficiency to dependence: mechanisms and factors important for autotransporter biogenesis. Nat Rev Microbiol 10, 213–225. https://doi.org/10.1038/nrmicro2733
Li, G.-W., Burkhardt, D., Gross, C., Weissman, J.S., 2014. Quantifying Absolute Protein Synthesis Rates Reveals Principles Underlying Allocation of Cellular Resources. Cell 157, 624–635. https://doi.org/10.1016/j.cell.2014.02.033
Li, Y., Gardner, J.J., Fortney, K.R., Leus, I.V., Bonifay, V., Zgurskaya, H.I., Pletnev, A.A., Zhang, S., Zhang, Z.-Y., Gribble, G.W., Spinola, S.M., Duerfeldt, A.S., 2019. First-generation structure-activity relationship studies of 2,3,4,9-tetrahydro-1H-carbazol-1-amines as CpxA phosphatase inhibitors. Bioorganic & Medicinal Chemistry Letters 29, 1836–1841. https://doi.org/10.1016/j.bmcl.2019.05.003
Liao, C., Santoscoy, M.C., Craft, J., Anderson, C., Soupir, M.L., Jarboe, L.R., 2022. Allelic variation of Escherichia coli outer membrane protein A: Impact on cell surface properties, stress tolerance and allele distribution. PLOS ONE 17, e0276046. https://doi.org/10.1371/journal.pone.0276046
Liebschner, D., Afonine, P.V., Baker, M.L., Bunkóczi, G., Chen, V.B., Croll, T.I., Hintze, B., Hung, L.-W., Jain, S., McCoy, A.J., Moriarty, N.W., Oeffner, R.D., Poon, B.K., Prisant, M.G., Read, R.J., Richardson, J.S., Richardson, D.C., Sammito, M.D., Sobolev, O.V., Stockwell, D.H., Terwilliger, T.C., Urzhumtsev, A.G., Videau, L.L., Williams, C.J., Adams, P.D., 2019. Macromolecular structure determination using X-rays, neutrons and electrons: recent developments in Phenix. Acta Crystallographica Section D 75, 861–877. https://doi.org/10.1107/S2059798319011471
Lithgow, T., Stubenrauch, C.J., Stumpf, M.P.H., 2023. Surveying membrane landscapes: a new look at the bacterial cell surface. Nat Rev Microbiol 21, 502–518. https://doi.org/10.1038/s41579-023-00862-w

Liu, B., Furevi, A., Perepelov, A.V., Guo, X., Cao, H., Wang, Q., Reeves, P.R., Knirel, Y.A., Wang, L., Widmalm, G., 2019. Structure and genetics of Escherichia coli O antigens. FEMS Microbiol Rev 44, 655–683. https://doi.org/10.1093/femsre/fuz028

Low, W.-Y., Thong, S., Chng, S.-S., 2021. ATP disrupts lipid-binding equilibrium to drive retrograde transport critical for bacterial outer membrane asymmetry. Proceedings of the National Academy of Sciences 118, e2110055118. https://doi.org/10.1073/pnas.2110055118

Lu, J., Peng, Y., Arutyunov, D., Frost, L.S., Glover, J.N.M., 2012. Error-Prone PCR Mutagenesis Reveals Functional Domains of a Bacterial Transcriptional Activator, TraJ. J Bacteriol 194, 3670–3677. https://doi.org/10.1128/JB.00312-12

Lu, J., Peng, Y., Wan, S., Frost, L.S., Raivio, T., Glover, J.N.M., 2018. Cooperative Function of TraJ and ArcA in Regulating the F Plasmid tra Operon. J Bacteriol 201, e00448-18. https://doi.org/10.1128/JB.00448-18

Luo, Q., Wang, C., Qiao, S., Yu, S., Chen, L., Kim, S., Wang, K., Zheng, J., Zhang, Y., Wu, F., Lei, X., Lou, J., Hennig, M., Im, W., Miao, L., Zhou, M., Huang, Y., 2022. Lipoprotein sorting to the cell surface via a crosstalk between the Lpt and Lol pathways during outer membrane biogenesis. https://doi.org/10.1101/2022.12.25.521893

Lycklama a Nijeholt, J.A., Driessen, A.J.M., 2012. The bacterial Sec-translocase: structure and mechanism. Philos Trans R Soc Lond B Biol Sci 367, 1016–1028. https://doi.org/10.1098/rstb.2011.0201

Ma, Q., Wood, T.K., 2009. OmpA influences *Escherichia coli* biofilm formation by repressing cellulose production through the CpxRA two-component system. Environmental Microbiology 11, 2735–2746. https://doi.org/10.1111/j.1462-2920.2009.02000.x

Machin, J.M., Kalli, A.C., Ranson, N.A., Radford, S.E., 2023. Protein–lipid charge interactions control the folding of outer membrane proteins into asymmetric membranes. Nat. Chem. 15, 1754–1764. https://doi.org/10.1038/s41557-023-01319-6

MacRitchie, D.M., Acosta, N., Raivio, T.L., 2012. DegP Is Involved in Cpx-Mediated Posttranscriptional Regulation of the Type III Secretion Apparatus in Enteropathogenic Escherichia coli. Infect Immun 80, 1766–1772. https://doi.org/10.1128/IAI.05679-11

MacRitchie, D.M., Ward, J.D., Nevesinjac, A.Z., Raivio, T.L., 2008. Activation of the Cpx Envelope Stress Response Down-Regulates Expression of Several Locus of Enterocyte Effacement-Encoded Genes in Enteropathogenic *Escherichia coli*. Infect Immun 76, 1465–1475. https://doi.org/10.1128/IAI.01265-07

Magnet, S., Bellais, S., Dubost, L., Fourgeaud, M., Mainardi, J.-L., Petit-Frère, S., Marie, A., Mengin-Lecreulx, D., Arthur, M., Gutmann, L., 2007. Identification of the l,d-Transpeptidases Responsible for Attachment of the Braun Lipoprotein to Escherichia coli Peptidoglycan. Journal of Bacteriology 189, 3927–3931. https://doi.org/10.1128/jb.00084-07

Maher, C., Hassan, K.A., 2023. The Gram-negative permeability barrier: tipping the balance of the in and the out. mBio 14, e01205-23. https://doi.org/10.1128/mbio.01205-23

Majdalani, N., Gottesman, S., 2005. The Rcs phosphorelay: a complex signal transduction system. Annu Rev Microbiol 59, 379–405. https://doi.org/10.1146/annurev.micro.59.050405.101230

Majdalani, N., Heck, M., Stout, V., Gottesman, S., 2005. Role of RcsF in Signaling to the Rcs Phosphorelay Pathway in Escherichia coli. J Bacteriol 187, 6770–6778. https://doi.org/10.1128/JB.187.19.6770-6778.2005

Majdalani, N., Hernandez, D., Gottesman, S., 2002. Regulation and mode of action of the second small RNA activator of RpoS translation, RprA. Mol Microbiol 46, 813–826. https://doi.org/10.1046/j.1365-2958.2002.03203.x

Malinverni, J.C., Silhavy, T.J., 2009. An ABC transport system that maintains lipid asymmetry in the gram-negative outer membrane. Proc Natl Acad Sci U S A 106, 8009–8014. https://doi.org/10.1073/pnas.0903229106
Malojčić, G., Andres, D., Grabowicz, M., George, A.H., Ruiz, N., Silhavy, T.J., Kahne, D., 2014. LptE binds to and alters the physical state of LPS to catalyze its assembly at the cell surface. Proceedings of the National Academy of Sciences 111, 9467–9472. https://doi.org/10.1073/pnas.1402746111
Maloney, P.C., Kashket, E.R., Wilson, T.H., 1974. A Protonmotive Force Drives ATP Synthesis in Bacteria. Proc Natl Acad Sci U S A 71, 3896–3900.
Mamou, G., Corona, F., Cohen-Khait, R., Housden, N.G., Yeung, V., Sun, D., Sridhar, P., Pazos, M., Knowles, T.J., Kleanthous, C., Vollmer, W., 2022. Peptidoglycan maturation controls outer membrane protein assembly. Nature 606, 953–959. https://doi.org/10.1038/s41586-022-04834-7
Mandela, E., Stubenrauch, C.J., Ryoo, D., Hwang, H., Cohen, E.J., Torres, V.L., Deo, P., Webb, C.T., Huang, C., Schittenhelm, R.B., Beeby, M., Gumbart, J., Lithgow, T., Hay, I.D., n.d. Adaptation of the periplasm to maintain spatial constraints essential for cell envelope processes and cell viability. eLife 11, e73516. https://doi.org/10.7554/eLife.73516
Marcoux, J., Politis, A., Rinehart, D., Marshall, D.P., Wallace, M.I., Tamm, L.K., Robinson, C.V., 2014. Mass Spectrometry Defines the C-Terminal Dimerization Domain and Enables Modeling of the Structure of Full-Length OmpA. Structure 22, 781–790. https://doi.org/10.1016/j.str.2014.03.004
Marotta, J., May, K.L., Bae, C.Y., Grabowicz, M., 2023a. Molecular insights into Escherichia coli Cpx envelope stress response activation by the sensor lipoprotein NlpE. Molecular Microbiology 119, 586–598. https://doi.org/10.1111/mmi.15054
Marotta, J., May, K.L., Bae, C.Y., Grabowicz, M., 2023b. Molecular insights into *Escherichia coli* Cpx envelope stress response activation by the sensor lipoprotein NL p E. Molecular Microbiology mmi.15054. https://doi.org/10.1111/mmi.15054
Marx, D.C., Plummer, A.M., Faustino, A.M., Devlin, T., Roskopf, M.A., Leblanc, M.J., Lessen, H.J., Amann, B.T., Fleming, P.J., Krueger, S., Fried, S.D., Fleming, K.G., 2020. SurA is a cryptically grooved chaperone that expands unfolded outer membrane proteins. Proceedings of the National Academy of Sciences 117, 28026–28035. https://doi.org/10.1073/pnas.2008175117
Mascarenhas, N.M., Gosavi, S., 2017. Understanding protein domain-swapping using structure-based models of protein folding. Prog Biophys Mol Biol 128, 113–120. https://doi.org/10.1016/j.pbiomolbio.2016.09.013
Mascher, T., Helmann, J.D., Unden, G., 2006. Stimulus Perception in Bacterial Signal-Transducing Histidine Kinases. Microbiol Mol Biol Rev 70, 910–938. https://doi.org/10.1128/MMBR.00020-06
Masi, M., Pinet, E., Pagès, J.-M., 2020. Complex Response of the CpxAR Two-Component System to β-Lactams on Antibiotic Resistance and Envelope Homeostasis in Enterobacteriaceae. Antimicrob Agents Chemother 64, e00291-20. https://doi.org/10.1128/AAC.00291-20
Mathelié-Guinlet, M., Asmar, A.T., Collet, J.-F., Dufrêne, Y.F., 2020. Lipoprotein Lpp regulates the mechanical properties of the E. coli cell envelope. Nat Commun 11, 1789. https://doi.org/10.1038/s41467-020-15489-1
May, K.L., Lehman, K.M., Mitchell, A.M., Grabowicz, M., 2019. A Stress Response Monitoring Lipoprotein Trafficking to the Outer Membrane. mBio 10, e00618-19. https://doi.org/10.1128/mBio.00618-19
May, K.L., Silhavy, T.J., 2018. The Escherichia coli Phospholipase PldA Regulates Outer Membrane Homeostasis via Lipid Signaling. mBio 9, 10.1128/mbio.00379-18. https://doi.org/10.1128/mbio.00379-18

McCoy, A.J., Grosse-Kunstleve, R.W., Adams, P.D., Winn, M.D., Storoni, L.C., Read, R.J., 2007. Phaser crystallographic software. Journal of Applied Crystallography 40, 658–674. https://doi.org/10.1107/S0021889807021206
McDonald, C., Jovanovic, G., Ces, O., Buck, M., 2015. Membrane Stored Curvature Elastic Stress Modulates Recruitment of Maintenance Proteins PspA and Vipp1. mBio 6, e01188-01115. https://doi.org/10.1128/mBio.01188-15
McEwen, J., Sambucetti, L., Silverman, P.M., 1983. Synthesis of outer membrane proteins in cpxA cpxB mutants of Escherichia coli K-12. J Bacteriol 154, 375–382. https://doi.org/10.1128/jb.154.1.375-382.1983
McEwen, J., Silverman, P., 1980a. Genetic analysis of Escherichia coli K-12 chromosomal mutants defective in expression of F-plasmid functions: identification of genes cpxA and cpxB. J Bacteriol 144, 60–67. https://doi.org/10.1128/jb.144.1.60-67.1980
McEwen, J., Silverman, P., 1980b. Chromosomal mutations of Escherichia coli that alter expression of conjugative plasmid functions. Proc. Natl. Acad. Sci. U.S.A. 77, 513–517. https://doi.org/10.1073/pnas.77.1.513
McEwen, J., Silverman, P., 1980c. Mutations in genes cpxA and cpxB of Escherichia coli K-12 cause a defect in isoleucine and valine syntheses. J Bacteriol 144, 68–73. https://doi.org/10.1128/jb.144.1.68-73.1980
McEwen, J., Silverman, P.M., 1982. Mutations in genes cpxA and cpxB alter the protein composition of Escherichia coli inner and outer membranes. J Bacteriol 151, 1553–1559. https://doi.org/10.1128/jb.151.3.1553-1559.1982
McLeod, S.M., Fleming, P.R., MacCormack, K., McLaughlin, R.E., Whiteaker, J.D., Narita, S., Mori, M., Tokuda, H., Miller, A.A., 2015. Small-Molecule Inhibitors of Gram-Negative Lipoprotein Trafficking Discovered by Phenotypic Screening. J Bacteriol 197, 1075–1082. https://doi.org/10.1128/JB.02352-14
Mechaly, A.E., Diaz, S.S., Sassoon, N., Buschiazzo, A., Betton, J.-M., Alzari, P.M., 2017. Structural Coupling between Autokinase and Phosphotransferase Reactions in a Bacterial Histidine Kinase. Structure 25, 939-944.e3. https://doi.org/10.1016/j.str.2017.04.011
Mechaly, A.E., Haouz, A., Sassoon, N., Buschiazzo, A., Betton, J.-M., Alzari, P.M., 2018. Conformational plasticity of the response regulator CpxR, a key player in Gammaproteobacteria virulence and drug-resistance. Journal of Structural Biology 204, 165–171. https://doi.org/10.1016/j.jsb.2018.08.001
Mechaly, A.E., Sassoon, N., Betton, J.-M., Alzari, P.M., 2014. Segmental Helical Motions and Dynamical Asymmetry Modulate Histidine Kinase Autophosphorylation. PLoS Biol 12, e1001776. https://doi.org/10.1371/journal.pbio.1001776
Megrian, D., Taib, N., Witwinowski, J., Beloin, C., Gribaldo, S., 2020. One or two membranes? Diderm Firmicutes challenge the Gram-positive/Gram-negative divide. Mol Microbiol 113, 659–671. https://doi.org/10.1111/mmi.14469
Mensa, B., Polizzi, N.F., Molnar, K.S., Natale, A.M., Lemmin, T., DeGrado, W.F., 2021. Allosteric mechanism of signal transduction in the two-component system histidine kinase PhoQ. eLife 10, e73336. https://doi.org/10.7554/eLife.73336
Mi, W., Li, Y., Yoon, S.H., Ernst, R.K., Walz, T., Liao, M., 2017. Structural basis of MsbA-mediated lipopolysaccharide transport. Nature 549, 233–237. https://doi.org/10.1038/nature23649
Mikheyeva, I.V., Sun, J., Huang, K.C., Silhavy, T.J., 2023. Mechanism of outer membrane destabilization by global reduction of protein content. Nat Commun 14, 5715. https://doi.org/10.1038/s41467-023-40396-6
Mileykovskaya, E., Dowhan, W., 1997. The Cpx two-component signal transduction pathway is activated in Escherichia coli mutant strains lacking phosphatidylethanolamine. J Bacteriol 179, 1029–1034. https://doi.org/10.1128/jb.179.4.1029-1034.1997

Miller, J.H., 1972. Experiments in molecular genetics. Cold Spring Harbor Laboratory.
Miller, S.I., Salama, N.R., 2018. The gram-negative bacterial periplasm: Size matters. PLoS Biol 16, e2004935. https://doi.org/10.1371/journal.pbio.2004935
Miot, M., Betton, J.-M., 2004. Protein quality control in the bacterial periplasm. Microb Cell Fact 3, 4. https://doi.org/10.1186/1475-2859-3-4
Mirdita, M., Schütze, K., Moriwaki, Y., Heo, L., Ovchinnikov, S., Steinegger, M., 2022. ColabFold: making protein folding accessible to all. Nat Methods 19, 679–682. https://doi.org/10.1038/s41592-022-01488-1
Misra, R., Miao, Y., 1995. Molecular analysis of asmA, a locus identified as the suppressor of OmpF assembly mutants of Escherichia coli K-12. Mol Microbiol 16, 779–788. https://doi.org/10.1111/j.1365-2958.1995.tb02439.x
Mitchell, A.M., Silhavy, T.J., 2019. Envelope stress responses: balancing damage repair and toxicity. Nat Rev Microbiol 17, 417–428. https://doi.org/10.1038/s41579-019-0199-0
Mitra, R., Gadkari, V.V., Meinen, B.A., van Mierlo, C.P.M., Ruotolo, B.T., Bardwell, J.C.A., 2021. Mechanism of the small ATP-independent chaperone Spy is substrate specific. Nat Commun 12, 851. https://doi.org/10.1038/s41467-021-21120-8
Mitrophanov, A.Y., Groisman, E.A., 2008. Signal integration in bacterial two-component regulatory systems. Genes Dev 22, 2601–2611. https://doi.org/10.1101/gad.1700308
Miyadai, H., Tanaka-Masuda, K., Matsuyama, S., Tokuda, H., 2004. Effects of Lipoprotein Overproduction on the Induction of DegP (HtrA) Involved in Quality Control in the Escherichia coli Periplasm. Journal of Biological Chemistry 279, 39807–39813. https://doi.org/10.1074/jbc.M406390200
Mizutani, M., Mukaiyama, K., Xiao, J., Mori, M., Satou, R., Narita, S., Okuda, S., Tokuda, H., 2013. Functional differentiation of structurally similar membrane subunits of the ABC transporter LolCDE complex. FEBS Letters 587, 23–29. https://doi.org/10.1016/j.febslet.2012.11.009
Moffatt, J.H., Harper, M., Harrison, P., Hale, J.D.F., Vinogradov, E., Seemann, T., Henry, R., Crane, B., St Michael, F., Cox, A.D., Adler, B., Nation, R.L., Li, J., Boyce, J.D., 2010. Colistin resistance in Acinetobacter baumannii is mediated by complete loss of lipopolysaccharide production. Antimicrob Agents Chemother 54, 4971–4977. https://doi.org/10.1128/AAC.00834-10
Möglich, A., Ayers, R.A., Moffat, K., 2009. Structure and Signaling Mechanism of Per-ARNT-Sim Domains. Structure 17, 1282–1294. https://doi.org/10.1016/j.str.2009.08.011
Morè, N., Martorana, A.M., Biboy, J., Otten, C., Winkle, M., Serrano, C.K.G., Montón Silva, A., Atkinson, L., Yau, H., Breukink, E., den Blaauwen, T., Vollmer, W., Polissi, A., 2019. Peptidoglycan Remodeling Enables Escherichia coli To Survive Severe Outer Membrane Assembly Defect. mBio 10, 10.1128/mbio.02729-18. https://doi.org/10.1128/mbio.02729-18
Morgenstein, R.M., Rather, P.N., 2012. Role of the Umo Proteins and the Rcs Phosphorelay in the Swarming Motility of the Wild Type and an O-Antigen (*waaL*) Mutant of Proteus mirabilis. J Bacteriol 194, 669–676. https://doi.org/10.1128/JB.06047-11
Mori, H., Ito, K., 2001. The Sec protein-translocation pathway. Trends in Microbiology 9, 494–500. https://doi.org/10.1016/S0966-842X(01)02174-6
Moukhametzianov, R., Klare, J.P., Efremov, R., Baeken, C., Göppner, A., Labahn, J., Engelhard, M., Büldt, G., Gordeliy, V.I., 2006. Development of the signal in sensory rhodopsin and its transfer to the cognate transducer. Nature 440, 115–119. https://doi.org/10.1038/nature04520
Mouslim, C., Groisman, E.A., 2003. Control of the Salmonella ugd gene by three two-component regulatory systems. Mol Microbiol 47, 335–344. https://doi.org/10.1046/j.1365-2958.2003.03318.x

Mukhopadhyay, A., Kumar, M., 2023. Phage Shock Protein-Mediated Stress Response in Bacteria, in: Microbial Stress Response: Mechanisms and Data Science, ACS Symposium Series. American Chemical Society, pp. 43–57. https://doi.org/10.1021/bk-2023-1434.ch003

Murata, T., Tseng, W., Guina, T., Miller, S.I., Nikaido, H., 2007. PhoPQ-Mediated Regulation Produces a More Robust Permeability Barrier in the Outer Membrane of Salmonella enterica Serovar Typhimurium. J Bacteriol 189, 7213–7222. https://doi.org/10.1128/JB.00973-07

Murray, C.J.L., Ikuta, K.S., Sharara, F., Swetschinski, L., Robles Aguilar, G., Gray, A., Han, C., Bisignano, C., Rao, P., Wool, E., Johnson, S.C., Browne, A.J., Chipeta, M.G., Fell, F., Hackett, S., Haines-Woodhouse, G., Kashef Hamadani, B.H., Kumaran, E.A.P., McManigal, B., Achalapong, S., Agarwal, R., Akech, S., Albertson, S., Amuasi, J., Andrews, J., Aravkin, A., Ashley, E., Babin, F.-X., Bailey, F., Baker, S., Basnyat, B., Bekker, A., Bender, R., Berkley, J.A., Bethou, A., Bielicki, J., Boonkasidecha, S., Bukosia, J., Carvalheiro, C., Castañeda-Orjuela, C., Chansamouth, V., Chaurasia, S., Chiurchiù, S., Chowdhury, F., Clotaire Donatien, R., Cook, A.J., Cooper, B., Cressey, T.R., Criollo-Mora, E., Cunningham, M., Darboe, S., Day, N.P.J., De Luca, M., Dokova, K., Dramowski, A., Dunachie, S.J., Duong Bich, T., Eckmanns, T., Eibach, D., Emami, A., Feasey, N., Fisher-Pearson, N., Forrest, K., Garcia, C., Garrett, D., Gastmeier, P., Giref, A.Z., Greer, R.C., Gupta, V., Haller, S., Haselbeck, A., Hay, S.I., Holm, M., Hopkins, S., Hsia, Y., Iregbu, K.C., Jacobs, J., Jarovsky, D., Javanmardi, F., Jenney, A.W.J., Khorana, M., Khusuwan, S., Kissoon, N., Kobeissi, E., Kostyanev, T., Krapp, F., Krumkamp, R., Kumar, A., Kyu, H.H., Lim, C., Lim, K., Limmathurotsakul, D., Loftus, M.J., Lunn, M., Ma, J., Manoharan, A., Marks, F., May, J., Mayxay, M., Mturi, N., Munera-Huertas, T., Musicha, P., Musila, L.A., Mussi-Pinhata, M.M., Naidu, R.N., Nakamura, T., Nanavati, R., Nangia, S., Newton, P., Ngoun, C., Novotney, A., Nwakanma, D., Obiero, C.W., Ochoa, T.J., Olivas-Martinez, A., Olliaro, P., Ooko, E., Ortiz-Brizuela, E., Ounchanum, P., Pak, G.D., Paredes, J.L., Peleg, A.Y., Perrone, C., Phe, T., Phommasone, K., Plakkal, N., Ponce-de-Leon, A., Raad, M., Ramdin, T., Rattanavong, S., Riddell, A., Roberts, T., Robotham, J.V., Roca, A., Rosenthal, V.D., Rudd, K.E., Russell, N., Sader, H.S., Saengchan, W., Schnall, J., Scott, J.A.G., Seekaew, S., Sharland, M., Shivamallappa, M., Sifuentes-Osornio, J., Simpson, A.J., Steenkeste, N., Stewardson, A.J., Stoeva, T., Tasak, N., Thaiprakong, A., Thwaites, G., Tigoi, C., Turner, C., Turner, P., van Doorn, H.R., Velaphi, S., Vongpradith, A., Vongsouvath, M., Vu, H., Walsh, T., Walson, J.L., Waner, S., Wangrangsimakul, T., Wannapinij, P., Wozniak, T., Young Sharma, T.E.M.W., Yu, K.C., Zheng, P., Sartorius, B., Lopez, A.D., Stergachis, A., Moore, C., Dolecek, C., Naghavi, M., 2022. Global burden of bacterial antimicrobial resistance in 2019: a systematic analysis. The Lancet 399, 629–655. https://doi.org/10.1016/S0140-6736(21)02724-0

Mychack, A., Amrutha, R.N., Chung, C., Cardenas Arevalo, K., Reddy, M., Janakiraman, A., 2019. A synergistic role for two predicted inner membrane proteins of *Escherichia coli* in cell envelope integrity. Mol Microbiol 111, 317–337. https://doi.org/10.1111/mmi.14157

Mychack, A., Janakiraman, A., 2021. Defects in The First Step of Lipoprotein Maturation Underlie The Synthetic Lethality of Escherichia coli Lacking The Inner Membrane Proteins YciB And DcrB. J Bacteriol 203, e00640-20, JB.00640-20. https://doi.org/10.1128/JB.00640-20

Nagakubo, S., Nishino, K., Hirata, T., Yamaguchi, A., 2002. The putative response regulator BaeR stimulates multidrug resistance of Escherichia coli via a novel multidrug exporter system, MdtABC. J Bacteriol 184, 4161–4167. https://doi.org/10.1128/JB.184.15.4161-4167.2002

Narita, S., Tokuda, H., 2017. Bacterial lipoproteins; biogenesis, sorting and quality control. Biochimica et Biophysica Acta (BBA) - Molecular and Cell Biology of Lipids 1862, 1414–1423. https://doi.org/10.1016/j.bbalip.2016.11.009

Natale, P., Brüser, T., Driessen, A.J.M., 2008. Sec- and Tat-mediated protein secretion across the bacterial cytoplasmic membrane—Distinct translocases and mechanisms. Biochimica et Biophysica Acta (BBA) - Biomembranes 1778, 1735–1756. https://doi.org/10.1016/j.bbamem.2007.07.015

Nevesinjac, A.Z., Raivio, T.L., 2005. The Cpx Envelope Stress Response Affects Expression of the Type IV Bundle-Forming Pili of Enteropathogenic *Escherichia coli*. J Bacteriol 187, 672–686. https://doi.org/10.1128/JB.187.2.672-686.2005

Newell, N.E., 2015. Mapping side chain interactions at protein helix termini. BMC Bioinformatics 16, 231. https://doi.org/10.1186/s12859-015-0671-4

Nickerson, N.N., Jao, C.C., Xu, Y., Quinn, J., Skippington, E., Alexander, M.K., Miu, A., Skelton, N., Hankins, J.V., Lopez, M.S., Koth, C.M., Rutherford, S., Nishiyama, M., 2018. A Novel Inhibitor of the LolCDE ABC Transporter Essential for Lipoprotein Trafficking in Gram-Negative Bacteria. Antimicrob Agents Chemother 62, e02151-17. https://doi.org/10.1128/AAC.02151-17

Nikaido, H., 2003. Molecular Basis of Bacterial Outer Membrane Permeability Revisited. Microbiol Mol Biol Rev 67, 593–656. https://doi.org/10.1128/MMBR.67.4.593-656.2003

Nishino, K., Honda, T., Yamaguchi, A., 2005. Genome-wide analyses of Escherichia coli gene expression responsive to the BaeSR two-component regulatory system. J Bacteriol 187, 1763–1772. https://doi.org/10.1128/JB.187.5.1763-1772.2005

Noinaj, N., Guillier, M., Barnard, T.J., Buchanan, S.K., 2010. TonB-Dependent Transporters: Regulation, Structure, and Function. Annu. Rev. Microbiol. 64, 43–60. https://doi.org/10.1146/annurev.micro.112408.134247

Noinaj, N., Kuszak, A.J., Balusek, C., Gumbart, J.C., Buchanan, S.K., 2014. Lateral opening and exit pore formation are required for BamA function. Structure 22, 1055–1062. https://doi.org/10.1016/j.str.2014.05.008

Noland, C.L., Kattke, M.D., Diao, J., Gloor, S.L., Pantua, H., Reichelt, M., Katakam, A.K., Yan, D., Kang, J., Zilberleyb, I., Xu, M., Kapadia, S.B., Murray, J.M., 2017. Structural insights into lipoprotein N-acylation by Escherichia coli apolipoprotein N-acyltransferase. Proceedings of the National Academy of Sciences 114, E6044–E6053. https://doi.org/10.1073/pnas.1707813114

Okuda, S., Freinkman, E., Kahne, D., 2012. Cytoplasmic ATP Hydrolysis Powers Transport of Lipopolysaccharide Across the Periplasm in E. coli. Science 338, 1214–1217. https://doi.org/10.1126/science.1228984

Okuda, S., Sherman, D.J., Silhavy, T.J., Ruiz, N., Kahne, D., 2016. Lipopolysaccharide transport and assembly at the outer membrane: the PEZ model. Nat Rev Microbiol 14, 337–345. https://doi.org/10.1038/nrmicro.2016.25

Okuda, S., Tokuda, H., 2011. Lipoprotein Sorting in Bacteria. Annu. Rev. Microbiol. 65, 239–259. https://doi.org/10.1146/annurev-micro-090110-102859

Olatunji, S., Yu, X., Bailey, J., Huang, C.-Y., Zapotoczna, M., Bowen, K., Remškar, M., Müller, R., Scanlan, E.M., Geoghegan, J.A., Olieric, V., Caffrey, M., 2020. Structures of lipoprotein signal peptidase II from Staphylococcus aureus complexed with antibiotics globomycin and myxovirescin. Nat Commun 11, 140. https://doi.org/10.1038/s41467-019-13724-y

O'Neal, L., Baraquet, C., Suo, Z., Dreifus, J.E., Peng, Y., Raivio, T.L., Wozniak, D.J., Harwood, C.S., Parsek, M.R., 2022. The Wsp system of Pseudomonas aeruginosa links surface sensing and cell envelope stress. Proceedings of the National Academy of Sciences 119, e2117633119. https://doi.org/10.1073/pnas.2117633119

Onufryk, C., Crouch, M.-L., Fang, F.C., Gross, C.A., 2005. Characterization of six lipoproteins in the sigmaE regulon. J Bacteriol 187, 4552–4561. https://doi.org/10.1128/JB.187.13.4552-4561.2005
Orme, R., Douglas, C.W.I., Rimmer, S., Webb, M., 2006. Proteomic analysis ofEscherichia coli biofilms reveals the overexpression of the outer membrane protein OmpA. Proteomics 6, 4269–4277. https://doi.org/10.1002/pmic.200600193
Ortiz-Suarez, M.L., Samsudin, F., Piggot, T.J., Bond, P.J., Khalid, S., 2016. Full-Length OmpA: Structure, Function, and Membrane Interactions Predicted by Molecular Dynamics Simulations. Biophysical Journal 111, 1692–1702. https://doi.org/10.1016/j.bpj.2016.09.009
Oswald, J., Njenga, R., Natriashvili, A., Sarmah, P., Koch, H.-G., 2021. The Dynamic SecYEG Translocon. Front. Mol. Biosci. 8. https://doi.org/10.3389/fmolb.2021.664241
O'Toole, G., Kaplan, H.B., Kolter, R., 2000. Biofilm Formation as Microbial Development. Annu. Rev. Microbiol. 54, 49–79. https://doi.org/10.1146/annurev.micro.54.1.49
O'Toole, G.A., Wong, G.C., 2016. Sensational biofilms: surface sensing in bacteria. Current Opinion in Microbiology 30, 139–146. https://doi.org/10.1016/j.mib.2016.02.004
Otto, K., Silhavy, T.J., 2002. Surface sensing and adhesion of *Escherichia coli* controlled by the Cpx-signaling pathway. Proc. Natl. Acad. Sci. U.S.A. 99, 2287–2292. https://doi.org/10.1073/pnas.042521699
Ouellette, S.P., Gauliard, E., Antosová, Z., Ladant, D., 2014. A Gateway ® -compatible bacterial adenylate cyclase-based two-hybrid system: A Gateway-compatible bacterial two-hybrid system. Environmental Microbiology Reports 6, 259–267. https://doi.org/10.1111/1758-2229.12123
Palmer, T., Berks, B.C., 2012. The twin-arginine translocation (Tat) protein export pathway. Nat Rev Microbiol 10, 483–496. https://doi.org/10.1038/nrmicro2814
Pardue, E.J., Sartorio, M.G., Jana, B., Scott, N.E., Beatty, W.L., Ortiz-Marquez, J.C., Van Opijnen, T., Hsu, F.-F., Potter, R.F., Feldman, M.F., 2024. Dual membrane-spanning anti-sigma factors regulate vesiculation in Bacteroides thetaiotaomicron. Proceedings of the National Academy of Sciences 121, e2321910121. https://doi.org/10.1073/pnas.2321910121
Park, H., Kim, Y.T., Choi, C., Kim, S., 2017. Tripodal Lipoprotein Variants with C-Terminal Hydrophobic Residues Allosterically Modulate Activity of the DegP Protease. Journal of Molecular Biology 429, 3090–3101. https://doi.org/10.1016/j.jmb.2017.09.011
Park, J.S., Lee, W.C., Yeo, K.J., Ryu, K., Kumarasiri, M., Hesek, D., Lee, M., Mobashery, S., Song, J.H., Kim, S.I., Lee, J.C., Cheong, C., Jeon, Y.H., Kim, H., 2012. Mechanism of anchoring of OmpA protein to the cell wall peptidoglycan of the gram-negative bacterial outer membrane. FASEB j. 26, 219–228. https://doi.org/10.1096/fj.11-188425
Perez, J.C., Shin, D., Zwir, I., Latifi, T., Hadley, T.J., Groisman, E.A., 2009. Evolution of a Bacterial Regulon Controlling Virulence and Mg2+ Homeostasis. PLOS Genetics 5, e1000428. https://doi.org/10.1371/journal.pgen.1000428
Persat, A., 2017. Bacterial mechanotransduction. Curr Opin Microbiol 36, 1–6. https://doi.org/10.1016/j.mib.2016.12.002
Persat, A., Inclan, Y.F., Engel, J.N., Stone, H.A., Gitai, Z., 2015. Type IV pili mechanochemically regulate virulence factors in Pseudomonas aeruginosa. Proceedings of the National Academy of Sciences 112, 7563–7568. https://doi.org/10.1073/pnas.1502025112
Petit-Härtlein, I., Rome, K., de Rosny, E., Molton, F., Duboc, C., Gueguen, E., Rodrigue, A., Covès, J., 2015. Biophysical and physiological characterization of ZraP from *Escherichia coli* , the periplasmic accessory protein of the atypical ZraSR two-component system. Biochemical Journal 472, 205–216. https://doi.org/10.1042/BJ20150827

Pogliano, J., Lynch, A.S., Belin, D., Lin, E.C., Beckwith, J., 1997. Regulation of Escherichia coli cell envelope proteins involved in protein folding and degradation by the Cpx two-component system. Genes Dev. 11, 1169–1182. https://doi.org/10.1101/gad.11.9.1169
Poole, K., Hay, T., Gilmour, C., Fruci, M., 2019. The aminoglycoside resistance-promoting AmgRS envelope stress-responsive two-component system in Pseudomonas aeruginosa is zinc-activated and protects cells from zinc-promoted membrane damage. Microbiology 165, 563–571. https://doi.org/10.1099/mic.0.000787
Powers, M.J., Simpson, B.W., Trent, M.S., 2020. The Mla pathway in Acinetobacter baumannii has no demonstrable role in anterograde lipid transport. eLife 9, e56571. https://doi.org/10.7554/eLife.56571
Powers, M.J., Trent, M.S., 2019. Intermembrane transport: Glycerophospholipid homeostasis of the Gram-negative cell envelope. Proceedings of the National Academy of Sciences 116, 17147–17155. https://doi.org/10.1073/pnas.1902026116
Price, N.L., Raivio, T.L., 2009. Characterization of the Cpx Regulon in *Escherichia coli* Strain MC4100. J Bacteriol 191, 1798–1815. https://doi.org/10.1128/JB.00798-08
Prigent-Combaret, C., Brombacher, E., Vidal, O., Ambert, A., Lejeune, P., Landini, P., Dorel, C., 2001. Complex Regulatory Network Controls Initial Adhesion and Biofilm Formation in *Escherichia coli* via Regulation of the *csgD* Gene. J Bacteriol 183, 7213–7223. https://doi.org/10.1128/JB.183.24.7213-7223.2001
Prost, L.R., Daley, M.E., Le Sage, V., Bader, M.W., Le Moual, H., Klevit, R.E., Miller, S.I., 2007. Activation of the bacterial sensor kinase PhoQ by acidic pH. Mol Cell 26, 165–174. https://doi.org/10.1016/j.molcel.2007.03.008
Qiao, S., Luo, Q., Zhao, Y., Zhang, X.C., Huang, Y., 2014. Structural basis for lipopolysaccharide insertion in the bacterial outer membrane. Nature 511, 108–111. https://doi.org/10.1038/nature13484
Quan, S., Koldewey, P., Tapley, T., Kirsch, N., Ruane, K.M., Pfizenmaier, J., Shi, R., Hofmann, S., Foit, L., Ren, G., Jakob, U., Xu, Z., Cygler, M., Bardwell, J.C.A., 2011. Genetic selection designed to stabilize proteins uncovers a chaperone called Spy. Nat Struct Mol Biol 18, 262–269. https://doi.org/10.1038/nsmb.2016
Raetz, C.R.H., Whitfield, C., 2002. Lipopolysaccharide endotoxins. Annu Rev Biochem 71, 635–700. https://doi.org/10.1146/annurev.biochem.71.110601.135414
Raffa, R.G., Raivio, T.L., 2002. A third envelope stress signal transduction pathway in Escherichia coli: Envelope stress signal transduction. Molecular Microbiology 45, 1599–1611. https://doi.org/10.1046/j.1365-2958.2002.03112.x
Rainwater, S., Silverman, P.M., 1990. The Cpx proteins of Escherichia coli K-12: evidence that cpxA, ecfB, ssd, and eup mutations all identify the same gene. J Bacteriol 172, 2456–2461. https://doi.org/10.1128/jb.172.5.2456-2461.1990
Raivio, T.L., 2019. Regulatory Systems: Two-Component, in: John Wiley & Sons, Ltd (Ed.), eLS. Wiley, pp. 1–16. https://doi.org/10.1002/9780470015902.a0000856.pub3
Raivio, T.L., 2014. Everything old is new again: An update on current research on the Cpx envelope stress response. Biochimica et Biophysica Acta (BBA) - Molecular Cell Research 1843, 1529–1541. https://doi.org/10.1016/j.bbamcr.2013.10.018
Raivio, T.L., 2005. MicroReview: Envelope stress responses and Gram-negative bacterial pathogenesis: Envelope stress responses and virulence. Molecular Microbiology 56, 1119–1128. https://doi.org/10.1111/j.1365-2958.2005.04625.x
Raivio, T.L., Laird, M.W., Joly, J.C., Silhavy, T.J., 2000. Tethering of CpxP to the inner membrane prevents spheroplast induction of the Cpx envelope stress response. Mol Microbiol 37, 1186–1197. https://doi.org/10.1046/j.1365-2958.2000.02074.x
Raivio, T.L., Leblanc, S.K.D., Price, N.L., 2013. The Escherichia coli Cpx Envelope Stress Response Regulates Genes of Diverse Function That Impact Antibiotic Resistance and Membrane Integrity. J Bacteriol 195, 2755–2767. https://doi.org/10.1128/JB.00105-13

Raivio, T.L., Popkin, D.L., Silhavy, T.J., 1999. The Cpx Envelope Stress Response Is Controlled by Amplification and Feedback Inhibition. J Bacteriol 181, 5263–5272. https://doi.org/10.1128/JB.181.17.5263-5272.1999
Raivio, T.L., Silhavy, T.J., 1997. Transduction of envelope stress in Escherichia coli by the Cpx two-component system. J Bacteriol 179, 7724–7733. https://doi.org/10.1128/jb.179.24.7724-7733.1997
Reinelt, S., Hofmann, E., Gerharz, T., Bott, M., Madden, D.R., 2003. The Structure of the Periplasmic Ligand-binding Domain of the Sensor Kinase CitA Reveals the First Extracellular PAS Domain*. Journal of Biological Chemistry 278, 39189–39196. https://doi.org/10.1074/jbc.M305864200
Rhodius, V.A., Suh, W.C., Nonaka, G., West, J., Gross, C.A., 2005. Conserved and Variable Functions of the σE Stress Response in Related Genomes. PLOS Biology 4, e2. https://doi.org/10.1371/journal.pbio.0040002
Rice, L.B., 2008. Federal funding for the study of antimicrobial resistance in nosocomial pathogens: no ESKAPE. J Infect Dis 197, 1079–1081. https://doi.org/10.1086/533452
Rodríguez-Alonso, R., Létoquart, J., Nguyen, V.S., Louis, G., Calabrese, A.N., Iorga, B.I., Radford, S.E., Cho, S.-H., Remaut, H., Collet, J.-F., 2020. Structural insight into the formation of lipoprotein-β-barrel complexes. Nat Chem Biol 16, 1019–1025. https://doi.org/10.1038/s41589-020-0575-0
Rojas, E.R., Billings, G., Odermatt, P.D., Auer, G.K., Zhu, L., Miguel, A., Chang, F., Weibel, D.B., Theriot, J.A., Huang, K.C., 2018. The outer membrane is an essential load-bearing element in Gram-negative bacteria. Nature 559, 617–621. https://doi.org/10.1038/s41586-018-0344-3
Rojas, E.R., Huang, K.C., 2018. Regulation of microbial growth by turgor pressure. Current Opinion in Microbiology, Cell Regulation 42, 62–70. https://doi.org/10.1016/j.mib.2017.10.015
Rome, K., Borde, C., Taher, R., Cayron, J., Lesterlin, C., Gueguen, E., De Rosny, E., Rodrigue, A., 2018. The Two-Component System ZraPSR Is a Novel ESR that Contributes to Intrinsic Antibiotic Tolerance in Escherichia coli. Journal of Molecular Biology 430, 4971–4985. https://doi.org/10.1016/j.jmb.2018.10.021
Rubin, E.J., Herrera, C.M., Crofts, A.A., Trent, M.S., 2015. PmrD Is Required for Modifications to Escherichia coli Endotoxin That Promote Antimicrobial Resistance. Antimicrob Agents Chemother 59, 2051–2061. https://doi.org/10.1128/AAC.05052-14
Ruiz, N., Davis, R.M., Kumar, S., 2021. YhdP, TamB, and YdbH Are Redundant but Essential for Growth and Lipid Homeostasis of the Gram-Negative Outer Membrane. mBio 12, e02714-21. https://doi.org/10.1128/mBio.02714-21
Sambucetti, L., Eoyang, L., Silverman, P.M., 1982. Cellular control of conjugation in Escherichia coli K12. Journal of Molecular Biology 161, 13–31. https://doi.org/10.1016/0022-2836(82)90275-3
Samsudin, F., Boags, A., Piggot, T.J., Khalid, S., 2017. Braun's Lipoprotein Facilitates OmpA Interaction with the Escherichia coli Cell Wall. Biophys J 113, 1496–1504. https://doi.org/10.1016/j.bpj.2017.08.011
Samsudin, F., Ortiz-Suarez, M.L., Piggot, T.J., Bond, P.J., Khalid, S., 2016. OmpA: A Flexible Clamp for Bacterial Cell Wall Attachment. Structure 24, 2227–2235. https://doi.org/10.1016/j.str.2016.10.009
Samuel, G., Reeves, P., 2003. Biosynthesis of O-antigens: genes and pathways involved in nucleotide sugar precursor synthesis and O-antigen assembly. Carbohydrate Research, Bacterial Antigens and Vaccines 338, 2503–2519. https://doi.org/10.1016/j.carres.2003.07.009
Sankaran, K., Wu, H.C., 1994. Lipid modification of bacterial prolipoprotein. Transfer of diacylglyceryl moiety from phosphatidylglycerol. J Biol Chem 269, 19701–19706.

Sardis, M.F., Bohrhunter, J.L., Greene, N.G., Bernhardt, T.G., 2021. The LpoA activator is required to stimulate the peptidoglycan polymerase activity of its cognate cell wall synthase PBP1a. Proc Natl Acad Sci U S A 118, e2108894118. https://doi.org/10.1073/pnas.2108894118

Sarkar, M.K., Paul, K., Blair, D., 2010. Chemotaxis signaling protein CheY binds to the rotor protein FliN to control the direction of flagellar rotation in Escherichia coli. Proc Natl Acad Sci U S A 107, 9370–9375. https://doi.org/10.1073/pnas.1000935107

Sato, T., Takano, A., Hori, N., Izawa, T., Eda, T., Sato, K., Umekawa, M., Miyagawa, H., Matsumoto, Kenji, Muramatsu-Fujishiro, A., Matsumoto, Kouji, Matsuoka, S., Hara, H., 2017. Role of the inner-membrane histidine kinase RcsC and outer-membrane lipoprotein RcsF in the activation of the Rcs phosphorelay signal transduction system in Escherichia coli. Microbiology 163, 1071–1080. https://doi.org/10.1099/mic.0.000483

Saul, F.A., Arié, J.-P., Vulliez-le Normand, B., Kahn, R., Betton, J.-M., Bentley, G.A., 2004. Structural and functional studies of FkpA from Escherichia coli, a cis/trans peptidyl-prolyl isomerase with chaperone activity. J Mol Biol 335, 595–608. https://doi.org/10.1016/j.jmb.2003.10.056

Sauvage, E., Kerff, F., Terrak, M., Ayala, J.A., Charlier, P., 2008. The penicillin-binding proteins: structure and role in peptidoglycan biosynthesis. FEMS Microbiology Reviews 32, 234–258. https://doi.org/10.1111/j.1574-6976.2008.00105.x

Scheurwater, E., Reid, C.W., Clarke, A.J., 2008. Lytic transglycosylases: Bacterial space-making autolysins. The International Journal of Biochemistry & Cell Biology 40, 586–591. https://doi.org/10.1016/j.biocel.2007.03.018

Schiffrin, B., Calabrese, A.N., Devine, P.W.A., Harris, S.A., Ashcroft, A.E., Brockwell, D.J., Radford, S.E., 2016. Skp is a multivalent chaperone of outer-membrane proteins. Nat Struct Mol Biol 23, 786–793. https://doi.org/10.1038/nsmb.3266

Schultz, K.M., Lundquist, T.J., Klug, C.S., 2017. Lipopolysaccharide binding to the periplasmic protein LptA. Protein Sci 26, 1517–1523. https://doi.org/10.1002/pro.3177

Schulze, R.J., Zückert, W.R., 2006. Borrelia burgdorferi lipoproteins are secreted to the outer surface by default. Mol Microbiol 59, 1473–1484. https://doi.org/10.1111/j.1365-2958.2006.05039.x

Schwarzenbacher, R., Godzik, A., Grzechnik, S.K., Jaroszewski, L., 2004. The importance of alignment accuracy for molecular replacement. Acta Cryst D 60, 1229–1236. https://doi.org/10.1107/S0907444904010145

Sean Peacock, R., Weljie, A.M., Peter Howard, S., Price, F.D., Vogel, H.J., 2005. The Solution Structure of the C-terminal Domain of TonB and Interaction Studies with TonB Box Peptides. Journal of Molecular Biology 345, 1185–1197. https://doi.org/10.1016/j.jmb.2004.11.026

Seo, J., Savitzky, D.C., Ford, E., Darwin, A.J., 2007. Global analysis of tolerance to secretin-induced stress in Yersinia enterocolitica suggests that the phage-shock-protein system may be a remarkably self-contained stress response. Mol Microbiol 65, 714–727. https://doi.org/10.1111/j.1365-2958.2007.05821.x

Sevvana, M., Vijayan, V., Zweckstetter, M., Reinelt, S., Madden, D.R., Herbst-Irmer, R., Sheldrick, G.M., Bott, M., Griesinger, C., Becker, S., 2008. A Ligand-Induced Switch in the Periplasmic Domain of Sensor Histidine Kinase CitA. Journal of Molecular Biology 377, 512–523. https://doi.org/10.1016/j.jmb.2008.01.024

Sham, L.-T., Butler, E.K., Lebar, M.D., Kahne, D., Bernhardt, T.G., Ruiz, N., 2014. MurJ is the flippase of lipid-linked precursors for peptidoglycan biogenesis. Science 345, 220–222. https://doi.org/10.1126/science.1254522

Shiba, Y., Miyagawa, H., Nagahama, H., Matsumoto, Kenji, Kondo, D., Matsuoka, S., Matsumoto, Kouji, Hara, H., 2012. Exploring the relationship between lipoprotein

mislocalization and activation of the Rcs signal transduction system in Escherichia coli. Microbiology (Reading) 158, 1238–1248. https://doi.org/10.1099/mic.0.056945-0
Shimizu, T., Ichimura, K., Noda, M., 2016. The Surface Sensor NlpE of Enterohemorrhagic Escherichia coli Contributes to Regulation of the Type III Secretion System and Flagella by the Cpx Response to Adhesion. Infect Immun 84, 537–549. https://doi.org/10.1128/IAI.00881-15
Shimohata, N., Chiba, S., Saikawa, N., Ito, K., Akiyama, Y., 2002. The Cpx stress response system of Escherichia coli senses plasma membrane proteins and controls HtpX, a membrane protease with a cytosolic active site. Genes to Cells 7, 653–662.
Shrivastava, R., Chng, S.-S., 2019. Lipid trafficking across the Gram-negative cell envelope. Journal of Biological Chemistry 294, 14175–14184. https://doi.org/10.1074/jbc.AW119.008139
Shrivastava, R., Jiang, X., Chng, S.-S., 2017. Outer membrane lipid homeostasis via retrograde phospholipid transport in Escherichia coli. Molecular Microbiology 106, 395–408. https://doi.org/10.1111/mmi.13772
Silale, A., Zhu, Y., Witwinowski, J., Smith, R.E., Newman, K.E., Bhamidimarri, S.P., Baslé, A., Khalid, S., Beloin, C., Gribaldo, S., van den Berg, B., 2023. Dual function of OmpM as outer membrane tether and nutrient uptake channel in diderm Firmicutes. Nat Commun 14, 7152. https://doi.org/10.1038/s41467-023-42601-y
Silhavy, T.J., Kahne, D., Walker, S., 2010. The Bacterial Cell Envelope. Cold Spring Harbor Perspectives in Biology 2, a000414–a000414. https://doi.org/10.1101/cshperspect.a000414
Silipo, A., Molinaro, A., 2010. The diversity of the core oligosaccharide in lipopolysaccharides. Subcell Biochem 53, 69–99. https://doi.org/10.1007/978-90-481-9078-2_4
Singh, S., Singh, S.K., Chowdhury, I., Singh, R., 2017. Understanding the Mechanism of Bacterial Biofilms Resistance to Antimicrobial Agents. Open Microbiol J 11, 53–62. https://doi.org/10.2174/1874285801711010053
Singh, S.P., Williams, Y.U., Miller, S., Nikaido, H., 2003. The C-Terminal Domain of Salmonella enterica Serovar Typhimurium OmpA Is an Immunodominant Antigen in Mice but Appears To Be Only Partially Exposed on the Bacterial Cell Surface. Infect Immun 71, 3937–3946. https://doi.org/10.1128/IAI.71.7.3937-3946.2003
Siroy, A., Cosette, P., Seyer, D., Lemaître-Guillier, C., Vallenet, D., Van Dorsselaer, A., Boyer-Mariotte, S., Jouenne, T., Dé, E., 2006. Global Comparison of the Membrane Subproteomes between a Multidrug-Resistant *Acinetobacter baumannii* Strain and a Reference Strain. J. Proteome Res. 5, 3385–3398. https://doi.org/10.1021/pr060372s
Slamti, L., Waldor, M.K., 2009. Genetic Analysis of Activation of the *Vibrio cholerae* Cpx Pathway. J Bacteriol 191, 5044–5056. https://doi.org/10.1128/JB.00406-09
Slauch, J.M., Silhavy, T.J., 1991. cis-acting ompF mutations that result in OmpR-dependent constitutive expression. J Bacteriol 173, 4039–4048. https://doi.org/10.1128/jb.173.13.4039-4048.1991
Smith, S.G.J., Mahon, V., Lambert, M.A., Fagan, R.P., 2007. A molecular Swiss army knife: OmpA structure, function and expression. FEMS Microbiology Letters 273, 1–11. https://doi.org/10.1111/j.1574-6968.2007.00778.x
Snijder, H.J., Kingma, R.L., Kalk, K.H., Dekker, N., Egmond, M.R., Dijkstra, B.W., 2001. Structural investigations of calcium binding and its role in activity and activation of outer membrane phospholipase A from *Escherichia coli*1. Journal of Molecular Biology 309, 477–489. https://doi.org/10.1006/jmbi.2001.4675
Snijder, H.J., Ubarretxena-Belandia, I., Blaauw, M., Kalk, K.H., Verheij, H.M., Egmond, M.R., Dekker, N., Dijkstra, B.W., 1999. Structural evidence for dimerization-regulated activation of an integral membrane phospholipase. Nature 401, 717–721. https://doi.org/10.1038/44890

Snyder, W.B., Davis, L.J., Danese, P.N., Cosma, C.L., Silhavy, T.J., 1995. Overproduction of NlpE, a new outer membrane lipoprotein, suppresses the toxicity of periplasmic LacZ by activation of the Cpx signal transduction pathway. J Bacteriol 177, 4216–4223. https://doi.org/10.1128/jb.177.15.4216-4223.1995

Snyder, W.B., Silhavy, T.J., 1995. Beta-galactosidase is inactivated by intermolecular disulfide bonds and is toxic when secreted to the periplasm of Escherichia coli. Journal of Bacteriology 177, 953–963. https://doi.org/10.1128/jb.177.4.953-963.1995

Spangler, C., Kaever, V., Seifert, R., 2011. Interaction of the diguanylate cyclase YdeH of Escherichia coli with 2',(3')-substituted purine and pyrimidine nucleotides. J Pharmacol Exp Ther 336, 234–241. https://doi.org/10.1124/jpet.110.170993

Spiess, C., Beil, A., Ehrmann, M., 1999. A temperature-dependent switch from chaperone to protease in a widely conserved heat shock protein. Cell 97, 339–347. https://doi.org/10.1016/s0092-8674(00)80743-6

Spinola, S.M., Fortney, K.R., Baker, B., Janowicz, D.M., Zwickl, B., Katz, B.P., Blick, R.J., Munson, R.S., 2010. Activation of the CpxRA System by Deletion of *cpxA* Impairs the Ability of *Haemophilus ducreyi* To Infect Humans. Infect Immun 78, 3898–3904. https://doi.org/10.1128/IAI.00432-10

Steyn, A.J.C., Joseph, J., Bloom, B.R., 2003. Interaction of the sensor module of Mycobacterium tuberculosis H37Rv KdpD with members of the Lpr family. Molecular Microbiology 47, 1075–1089. https://doi.org/10.1046/j.1365-2958.2003.03356.x

Stubenrauch, C., Belousoff, M.J., Hay, I.D., Shen, H.-H., Lillington, J., Tuck, K.L., Peters, K.M., Phan, M.-D., Lo, A.W., Schembri, M.A., Strugnell, R.A., Waksman, G., Lithgow, T., 2016. Effective assembly of fimbriae in Escherichia coli depends on the translocation assembly module nanomachine. Nat Microbiol 1, 1–8. https://doi.org/10.1038/nmicrobiol.2016.64

Sugawara, E., Nagano, K., Nikaido, H., 2010. Factors Affecting the Folding of Pseudomonas aeruginosa OprF Porin into the One-Domain Open Conformer. mBio 1, 10.1128/mbio.00228-10. https://doi.org/10.1128/mbio.00228-10

Suits, M.D.L., Sperandeo, P., Dehò, G., Polissi, A., Jia, Z., 2008. Novel structure of the conserved gram-negative lipopolysaccharide transport protein A and mutagenesis analysis. J Mol Biol 380, 476–488. https://doi.org/10.1016/j.jmb.2008.04.045

Šulskis, D., Thoma, J., Burmann, B.M., 2021. Structural basis of DegP protease temperature-dependent activation. Sci Adv 7, eabj1816. https://doi.org/10.1126/sciadv.abj1816

Sun, J., Rutherford, S.T., Silhavy, T.J., Huang, K.C., 2022. Physical properties of the bacterial outer membrane. Nat Rev Microbiol 20, 236–248. https://doi.org/10.1038/s41579-021-00638-0

Sutcliffe, I.C., Harrington, D.J., 2004. Lipoproteins of Mycobacterium tuberculosis: an abundant and functionally diverse class of cell envelope components. FEMS Microbiology Reviews 28, 645–659. https://doi.org/10.1016/j.femsre.2004.06.002

Sutterlin, H.A., Shi, H., May, K.L., Miguel, A., Khare, S., Huang, K.C., Silhavy, T.J., 2016. Disruption of lipid homeostasis in the Gram-negative cell envelope activates a novel cell death pathway. Proc Natl Acad Sci U S A 113, E1565-1574. https://doi.org/10.1073/pnas.1601375113

Sutton, A., Newman, T., McEwen, J., Silverman, P.M., Freundlich, M., 1982. Mutations in genes cpxA and cpxB of Escherichia coli K-12 cause a defect in acetohydroxyacid synthase I function in vivo. J Bacteriol 151, 976–982. https://doi.org/10.1128/jb.151.2.976-982.1982

Szczepaniak, J., Holmes, P., Rajasekar, K., Kaminska, R., Samsudin, F., Inns, P.G., Rassam, P., Khalid, S., Murray, S.M., Redfield, C., Kleanthous, C., 2020. The lipoprotein Pal stabilises the bacterial outer membrane during constriction by a mobilisation-and-capture mechanism. Nat Commun 11, 1305. https://doi.org/10.1038/s41467-020-15083-5

Szwedziak, P., Löwe, J., 2013. Do the divisome and elongasome share a common evolutionary past? Curr Opin Microbiol 16, 745–751. https://doi.org/10.1016/j.mib.2013.09.003

Taib, N., Megrian, D., Witwinowski, J., Adam, P., Poppleton, D., Borrel, G., Beloin, C., Gribaldo, S., 2020. Genome-wide analysis of the Firmicutes illuminates the diderm/monoderm transition. Nat Ecol Evol 4, 1661–1672. https://doi.org/10.1038/s41559-020-01299-7
Takeda, K., Miyatake, H., Yokota, N., Matsuyama, S., Tokuda, H., Miki, K., 2003. Crystal structures of bacterial lipoprotein localization factors, LolA and LolB. EMBO J 22, 3199–3209. https://doi.org/10.1093/emboj/cdg324
Tan, W.B., Chng, S.-S., 2024. Primary role of the Tol-Pal complex in bacterial outer membrane lipid homeostasis. https://doi.org/10.1101/2024.05.08.593160
Tang, X., Chang, S., Luo, Q., Zhang, Zhengyu, Qiao, W., Xu, C., Zhang, C., Niu, Y., Yang, W., Wang, T., Zhang, Zhibo, Zhu, X., Wei, X., Dong, C., Zhang, X., Dong, H., 2019. Cryo-EM structures of lipopolysaccharide transporter LptB2FGC in lipopolysaccharide or AMP-PNP-bound states reveal its transport mechanism. Nat Commun 10, 4175. https://doi.org/10.1038/s41467-019-11977-1
Tang, X., Chang, S., Qiao, W., Luo, Q., Chen, Y., Jia, Z., Coleman, J., Zhang, K., Wang, T., Zhang, Z., Zhang, C., Zhu, X., Wei, X., Dong, C., Zhang, X., Dong, H., 2021. Structural insights into outer membrane asymmetry maintenance in Gram-negative bacteria by MlaFEDB. Nat Struct Mol Biol 28, 81–91. https://doi.org/10.1038/s41594-020-00532-y
Tao, K., Watanabe, S., Narita, S., Tokuda, H., 2010. A Periplasmic LolA Derivative with a Lethal Disulfide Bond Activates the Cpx Stress Response System. J Bacteriol 192, 5657–5662. https://doi.org/10.1128/JB.00821-10
Tata, M., Konovalova, A., 2019. Improper Coordination of BamA and BamD Results in Bam Complex Jamming by a Lipoprotein Substrate. mBio 10, e00660-19. https://doi.org/10.1128/mBio.00660-19
Tata, M., Kumar, S., Lach, S.R., Saha, S., Hart, E.M., Konovalova, A., 2021. High-throughput suppressor screen demonstrates that RcsF monitors outer membrane integrity and not Bam complex function. Proceedings of the National Academy of Sciences 118, e2100369118. https://doi.org/10.1073/pnas.2100369118
Teese, M.G., Langosch, D., 2015. Role of GxxxG Motifs in Transmembrane Domain Interactions. Biochemistry 54, 5125–5135. https://doi.org/10.1021/acs.biochem.5b00495
Terwilliger, T.C., Grosse-Kunstleve, R.W., Afonine, P.V., Moriarty, N.W., Zwart, P.H., Hung, L.W., Read, R.J., Adams, P.D., 2008. Iterative model building, structure refinement and density modification with the PHENIX AutoBuild wizard. Acta Crystallogr D Biol Crystallogr 64, 61–69. https://doi.org/10.1107/S090744490705024X
Thanassi, D.G., Stathopoulos, C., Karkal, A., Li, H., 2005. Protein secretion in the absence of ATP: the autotransporter, two-partner secretion and chaperone/usher pathways of Gram-negative bacteria (Review). Molecular Membrane Biology 22, 63–72. https://doi.org/10.1080/09687860500063290
Thede, G.L., Arthur, D.C., Edwards, R.A., Buelow, D.R., Wong, J.L., Raivio, T.L., Glover, J.N.M., 2011. Structure of the Periplasmic Stress Response Protein CpxP. J Bacteriol 193, 2149–2157. https://doi.org/10.1128/JB.01296-10
Thomason, L.C., Sawitzke, J.A., Li, X., Costantino, N., Court, D.L., 2014. Recombineering: genetic engineering in bacteria using homologous recombination. Curr Protoc Mol Biol 106, 1.16.1-1.16.39. https://doi.org/10.1002/0471142727.mb0116s106
Thomassin, J.-L., Giannakopoulou, N., Zhu, L., Gross, J., Salmon, K., Leclerc, J.-M., Daigle, F., Le Moual, H., Gruenheid, S., 2015. The CpxRA Two-Component System Is Essential for Citrobacter rodentium Virulence. Infect Immun 83, 1919–1928. https://doi.org/10.1128/IAI.00194-15
Thomassin, J.-L., Leclerc, J.-M., Giannakopoulou, N., Zhu, L., Salmon, K., Portt, A., Daigle, F., Le Moual, H., Gruenheid, S., 2017. Systematic Analysis of Two-Component Systems in Citrobacter rodentium Reveals Positive and Negative Roles in Virulence. Infect Immun 85, e00654-16. https://doi.org/10.1128/IAI.00654-16

Thompson, B.G., Murray, R.G.E., Boyce, J.F., 1982. The association of the surface array and the outer membrane of Deinococcus radiodurans. Can. J. Microbiol. 28, 1081–1088. https://doi.org/10.1139/m82-161
Tocheva, E.I., Ortega, D.R., Jensen, G.J., 2016. Sporulation, bacterial cell envelopes and the origin of life. Nat Rev Microbiol 14, 535–542. https://doi.org/10.1038/nrmicro.2016.85
Tokunaga, M., Tokunaga, H., Wu, H.C., 1982. Post-translational modification and processing of Escherichia coli prolipoprotein in vitro. Proceedings of the National Academy of Sciences 79, 2255–2259. https://doi.org/10.1073/pnas.79.7.2255
Tran, A.X., Dong, C., Whitfield, C., 2010. Structure and Functional Analysis of LptC, a Conserved Membrane Protein Involved in the Lipopolysaccharide Export Pathway in Escherichia coli. J Biol Chem 285, 33529–33539. https://doi.org/10.1074/jbc.M110.144709
Tsang, M.-J., Yakhnina, A.A., Bernhardt, T.G., 2017. NlpD links cell wall remodeling and outer membrane invagination during cytokinesis in Escherichia coli. PLOS Genetics 13, e1006888. https://doi.org/10.1371/journal.pgen.1006888
Tschauner, K., Hörnschemeyer, P., Müller, V.S., Hunke, S., 2014. Dynamic Interaction between the CpxA Sensor Kinase and the Periplasmic Accessory Protein CpxP Mediates Signal Recognition in E. coli. PLoS ONE 9, e107383. https://doi.org/10.1371/journal.pone.0107383
Tsukahara, J., Mukaiyama, K., Okuda, S., Narita, S., Tokuda, H., 2009. Dissection of LolB function--lipoprotein binding, membrane targeting and incorporation of lipoproteins into lipid bilayers. FEBS J 276, 4496–4504. https://doi.org/10.1111/j.1742-4658.2009.07156.x
Tsukazaki, T., 2019. Structural Basis of the Sec Translocon and YidC Revealed Through X-ray Crystallography. Protein J 38, 249–261. https://doi.org/10.1007/s10930-019-09830-x
Tsukazaki, T., Mori, H., Echizen, Y., Ishitani, R., Fukai, S., Tanaka, T., Perederina, A., Vassylyev, D.G., Kohno, T., Maturana, A.D., Ito, K., Nureki, O., 2011. Structure and function of a membrane component SecDF that enhances protein export. Nature 474, 235–238. https://doi.org/10.1038/nature09980
Tsviklist, V., Guest, R.L., Raivio, T.L., 2022. The Cpx Stress Response Regulates Turnover of Respiratory Chain Proteins at the Inner Membrane of Escherichia coli. Front. Microbiol. 12, 732288. https://doi.org/10.3389/fmicb.2021.732288
Ünal, C.M., Steinert, M., 2014. Microbial Peptidyl-Prolyl cis/trans Isomerases (PPIases): Virulence Factors and Potential Alternative Drug Targets. Microbiol Mol Biol Rev 78, 544–571. https://doi.org/10.1128/MMBR.00015-14
Unden, G., Bongaerts, J., 1997. Alternative respiratory pathways of Escherichia coli: energetics and transcriptional regulation in response to electron acceptors. Biochim Biophys Acta 1320, 217–234. https://doi.org/10.1016/s0005-2728(97)00034-0
Upadhyay, A.A., Fleetwood, A.D., Adebali, O., Finn, R.D., Zhulin, I.B., 2016. Cache Domains That are Homologous to, but Different from PAS Domains Comprise the Largest Superfamily of Extracellular Sensors in Prokaryotes. PLOS Computational Biology 12, e1004862. https://doi.org/10.1371/journal.pcbi.1004862
Vaara, M., 1993. Antibiotic-supersusceptible mutants of Escherichia coli and Salmonella typhimurium. Antimicrob Agents Chemother 37, 2255–2260.
van der Heijden, J., Reynolds, L.A., Deng, W., Mills, A., Scholz, R., Imami, K., Foster, L.J., Duong, F., Finlay, B.B., 2016. Salmonella Rapidly Regulates Membrane Permeability To Survive Oxidative Stress. mBio 7, 10.1128/mbio.01238-16. https://doi.org/10.1128/mbio.01238-16
van Rensburg, J.J., Fortney, K.R., Chen, L., Krieger, A.J., Lima, B.P., Wolfe, A.J., Katz, B.P., Zhang, Z., Spinola, S.M., 2015. Development and Validation of a High-Throughput Cell-Based Screen To Identify Activators of a Bacterial Two-Component Signal Transduction

System. Antimicrob Agents Chemother 59, 3789–3799. https://doi.org/10.1128/AAC.00236-15
van Stelten, J., Silva, F., Belin, D., Silhavy, T.J., 2009. Effects of Antibiotics and a Proto-Oncogene Homolog on Destruction of Protein Translocator SecY. Science 325, 753–756. https://doi.org/10.1126/science.1172221
Vandeputte-Rutten, L., Kramer, R.A., Kroon, J., Dekker, N., Egmond, M.R., Gros, P., 2001. Crystal structure of the outer membrane protease OmpT from Escherichia coli suggests a novel catalytic site. The EMBO Journal 20, 5033–5039. https://doi.org/10.1093/emboj/20.18.5033
Vázquez-Torres, A., 2012. Redox Active Thiol Sensors of Oxidative and Nitrosative Stress. Antioxid Redox Signal 17, 1201–1214. https://doi.org/10.1089/ars.2012.4522
Vergalli, J., Bodrenko, I.V., Masi, M., Moynié, L., Acosta-Gutiérrez, S., Naismith, J.H., Davin-Regli, A., Ceccarelli, M., van den Berg, B., Winterhalter, M., Pagès, J.-M., 2020. Porins and small-molecule translocation across the outer membrane of Gram-negative bacteria. Nat Rev Microbiol 18, 164–176. https://doi.org/10.1038/s41579-019-0294-2
Vogt, J., Schulz, G.E., 1999. The structure of the outer membrane protein OmpX from Escherichia coli reveals possible mechanisms of virulence. Structure 7, 1301–1309. https://doi.org/10.1016/s0969-2126(00)80063-5
Vogt, S.L., Nevesinjac, A.Z., Humphries, R.M., Donnenberg, M.S., Armstrong, G.D., Raivio, T.L., 2010. The Cpx envelope stress response both facilitates and inhibits elaboration of the enteropathogenic Escherichia coli bundle-forming pilus: Cpx regulation of EPEC pilus elaboration. Molecular Microbiology 76, 1095–1110. https://doi.org/10.1111/j.1365-2958.2010.07145.x
Vogt, S.L., Raivio, T.L., 2014. Hfq reduces envelope stress by controlling expression of envelope-localized proteins and protein complexes in enteropathogenic *E scherichia coli*: Hfq reduces envelope stress in *E. coli*. Molecular Microbiology 92, 681–697. https://doi.org/10.1111/mmi.12581
Vogt, S.L., Raivio, T.L., 2012. Just scratching the surface: an expanding view of the Cpx envelope stress response. FEMS Microbiol Lett 326, 2–11. https://doi.org/10.1111/j.1574-6968.2011.02406.x
Vollmer, W., Bertsche, U., 2008. Murein (peptidoglycan) structure, architecture and biosynthesis in Escherichia coli. Biochimica et Biophysica Acta (BBA) - Biomembranes 1778, 1714–1734. https://doi.org/10.1016/j.bbamem.2007.06.007
Vollmer, W., Joris, B., Charlier, P., Foster, S., 2008. Bacterial peptidoglycan (murein) hydrolases. FEMS Microbiology Reviews 32, 259–286. https://doi.org/10.1111/j.1574-6976.2007.00099.x
von Heijne, G., 1990. The signal peptide. J. Membrain Biol. 115, 195–201. https://doi.org/10.1007/BF01868635
von Kügelgen, A., van Dorst, S., Alva, V., Bharat, T.A.M., 2022. A multidomain connector links the outer membrane and cell wall in phylogenetically deep-branching bacteria. Proceedings of the National Academy of Sciences 119, e2203156119. https://doi.org/10.1073/pnas.2203156119
Voss, B.J., Trent, M.S., 2018. LPS Transport: Flipping Out over MsbA. Current Biology 28, R30–R33. https://doi.org/10.1016/j.cub.2017.10.067
Vreede, J., van der Horst, M.A., Hellingwerf, K.J., Crielaard, W., van Aalten, D.M.F., 2003. PAS domains. Common structure and common flexibility. J Biol Chem 278, 18434–18439. https://doi.org/10.1074/jbc.M301701200
Wall, E., Majdalani, N., Gottesman, S., 2018. The Complex Rcs Regulatory Cascade. Annual Review of Microbiology 72, 111–139. https://doi.org/10.1146/annurev-micro-090817-062640

Wall, E.A., Majdalani, N., Gottesman, S., 2020. IgaA negatively regulates the Rcs Phosphorelay via contact with the RcsD Phosphotransfer Protein. PLoS Genet 16, e1008610. https://doi.org/10.1371/journal.pgen.1008610
Walsh, N.P., Alba, B.M., Bose, B., Gross, C.A., Sauer, R.T., 2003. OMP Peptide Signals Initiate the Envelope-Stress Response by Activating DegS Protease via Relief of Inhibition Mediated by Its PDZ Domain. Cell 113, 61–71. https://doi.org/10.1016/S0092-8674(03)00203-4
Wang, S., Huang, C.-H., Lin, T.-S., Yeh, Y.-Q., Fan, Y.-S., Wang, S.-W., Tseng, H.-C., Huang, S.-J., Chang, Y.-Y., Jeng, U.-S., Chang, C.-I., Tzeng, S.-R., 2024. Structural basis for recruitment of peptidoglycan endopeptidase MepS by lipoprotein NlpI. Nat Commun 15, 5461. https://doi.org/10.1038/s41467-024-49552-y
Wang, X., Quinn, P.J., 2010. Lipopolysaccharide: Biosynthetic pathway and structure modification. Progress in Lipid Research 49, 97–107. https://doi.org/10.1016/j.plipres.2009.06.002
Wang, Y., 2002. The Function of OmpA in Escherichia coli. Biochemical and Biophysical Research Communications 292, 396–401. https://doi.org/10.1006/bbrc.2002.6657
Warner, L.R., Gatzeva-Topalova, P.Z., Doerner, P.A., Pardi, A., Sousa, M.C., 2017. Flexibility in the Periplasmic Domain of BamA Is Important for Function. Structure 25, 94–106. https://doi.org/10.1016/j.str.2016.11.013
Watanabe, N., Savchenko, A., 2024. Molecular insights into the initiation step of the Rcs signaling pathway. Structure 0. https://doi.org/10.1016/j.str.2024.06.003
Waterhouse, A., Bertoni, M., Bienert, S., Studer, G., Tauriello, G., Gumienny, R., Heer, F.T., de Beer, T.A.P., Rempfer, C., Bordoli, L., Lepore, R., Schwede, T., 2018. SWISS-MODEL: homology modelling of protein structures and complexes. Nucleic Acids Research 46, W296–W303. https://doi.org/10.1093/nar/gky427
Weatherspoon-Griffin, N., Zhao, G., Kong, W., Kong, Y., Morigen, Andrews-Polymenis, H., McClelland, M., Shi, Y., 2011. The CpxR/CpxA Two-component System Up-regulates Two Tat-dependent Peptidoglycan Amidases to Confer Bacterial Resistance to Antimicrobial Peptide. Journal of Biological Chemistry 286, 5529–5539. https://doi.org/10.1074/jbc.M110.200352
Webby, M.N., Williams-Jones, D.P., Press, C., Kleanthous, C., 2022. Force-Generation by the Trans-Envelope Tol-Pal System. Front. Microbiol. 13. https://doi.org/10.3389/fmicb.2022.852176
Weber, R.F., Silverman, P.M., 1988. The Cpx proteins of Escherichia coli K12. Journal of Molecular Biology 203, 467–478. https://doi.org/10.1016/0022-2836(88)90013-7
Weiner, L., Brissette, J.L., Ramani, N., Model, P., 1995. Analysis of the proteins and cis-acting elements regulating the stress-induced phage shock protein operon. Nucleic Acids Res 23, 2030–2036. https://doi.org/10.1093/nar/23.11.2030
Whitfield, C., Williams, D.M., Kelly, S.D., 2020. Lipopolysaccharide O-antigens—bacterial glycans made to measure. J Biol Chem 295, 10593–10609. https://doi.org/10.1074/jbc.REV120.009402
WHO bacterial priority pathogens list, 2024: Bacterial pathogens of public health importance to guide research, development and strategies to prevent and control antimicrobial resistance, 2024.
Winkle, M., Hernández-Rocamora, V.M., Pullela, K., Goodall, E.C.A., Martorana, A.M., Gray, J., Henderson, I.R., Polissi, A., Vollmer, W., 2021. DpaA Detaches Braun's Lipoprotein from Peptidoglycan. mBio 12, 10.1128/mbio.00836-21. https://doi.org/10.1128/mbio.00836-21
Witwinowski, J., Sartori-Rupp, A., Taib, N., Pende, N., Tham, T.N., Poppleton, D., Ghigo, J.-M., Beloin, C., Gribaldo, S., 2022. An ancient divide in outer membrane tethering systems in bacteria suggests a mechanism for the diderm-to-monoderm transition. Nat Microbiol 7, 411–422. https://doi.org/10.1038/s41564-022-01066-3

Wu, R., Bakelar, J.W., Lundquist, K., Zhang, Z., Kuo, K.M., Ryoo, D., Pang, Y.T., Sun, C., White, T., Klose, T., Jiang, W., Gumbart, J.C., Noinaj, N., 2021. Plasticity within the barrel domain of BamA mediates a hybrid-barrel mechanism by BAM. Nat Commun 12, 7131. https://doi.org/10.1038/s41467-021-27449-4

Wu, T., Malinverni, J., Ruiz, N., Kim, S., Silhavy, T.J., Kahne, D., 2005. Identification of a Multicomponent Complex Required for Outer Membrane Biogenesis in Escherichia coli. Cell 121, 235–245. https://doi.org/10.1016/j.cell.2005.02.015

Yaeger, L.N., Ranieri, M.R.M., Chee, J., Karabelas-Pittman, S., Rudolph, M., Giovannoni, A.M., Harvey, H., Burrows, L.L., 2024. A genetic screen identifies a role for oprF in Pseudomonas aeruginosa biofilm stimulation by subinhibitory antibiotics. npj Biofilms Microbiomes 10, 1–12. https://doi.org/10.1038/s41522-024-00496-7

Yakhnina, A.A., Bernhardt, T.G., 2020. The Tol-Pal system is required for peptidoglycan-cleaving enzymes to complete bacterial cell division. Proceedings of the National Academy of Sciences 117, 6777–6783. https://doi.org/10.1073/pnas.1919267117

Yakhnina, A.A., McManus, H.R., Bernhardt, T.G., 2015. The cell wall amidase AmiB is essential for *P seudomonas aeruginosa* cell division, drug resistance and viability: *Pseudomonas* amidases. Molecular Microbiology 97, 957–973. https://doi.org/10.1111/mmi.13077

Yamamoto, K., Hirao, K., Oshima, T., Aiba, H., Utsumi, R., Ishihama, A., 2005. Functional Characterization in Vitro of All Two-component Signal Transduction Systems from Escherichia coli. Journal of Biological Chemistry 280, 1448–1456. https://doi.org/10.1074/jbc.M410104200

Yamamoto, K., Ishihama, A., 2006. Characterization of Copper-Inducible Promoters Regulated by CpxA/CpxR in *Escherichia coli*. Bioscience, Biotechnology, and Biochemistry 70, 1688–1695. https://doi.org/10.1271/bbb.60024

Yamamoto, K., Ishihama, A., 2005. Transcriptional response of Escherichia coli to external copper: Transcriptional response of E. coli to external copper. Molecular Microbiology 56, 215–227. https://doi.org/10.1111/j.1365-2958.2005.04532.x

Yamashita, S., Lukacik, P., Barnard, T.J., Noinaj, N., Felek, S., Tsang, T.M., Krukonis, E.S., Hinnebusch, B.J., Buchanan, S.K., 2011. Structural Insights into Ail-Mediated Adhesion in *Yersinia pestis*. Structure 19, 1672–1682. https://doi.org/10.1016/j.str.2011.08.010

Yang, Y., Chen, H., Corey, R.A., Morales, V., Quentin, Y., Froment, C., Caumont-Sarcos, A., Albenne, C., Burlet-Schiltz, O., Ranava, D., Stansfeld, P.J., Marcoux, J., Ieva, R., 2023. LptM promotes oxidative maturation of the lipopolysaccharide translocon by substrate binding mimicry. Nat Commun 14, 6368. https://doi.org/10.1038/s41467-023-42007-w

Yasuhiro, K., Yuzuru, A., Shoshichi, N., 1967. Composition and turnover of the phospholipids in *Escherichia coli*. Biochimica et Biophysica Acta (BBA) - Lipids and Lipid Metabolism 144, 382–390. https://doi.org/10.1016/0005-2760(67)90167-1

Yeow, J., Chng, S.-S., 2022. Of zones, bridges and chaperones – phospholipid transport in bacterial outer membrane assembly and homeostasis. Microbiology 168, 001177. https://doi.org/10.1099/mic.0.001177

Yeow, J., Luo, M., Chng, S.-S., 2023. Molecular mechanism of phospholipid transport at the bacterial outer membrane interface. Nat Commun 14, 8285. https://doi.org/10.1038/s41467-023-44144-8

Yu, L., Cao, Q., Chen, W., Yang, N., Yang, C.-G., Ji, Q., Wu, M., Bae, T., Lan, L., 2022. A novel copper-sensing two-component system for inducing Dsb gene expression in bacteria. Science Bulletin 67, 198–212. https://doi.org/10.1016/j.scib.2021.03.003

Zakharian, E., Reusch, R.N., 2005. Kinetics of Folding of Escherichia coli OmpA from Narrow to Large Pore Conformation in a Planar Bilayer. Biochemistry 44, 6701–6707. https://doi.org/10.1021/bi047278e

Zakharian, E., Reusch, R.N., 2003. Outer membrane protein A of Escherichia coli forms temperature-sensitive channels in planar lipid bilayers. FEBS Lett 555, 229–235. https://doi.org/10.1016/s0014-5793(03)01236-5

Zhang, S., Cheng, Y., Ma, J., Wang, Y., Chang, Z., Fu, X., 2019. Degp degrades a wide range of substrate proteins in Escherichia coli under stress conditions. Biochem J 476, 3549–3564. https://doi.org/10.1042/BCJ20190446

Zheng, C., Yang, L., Hoopmann, M.R., Eng, J.K., Tang, X., Weisbrod, C.R., Bruce, J.E., 2011. Cross-linking Measurements of In Vivo Protein Complex Topologies. Molecular & Cellular Proteomics 10.

Zhou, X., Keller, R., Volkmer, R., Krauss, N., Scheerer, P., Hunke, S., 2011. Structural Basis for Two-component System Inhibition and Pilus Sensing by the Auxiliary CpxP Protein. Journal of Biological Chemistry 286, 9805–9814. https://doi.org/10.1074/jbc.M110.194092

Zhou, Z., White, K.A., Polissi, A., Georgopoulos, C., Raetz, C.R.H., 1998. Function of *Escherichia coli* MsbA, an Essential ABC Family Transporter, in Lipid A and Phospholipid Biosynthesis*. Journal of Biological Chemistry 273, 12466–12475. https://doi.org/10.1074/jbc.273.20.12466

Zückert, W.R., 2014. Secretion of Bacterial Lipoproteins: Through the Cytoplasmic Membrane, the Periplasm and Beyond. Biochimica et Biophysica Acta (BBA) - Molecular Cell Research, Protein trafficking and secretion in bacteria 1843, 1509–1516. https://doi.org/10.1016/j.bbamcr.2014.04.022

Zwir, I., Shin, D., Kato, A., Nishino, K., Latifi, T., Solomon, F., Hare, J.M., Huang, H., Groisman, E.A., 2005. Dissecting the PhoP regulatory network of Escherichia coli and Salmonella enterica. Proc Natl Acad Sci U S A 102, 2862–2867. https://doi.org/10.1073/pnas.0408238102

Appendix – Evolution of NlpE across bacterial species

Appendix Results and Discussion

Type I and II variants of NlpE

Throughout our studies of the outer membrane lipoprotein NlpE, we have always been intrigued by the observation that NlpE homologs differ significantly across Gram-negative bacteria. The original structural study noted that NlpE homologs fell into two broad categories (Hirano et al., 2007). The first are those that possess both N- and C-terminal domains in a similar configuration to NlpE in *E. coli* (named type I NlpE). Interestingly, all the identified type I variants of NlpE in this study hailed from species in Order Enterobacterales (e.g. from genera such as *Escherichia, Yersinia, Salmonella,* and *Shigella*). In contrast, Hirano and colleagues (2007) noticed that several species possessed a truncated variant of NlpE lacking the C-terminal domain. These variants were named type II NlpE, and included homologs from species such as *Vibrio cholerae*, *Shewanella oneidensis*, *Acinetobacter* sp., *Bordatella parapertussis*, and *Bacteroides fragilis*. These species are found in a much broader range of bacterial taxa, differing from up to the phylum level between *Bacteroides fragilis* (Phylum Bacteroidota) and all other species (which belong to Phylum Pseudomonadota).

The relevance of this diversity in NlpE domain organization is unknown. Part of the mystery comes from lack of studies of NlpE in species outside of Enterobacteriaceae. *Acinetobacter baumanii*'s type II NlpE homolog is produced at higher-than-normal abundance in a multi-drug resistant strain that also strongly produces biofilms (Siroy et al., 2006), and a recent study in a different strain reports that NlpE is upregulated in response to exogenous sulfide (Walsh et al., 2020). However, the Cpx response of *A. baumanii* has not been characterized (if it

even possesses a homologous system at all) so it's difficult to know if NlpE in this species functions similarly to enterobacterial NlpE.

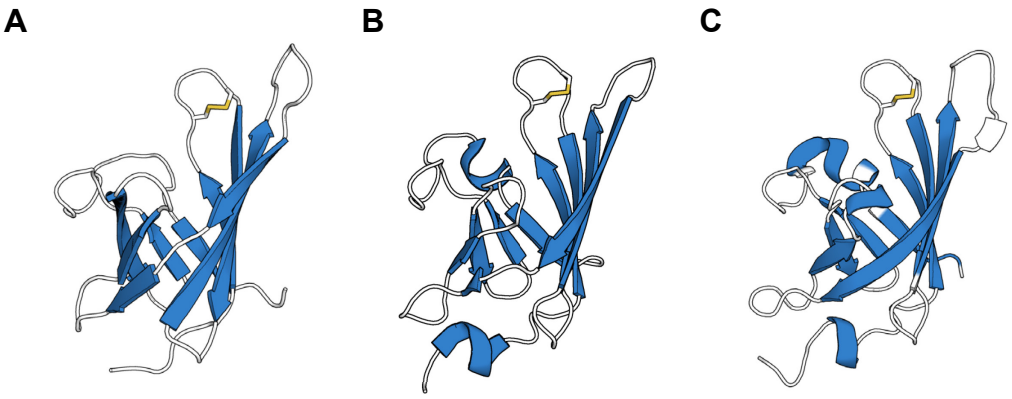

Figure 0-1. Type I and II variants of NlpE.

Representative structures of the N-terminal domains of **(A)** type I (from *E. coli*) (from the AlphaFold database) and **(B)** type II (from *Shewanella oneidensis*) NlpE (PDB 3LHN) variants of NlpE. **(C)** shows the N-terminal domain of the type II *Acinetobacter baumanii* NlpE. The universally conserved CXXC disulfide motif is shown in yellow.

AlphaFold models predict that, despite relatively low sequence conservation, type I and II homologues of NlpE, adopt highly similar folds (Appendix Figure 0-1). Coincidentally, we found that the crystal structure of the type II NlpE from *Shewanella oneidensis* was deposited to the Protein Data Bank (PDB code 3LHN). This crystal structure again confirms that N-terminal domains across type I and II homologs adopt similar β-barrel folds (Appendix Figure 0-1). An expanded alignment of type I and II NlpE is shown in Appendix Figure 0-2. These alignments show that the most universally conserved features (outside of the acylated N-temrinal cysteine) are two sets of disulfide bonds, one per domain.

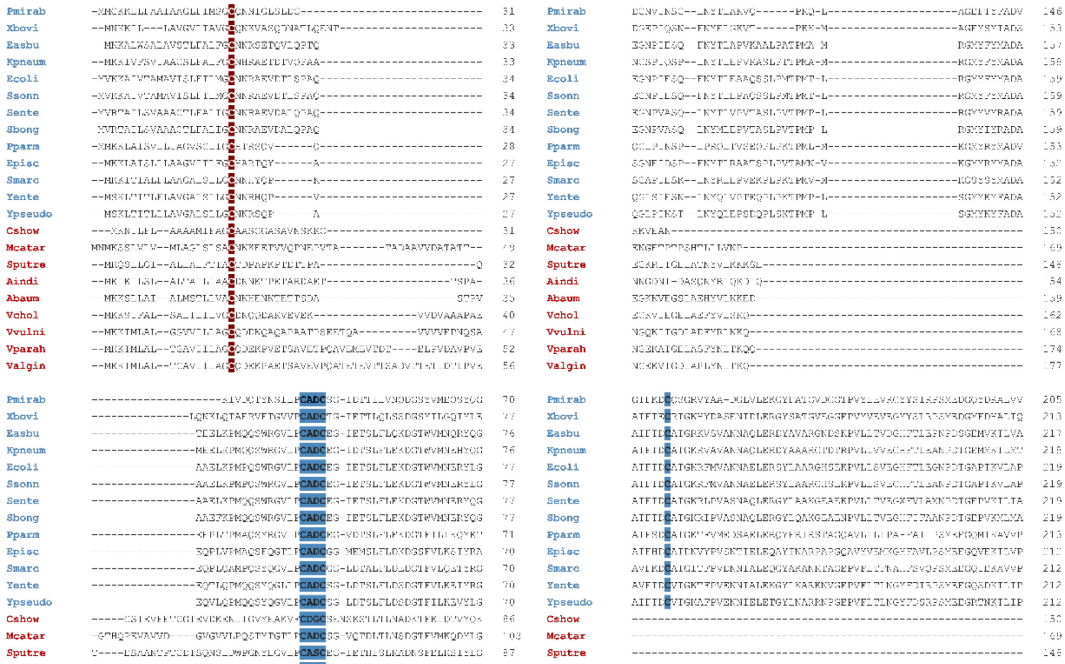

Figure 0-2. Expanded alignment of type I and II NlpE sequences.

Protein sequences of NlpE (CutF) homologs in multiple Gram-negative species were aligned using Clustal Omega. The organisms used here are: Type I-containing (blue) - *Proteus mirabilis, Xenorhabdus bovienii, Enterobacter asburiae, Klebsiella pneumoniae, Escherichia coli, Shigella sonnei, Salmonella enterica, Salmonella bongori, Pectobacterium parmentieri, Edwardsiella piscicida, Serratia marcescens, Yersinia enterocolitica, Yersinia pseudotuberculosis,* and Type II-containing (Red) - *Campylobacter showae, Moraxella catarrhalis, Shewanella putrefaciens, Acinetobacter indicus, Acinetobacter baumanii, Vibrio cholerae, Vibrio vulnificus, Vibrio parahaemolyticus, Vibrio alginolyticus.* Universally conserved Cys21 is highlighted in red and disulfide bond forming cysteines in blue.

Figure 0-3. R93 is only conserved in C-terminal domain containing NlpE.

R93 is highlighted in cyan and neighbouring K97 is highlighted in blue (both numbered based on residues in *E. coli*).

In Chapter 3, we reported that the positively charged arginine 93 residue is critical for activating CpxA at the inner membrane. This residue was also independently reported as the key residue for NlpE-CpxA interactions by others (Marotta et al., 2023). Interestingly, we find that this critical residue is only conserved in type I homologs of NlpE that also possess a C-terminal domain (Appendix Figure 0-3). This is somewhat puzzling as the C-terminal domain is completely dispensable for the ability of NlpE to alert CpxA to defective lipoprotein biogenesis; the C-terminal domain does not appear to physically interact with CpxA, nor is it required to activate CpxA when NlpE is mislocalized to the inner membrane (see Chapter 3 of this thesis and (Delhaye et al., 2019; May et al., 2019)). If the N-terminal domain's ancestral function is to activate CpxA at the inner membrane, why is this key residue not conserved in all N-terminal domain containing species?

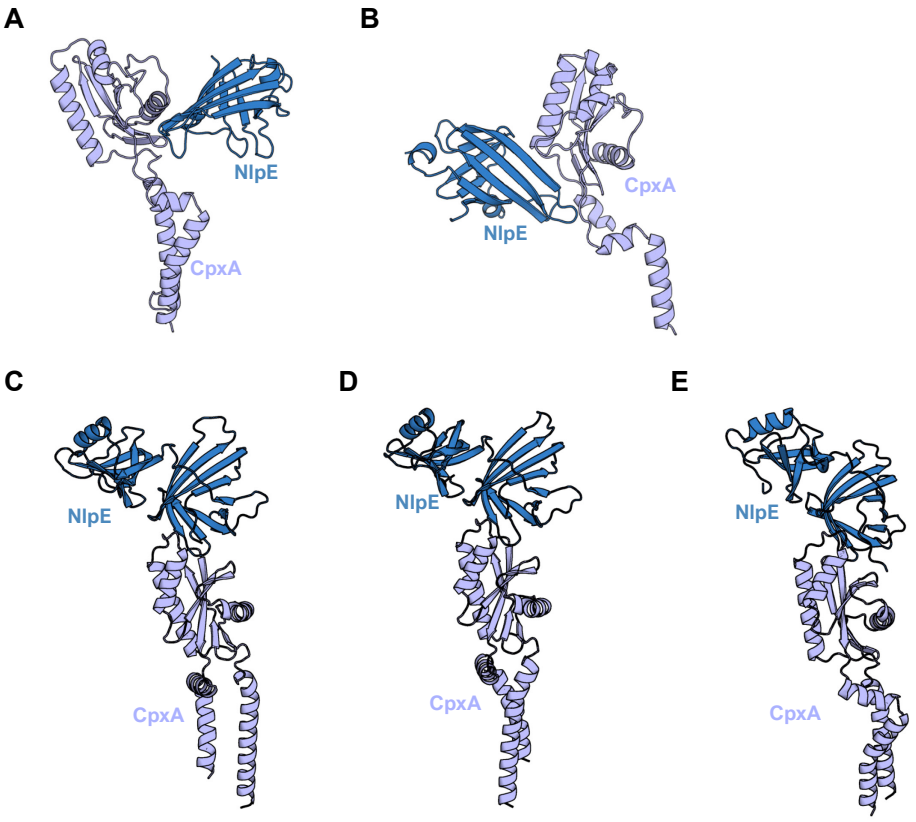

Figure 0-4. AlphaFold3 modeling of NlpE-CpxA complexes across species.

Low confidence models of NlpE-CpxA complexes are shown in **(A)** *V. cholerae* (ipTM = 0.18, pTM = 0.43) and **(B)** *Shewanella oneidensis* (ipTM = 0.15, pTM = 0.4). Higher confidence models of complexes in **(C)** *E. coli* (ipTM = 0.75, pTM = 0.73), **(D)** *Yersinia* sp. (ipTM = 0.75, pTM = 0.72), and **(E)** *Klebsiella* sp. (ipTM = 0.72, pTM = 0.73) are also shown.

It's possible that the N-terminal domain of type II NlpEs still interact with the CpxA homologs in their respective species, but just by different residues. However, preliminary investigations do not bear this out. AlphaFold3 does not confidently predict interactions between CpxA and NlpE in two organisms with type II NlpE (*V. cholerae* and *Shewanella oneidensis*) (Appendix Figure 0-4AB) with interface predicted template modeling (ipTM) scores of less than 0.2, significantly below the 0.6 value score for potentially failed predictions. In contrast, AlphaFold3 provides relatively confident predictions for NlpE-CpxA complexes in *Yersinia pestis*

and *Klebsiella pneumoniae* that are essentially identical to complexes predicted for *E. coli* homologs (Appendix Figure 0-4CDE). Furthermore, studies of the Cpx response in *V. cholerae* report that overexpression of *V. cholerae*'s NlpE does not activate CpxA in that organism (Slamti and Waldor, 2009). This is in contrast to *E. coli* and closely related organism *Salmonella enterica* serovar Typhimurium where overexpression is a strong inducing signal (Humphreys et al., 2004; Snyder and Silhavy, 1995). Overall, these results suggest that the ability of NlpE to activate CpxA at the inner membrane is limited to a relatively specific subset of Gram-negative bacteria.

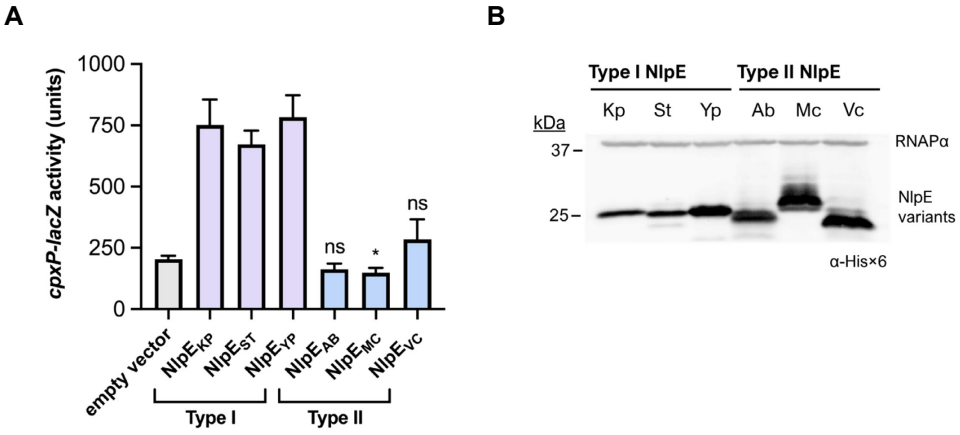

Figure 0-5. Overexpression of type I but not type II NlpE activates CpxA in *E. coli.*

(A) Ability of type I and II NlpE to activate CpxA in *E. coli* as measured by *cpxP-lacZ* reporter activity. Shown are means of three replicates with standard deviation. Data were analyzed with Tukey HSD post-hoc test (ns = nonsignificant, *p<0.05). Type I NlpE are: KP = *Klebsiella pneumoniae*; ST = *Salmonella typhimurium*; YP = *Yersinia pseudotuberculosis*. Type II NlpE are: AB = *Acinetobacter baumanii*; MC = *Moraxella catarrhalis;* VC = *Vibrio cholerae.* **(B)** shows a Western blot with anti-His×6 antibody to detect the expression levels of the tested NlpE variants. RNAPα was used as a loading control.

To further examine the ability of type I and II NlpE to activate CpxA, we ordered gene fragments (Twist Bioscience) of three non-*E. coli* type I *nlpE* (*Klebsiella pneumoniae, Salmonella*

Typhimurium, and *Yersinia pseudotuberculosis*) from and three type II *nlpE* (*Acinetobacter baumanii*, *Moraxella catarrhalis*, and *Vibrio cholerae*). All gene fragments encode for a C-terminal His×6 tag and were cloned into expression vector pTrc99A as described in other chapters. Expression vectors were then transformed into *E. coli* TR50 and expression of NlpE variants was induced with IPTG before *cpxP-lacZ* activity was quantified as described previously. Here, we found that overexpression of any type I NlpE is able to activate CpxA in *E. coli* (Appendix Figure 0-5A). However, none of the type II variants activated CpxA. All variants were stably expressed (Appendix Figure 0-5B).

This evidence, while very preliminary, implies that NlpE's ancestral function was not to activate CpxA at the inner membrane as a sensor of lipoprotein biogenesis defects. Instead, we hypothesize that NlpE evolved to interact with CpxA at the inner membrane only in a specific subset of species, namely those that possess a C-terminal domain that signals to the Cpx response. We showed in Chapter 4 that the C-terminal domain of NlpE transduces an outer membrane associated signal to the Cpx response, and work from the Collet group has shown that NlpE's C-terminal domain disulfide bonds are involved in activating CpxA in the presence of redox stress in the envelope (Delhaye et al., 2019). Because these signaling roles are associated with the outer membrane, we propose that NlpE only evolved to activate CpxA at the inner because it has an important signaling role at the outer membrane. In species that lack a domain capable of signaling from the outer membrane to CpxA, there is likely little selective pressure to accumulate mutations that allow for NlpE-CpxA interactions at the inner membrane, hence why type II variants do not appear to interact with or activate CpxA in their respective organisms (Slamti and Waldor, 2009).

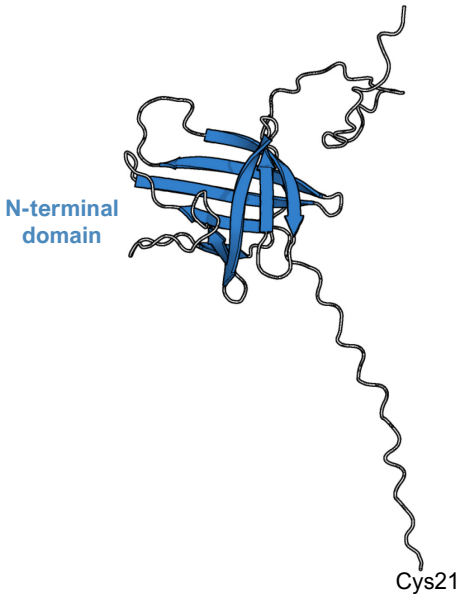

Figure 0-6. AlphaFold3 model of *Salmonella* Typhimurium LT2 NlpE with a truncated C-terminal domain.

How might have the type I and II divergence have occurred? The simplest and most likely explanation is that type II NlpE arises from a deletion of the C-terminal domain in an ancestral type I NlpE. Such events can be observed in modern strains; NlpE in *Salmonella* Typhimurium strain LT2 contains a frameshift mutation that causes it to express a truncated version of NlpE without an intact C-terminal domain, while other strains of *Salmonella* spp. carry intact NlpE (Appendix Figure 0-6) (Humphreys et al., 2004). We have noticed that overexpression of the C-terminal domain of NlpE in *E. coli* alone is quite toxic to cells (data not shown), which may underly the selective pressure to lose this domain in some species. Interestingly, we have also found a study that reports that NlpE may be present on mobile genetic elements such as large plasmids in some species, which may facilitate the evolution of NlpE across species (Marathe et al., 2022).

The diversity of NlpE homologs across Kingdom Bacteria

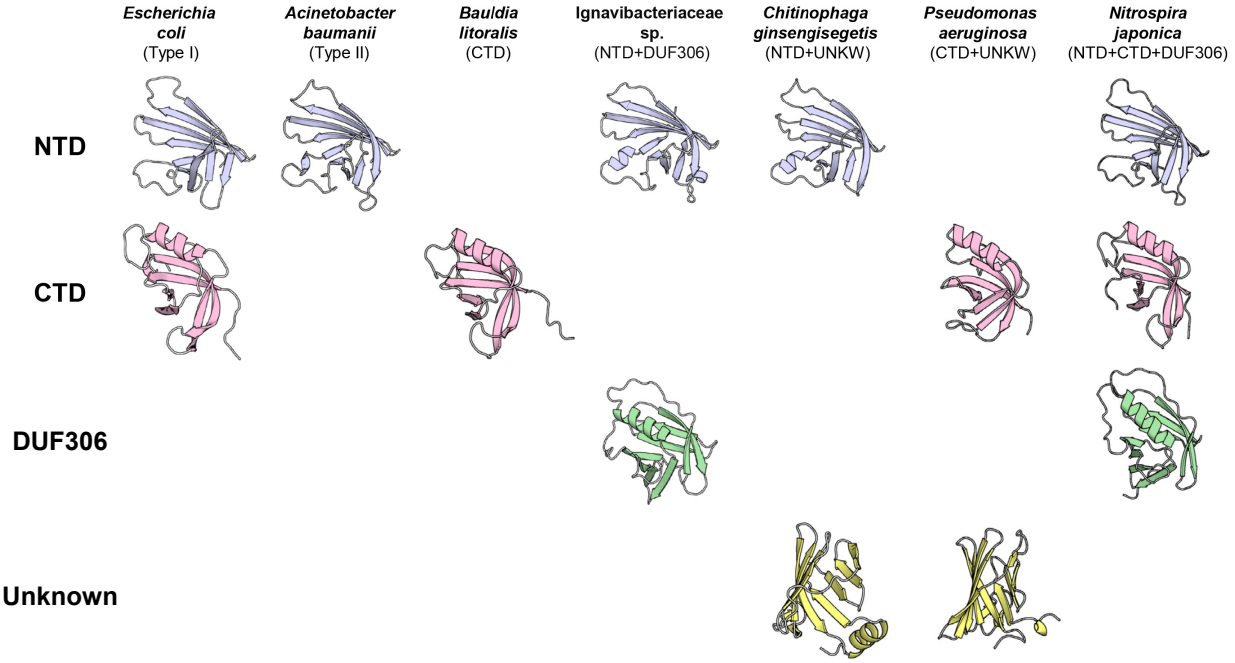

Figure 0-7. NlpE homologs across bacterial species possess diverse domain architecture. Structures of representative NlpE types found by bioinformatic searches were pulled from the AlphaFold database. NTD = domain resembling *E. coli*'s N-terminal domain; CTD = domain resembling *E. coli*'s C-terminal domain; UNKW = unannotated domains; DUF306 = domain of unknown function 306.

The fact that NlpE homologs comes in at least two variants raised an important question: if type II variants can arise from (the presumed) loss of the C-terminal domain in an ancestral type I-like variant, is it possible that other homologs of NlpE possess other combinations of domains? To investigate this, we used both the structures published on the AlphaFold database and the protein basic local alignment search tool (BLASTp) on the UniProt database to conduct searches for NlpE variants across bacterial species. Specifically, we started with the sequences of the *E. coli* N- and C-terminal domains separately and then searched for proteins containing

similar domains via BLASTp. Predictably, many type I and II variants of NlpE came up in these searches. To our surprise, however, we found several homologs of NlpE that contained extra domains (Appendix Figure 0-7). These searches revealed that NlpE homologs are not limited to just type I and II variants but instead comprise a diverse family of proteins that contain *E. coli*-like N-terminal and/or C-terminal domains and several domains of unknown function. Altogether, we identified at least seven different variants of NlpE across species possessing these domains in different combinations. Many of these NlpE homologs are from species that are outside of Phylum Pseudomonadota (AKA Proteobacteria). Strikingly, we noticed that several homologs of NlpE are predicted to encode for three domains, with the third domain being either an unannotated domain of unknown function (DUF) or a DUF306/Meta/HslJ domain.

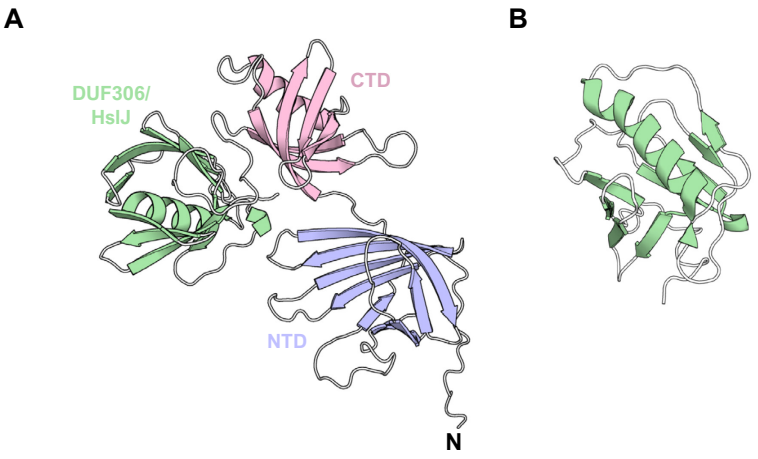

Figure 0-8. DUF306/HslJ-like domains in NlpE homologs.

(A) The AlphaFold model of Alkalimonas amylolytica's HslJ (which possesses domains resembling NlpE from *E. coli*). **(B)** NMR structure of the globular domain of HslJ (PDB 2KTS).

Three domain NlpE with a DUF306 are particularly interesting (Appendix Figure 0-8A). All examples that we could identified had the same order of domains: NTD-CTD-DUF306. Literature on this particular domain is scarce. *E. coli* encodes for HslJ outer membrane lipoprotein that is

solely composed of this domain. While initially identified as a potential heat shock protein (Chuang and Blattner, 1993), later studies disproved that its involvement in heat shock but instead found it to be involved in increasing resistance to the antibiotic novobiocin (Lilic et al., 2003). The structure of HslJ was solved by nuclear magnetic resonance (NMR) and deposited to the Protein Data Bank (PDB code 2KTS) (Appendix Figure 0-8B); however, no subsequent manuscript was published on this structure, leaving its function and mechanism shrouded in mystery. While its structure is superficially similar to the C-terminal domain of NlpE, with a partial β-barrel capped by an α-helix, it does not share the same disulfide bond as the C-terminal domain, making it unlikely that these structures are derived from one another.

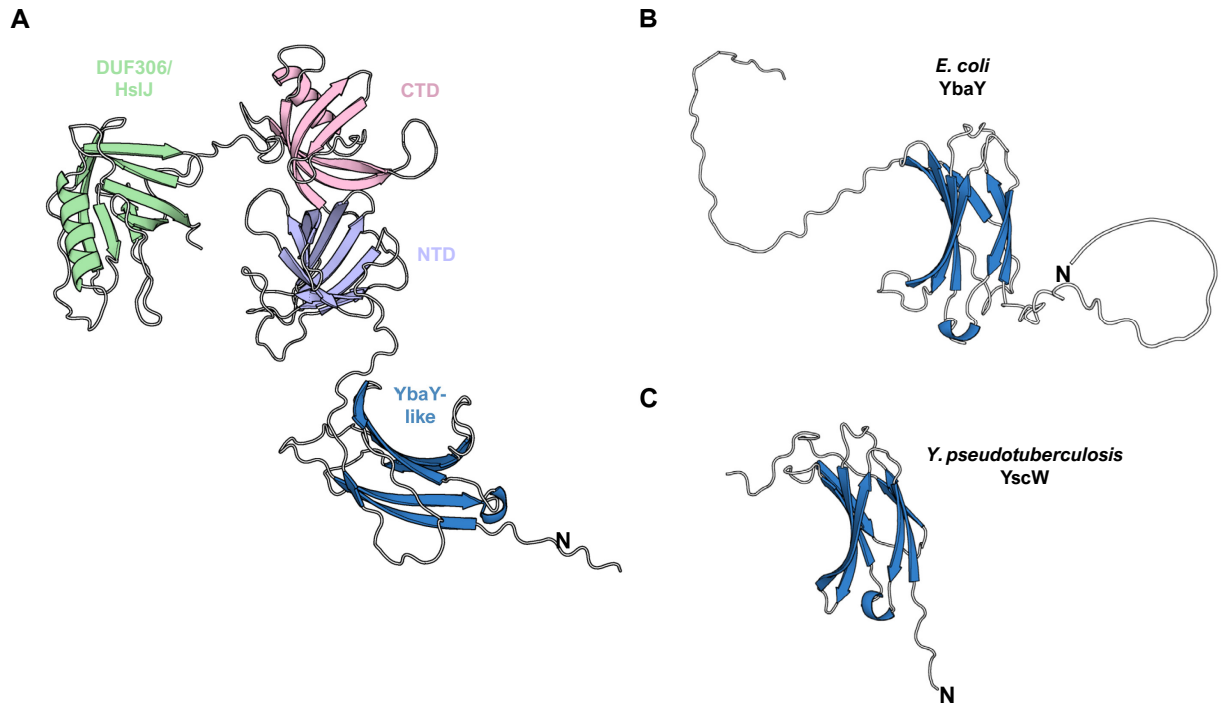

Figure 0-9. YbaY/YcsW/pilotin-like domains in NlpE homologs.

AlphaFold models of **(A)** *Niveibacterium umoris* NlpE/HslJ/YbaY-like lipoprotein, **(B)** *E. coli*'s YbaY, and **(C)** *Yersinia pseudotuberculosis* YscW.

Digging further into these results reveals even more bizarre variants of NlpE. One example is an NlpE variant that contains four independently folding domains from the Betaproteobacterial *Niveibacterium umoris* (Appendix Figure 0-9A). This protein contains an extra domain inserted before the *E. coli*-like N-terminal domain. This domain is annotated as a putative lipoprotein YbaY-like domain. Its overall domain architecture from this domain resembles the three domain NlpE discussed previously: YbaY-NTD-CTD-DUF306. Interestingly, YbaY is annotated in the same family of proteins as pilotin lipoproteins such as YscW and ExsB (Burghout et al., 2004; Perdu et al., 2015). AlphaFold models predict that the YbaY domain of the four-domain NlpE in *Niveibacterium umoris*, YbaY from *E. coli*, and YscW all resemble each other (Appendix Figure 0-9). Pilotins such as YscW are lipoproteins that facilitate the assembly of secretins, which form the outer membrane channels of secretion systems such as the type II and III secretion systems, into the outer membrane (Gu et al., 2012; Koo et al., 2012; Silva et al., 2020). While the function of YbaY in *E. coli* is unknown, the presence of a pilotin-like domain in NlpE homologues may suggest an ancestral role for NlpE in facilitating protein folding.

Taken together, NlpE appears to be a highly modular protein that serves as the platform for many different domains, some of which may be involved in stress response or envelope protein folding. The domains contained in these homologs differ across species but tends to follow a generally conserved domain organization. Significantly, all the NlpE homologs we studied which possess *E. coli*-like N- and C-terminal domains order these domains in the same way as they are in *E. coli*. Other domains appear to be added and removed from NlpE over evolutionary time and across bacterial species, leading to the diverse array presented here. It is also significant that while these domains are not found on the NlpE in *E. coli*, genes encoding other lipoproteins with the domains explored here (such as HslJ or YbaY) exist elsewhere in the genome. Thus, it's tempting to speculate that these lipoproteins may still be functionally linked to

NlpE in *E. coli*, just not as members of the same unit; future studies should examine if any such connection exists. Overall, our foray into the impossibly vast landscape of protein homologues across bacterial species, facilitated by advances in protein structure prediction and the availability of predicted structures on the AlphaFold database, may help generate novel hypotheses about the function of NlpE in our model organism, *E. coli*.

Appendix Tables

Table 0-1. Strains used in this study

Strain	Description	Source
TR50	MC4100 λRS88[*cpxP'-lacZ*$^{+}$*]*	(Raivio and Silhavy, 1997)
VM36	TR50 Δ*nlpE*	Vincent Man
TC772	VM36 + pTrc99A	This study
TC773	VM36 + pTrc-*nlpE*$_{AB}$	This study
TC777	VM36 + pTrc-*nlpE*$_{VC}$	This study
TC775	VM36 + pTrc-*nlpE*$_{MC}$	This study
TC778	VM36 + pTrc-*nlpE*$_{YP}$	This study
TC776	VM36 + pTrc-*nlpE*$_{ST}$	This study
TC774	VM36 + pTrc-*nlpE*$_{KP}$	This study

Appendix References

Burghout, P., Beckers, F., de Wit, E., van Boxtel, R., Cornelis, G.R., Tommassen, J., Koster, M., 2004. Role of the Pilot Protein YscW in the Biogenesis of the YscC Secretin in Yersinia enterocolitica. J Bacteriol 186, 5366–5375. https://doi.org/10.1128/JB.186.16.5366-5375.2004

Chuang, S.E., Blattner, F.R., 1993. Characterization of twenty-six new heat shock genes of Escherichia coli. Journal of Bacteriology 175, 5242–5252. https://doi.org/10.1128/jb.175.16.5242-5252.1993

Delhaye, A., Laloux, G., Collet, J.-F., 2019. The Lipoprotein NlpE Is a Cpx Sensor That Serves as a Sentinel for Protein Sorting and Folding Defects in the *Escherichia coli* Envelope. J Bacteriol 201. https://doi.org/10.1128/JB.00611-18

Gu, S., Rehman, S., Wang, X., Shevchik, V.E., Pickersgill, R.W., 2012. Structural and Functional Insights into the Pilotin-Secretin Complex of the Type II Secretion System. PLoS Pathog 8, e1002531. https://doi.org/10.1371/journal.ppat.1002531

Hirano, Y., Hossain, Md.M., Takeda, K., Tokuda, H., Miki, K., 2007. Structural Studies of the Cpx Pathway Activator NlpE on the Outer Membrane of Escherichia coli. Structure 15, 963–976. https://doi.org/10.1016/j.str.2007.06.014

Humphreys, S., Rowley, G., Stevenson, A., Anjum, M.F., Woodward, M.J., Gilbert, S., Kormanec, J., Roberts, M., 2004. Role of the Two-Component Regulator CpxAR in the Virulence of *Salmonella enterica* Serotype Typhimurium. Infect Immun 72, 4654–4661. https://doi.org/10.1128/IAI.72.8.4654-4661.2004

Koo, J., Burrows, L.L., Lynne Howell, P., 2012. Decoding the roles of pilotins and accessory proteins in secretin escort services. FEMS Microbiology Letters 328, 1–12. https://doi.org/10.1111/j.1574-6968.2011.02464.x

Lilic, M., Jovanovic, M., Jovanovic, G., Savic, D.J., 2003. Identification of the CysB-regulated gene, hslJ, related to the Escherichia coli novobiocin resistance phenotype. FEMS Microbiology Letters 224, 239–246. https://doi.org/10.1016/S0378-1097(03)00441-5

Marathe, N.P., Salvà-Serra, F., Nimje, P.S., Moore, E.R.B., 2022. Novel Plasmid Carrying Mobile Colistin Resistance Gene mcr-4.3 and Mercury Resistance Genes in Shewanella baltica: Insights into Mobilization of mcr-4.3 in Shewanella Species. Microbiology Spectrum 10, e02037-22. https://doi.org/10.1128/spectrum.02037-22

Marotta, J., May, K.L., Bae, C.Y., Grabowicz, M., 2023. Molecular insights into Escherichia coli Cpx envelope stress response activation by the sensor lipoprotein NlpE. Molecular Microbiology 119, 586–598. https://doi.org/10.1111/mmi.15054

May, K.L., Lehman, K.M., Mitchell, A.M., Grabowicz, M., 2019. A Stress Response Monitoring Lipoprotein Trafficking to the Outer Membrane. mBio 10, e00618-19. https://doi.org/10.1128/mBio.00618-19

Perdu, C., Huber, P., Bouillot, S., Blocker, A., Elsen, S., Attrée, I., Faudry, E., 2015. ExsB Is Required for Correct Assembly of the Pseudomonas aeruginosa Type III Secretion Apparatus in the Bacterial Membrane and Full Virulence In Vivo. Infect Immun 83, 1789–1798. https://doi.org/10.1128/IAI.00048-15

Raivio, T.L., Silhavy, T.J., 1997. Transduction of envelope stress in Escherichia coli by the Cpx two-component system. J Bacteriol 179, 7724–7733. https://doi.org/10.1128/jb.179.24.7724-7733.1997

Silva, Y.R. de O., Contreras-Martel, C., Macheboeuf, P., Dessen, A., 2020. Bacterial secretins: Mechanisms of assembly and membrane targeting. Protein Sci 29, 893–904. https://doi.org/10.1002/pro.3835

Siroy, A., Cosette, P., Seyer, D., Lemaître-Guillier, C., Vallenet, D., Van Dorsselaer, A., Boyer-Mariotte, S., Jouenne, T., Dé, E., 2006. Global Comparison of the Membrane Subproteomes between a Multidrug-Resistant *Acinetobacter baumannii* Strain and a Reference Strain. J. Proteome Res. 5, 3385–3398. https://doi.org/10.1021/pr060372s

Slamti, L., Waldor, M.K., 2009. Genetic Analysis of Activation of the *Vibrio cholerae* Cpx Pathway. J Bacteriol 191, 5044–5056. https://doi.org/10.1128/JB.00406-09

Snyder, W.B., Silhavy, T.J., 1995. Beta-galactosidase is inactivated by intermolecular disulfide bonds and is toxic when secreted to the periplasm of Escherichia coli. J Bacteriol 177, 953–963. https://doi.org/10.1128/jb.177.4.953-963.1995

Walsh, B.J.C., Wang, J., Edmonds, K.A., Palmer, L.D., Zhang, Y., Trinidad, J.C., Skaar, E.P., Giedroc, D.P., 2020. The Response of Acinetobacter baumannii to Hydrogen Sulfide Reveals Two Independent Persulfide-Sensing Systems and a Connection to Biofilm Regulation. mBio 11, e01254-20. https://doi.org/10.1128/mBio.01254-20